Late Quaternary Indian Monsoon Variability: Inferences from Marine and Continental Records

A Thesis submitted during 2020 to the University of Hyderabad in partial fulfilment of the award of a Ph.D. degree in Centre for Earth, Ocean and Atmospheric Sciences, School of Physics

by

Pawan Kumar Gautam

Centre for Earth, Ocean and Atmospheric Sciences
School of Physics
University of Hyderabad
(P.O.) Central University, Gachibowli
Hyderabad-500 046
India

December 2020

Late Quaternary Indian Monsoon Variability: Inferences from Marine and Continental Records

A Thesis submitted during 2020 to the University of Hyderabad in partial fulfilment of the award of a Ph.D. degree in Centre for Earth, Ocean and Atmospheric Sciences, School of Physics

by

Pawan Kumar Gautam

Centre for Earth, Ocean and Atmospheric Sciences
School of Physics
University of Hyderabad
(P.O.) Central University, Gachibowli
Hyderabad-500 046
India

December 2020

CERTIFICATE

This is to certify that the thesis entitled, **"Late Quaternary Indian Monsoon Variability: Inferences from Marine and Continental Records"** Submitted by **Pawan Kumar Gautam** bearing Registration No. **12ESPE04** in partial fulfilment of the requirements for the award of Doctor of Philosophy in **Earth Sciences** is a bonafide work carried out by him under my supervision and guidance.

The thesis has not been submitted previously in part or in full to this or any other University or Institution for the award of any degree or diploma.

Prof. A. C. Narayana
(Research Supervisor)

//Countersigned//

Head,
Centre for Earth, Ocean
and Atmospheric Sciences

Dr. K.S.Krishna, FNA, FASc, FNASc
Professor & Head
Centre for Earth, Ocean and Atmospheric Sciences
University of Hyderabad
Hyderabad-500 046, Telangana. India

Dean,
School of Physics

DEAN
School of Physics
University of Hyderabad
Hyderabad-500 046, INDIA

DECLARATION

I **Pawan Kumar Gautam** hereby declare that this thesis entitled "**Late Quaternary Indian Monsoon Variability: Inferences from Marine and Continental Records**" Submitted by me under the guidance and supervision of **Prof. A. C. Narayana** is a bonafide research work. I also declare that it has not been submitted previously in part or in full to this University or any other University or Institution for the award of any degree or diploma.

Date: 12.12.2020

Name: **Pawan Kumar Gautam**

Signature of the Student: Pawan Ku. Gautam 12.12.2020

Regd. No. 12ESPE04

Acknowledgements

It is dreadful to express fully the gratitude I feel towards the people in my life who have contributed time, effort, thought, support, and humor to me during my PhD. In reaching this goal, I have remarkably become engulfed in geopolitics, absorbed multiple religions, been immersed in even and odd culture across the country, and witnessed apex science. Beyond the field and labs, this project has helped me broaden my small scope on the huge galaxy of research arena. For this, at the onset, I would like to thank Professor A. C. Narayana for shaping my research and personality like a perfectionist and to make me capable for opting research as career. I also would like to thank him for introducing me to the other scientific and social endeavours which has strengthened me towards achieving the goals of life.

I wish to express my sincere gratitude to late Professor R. Ramesh, an outstanding scientist and human being, formerly from Physical Research Laboratory, Ahmedabad for his all-time support and mentorship during my research planning, execution and excellent research collaboration through ISRO-GBP Project. I also pay my deep regards to Dr. M. G. Yadava, Senior Scientist from Physical Research Laboratory, Ahmedabad for his all-time support, for his priceless guidance, suggestions, and motivation to carry out research. I Thank Prof. Ramesh and Dr. Yadava for providing all lab facilities. I also thank PRL administration for their support during my stay at PRL

I thank Prof. C-C Shen alias and his lab associates from HISPEC, National Taiwan university, Taiwan for providing U-Th ages of the samples. Similarly, Prof. Hai Cheng, Dr. Gayatri Kathayat and their lab associates of Institute of Global Environmental Change, Xi'an Jiaotong University, Xi'an, China are also thanked for U-Th ages. Prof. Jull, formerly from University of Arizona is acknowledged for ^{14}C AMS ages.

I want to thank my doctoral committee member, Dr. Masood Ahmad, Senior Scientist (Retd.) from National Geophysical Research Laboratory (NGRI), Hyderabad for sparing his time to review my work progress and boosting me up with the best suggestions. I owe a thank you to the other doctoral committee members as well along with Head, Centre for Earth, Ocean and Atmospheric Sciences (CEOAS), faculties, colleagues, and all the staff members of CEOAS for their affection and support while pursuing my PhD. I especially thank my fellow group members, namely, Dr. Shiva Kumar G., Mr. Anjaiah B., and Dr. Sravanthi N. for their wonderful company and for the happiness we exchanged while being at the centre. UoH administration is acknowledged for the fellowship and all other administrative issues.

I am very much thankful to Mr. C. P. Panigrahi, Scientist from Atomic Mineral Directorate (AMD) for his help in field work and collection of the stalagmite samples. Mr. N. Vaghela from PRL is acknowledged for his assistance during sample cutting and processing at PRL. I am indebted to the technical support received from Dr. Shraddha T. Band, and Dr. P. Kiran Kumar from PRL during the sub-sampling and chemical analyses.

XRD and SEM labs of Central Instrumentation Laboratory (CIL), UoH are thanked for providing the technical support during analyses. Also, XRD lab of CEST, UoH is also acknowledged for the same.

I am indebted to Dr. Pradeep Kumar G. for his unconditional help in collecting the research articles needed for the research work. Dr. Venu keerthi is also acknowledged for providing many research papers I requested for.

Dr. Bivin Geo George, Dr. Ikshu Gautam, Dr. Anirban Chaterjee, Dr. Ananta Mishra, Dr. P. Kiran Kumar, Mr. Sachin Kumar, Dr. Midhun, Dr. Shrema, Dr. Sateesh R. V, and others from PRL are acknowledged for their help and support during my stay at PRL. Miss. Deepa Verma is specially acknowledged for her company while being at Ahmedabad.

I take this opportunity thank Mr. Kumar Ashish, elder brother from another mother, for his love, support, guidance, and priceless suggestions since childhood. I am indebted to him for shaping a raw of me into a polished one.

My stay at UoH was cheerful because of the company of most wonderful people around me. I am indebted Mr. Hemant Khanchi, Mr. Akshay Rastogi, Dr. Bhanu Pratap Singh, Dr. Shubham Tripathi, Mr. Kushagra Krishnan, My roommate Dr. Durga Rao B., etc. for their crème-de-la-crème affection while being at UoH campus. Mr. Raghvendra Kushwaha and Mr. Subhash Kumar are thanked for their help and support during COVID-19 lockdown days. Mr Abhishek Kumar and Mrs. Mona are also acknowledged for the same. Prof. Appa Rao, Vice Chancellor, UoH is especially thanked for allowing me to stay in guest house.

I thank my colleagues from Geological survey of India for their support. Especially, Miss. Namrata Singh Chauhan is highly thanked for her unconditional support and affection during my offbeat dispositions in connection with the research workloads. I sincerely thank the administration of GSI for providing the no objection certificate (NOC) to pursue my PhD and providing comfortable environment in discharging my duties without any obstacle.

I am thankful to my teachers from my school days and Pondicherry University for their magnificent skills in orienting me to achieve the desired. I also thank my seniors, batch mates, and juniors from school and university for being always there for me.

Now, a little closer to home, words cannot express the gratitude I have for my family. They have shown nothing but love and encouragement throughout my entire life as well as my academic career. I am truly grateful to have such an amazing family. I want especially to thank my parents, grand-parents, uncles-aunts, sisters, brother-in-laws, and cousins for their belief in me. I dedicate this thesis to my parents.

At the end, I thank almighty GOD for controlling all the stuff I have done so far!

Pawan Kumar Gautam

Abstract

Indian monsoon is considered as one of the most powerful circulation system manifested by the seasonal wind reversal driven by the north-south movement of the Inter-Tropical Convergence Zone across the equator causing enormous change in the hydrological system. This change of hydrological system affects the economy, culture, society, land use, vegetation, etc., across the Indian subcontinent. To understand the variability of the monsoon rainfall and its associated causative factors, continuous monitoring of meteorological parameters is essential for climate modeling and future prediction. However, long term study from the past is not possible as the instrumental data is available only for about a century. Hence, long term records of monsoonal variability are studied from several natural proxies. A chronological parameter is also essential in assigning the temporal range to the proxy based climatic reconstruction in geological time scale. The proxy based studies together with geochronology make the scientific explanations stronger in reconstructing the paleoclimate. Paleoclimatic studies using various proxies such as marine sediments, lacustrine sediments, tree rings, stalagmites, etc., have been carried out from Indian region. Studies on monsoon reconstruction from the past indicate that several ancient civilizations suffered due to the adverse changes in Indian monsoon causing severe drought and/or floods. The literature review of Indian monsoon reconstruction from various proxies of marine and continental domains give an insight in to the Indian monsoon mechanism and its dynamics, which is very complex and has varied truly out of the box of its convenient mode of variability at different time intervals. Hence, it is very important to have its reconstruction at high resolution so that the minute

changes and the variabilities on the cyclic pattern of the monsoon system can be understood. Thus, to understand the Indian monsoon variability, $\delta^{18}O$ and $\delta^{13}C$ isotopic studies of two planktic foraminifera: *Globigerina bulloides* and *Orbulina universa,* as a proxy for marine record and speleothems (stalagmites) for continental records have been studied. The study area covers the southwestern Bay of Bengal (BoB) and the two limestone caves from Indian subcontinent - Kailash cave, Kanger valley, Chhattisgarh, and Borra Cave, Araku valley, Andhra Pradesh, eastern part of India. The $\delta^{18}O$ and $\delta^{13}C$ isotopic records of *Globigerina bulloides* and *Orbulina universa* from southwestern Bay of Bengal unravel the Indian monsoon variability during the last 46 ka BP. The isotopic variability records of *Globigerina bulloides* and *Orbulina universa* are inferred to reflect Northeast Monsoon (NEM) and Southwest Monsoon (SWM) variability, respectively. The $\Delta\delta^{18}O_{bulloides\text{-}universa}$ indicates that the intensity of Indian monsoon in the southwestern Bay of Bengal (BoB) was significantly different during MIS-1, MIS-2, and MIS-3 where monsoon was strongest during MIS-1 followed by MIS-3, but was weaker during MIS-2. Most enriched $\delta^{13}C$ concentrations of *Globigerina bulloides* during MIS-1 also indicate intense stratification and weak upwelling. On the contrary, MIS-2 indicates weakest stratification due to the supply of nutrient rich cold water along with depleted $\delta^{13}C$ to the ocean surface. Similarly, a moderate $\delta^{13}C$ value during MIS-3 supports the fact that MIS-3 was associated with higher productivity than MIS-2 but lower than MIS-1. Sea surface height anomaly data suggest that the core location lies in the region of persistent cyclonic eddies as the southwestern BoB experiences more cyclonic events. It is inferred that downwind transport of atmospheric signal from the North Atlantic drives the changes in the Indian monsoon. The study further reveals that high productivity during early Holocene, i.e. onset of active interglacial stage, was due to

enhanced photosynthesis. The study supports *Globigerina bulloides* and *Orbulina universa* $\delta^{18}O$ and $\delta^{13}C$ as a reliable proxy for Indian monsoon reconstruction. Regional correlation of $\delta^{18}O$ records suggest that hydroclimate in southwestern BoB were similar to the other parts of BoB and Andaman Sea. Significant high resolution southwest monsoon variability was reconstructed between Bolling-Allerod (B-A) and Younger Dryas from KG-6 stalagmite of Kailash Cave, Central India. The isotopic time series records show monsoonal variability and their periodicities were the consequence of the changes that occurred in dominant coupled ocean-atmospheric system. Results indicate significant Southern Hemisphere contribution in modulating the climate pattern of southwest monsoon. The stalagmite (BRA-3B) $\delta^{18}O$ and $\delta^{13}C$ records from Borra cave have helped in clearly demarcating six wet and four dry phases during ~4.8- ~3.8 ka BP. The isotopic variability records suggest a ~25 years and ~10 years cycles before and after 4.2 ka event. Records also show that dry phases were dominant during ~4.5 ka to ~4.1 ka with small but intense intermittent wet phase caused due to intensified local moisture. Major dry period existed in three phases with intermittent short wet phases during 4.2 ka. Intermittent wet periods may be associated with flood events. Major dry phase caused global extinction and/or migration of civilizations Centennial periodicities inferred from $\delta^{18}O$ and $\delta^{13}C$ time series strongly suggest that the ISM variability has been directly modulated by solar cycles. Centennial periodicities inferred from $\delta^{18}O$ and $\delta^{13}C$ time series strongly suggest that the ISM variability has been directly modulated by solar cycles.

List of Figures

List of Tables

Late Quaternary Indian Monsoon Variability: Inferences from Marine and Continental Records

Contents

Chapter 1

Introduction

Chapter 1
Introduction

1.1 Introduction

The Indian monsoon is one of the most dynamic and powerful circulation system manifested by the seasonal wind reversal driven by the north-south movement of the Inter-Tropical Convergence Zone (ITCZ) across the equator causing enormous change in the hydrological system (Wyrtki, 1971).The monsoon system directly and/or indirectly controls the hydrology, economy, culture, society, land use, vegetation, etc., across the Indian subcontinent. To understand the variability of the monsoon rainfall and its associated causative factors, continuous monitoring of meteorological parameters is essential for climate modeling and future prediction. However, long term study from the past is not possible as the instrumental data is available only for about a century. Hence, long term records of monsoonal variability are studied from several natural proxies. The proxy based study of reconstructing the climate from geological past is dealt in Paleoclimate (Bradley, 2014). Paleoclimatic study of any region of the world is of great importance particularly in gaining knowledge of how, why and when changes have occurred and also to identify possible mechanism for those changes. A chronological parameter is also essential in assigning the temporal range to the proxy based climatic reconstruction in geological time scale. Hence, proxy studies together with geochronology make the scientific

explanations stronger in reconstructing the paleoclimate. Brief description about paleoclimate and proxies used in paleoclimatic studies are discussed below.

1.2. Paleoclimate

Spatial and temporal reconstruction of long term weather conditions (i.e. climate) are dealt in paleoclimatic studies which invariably enhances the control on understanding the forcing mechanisms and natural agents responsible for modulating the climate change in the geological past. The paleoclimatic reconstruction is very important topic of scientific research as it increases the knowledge of the changes occurred in global ecological, cultural and economical system. Paleoclimatic study of any region of the world is of great importance particularly in gaining knowledge of how, why and when changes have occurred and also to identify possible mechanism for those changes.

The major natural causative factors involved in modulating the global climate system has been so far related with Earth's orbital parameter, variations in the Sun's output and volcanic eruptions. Cyclic variability in the amount of energy emitted by Sun inferred from sunspots is now linked to change in global climate. For example, cooling or little ice ages such as Oort Minimum, Wolf minimum, Spörer minimum, Maundar minimum, etc., (during the 17^{th} and 18^{th} century) and the warming in 20^{th} century have been directly correlated to solar insolation cycles. Similarly, on larger temporal scale, cyclic occurrences of Glacial and Interglacial periods in the geological past also have been linked to Earth's orbital parameters (Croll, 1867).

Milankovitch (1941) first identified the cyclic changes in the Earth's orbital parameters: eccentricity, axial tilt and precession and these cycles are known as Milankovitch cycles (Fig. 1.1). The eccentricity changes between more or less elliptical and circular at an interval of approximately 100,000 years. Changes in the Earth's axial tilt between 21.5^{o} to 24.5 ^{o} occur once with periodicity of 41,000 years. The precession, the Earth's slow wobble as it spins on its axis, occurs with a periodicity of 23,000 years. These cycles cause changes in the Earth's climate. Furthermore, volcanic eruptions inject dusty materials into the atmosphere that decrease the net solar radiation reaching the earth's surface. These cause change in the energy balance and hence alter the atmospheric circulation patterns. However, volcanic eruptions are short lived phenomena and hence are responsible for short term climatic changes.

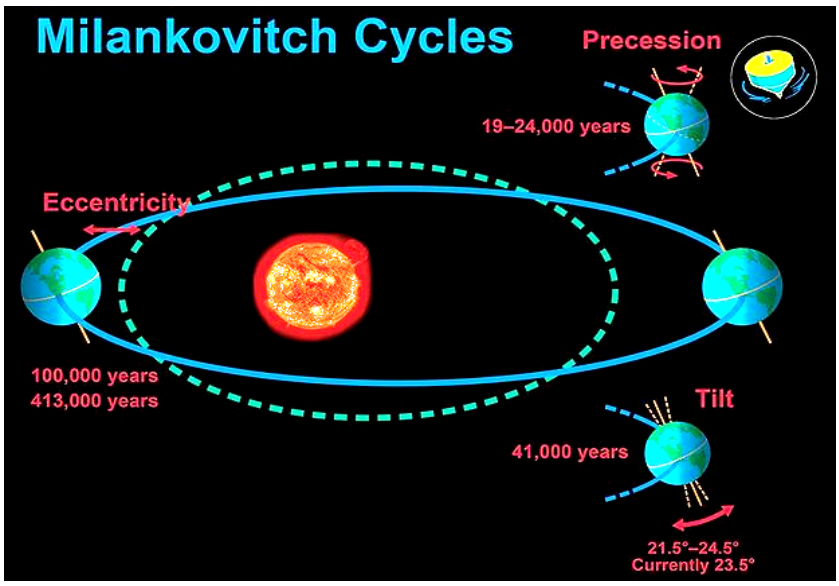

Fig. 1.1. Milankovitch Cycle (Milankovitch, 1941)

1.2.1. Proxies

The knowledge of the past prepares us for current and future climatic changes (Bradley and Eddy, 1991). Hence, paleoclimatic reconstruction helps in modeling the contemporary and future climate patterns for particular region or entire earth. Paleoclimatic studies are different from contemporary climate study as they are totally based on instrumental records and modeling. While climatic data for the past 100 years or so may be available, older data can only be found in the form of some kind of proxy. A climate proxy (Fig. 1.2) is physical, chemical or biological property of the natural system which enables quantification of the change in climate in the past and a chronometer to assign a time to this proxy. A chronological parameter is also essential in assigning the temporal range to the proxy based climatic reconstruction in geological time scale. Hence, proxy along with geochronology together makes the scientific methodology for paleoclimate reconstruction.

Proxies (Fig. 1.2) are basically measurable parameters which provide quantitative or qualitative information about climate and hydrological variables such as temperature, precipitations, run off, discharge, and sedimentation rates. The choice of particular proxy depends on the period for which paleoclimatic information is being retrieved, the site and availability of suitable material for extracting the proxy data. Evidence of past climatic conditions is commonly preserved in natural archives such as marine and lacustrine sediments, loess, ice, cave deposits (speleothems), sub-fossil biological material, geomorphological features (glacial deposits, erosional features, paleosols, and periglacial phenomena), etc. By definition, such proxy

records of climate contain a climatic signal but that signal may be relatively weak, embedded in a great deal of extraneous “noise” arising from the effects of other (nonclimatic) influences. Hence, to extract the paleoclimatic signal from proxy data, the record must first be calibrated for actual interpretation. Calibration is done using modern climatic records and climate-dependent proxy materials. It is assumed that the modern relationships observed have operated, unchanged, throughout the period of interest (Theory of Uniformitarianism).For the reconstruction of recent climatic changes, tree rings, corals, lakes and ice core records are commonly used. In this study, foraminifera and stalagmite (speleothem) have been used (explained in Chapter 3) for the reconstruction of Indian Monsoon using stable isotopes of carbon and oxygen. Brief information about planktonic foraminifera and stalagmite use for paleoclimatic interpretation is discussed in sections 1.12 and 1.13, respectively.

Marine Proxy: Planktic Foraminifera

Applications of planktic foraminifera in the field of paleoceanography and paleoclimate have increased substantially since the pioneering work of Schott (1935). The growth of planktic foraminifera shells have been proved as a function of ambient sea water condition, and the relative abundance and chemistry of the foraminifera shells are now very well used to interpret paleoceanographic or paleoclimatic signatures. Foraminifera are classified into two types - Planktonic and Benthic - based on their depth of dwelling or habitat. There exist more than 4000 species of

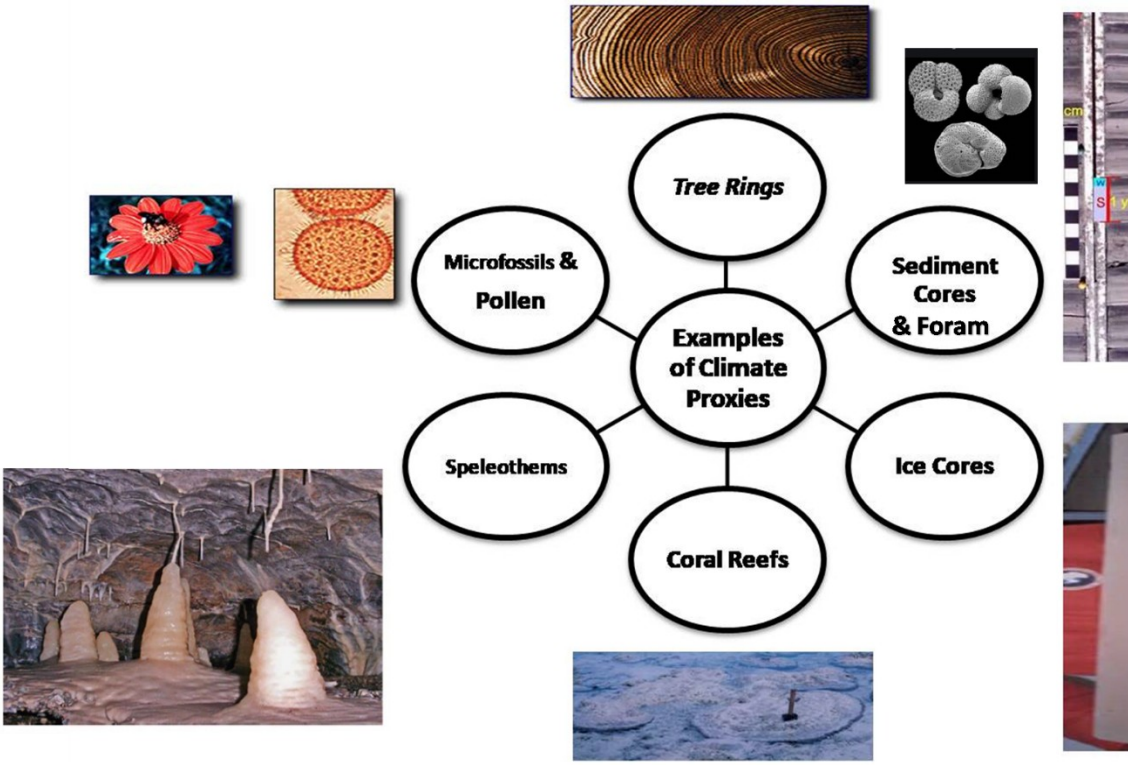

Fig. 1.2. Paleoclimate Proxies used to infer climate of the geological past.

foraminifera out of which less than 50 species are planktonic and rest of them are benthic. Basically, planktonic foraminifera are evolved from benthic species itself during late Jurassic to Cretaceous (Darling et al., 1997). Planktic foraminifera are basically surface dwelling species and record the surficial oceanographic change in their shells. Several planktic and benthic species have been studied for paleoceanographic reconstruction. Paleoceanographic studies are done by the population studies of the species or by chemical analyses of the foraminifera shells. Species like *G. ruber*, *G. menardii, G. Hirsuta, G. Sacculifer, O. universa, G. bulloides,* etc have been used globally for paleoceanographic studies. In this study, two planktonic foraminifera: *Globigerina bulloides* (Fig. 1.3A) and *Orbulina*

universa (Fig. 1.3B) have been studied for the interpretation of monsoon from southwestern Bay of Bengal.

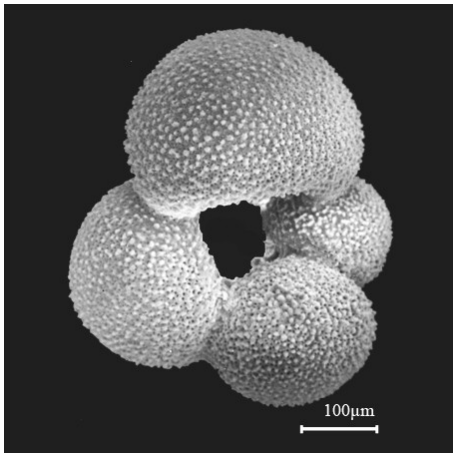

Fig. 1.3A. *Globigerina bulloides*

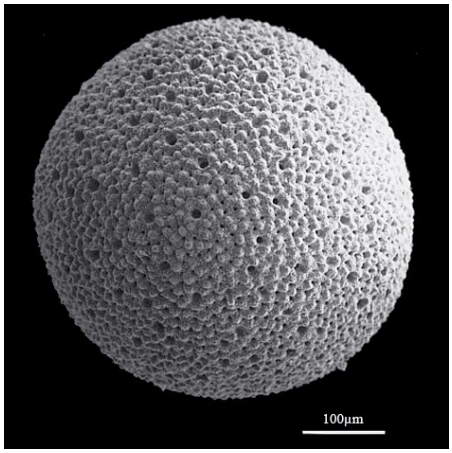

Fig. 1.3B. *Orbulina universa*

Continental Proxy: Speleothem (Stalagmite)

The terminology speleothem is derived from the Greek words *spelaion* (cave) and *thema* (deposit) (Schwarcz 1986). Speleothems are basically secondary calcium carbonate deposits occurring in the caves of karst region by the action of rain water percolating through the cave and dripping from the ceiling or walls of a cave. Schematic model of speleothem deposition, explained by Fairchild *et al.* (2007), is shown in figure 1.4. Soil is acidic in nature as the pCO_2 of soul is considerably high due to decomposition of organic matter and root respiration. Hence, the water mixed with soil carry ions such as HCO^{3-}, $CO3^{2-}$, and Ca^{2+}, etc., while seeping into caves through fractures. Since the pCO_2 of the cave is relatively low (due to ventilation) than the outer atmosphere, automatic CO_2 degassing takes place which leads to

supersaturation of carbonates and then ultimately their deposition (Emrich *et al.,* 1970). This continued process causes the growth of speleothems. Sometimes, growing stalactite and stalagmite join together to form a pillar.

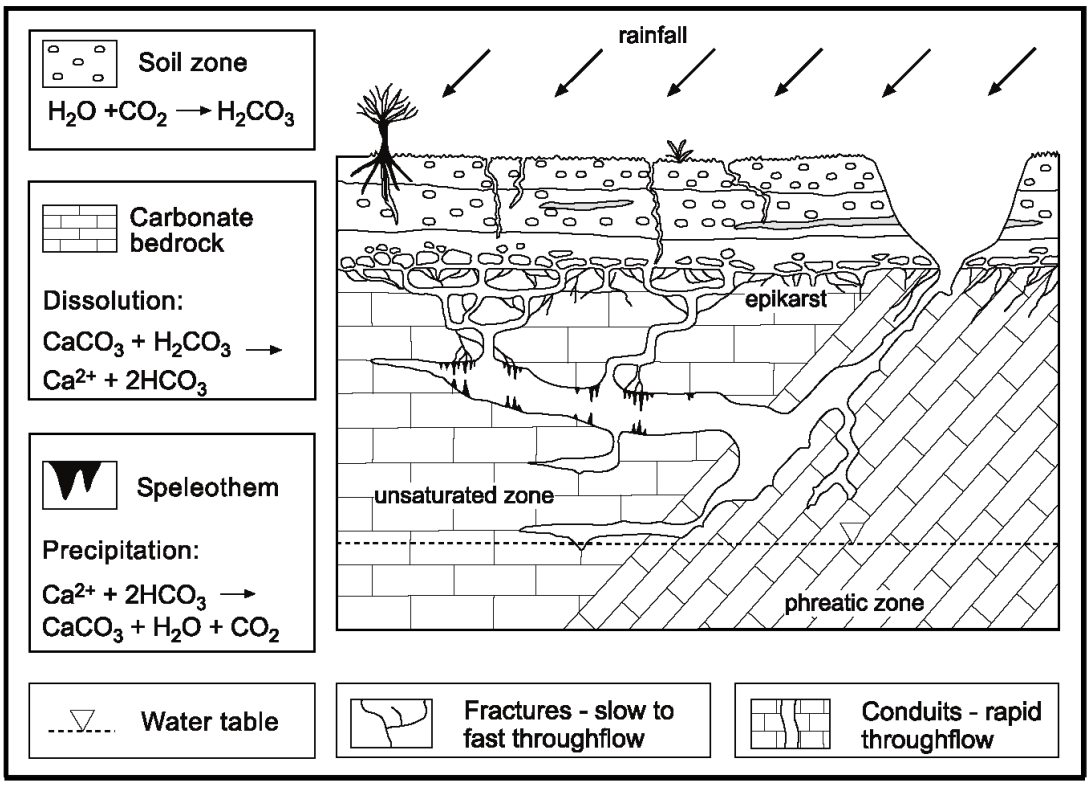

Fig. 1.4. Process of speleothem formation and growth in a Karst environment (Fairchild *et al.,* 2007).

Stalagmites have been considered best for paleoclimatic interpretation because of their layered sequential growth with time without mixing. Hendy (1969, 1971) in his initial researches on stalagmites showed that only those stalagmites which have been deposition under isotopic equilibrium are good for paleoclimatic

interpretation. This means that the oxygen and carbon isotopic value along a growth layer should be uniform and there should not be any correlation between oxygen and carbon isotope of each layer. Any such relation will indicate fractionation during deposition. Isotopic fractionations are dealt in Chapter 4. Stalagmites deposited in isotopic equilibrium are typically found in caves having poor ventilation.

1.2.2. Geochronology

Geochronology helps in fixing the temporal disposition of the reconstructed climate in geological time series. This is done by estimating the relative or absolute stratigraphic age estimation of the proxy geological material used for the reconstruction. The output of the present research work is confined to the Quaternary age as this period is very important in paleoclimatic studies as the earth has witnessed large climatic variability during this time period. Based on the age estimation criteria, geochronological methods for Quaternary age are classified as following.

- **Sidereal**: Calendar or annual methods which determine calendar dates or count annual events.
- **Isotopic**: This measures changes in isotopic composition due to radioactive decay and/or growth
- **Radiogenic**: This measures the cumulative effects of radioactive decay such as crystal damage and electron energy traps.

- **Chemical and Biological**: This measures the time dependent chemical and biological processes.
- **Geomorphic**: This measures the cumulative results of complex, interrelated physical, chemical, and biological processes on the landscape.
- **Correlation**: It establishes age equivalence using time-independent properties.

Several age estimation methods are classified into aforementioned six types as shown in Table 1.1. For the age estimations of the results produced from the foraminiferal species, radiocarbon geochronological method has been applied; whereas U-Th dating methods have been applied for stalagmites' age estimations. The procedures of Radiocarbon and U-Series age estimation methods have been described in detail in Chapter 3.

1.3. CO_2 Stable Isotopologues

Isotopologues are referred to the different combinations of isotopic masses of CO_2 molecule which involve the combinations of isotopes of Carbon and Oxygen. There are three major stable isotopologues of CO_2 having molecular masses of 44, 45, and 46. These isotopologues along with their abundance percentage as reported by NOAA are tabulated in Table 1.2 where the majority of the mass is comprised of 44 isotopologues and isotopologues of mass 45 and 46 contribute a small fraction or

Table 1.1. Geochronological methods for the age estimation

Numerical Age					
	Calibrated Age				
	Relative Age				
			Correlated Age		
Sidereal	**Isotopic**	**Radiogenic**	**Chemical and Biological**	**Geomorphic**	**Correlation**
Dendrochronology	Radiocarbon (^{14}C)	Fission Track	Amino acid racemization	Rock and mineral weathering	Stratigraphy
Sclero-chronology	^{10}Be, ^{26}Al, ^{36}Cl, ^{3}He, etc.	Thermo-Luminescence (TL)	Obsidian hydration and tephra hydration	Soil profile development	Paleomagnetism
Varve Chronology	K-Ar and Ar-Ar	Optically Stimulated Luminescence (OSL)	Rock varnish cation ratio	Rate of deposition	Tephrachronology
Historical Records	U-Th Series	Electron Spin Resonance	Lichenometry	Rate of deformation	Paleontology
			Soil Chemistry	Scarp morphology	Archealogy
				Stone coating (Calcium carbonate)	Climatic correlation
					Astronomical Correlation
					Marine Isotopic Stage (MIS)
					Tectites and microtectites

Note: Grey bars indicate the control of type of geochronological methods

Table 1.2. CO_2 Stable Isotopologues		
Molecular Mass	**Isotopologues**	**Abundance %**
44	$^{12}C^{16}O_2$	98.40
45	$^{13}C^{16}O_2$	1.19
	$^{12}C^{17}O^{16}O$	0.0748
46	$^{12}C^{18}O^{16}O$	0.41
	$^{13}C^{17}O^{16}O$	.00084
	$^{12}C^{17}O_2$	0.0000142

their abundance is very low when compared to mass of 45. In order to infer the paleoclimate signatures from these isotopologues, ^{13}C and ^{18}O are taken into account. Thus, Criag corrections (Criag, 1957; dealt in Chapter 3) are required for the removal of effects from the isotopologues of lower abundance.

1.3.1. Isotopic Notations

Based on the isotopic masses, the relative abundance (R) of the isotopes is represented by the ratio of the higher to the lower isotopic mass of the element. The isotopic ratios are further represented as δ in comparison to their international standard as measurement of their absolute abundance is very difficult.

$$\delta = [(R_{Sample}/R_{Standard}) - 1] \times 10^3 \text{ ‰}$$

Where,

R = (Abundance of heavier isotope / Abundance of lighter isotope)

Isotopic standards are assigned the value of 0‰ on δ-scale of interest. Vienna Pee Dee Belemnite (VPDB) is considered as the international standard for carbonates as per International Atomic Energy Agency (IAEA). VPDB is basically belemnite of Cretaceous age from the Peedee Formation of South Carolina (Criag, 1957).

Due to the relative mass difference in molecules because of their zero point energy (energy at 0 Kelvin) and vibrational energy, isotopic fractionation takes place which causes variations in R value. This isotopic fractionation is mass dependent such that it is observed more in lighter element as the ratio of the difference between isotopic masses to the isotopic mass are also high for lighter elements than heavier elements. The fractionation becomes negligible for isotopic masses more than 40.

1.4. Indian Monsoon and its Variability

Paleoclimatic studies, in the Indian context, deals mostly with the Monsoon reconstruction. Indian monsoon is the most important single climate factor that determines the lives, ecology and economics of the region. Agriculture depends upon summer monsoon. Monsoon represents the seasonal reversal of wind direction over the subcontinent. During summer (June-August), the south westerly winds (the

summer monsoon) pick up moisture from the oceans, travel to land and precipitate their moisture over the region. During winter (December-February), however, the monsoon winds are dry and variable, blowing from the northeast, from land to sea. Most parts of the Indian region receive a major portion of their annual rainfall during the summer or southwest (SW) monsoon. Differential warming of South Asia and the surrounding ocean causes monsoons. The areas of the northern and central Indian subcontinent heats up during the northern summer season. This is responsible for development of a low pressure area over the northern and central Indian subcontinent. The moisture-laden winds from the Indian Ocean move in to fill this void via Bay of Bengal and the Arabian Sea. The monsoon winds are confined to the subcontinent and are not allowed to carry the moisture to central Asia by the mighty Himalaya Mountains, which form a physical barrier. The Indian monsoon along with Chinese monsoon plays an important role in modulating the global climate as well as controlling the global hydrologic cycle. The dynamics of Indian Monsoon is explained in detail in Chapter 2. Several workers have provided prolific records of Indian monsoon from the geologic past to the Recent. A brief description of the previous work carried out on Indian/Asian monsoon reconstruction is described below.

1.5. Previous Work

Pioneer projects like CLIMAP and COHMAP for paleoclimate reconstructions of marine and continental conditions at 3000-year intervals from 18,000 years BP to the present have been carried out on global scale (CLIMAP, 1976; COHMAP, 1988;

Webb et al., 1993). These were followed by other large-scale syntheses (EPILOG, GLAMAP, MARGO, etc.) accompanied by modeling and simulation (e.g., PMIP; Prentice et al., 2000) and further studies of surface conditions at the LGM (Kucera et al., 2005).

Paleomonsoon research on the Asian monsoon zone began with the study of loess profiles during 1950 which attracted scientist of different domain to study loess profiles in China and came up with the fact during late 1990s that monsoon is the main controlling force for paleo-environmental change in East Asia. This opened the door for spatial and temporal correlation of monsoon studies from different natural archives in Asia.

Paleoclimatic studies using various proxies for monsoonal reconstruction in the Indian region was emphasized by Prell *et al.,* (1980) and Bryson and Swain, (1981) and several others (Sirocko, *et al.,* 1993, 1996; Sarkar, *et al.,* 2000; Ramesh, 2001; Thamban *et al.,* 2001;Yadava and Ramesh, 2001, 2005; Anderson *et al.,* 2002; Staubwasser *et al.,* 2002, 2003; Fleitmann *et al.,* 2003; Gupta *et al.,* 2003, 2005; Yadava *et al.,* 2004; Singh *et al.,* 2006; Tiwari *et al.,* 2006; Rashid *et al.,* 2007; Yadava and Ramesh, 2007; Govil and Naidu, 2010; Ahmad *et al.,* 2012; Raza and Ahmad, 2013; Kotlia *et al.,* 2014; Lone *et al.,* 2014; Dixit *et al.,* 2016, Sijinkumar *et al.,* 2016; Narayana *et al.,* 2012, 2014, 2017, Kathayat *et al.,* 2016, 2017; Silva *et al.,* 2017; Kumar *et al.,* 2018; Gautam *et al.,* 2019; Band *et al.,* 2019, etc.). Proxies such as tree-rings (Bräuning and Griebinger, 2006, Managave and Ramesh, 2011; Managave *et al.,* 2019), lacustrine and marine sediments and their organic matter

(Enzel *et al.,* 1999; Agnihotri *et al.,* 2002; Ramesh and Tiwari, 2007; Ramesh *et al.,* 2007; Mishra *et al.,* 2019) and pollen records (Bhattacharyya *et al.,* 2006; Phadtare and Pant, 2006) have been used to obtain paleomonsoon records with different resolutions. Similarly, foraminiferal abundances and their stable oxygen and carbon isotope ratios have been well studied from Arabian sea (Sirocko *et al.,* 1993; Overpeck *et al.,* 1996; Naidu and Malmgren, 1996; Sarkar *et al.,* 2000; Gupta *et al.,* 2003; Anand *et al.,* 2008; Ramesh *et al.,* 2010; Singh *et al.,* 2010; Tiwari *et al.,*2005, 2010; Govil and Naidu., 2010; Naidu *et al.,*1999, 2011; Saraswat *et al.,* 2013; Partin *et al.,* 2015; Singh *et al.,* 2016), Andaman Sea, and BoB (Cullen *et al.,* 1981; Naidu *et al.,* 1999; Kudrass *et al.,* 2001; Rashid *et al.,* 2007, 2011; Govil and Naidu, 2011; Ahmad *et al.,* 2012; Raza *et al.,* 2014; Sijinkumar *et al.,* 2016; Gebregiorgis *et al.,* 2016; Silva *et al.,* 2017; Kumar *et al.,* 2018). Monsoonal reconstruction using speleothems/stalagmites have also been studied by many researchers (Neff *et al.,* 2001; Yadava and Ramesh, 2001, 2006; Yadava *et al.,* 2004; Fleitmann *et al.,* 2003, 2007; Laskar *et al.,* 2011, 2013; Kotlia *et al.,* 2012, 2014; Sanwal *et al.,* 2013; Lone *et al.,* 2014, Kathayat *et al.,* 2016, 2017; Gautam *et al.,* 2019, Band *et al.,* 2019). Brief description on the research work carried out on marine and continental records are described in sections 1.5.1 and 1.5.2, respectively.

Studies from the archeological evidences also indicate that the collapse of human civilizations caused due to abrupt climate changes, for example collapse of Indus, Mayan, Egyptian, Babylonian and Mesopotamian, Akkadian, etc., were attributed to comparatively rapid change in climatic conditions. Monsoonal

deviations drastically affected the agrarian system of Indus valley which ultimately caused major change or rather extinction of many crop patterns.

1.5.1. Marine Record: Foraminifera

Paleoceanographic and paleomonsoonal studies based on different proxies from the northern Indian Ocean have shown significant changes in monsoon in the past (Cullen, 1981; Duplessy, 1982; Kallel *et al.,* 1988; Sarkar *et al.,* 1990; Prell *et al.,* 1992; Sirocko *et al.,* 1993; Naqvi *et al.,* 1994; Schulz *et al.,* 1998; Kudrass *et al.,* 2001; Gupta *et al.,* 2003; Ahmad *et al,* 2005; Curry and Oppo, 2005; Kessarkar *et al.,* 2005; Molnar, 2005; Saraswat *et al.,* 2005; Yadavand Ramesh, 2005; Ruddiman, 2006; Clemens and Prell, 2007; Sinha *et al.,* 2007; Rao *et al. ,*2008; Clemens *et al.,* 2010; Tiwari *et al.,* 2010; Rashid *et al.,* 2011; Kale, 2012; Achyuthan *et al.,* 2014; Lone *et al.,* 2014; Singhvi and Krishnan, 2014; Sijinkumar *et al.,* 2016; Kumar *et al.,* 2018). The major conclusions derived from the studies of various researchers are stated below:

- Monsoon experienced weak or seized cycles during glacial/stadial and strong/open cycles during the interglacial interstadial periods.
- Monsoon cycles followed the Milankovitch cycles which directly or indirectly modulated the glacial/interglacial phases on planet earth (Duplessy, 1982; Schulz *et al.,* 1998; Sarkar *et al.,* 1990, Rashid *et al.,* 2007; Saher *et al.,* 2007; Kessarkar *et al.,* 2013).

- Salinity is directly proportional to the glacial cycles such that higher salinity was preserved during glacial phases (Cullen, 1981; Duplessy, 1982; Rashid *et al.,* 2007, 2011).
- The strength of Indian monsoon is directly linked to the cold (stadial) and warm (inter-stadial) events of North Atlantic (Prell *et al.,* 1992*;* Sirocko *et al.,* 1993; Schulz *et al.,* 1998; Kudrass *et al.,* 2001; Higginson *et al.,* 2004; Sijinkumar *et al.,* 2016).
- Several researches, based on various proxies such as salinity, fresh water flux, mg/ca ratio, etc, have linked low fresh water input and higher salinity (Gupta *et al.,* 2003; Naidu and Malmgren, 2005; Govil and Naidu, 2011; Ahmad *et al.,* 2012; Mir *et al.,* 2013; Saraswat *et al.,* 2013; Mahesh and Banakar, 2014; Raza *et al.,* 2014; Boll *et al.,* 2015).
- Increased foraminiferal diversity has been reported during Heincrich events (Singh *et al.,* 2015).
- Several researches on paleo-productivity in Arabian Sea, Bay of Bengal and Andaman sea conclude the fact that productivity changes is witnessed region-wise such that Western Arabian sea witnessed high productivity during interglacial period (Emeis *et al.,* 1995; Naidu and Malmgren, 1996; Shimmield *et al.,* 1990; Spaulding and Oba, 1992) and eastem Arabian Sea witnessed increasing productivity during glacial phase (Cayre and Bard, 1999; Rostek *et al.,* 1997; Schulte *et al.,* 1999; Thamban *et al.,* 2001).

- Numerous studies have been carried out in different regions of Arabian Sea which largely emphasize on the variability of upwelling strength, biological productivity, sedimentation rates using several proxies such as foraminifera, sediment organic carbon, calcium carbonate, stable isotopes, clay minerals, textural analysis, elemental geochemistry, etc (Duplessey, 1982; Karbassi, I989; Nigam and Nair, 1989;Nair *et al.,* l989;Nambiar *et al.,* 1991;Clemens *et al.,* 1991;Manjunatha and Shankar, 1992; Paropkari *et al.,* 1993; Nambiar and Rajagopalan, 1995; Pandarinath *et al.,* 1998; Ganeshram *et al.,* 1999; Somayajulu *et al.,* 1999; Prakash Babu *et al.,* 1999;Naidu and Malmgren, 1999; Rao and Veerayya, 2000; Thamban *et al.,* 2001, 2002; Kessarkar *et al.,* 2003; Agnihotri *et al.,* 2003; Pattan *et al.,* 2003; Niitsuma, 2003; Naidu., 2003; Gupta *et al.,* 2003; Pandarinath *et al.,* 2004).

1.5.2. Continental Record: Stalagmite

Speleothem based paleoclimate reconstruction was initiated by Hendy and Wilson 1968 followed by Thompson *et al.,* 1974 in terms of paleo-temperature estimate from the continents.However, the complex mechanism to interpret temperature from speleothem showed multiple sources of climatic signals (McDermott, 2004).During last two decade, speleothems have been extensively used worldwide for understanding of paleoclimatic changes with better resolution and proper understanding of its environment of deposition favorable for climatic interpretation.

Speleothems (mainly Stalagmites) have been used to infer monsoon from Indian subcontinent and adjacent regions like China, Nepal, Oman, Yemen, Southeast Asia, etc. Several stalagmite based paleoclimate records have been studied but they are still very sparse and require lot more researches for better understanding of Monsoon. The $\delta^{18}O$ signature from stalagmite has been considered as a reliable proxy for rainfall for Indian subcontinent on annual to centennial scale. Several workers (Yadava and Ramesh, 2001, 2005, 2006; Yadava *et al.,* 2004; Sinha *et al.,* 2005, 2007, 2011; Laskar *et al.,* 2011, 2013; Kotlia *et al.,* 2012, 2014; Sanwal *et al.,* 2013, Lone *et al.,* 2014; Kathayat *et al.,* 2016, 2017, 2018; Band *et al.,* 2018; Nikita *et al.,* 2019, etc.) have reported the signatures of monsoonal variability for different time periods using stable oxygen and carbon isotopic records decoded from Indian stalagmites. Studies from the Indian speleothems are very few but the records have provided remarkable climatic signatures in terms of monsoon interpretation. Yadava *et al.,* (2004) started speleothem studies in India with speleothems from Akalagavi Cave, Karnataka and reported several droughts as well as wet events. Yadava and Ramesh (2005) studied speleothems of Gupteshwar cave, Odisha and Dandak cave, Chhattisgarh and inferred ~14 year arid event around 2000 yr BP and a high rainfall event around 600 yrs BP. Sinha *et al.,* (2005) reported a 15.2 to 11.7 ka BP record of monsoon from a speleothem of Timta Cave, Himalaya. They correlated the intensity variations in monsoon with North Atlantic climate changes. Yadava and Ramesh (2006), further, studied speleothems from Gupteshwar cave, Odisha, Dandak cave, Chhattisgarh, Sota cave, Uttar Pradesh, and Akalagavi cave, Karnataka to investigate the causative

mechanisms for the monsoonal variations and their spatial coherence from the isotope signals retrieved from the high resolution speleothem samples. Annually resolved stalagmite from Dandak cave was further studied by Sinha *et al* (2007). Similarly, Berkelhammer *et al.,* (2010), generated sub-annually resolved speleothem oxygen isotope record from Dandak Cave, Chhattisgarh. Kotlia *et al.,* (2012) reported Little Ice Age records from a 400 year old stalagmite from Kumaon Himalaya and correlated it to westerlies. Berkelhammer *et al.* (2012) studied stalagmites from Mawmluh Cave, Meghalaya spanning middle Holocene and related it to Indus valley and Nile river civilizations. Later on, based on the records from Mawmluh cave 4.2 ka event has been marked as the beginning of Meghalayan age in the Geological time scale. Similarly, Kotlia *et al.,* (2014) reported past 4000 year record from a stalagmite of Himalaya and interpreted as combined westerlies and monsoon precipitation sources of rainfall in the area. Laskar *et al.,* (2013) studied speleothem from Andaman and reported asynchronous change of Indian monsoon and global climatic events like MWP and LIA. Lone *et al.,* (2014) have studied a stalagmite from Valmiki cave, Andhra Pradesh and discussed about the monsoon variability during last deglacial. Narayana *et al.,* (2014) have studied a stalagmite from Belum cave, Andhra Pradesh and reported about the divergent trend of Indian and East Asian summer monsoon system. Dutt *et al.* (2015) studied stalagmite of from Mawmluh Cave and revealed monsoon intensity during major climatic events like YD, BA and Heinrich Event. Kotlia *et al.* (2015) studied a stalagmite from Sainji Cave, Himalaya and correlated the results to Harappan/Indus civilization. Stalagmites from Bittoo

Cave and Sahiya Cave, Uttarakhand were studied by Kathayat *et al.* (2016) for the last 280 kyrs and linked Indian summer monsoon and East Asian monsoon. Kotlia *et al.,* (2016) studied stalagmite from Jammu and Kashmir and reported the records of Last Pleistocene-Holocene transition and global events like Older Dryas, Allerød period, and YD. Kotlia *et al.* (2017) have reported stalagmite records from Dharamjali Cave, Pithoragarh, Uttarakhand and inferred about Indian summer and winter monsoon variability during ~4.0 to 1.9 ka BP. Further, Joshi *et al.,* (2017) studied stalagmites from Tityana cave, Uttarakhand and reconstructed Indian summer monsoon variability during 4 to 1.6 ka BP. Band *et al.,* (2018) studied a stalagmite from Kotumsar cave, Chhattisgarh and inferred Indian summer monsoon signatures during mid Holocene. Kaushal *et al.,* (2018) reviewed the status of stalagmite researches in India and examined Indian stalagmite records collated in the Speleothem Isotope Synthesis and AnaLysis version 1 (SISAL_v1) database (http://researchdata.reading.ac.uk/139/). They highlighted the current debates and suggested the most useful time periods (climatic events) and locations for further work using tools such as data-model comparisons, spectral analysis methods, multi-proxy investigations, and monitoring.

Similarly, several stalagmite records from China have been interpreted for Indian and/or Asian monsoon system (Wang *et al.,* 2001; Yuan *et al.,* 2004; Dykoski *et al.,* 2005; Yuan *et al*., 2004; Cai *et al.,* 2006, 2010; Wang *et al.,* 2008; Hu *et al.,* 2008; Dong *et al.,* 2010; Cheng *et al.,* 2012; Jiang *et al.,* 2012; Duan *et al.,* 2014, etc.). Furthermore, Denniston *et al.,* (2000) have studied speleothem from Pokhra

Valley, Nepal and interpreted them for monsoonal behavior of the past the past 2,300 years. Similarly, several workers from Oman and Yemen have also deciphered monsoonal variability from the speleothem records (Neff *et al.,* 2001; Burns *et al.,* 2002; Fleitmann *et al.,* 2003, 2007; Shakun *et al.,* 2007; Yang *et al.,* 2010, etc.). The major outcomes from the stalagmite studies based on different time intervals and different temporal resolutions are summarized below.

- Strong coherence exists between the monsoon variability and solar insolation on decadal to centennial scale.
- Sea surface temperature increase is related to decrease in monsoonal intensity.
- Coupled ocean-atmospheric processes are the driving forces for the modulation of monsoonal intensity.
- ITCZ fluctuations are concurrent with monsoon intensity.
- Monsoonal variability is found to be in-phase linked to northern hemisphere climate change.
- Variations in the intensity of monsoon are also linked to North Atlantic climate with the meridional transport of heat and moisture from the warmest part of the ocean.
- Transition phases along with glacial-interglacial periods are linked to wet and dry phases as inferred from the speleothem records. Several events such as B-A, Heinrich, YD, Bond cycles, 8.2 ka, 4.2 ka, etc., have been precisely revealed from the speleothem records.

1.6. Motivation for the present study

Paleoclimatic researches have revealed many important aspects of earth's climatic changes in the past which include glacial-interglacial phases or stadial-interstadial stages. During the glacial phases, Ice sheets grew to such an enormous size that they depressed the earth's crust under their weight and forced air masses around them. With the growth of ice sheets, distribution and composition of the world's terrestrial and marine ecosystems changed drastically. As ecosystems were altered, the composition of the atmosphere changed repeatedly, with low levels of important greenhouse gases during glacial episodes and higher levels in interglacial periods.

The evidence for these changes has been successfully retrieved from marine and continental records as described in sections 1.5.1 and 1.5.2. Precise climatic signatures for particular time period have been successfully understood with the advanced geochronological methods. It has also helped in understanding the leads and lags in the system to be established and rates of change. Observations from the climatic changes on interannual and inter-decadal timescales over recent time, it can be inferred that important modes of climate variability, such as North Atlantic Oscillation (NAO), have been playing important role in past and they will remain as important agent for future climate changes also. However, the present day climatic studies are not adequate for understanding the changes happened in the past and also to predict the future climatic changes.

With the comprehensive literature review of Indian monsoon reconstruction from various proxies collected from marine and continent give an idea that Indian monsoon mechanism and its dynamics is very complex and has varied truly out of the box of its convenient mode of variability at different time interval. Therefore, it is very important to have its reconstruction at high resolution so that the minute changes and the variability on the cyclic pattern of the monsoon can be understood. Hence, to understand the Indian monsoon variability, foraminifera as marine proxy for the last 46ka and stalagmites as continental proxies presenting monsoonal variability during Bolling-Allerod and Mid-Holocene have been taken for research studies. The major objectives envisaged in the present study are listed below.

1.7. Objectives

The main objectives envisaged are as follows:

- To reconstruct Indian monsoon from the proxy records of foraminifera and speleothems.
- To test and evaluate the proxies particularly for *Globigerina bulloides* and *Orbulina universa* from marine sediment core.
- To identify the abrupt climatic events during Late Quaternary.
- To understand the feedback mechanism of Indian monsoon during Late Quaternary.

Chapter 2

Study Area

Chapter 2

Study Area

2.1 Introduction

The study area covers the Bay of Bengal (BoB) and the two caves from the eastern India - Kailash cave, Kanger valley Chhattisgarh, and Borra Cave, Araku valley, Andhra Pradesh. The marine core has been collected from southwestern BoB, Cauvery Basin off Nagapattinam coast at the continental slope. The stalagmite samples KG-6 from Kailash cave and BRA-3B from Borra cave have been collected (Fig.2.1) for reconstruction of Indian monsoon from marine and continent archives. The Indian monsoon and its intensity have been understood so far as the reflection of variations in inter tropical convergence zone (ITCZ) and currents in Indian Ocean.

2.1.1. ITCZ and Indian Monsoon

ITCZ, also known as Doldrums, is the area of low pressure in the vicinity of Equator where trade winds of Hadley cell converges (Fig.2.2). These trade winds are also called as northeasterly and southeasterly trade winds which are ultimately deflected towards west during convergence. The higher annual mean temperature at the Equator causes it to become a zone of low pressure which causes the trade winds to follow the path from a high pressure to low pressure and deflecting towards west at the convergence zone due to Coriolis Effect. This low pressure at the convergence zone in the vicinity of Equator causes intensive cloud formation and subsequent rainfall and frequent cyclones.

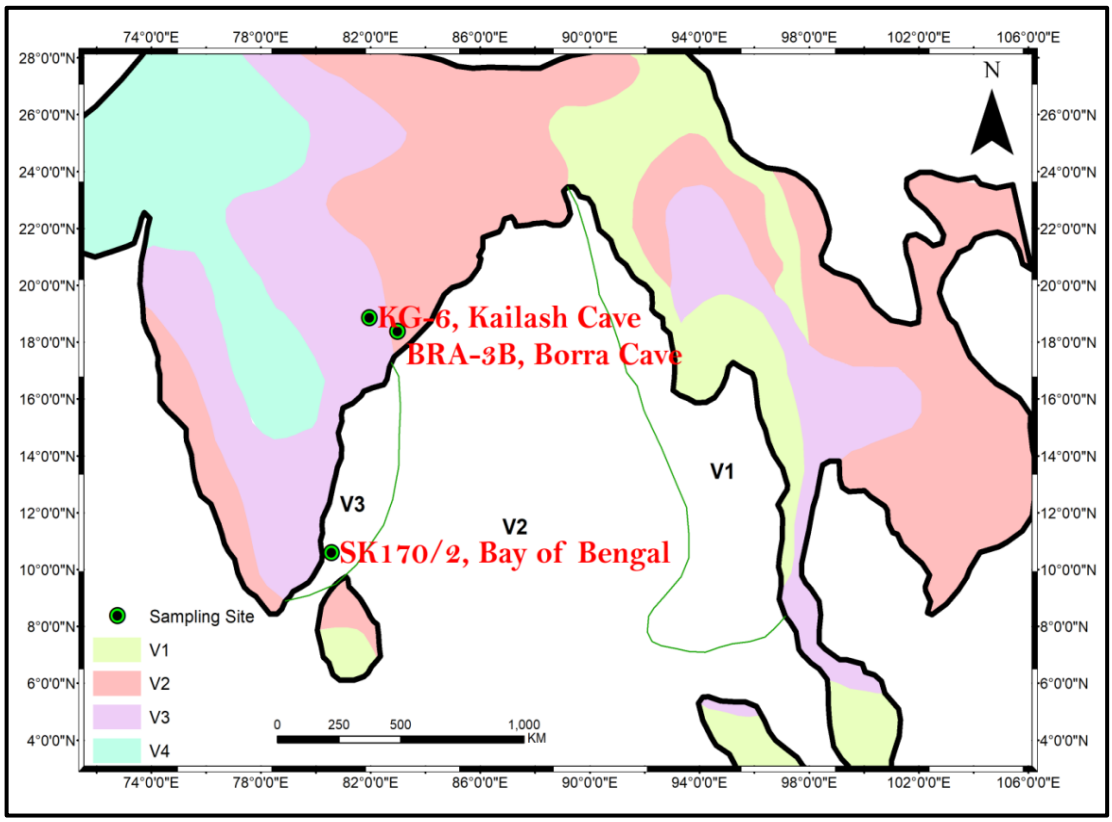

Figure 2.1. Sample Locations. Gravity core SK-170/2 (340 cm long; Latitude: 10.543°N, Longitude: 80.2921°E; water depth of 1000 m) was collected from Southwestern Bay of Bengal during October, 2001 Sagar Kanya cruise. Stalagmite samples were collected from Kailash Cave (KG-6), Kanger valley, Chhattisgarh and Borra Cave (BRA-3B), Araku valley, Andhra Pradesh. Figure shows the climate classification of the area where V1 is Tropical rainy climate, V2 corresponds to Tropical humid summer climate with humid winter, V3 is grouped under Wet and dry tropical climate and V4 as Tropical dry climate with humid winter (Redrawn after Landsberg *et al,* 1966).

As the Earth is tilted at an angle of 23.5˚, the Tropics of Cancer (23.5˚N) and Tropics of Capricorn (23.5˚S) receive the maximum solar insolation during equinoxes and solstices respectively. Hence, Tropics of Cancer and Capricorn act as vertical Equator during equinoxes and solstices respectively. This results in shift of convergence zone of the trade winds between the latitudes of Tropics of Cancer and Capricorn known as the variability in ITCZ. It has been observed that ITCZ shifts

between 25˚N in July to 20˚S in January. Relatively higher latitudinal shifts in Northern Hemisphere (NH) are because of larger continental exposure in NH. This can also be manifested as the ITCZ shifts in the continents are higher when compared to oceanic region.

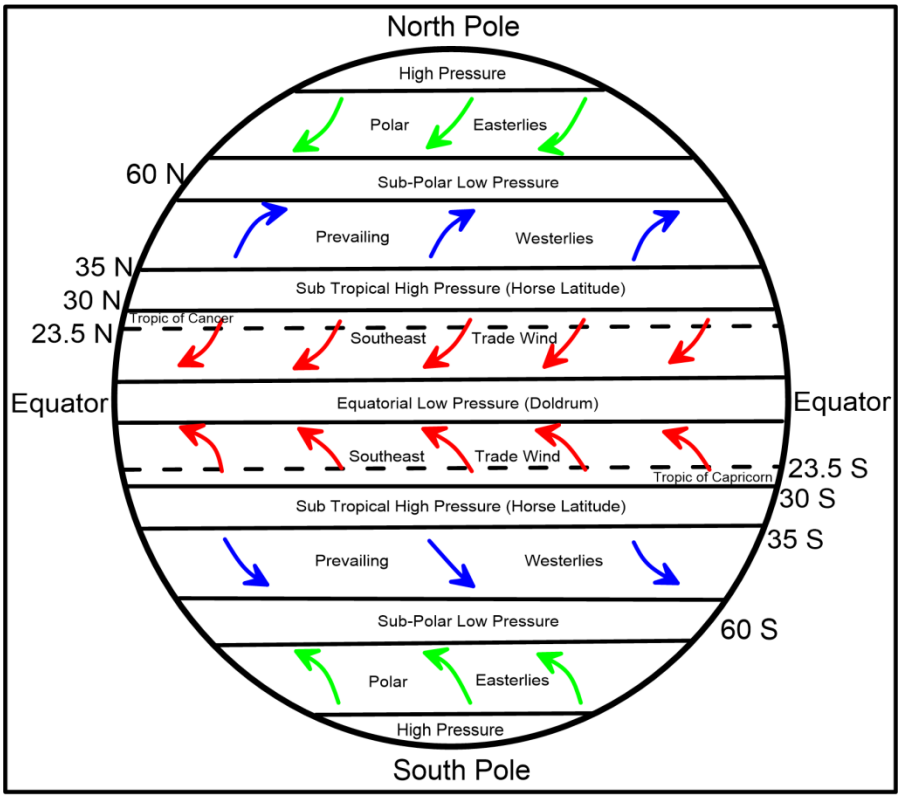

Fig.2.2. Major Global winds and Pressure distribution

The ITCZ shifts in the Indian Ocean region and Indian subcontinent reaches upto 25˚N in the Northern India resulting in the formation very low pressure zone over Indian subcontinent. This causes the winds to move towards low pressure zone during summer which persist till September. On the contrary, wind reversal is observed during winter when the ITCZ shifts towards Tropics of Capricorn. The formation of very low pressure zone over the Indian subcontinent is due to the fact

that the peninsular India comprises hard rocks and the northern part mostly comprises of Indo-Gangetic plain. These materials have low specific heat capacity such that they become hotter as when the solar insolation intensity increases causing a very low pressure over the Indian subcontinent which attracts the monsoon winds towards Indian subcontinent. Thus, the solar induced ITCZ convergence play a vital role in the variability of Indian Monsoon winds. However, the thick saline water of Indian Ocean (IO) also controls the mechanism of Monsoon modulations through various oceanic currents. The oceanography of IO is briefly described following in section 2.1.2.

2.1.2. Indian Ocean

Indian Ocean (IO) is surrounded by Indian subcontinent in the north and Antarctica in the south. Similarly, Africa and Madagascar on the western boundary whereas Australia, Indonesia, Sumatra and adjacent landmasses on the eastern boundary, respectively surround the IO. The IO south of the equator is called as Southern Indian Ocean (SIO) and the IO north of the equator is called as Northern Indian Ocean (NIO). Figures 2.3 and 2.4 illustrate the ocean currents of IO during the summer and winter monsoon respectively. The South Equatorial currents (SEC) and East Antarctica Circumpolar currents (EACC) supply northward Somali Currents during Summer Monsoon. Having crossed the Equator, part of the low-latitude Somali Current shift towards offshore near 4˚N causing upwelling and part re-circulates across the equator forming a gyre called as Southern Gyre whereas another gyre is formed in the North known as Great Whirl. Furthermore, a third gyre is formed northeast of Socotra known as Socotra Eddies.

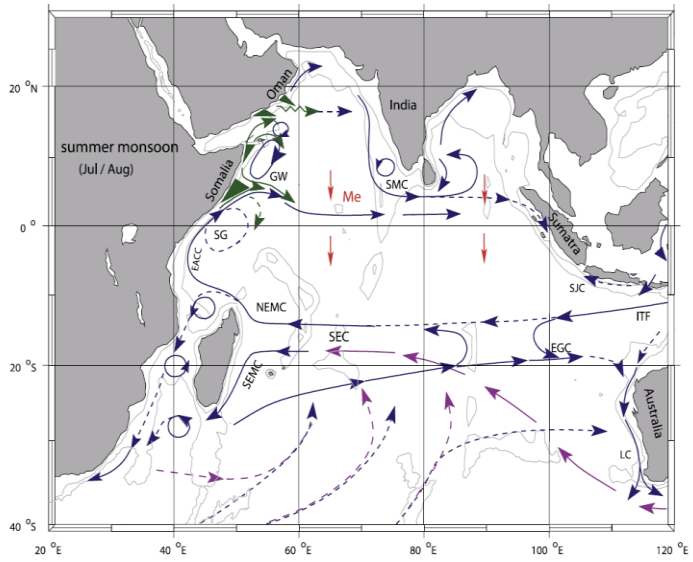

Fig. 2.3. Figure shows the oceanic currents in the IO during summer or southwest monsoon. The depth contours of 1000 and 3000m are shown in grey colours. SEC: South Equatorial Current; SECC: South Equatorial Counter Current. SMC: Southwest Monsoon Current; SEMC: South East Madagascar Current; NEMC: North East Madagascar Current; SC: Somali Current; SG: Somali Gyre; GW: Great Whirl; SJC: South Java Current; EGC: East Gyral Current; LC: Leeuwin current; ITF: Indonesian Trough Flow; Me: Meridional Ekman Transport. (Ref. McCreary *et al.,* 1993).

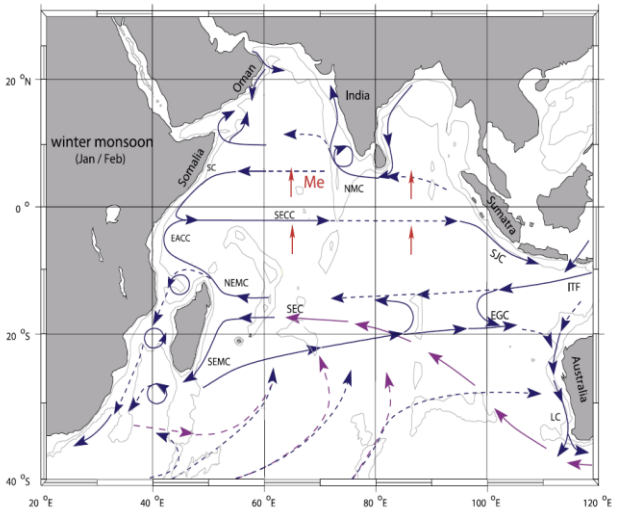

Fig. 2.4. Figure shows the oceanic currents in the IO during winter or northeast monsoon. The depth contours of 1000 and 3000 m are shown in grey colours. SEC: South Equatorial Current; SECC: South Equatorial Counter Current. SMC: Southwest Monsoon Current; SEMC: South East Madagascar Current; NEMC: North East Madagascar Current; SC: Somali Current; SG: Somali Gyre; GW: Great Whirl; SJC: South Java Current; EGC: East Gyral Current; LC: Leeuwin current; ITF: Indonesian Trough Flow; Me: Meridional Ekman Transport. (Ref. McCreary *et al.,* 1993)

The occurrence of strong eastward surface jets during the inter-monsoon periods; commonly referred to as Wyrtki Jets (WJs) are unique to the IO, owing their existence to the semiannual westerly equatorial winds. These WJs carry warm upper layer waters towards east which increases sea level and mixed layer thickness in the east and decrease in the west. The lack of sustained equatorial easterlies causes Eastward Equatorial Undercurrent (EUC) to exist only during February to June when the winds have an easterly component. The EUC can appear in other seasons as well but only when anomalous easterlies occur (Reppin *et al.,* 1999). The IO lacks sustained equatorial easterlies which results its primary upwelling regions off-equatorial regions where the thermocline is shallow and along the coasts of Somalia and Oman, near the tip of Peninsular India, and along the 5-10˚S thermocline ridge. The upwelling drives the ascending branches of the IO's primary shallow overturning circulations, namely, the CEC and the southern STC. Southwest and northeast monsoon winds are directed meridionally and against the Ekman transports at the Equator. This causes small near-surface equatorial overturning cell knowns as the equatorial roll (Miyama et al., 2003). This equatorial roll is confined totally to the surface-mixed layer and hence does not impact the oceanic heat budget or climate. Weak upwelling are also observed along eastern IO i.e. off Sumatra/Java and northwest Australia in the Arafura Sea (Godfrey and Mansbridge, 2000; Du *et al.,* 2005).

Further, the IO is connected to the global circulation through the Indonesian passages and its open southern boundary known as Indonesian Through Flow (ITF). The ITF transports North Pacific waters from the Mindanao Current (Gordon, 2005) into the IO within the upper ocean (<400 m). The ITF transport also has a subsurface

core at intermediate depths, most of which comes from the South Pacific (McCreary *et al.,* 2007).

The northern IO is comprised of main water bodies of Arabian Sea (AS), Bay of Bengal (BoB) and Andaman Sea (AnS). Northward (southward) precipitation trends over IO show a general migration during the boreal summer (winter). While, strong wintertime cooling in the northern AS is observed due to latent heat loss caused by cool and dry air, a strong cooling during summer in the western Arabian Sea is observed as a result of upwelling near the Somali and Oman coasts.

The summer monsoon winds following the low pressure converge towards the peninsular part and split into two parts such that one part follows the eastern AS and the other follows the western BoB. The winds cause rainfall across the country during southwest monsoon. A brief description of physiography and currents in BoB is given in section 2.2.

2.2. Bay of Bengal

BoB is the northeastern component of IO. The BoB marks a complex hydrographic setting as it receives a huge amount of fresh water and sediments by number of river systems. This river borne influx greatly influences the spatial extent of the physical, chemical and biological properties of BoB. Except a few (Indus, Narmada, Tapti, etc. into Arabian Sea), major rivers (viz. Ganga, Brahmaputra, Mahanadi, Godavari, Krishna, Cauvery, etc.) of India, and (Irrawaddy, Salween, Meghna, etc.) of adjacent countries debouch into Bay of Bengal (BoB) with a total water flux of 2.95×10^{12} m^3/year (Sijinkumar *et al.,* 2016; Silva *et al.,* 2017). Annual

rainfall over BoB varies between ~1m off the east coast of India to about 3m over the Andaman Islands.

2.2.1 Physiography

Major physiographic of BoB is Bengal submarine mega-fan which is one of the largest deep sea fans in the world's ocean and covers an area of ~3.0 x 10^6 sq. km with length of ~3000 km and maximum width of 1430 km with sediment thickness of 20 km. The bathymetry of the BoB sows shallow depth of ~1000 m which gradually increases up to ~4000 m at the southern tip of the Sri Lanka in the west and Ninety degree East Ridge in the eastern flank.

2.2.2. Salinity and SST

The sea surface temperature (SST), in the study area, varies from 27.5˚C to 29˚Cand 26.5˚C to 28.5˚Cduring SWM and NEM seasons respectively (Fig. 2.4), and sea surface salinity(SSS; Fig. 2.5)varies from~34.0psu during SWM to 32 psu during NEM (Narvekar and Prasanna Kumar, 2014).During SW monsoon high precipitation in the Bay of Bengal and more fresh water discharge from Ganges, Brahmaputra, Irrawaddy and Godavari forms a north-south salinity gradient in the Bay of Bengal, ranging from 26 to 34 psu (Levitus *et al.,* 1994).More evaporation and less river discharge and precipitation during NE monsoon increase the salinity of Bay of Bengal. During NE monsoon low salinity surface water of Bay of Bengal moves westward of the South Equatorial Current.

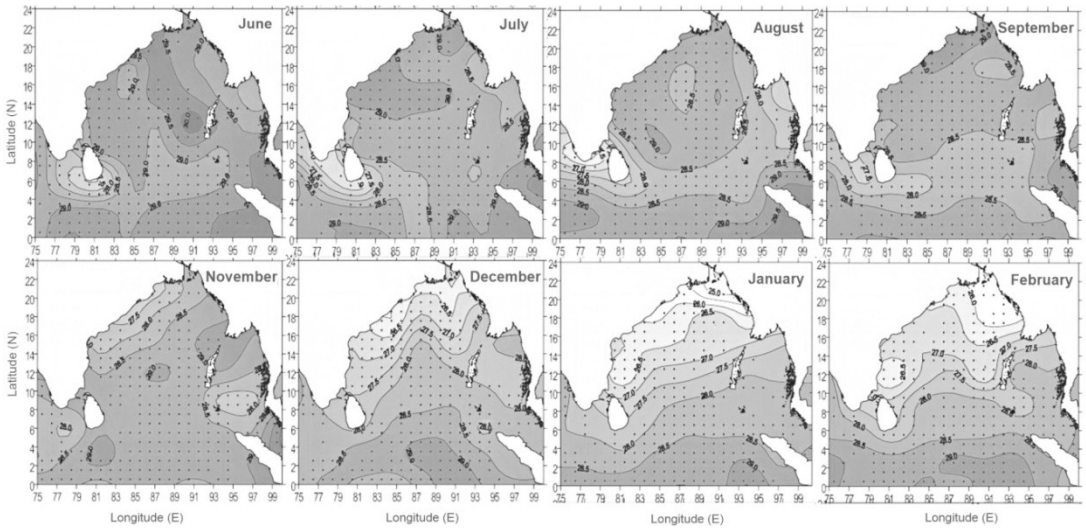

Figure 2.5. Sea Surface Temperature. The sea surface temperature (SST)at the core location varies from 27.5˚C to 29˚C and 26.5˚C to 28.5˚C during SWM and NEM time respectively (modified after Narvekar and Prasanna Kumar, 2014).

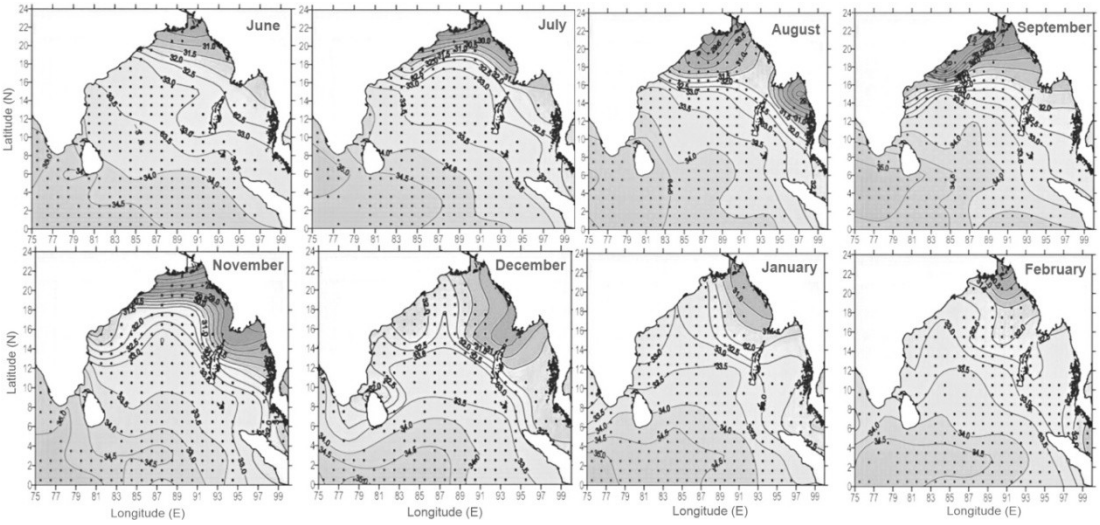

Figure 2.6. Sea Surface Salinity (SSS).SSS remains constant to ~34.0 psu during SWM and a lower value between 32.0 to 34.0 psu is noted during NEM at the core location. (modified after Narvekar and Prasanna Kumar, 2014).

2.2.3. BoB ocean current dynamics

The ocean dynamics of Bay of Bengal is observed to be very complex in terms of, massive freshwater influx, seasonal reversal of circulation (Martin *et al.,* 1981), eddies (Gopalan *et al.,* 2000) and planetary waves (McCreary *et al.,* 1993) which ultimately control the wind forcing, monsoon dynamics, cyclones, etc. over the

region. McCreary *et al.* (1993) carried out simulations and showed that the wind forcing act as a major mechanism of circulation in the coastal Bay of Bengal within the Bay throughout the year. It is also observed that during monsoon the circulation in BoB is not only driven by local winds but also by the Gyral circulation due to planetary waves. Numerous studies (Potemra *et al.,* 1991; Yu *et al.,* 1991; McCreary *et al.,* 1993; Sengupta *et al.,* 2001) have also shown that planetary waves act as dominant constituent in the ocean dynamics of BoB.

During April – May, abrupt change in the wind direction is observed in the equatorial region which results in upper ocean changes in terms of thermocline depression and rise in ocean surface propagating towards east long the equator as downwelling Kelvin wave (McCreary *et al.,* 1993). Having hot at the Sumatra coast, Kelvin wave split into two coastal Kelvin waves that is one towards north and another towards south. The northward coastal Kelvin wave propagates along the rim of BoB (Potemra *et al.,* 1991) and radiates Rossby waves with the same frequency. The radiating Rossby waves propagate towards west which results as the currents in the interior of the ocean and also in the western coast of BoB (McCreary *et al.,* 1996; Shetye *et al.,* 1996)

2.2.4. Climate

Longitudinally, the climate of BoB (Fig. 2.1) has been classified into three segments as V1, V2, and V3, by Landsberg *et al.* (1996). The V1 segment is observed to be of tropical rainy climate whereas the central segment of V2 is observed to have tropical humid summer and winter climate. Wet and dry tropical climate is observed at the western segment classified as V3. Althouh the northern and central portion of

western coast of BoB receives its major rain influx during southwest monsoon; the southern portion receives its major rainfall during northeast monsoon.

2.3. Carbonate rock distribution over Indian subcontinent

Carbonate rocks cover around 20 % of the world's continents and covers nearly for nearly 17 % of the world's settlement. About 3 % of India's total land surface is covered by carbonate rocks which are observed to be mostly karstified and are significant source of groundwater. Carbonates in India are either directly exposed at the surface or buried in geological Stratigraphy ranging from Precambrian to Tertiary periods mostly of limestone and dolomite composition (Fig. 2.8). The carbonate rock distribution in the country is tabulated below.

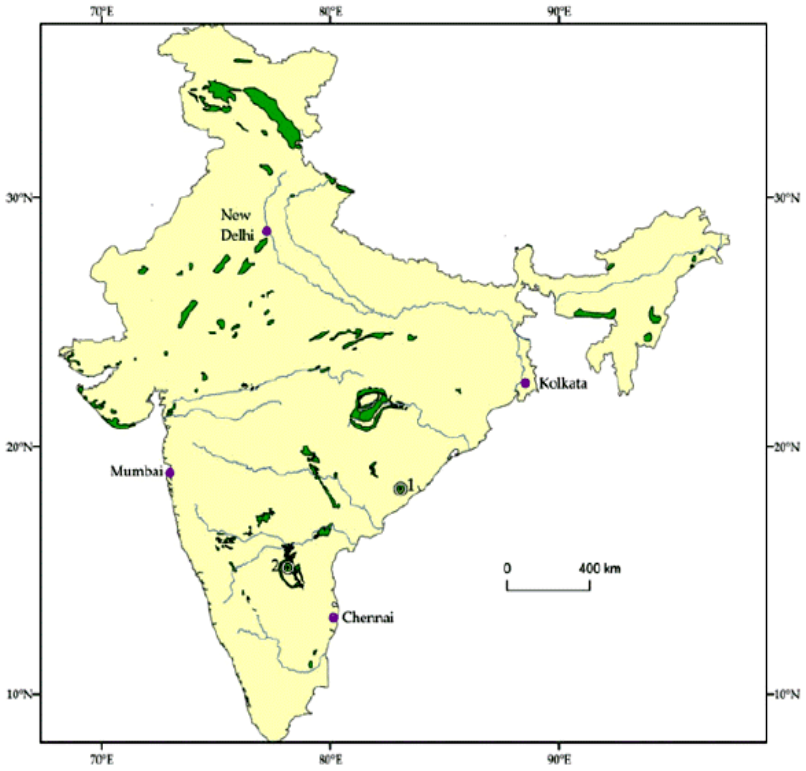

Fig. 2.8. Carbonate Distribution in India. Figure shows green coloured carbonate deposits over Indian territory (Narayana *et al.,* 2014).

Table 2.1. Carbonate rocks in Indian lithostratigraphy. Abbreviations: SG super group; Gr group; Fm formation; Ls limestone; Do dolomite. (Ref. Wadia 1939; Adyalkar 1977; Murty 1988; GSI 1997; Kumar 1985; Dar *et al.,* 2014)

Lithology	Formation	Group/Supergroup	Age	
Oolitic Lst	Miliolitic Lst (Gujarat)		Pleistocene	Cenozoic
Buff Lst	Nari and Gaj Fmn (Kutch)		Miocene-Oligocene	
Limestone	Baripada Beds (Odisha)			
Nummuitic Lst and shales	Subathu Series		Eocene	
Limestones	Ranikot and chharat Lst			
Limestone	Kopili and sylhet Lst			
Foraminiferal Lst	Kirthar Lst			
Nummulitic Lst	Ranikot Lst			
Nummulitic Lst	Lst (Pondicherry)		Palaeocene	
Fossiliferrous Lst	Chikkim Lst (Spiti)		Cretaceous	Mesozoic
Limestone	Kiogar Lst			
Sandy Limestone	Landpar Stage			
Coral Limestone	Bagh Beds			
Fossiliferrous Limestone	Turuvai and kalakadu Lst			
Oolitic Limestone	Niniyur Stage			
Shelly Limestone	Trichinopoly Stage			
Limestone and coral	Uttatur Stage			
Fossiliferrous Limestone	Mt. Everest Lst		Jurrassic	
Limestones	Kalhan Lst			
Limestone	Lilang Group Daonella			
Dolomite	Jaisalmer Lst			
Unfossiliferrous Lst	Kioto Lst			
Shelly Lst	Patcham Fmn.		Triassic	
Limestone and Dolomite	Other Himalayan Lst		Permian	Paleozoic
Limestone, Shale	Zewan Fmn			
Fossiliferrous Lst	Productus Lst			
Limestone	Lipak Beds		Carboniferrous	
Grey Limestone	Syringothyris Lst			
Limestone, Shale	Hapthanar Gr.		Silurian	

Limestone	Dhaulagiri and Nilgiri Lst		Ordovician	
Micritic Oolitic stromatolitic Lst	Rewa and Bhander Lst	Upper Vindhyan Gr	Upper Purana (Protorozoic)	Prote--rozoic
Massive and Flaggy Lst	Koikuntla Lst	Kurnool Grp		
Massive and Flaggy Lst	Narji Lst			
Limestone	Shahabad Lst	Bhima Grp		
Stromatolitic Lst	Katamdevari Lst			
Flaggy Dolomitic Lst	Kanger Lst	Indravati Grp.		
Dolomite	Jagdalpur Lst			
Dolomite	Hiri Dolomite	Chhattisgarh SG		
Stromatolitic Lst	Chandi Lst			
Limestone and Dolomite bands	Charmurial Lst			
Limestone and other rocks	Chatrela Fmn.			
Dolomite and marble	Saussar Series	Dongargarh SG		
Limestone	Nimbahara Lst	Lr. Vindhyan SG	Lower Purana (Proterozoic)	
Limestone	Kuteshwar Lst			
Stromatolitic dolomitic Lst	Fawn and Rohtas Lst			
Limestone and Shale	Kajrahat Lst			
Dolomite	Vempalle fmn	Cuddapah SG		
Dolomitic Lst	Chanda Lst			

2.4. Kailash Cave

2.4.1. Cave location and stalagmite sampling

The Kailash cave (18.8445°N; 81.9915°E, Fig. 2.1) is located ~40 km south of Jagdalpur, Chhattisgarh, India, atop a carbonate hill ~40 m above the ground in a thickly forested area of the Kanger National Park. Climatically, the area is tropical sub-humid, meso-thermal with dry winter. The main hall of the cave follows the shallow dip of the carbonate host rock with a steep slope.

Fig. 2.9. Kailash cave. Entrance of the Kailash cave and interior gallery showing various types of secondary carbonate deposits: stalagmite, stalactite, flowstone, etc.

2.4.2. Climate

Climatically, the area (Fig 2.1) is tropical sub-humid, meso-thermal with dry winter that is wet and dry topical climate. About 90% of the rainfall occurs from June to October with an average annual rainfall of 1200mm (Fig. 2.10). May is the hottest month when the daily maximum temperature varies from 38 °C to 40 °C, while December and January are the coldest months, with the daily maximum temperature varying from 14 °C to 28 °C (Fig. 2.10). Due to the intense rainfall, around 60% of the area is thickly forested with an uneven forest cover.Based on Thornthawaite's classification (1931),the region falls under CA'*w* (tropical sub-humid with rainfall deficient in winter) typeof climate, and based on Koppen classification the region can be classified as A*w* (Tropical wet and dry climate) and C*wg* (humid mesothermal warm climate with dry winter) types.

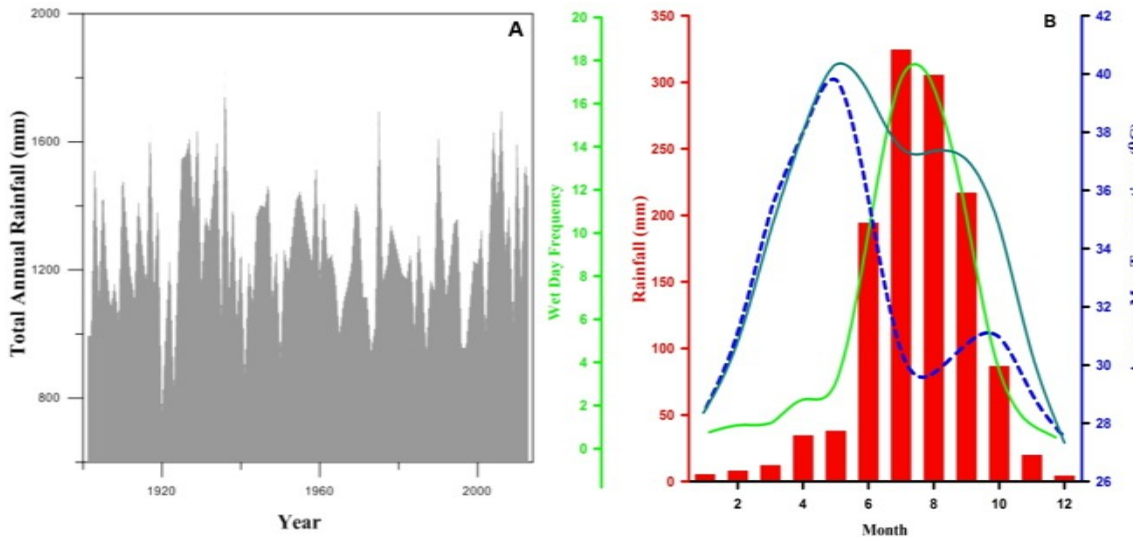

Fig. 2.10. Climate at Kailash cave. Climatic Research Unit (CRU, https://crudata.uea.ac.uk/cru/data/hrg/cru_ts_3.23/) and Indian Meteorological Data (IMD) data for total annual rainfall (mm) from 1900to 2014 at the cave location; B monthly average rainfall (red, mm), average maximum (blue dotted spline) and average minimum (dark cyan spline) temperatures (°C), and wet day frequency (green).

2.4.3. Geology

The Kailash cave lies in the Indrāvati Basin, resting over Bastar craton, falls in the core of Chhattisgarh hills and plateau (Fig. 2.1). The Indrāvati basin is characterized by late Proterozoic un-metamorphosed and unfossiliferous-sandstone-shale-limestone and stromatolitic dolomite rock types (Fig. 2.11). The sedimentary sequence rests non-conformably on the Archaean Granitic Complex. Kailash Cave is located in the Kanger Limestone Formation which is underlain by Cherakur Formation. The Kanger Limestone is hard and compact and breaks with conchoidal fracture and varies in colour from grayish grey to dark grey in which upper part of the formation is observed to be argillaceous. Major fault of Sirisguda has been considered as the main reason for abrupt change in the thickness and disposition of the limestone which passes through the north of the cave and results in small sympathetic parallel faults development which essentially have affected the

disposition of lithounits and created variance in characters and qualities. Northwest-southeast trending faults are also present in the vicinity of Kailash cave as shown in the figure 2.11. The area is covered by the red loamy and red sandy soils derived mainly from Archaean granites and gneisses. Gabhar (very fertile clayey soil), Tikra (Coarser than Gabhar and less fertile), Mal (coarse sandy and gravely soil), Marhan, and Bari (used in gardens; fertile) are the common local soil types in parts of the Bastar Plateau. The basalts and laterite formations in the region are covered with teak forests, which fall under 'Sal' forests. Indrāvati and Sabari, two tributaries of Godavari River, drain the area, while Indrāvati River flows from west to east and after travelling for a long distance it takes an abrupt turn towards south and joins the Godavari River. The Indrāvati Plain lies on the northeast Bastar Plateau (Dutt, 1963), which is situated at an altitude of 400-600 m, while the southern Bastar plateau is situated at 150-1000 m elevation.

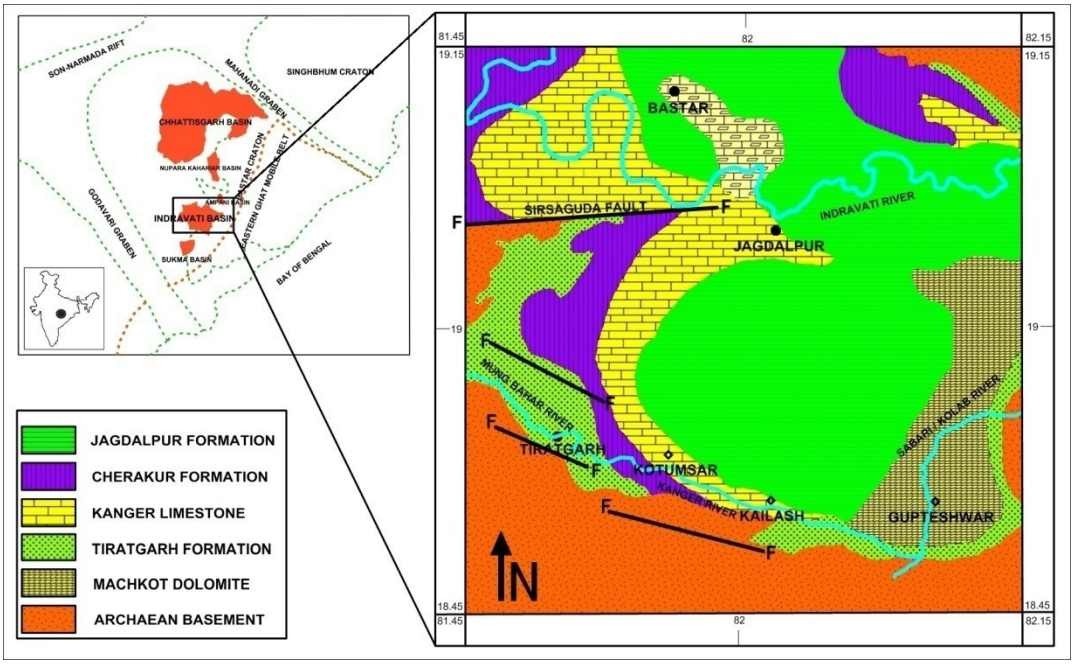

Fig.2.11. Geology around Kailash Cave. Figure shows the geology of the Kailash cave, Kanger valley of Proterozoic Indrāvati basin.

2.5. Borra Cave

2.5.1. Cave location and stalagmite sampling

Borra cave located (18.2807° N, 83.0397° E, Fig. 2.1) in the thickly forested Ananthagiri Hills of the Araku Valley in the Eastern Ghats, and about 90kms from Vishakhapatnam. The total length of the Borra Cave runs about 825 m, of which a distance of 200 m can be easily trekked. The entrance of the cave is at ~705 m above mean sea level (amsl). The deepest point of the cave is ~80 m below the entrance level. The main entrance of the cave is 35 m wide and 40 m deep, but the width of the main chamber is ~15 m. A narrow gallery of 150 m long is connected to the main chamber. A parallel chamber, from the central part of the cave, of 50 m wide and 10 m deep runs for a distance of 75 m. It is observed that this chamber is connected to a stream at the deeper levels. The interior of the cave distinctly exhibits a variety of impressive speleothems of various sizes and irregularly shaped stalactites and stalagmites. The stalactites range in length from ~0.1 to 3.5 m. The stalagmites are around 1.2 m long with columns of 6 m long and 0.75 m wide (Narayana, 2014). The Borra Cave is an important tourist spot with about half a million visitors annually, and has religious, historical, archaeological and economic importance. The stalagmite sample BRA-3B was collected in December 2015 from the deep interior narrow gallery of the cave located ~300 m south from the entrance of the cave.

Fig.2.12. Borra cave. Figure shows the entrance of the Borra cave and the various secondary carbonate deposits inside the cave.

2.5.2. Climate

Climatically, the Borra cave area falls under tropical humid summer climate with humid winter or V2 group (Fig. 2.1) as described by Landsberg *et al.,* (1995). The area experiences moderate humid climate and receives majority rainfall during summer monsoon (Fig. 2.13) with an average annual rainfall of 1800 mm (Fig. 2.13) with maximum wet day frequency of 12 days. The average maximum temperature and minimum temperature (Fig. 2.13) is observed to be 37˚C and 26˚C respectively. However, during peak summer the temperature raises anomalously upto 45˚C for some days with the enforcement of humidity in the area. During winter, the maximum and minimum temperatures (Fig.2.13) of the study area are recorded to be 25˚C and 10˚C respectively. The humidity in the cave site is recorded as 92% and air temperature 21±2˚C.

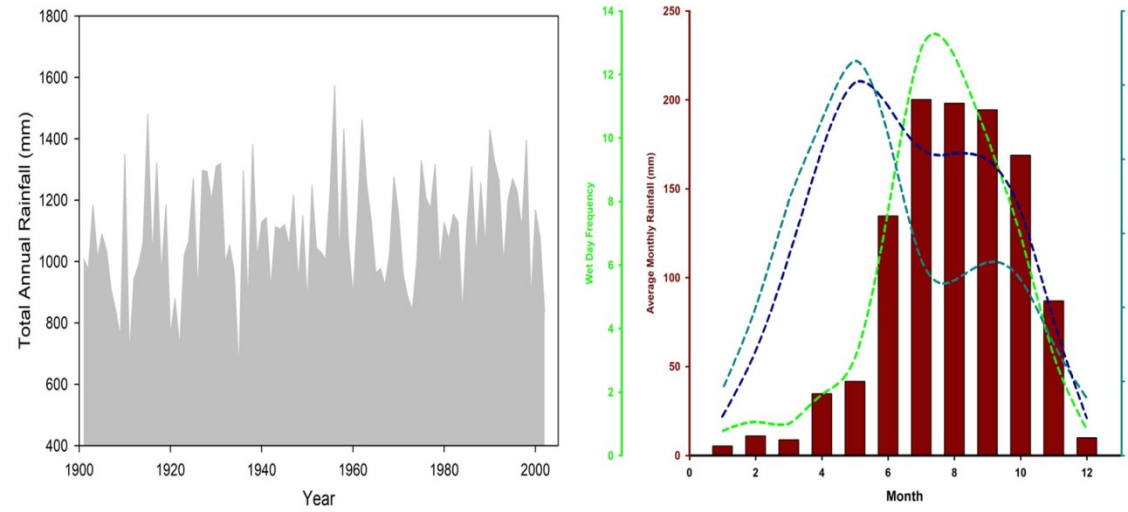

Fig. 2.13. Climate at Borra Cave. Figure show the Climatic Research Unit (CRU, https://crudata.uea.ac.uk/cru/data/hrg/cru_ts_3.23/) and IMD (Indian Meteorological Department) data for total annual rainfall (mm) at the cave location where average monthly rainfall (red, mm), average maximum (cyan dotted spline) and average minimum (blue dotted spline) temperatures (°C), and wet day frequency (green dotted spline) are also illustrated.

2.5.3. Geology

The Borra cave is developed in Proterozoic carbonate rocks of Eastern Ghat Granulite Mobile Belt, characterized by khondalite suite of Archean Age of Ananthagiri Hills of Araku valley. The evidence of active karstification inside the cave is provided by variety of speleothems such as dripstones (stalactites, stalagmites and pillars) and flow stones. The geology of this region is comprised of garnetiferrous sillimanite gneisses, quarto-feldsphathic garnet gneisses of Khondalites of Archean age followed by charnockite representing granulite facies metamorphism. The repetition of the khondalite and charnockite rock types in the Eastern Ghats is due to the tight isoclinals folds present in the mobile belt. At the cave location anticlinal fold is present which belong to doubly plunging anticline around Anantgiri. The calcite marbles frequently occur as minor patches and bands, and are interbedded with the Garnet-sillimanite gneisses. The major calcite marble unit, in an extensive scale, is

exposed around Borra and bordered by calc-granulite and diopsidities. The ubiquitous occurrence of garnet-sillimanite gneisses as layers and lenses within the marbles and vice versa indicate that these litho-units are gradational and confirm the metasedimentaries. The calcite marbles are observed to be devoid of impurities confined to the inner zone in the carbonate rocks which also show signs of migmatization in the mode of rhythmic bands of dolomites and calcites. Deformed and banded marbles extend over a triangular area of 2 sq. km at the Borra cave location.

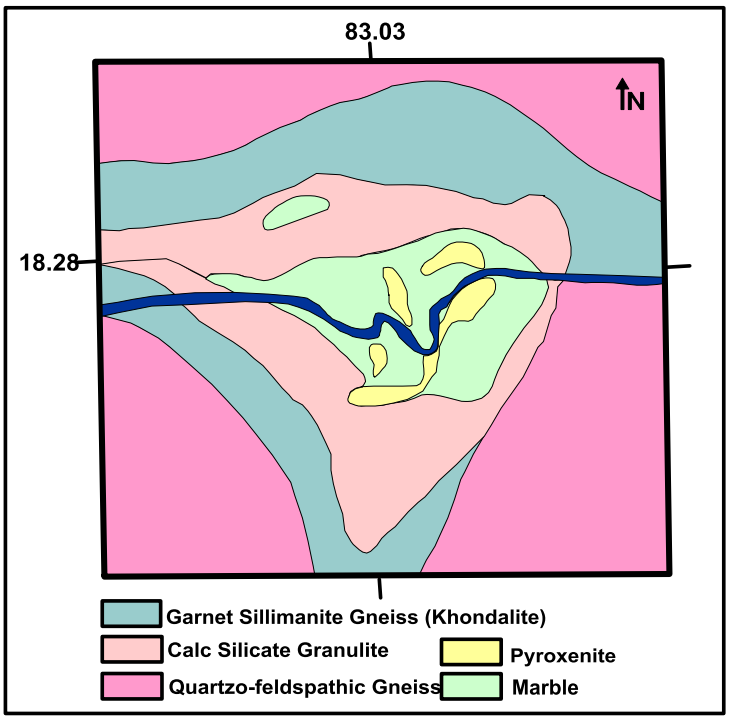

Fig. 2.14. Geology around Borra Cave. Figure shows the geological map around Borra cave. Borra cave is formed in deformed and banded marbles surrounded by diopside-scapolite-feldspar calc granulites (Redrawn after Baskar *et al.,* 2007).

Chapter 3

Material and Methods

Chapter 3

Materials and Methods

3.1. Introduction

In order to decipher the paleomonsoon, two main aspects are essential - one is the proxy and the other is chronology. The proxies can be from both marine and continental archives viz. marine sediments and cave deposits, where the compositions of the proxies are mostly of calcium carbonate. Further, chronological methods like Radiocarbon and/or U-Th series ages can be used to fit the proxy records in a time frame. Superimposed on the archives, proxy methods like carbon and oxygen stable isotopes and their variability in space and time help in reconstructing the monsoons of past. This chapter describes about the materials (section 3.2) used in reconstructing the Late Quaternary monsoon from marine and continental archives. Mineralogy (section 3.3) of stalagmites, essential for their U-Th age estimation (section 3.4), has been elucidated. Further, procedures of stable isotope analyses followed are explained (section 3.5), and their statistical analyses (section 3.6). Climate data (section 3.7) have been analyzed for paleoceanographic interpretation. GNIP data analyses are presented in section 3.8.

3.2. Samples and Sampling Procedures

In order to reconstruct paleomonsoon from marine proxies, foraminifera from a marine core from southwestern BoB (Fig.2.1) was collected whereas continental proxies that are stalagmites were collected from Kailash Cave, Kanger valley, Chhattisgarh (Fig. 2.1) and Borra Cave, Araku valley, Andhra Pradesh (Fig. 2.1). Detailed information about the sample location and sampling procedure is described below.

3.2.1. Marine Core Sediment

A 340 cm long gravity core SK 170/2 located at Latitude: 10.54°N and Longitude: 80.29°E (off Nagapattinam coast) from a water depth of 1000 m was collected by A C Narayana and his team in the month of October 2001 onboard Sagar Kanya during its cruise number 170. The core comprises of homogeneous sediments having earthy-pale brownish (0-80 cm); greenish brown (80-150cm); olive grey (150-200), and pale khaki grey (200-340) sediments. The sediment core was further sub-sampled at 2 cm intervals from 0 to 100 cm and remaining downcore part (100-340 cm) of the core at 4 cm intervals. Subsamples were soaked in water overnight and washed through 150 μm sieve. The retained fractions were collected on a filter paper and dried at 50°C in an oven.

Sub-sampling and Foraminifera separation

The dried samples were then taken for microscopic examination and identification of species. Planktonic species *Globigerina bulloides* and *Orbulina universa* of test sizes 200-250 μm and 300-350 μm, respectively were handpicked

under the stereo zoom microscope for isotopic measurements at Sedimentology lab, Centre for Earth, Ocean and Atmospheric Sciences, University of Hyderabad.

3.2.2. Stalagmites

Kailash Cave. Stalagmite sample KG-6, ~430 mm long, with an average diameter of ~100 mm was collected in May, 2014 from a ~250 m long Kailash Cave (18.8445°N; 81.9915°E) located in interior eastern India at about40 km south of Jagdalpur, Chhattisgarh, atop a carbonate hill ~40 m above the ground in a thickly forested area of the Kanger National Park. Kailash Cave (Fig. 2.1) with only one narrow entrance at the top where the lateral extent of the main hall is around 200 m long and ~20 m wide along with 5-10 m wide chambers (Fig. 2.9). Geometry of the cave follows shallow dip of the carbonate host rock with a steep slope. One can reach the hall, around 10 meters below the entrance, with the help of iron ladder and steeper down slope concrete ramp constructed by Chhattisgarh Tourism Department. Fringe zone is covered with spectacular multidimensional saw-tooth and curtain structures of secondary deposits along with sparkling whitish straws and flowstones. Stalactites, flowstones, terraced and isolated stalagmites and pillars can be seen in plenty while walking through the hall of the cave. The stalagmite (KG-6) was located on the ground ~200 m away from the entrance of the cave.

Fig. 3.1. Stalagmite Cutting. Stalagmites were cut into two equal halves and sliced for U-Th age estimations and stable isotopic analyses using Dramet cutting machine at PRL, Ahmedabad.

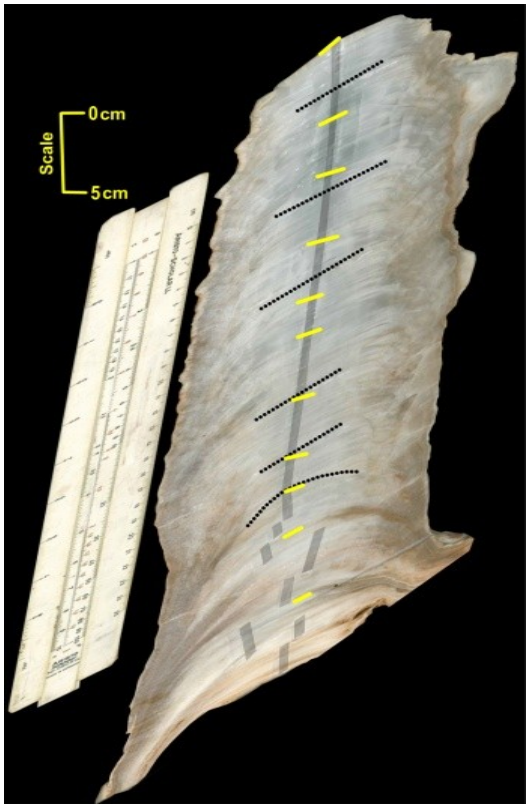

Fig. 3.2. Stalagmite Slicing for sub-sampling. Slice of KG-6 stalagmite with showing sum-sampling along growth layers (grey). Yellow points are U-Th age points and black dotted lines are selected growth layers for Hendy's Test.

Fig. 3.3. Micromilling. Sub-samples of stalagmites KG-6 and BRA-3B were drilled using an automated New Wave Research Micro-mill at PRL, Ahmedabad.

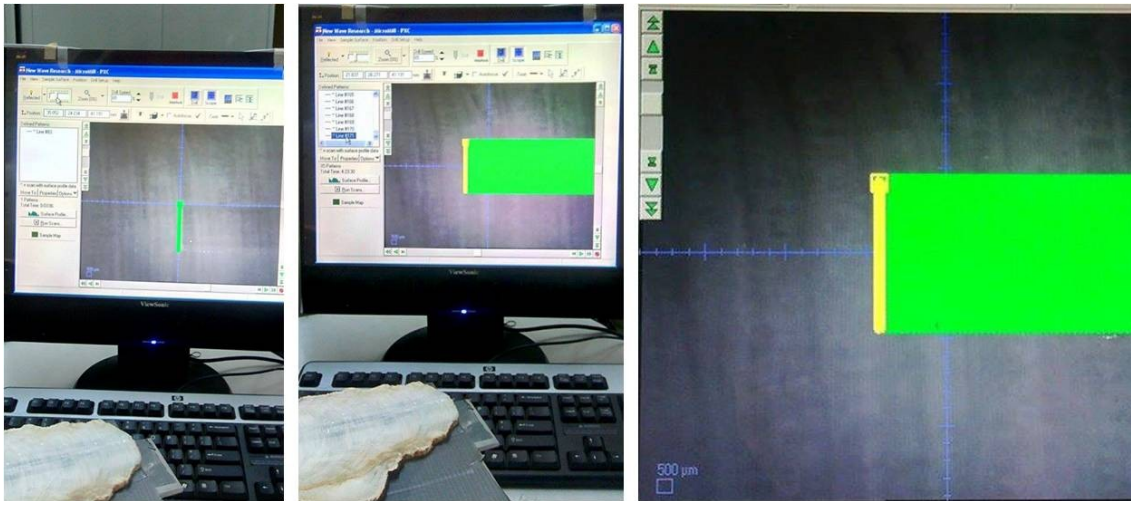

Fig. 3.4. Micromilling profile. Growth layer profiling for micromilling using an automated New Wave Research Micro-mill at PRL, Ahmedabad.

Borra Cave. The Borra Cave (18.2807° N, 83.0397° E), discovered by William King George in 1807 CE, is located in the thickly forested Ananthagiri Hills of the Araku Valley in the Eastern Ghats, about 93 km from Vishakhapatnam. The Borra Cave, having religious, historical, archaeological (e.g., Yadava *et al.* 2007) and economic importance, is an important tourist spot with about half a million visitors annually. The total length of the Borra Cave runs about 825 m, of which a distance of

200 m can be easily trekked. The entrance of the cave is at ~705 m amsl. The deepest point of the cave is ~80 m below the entrance level. The main entrance of the cave is 35 m wide and 40 m deep, but the width of the main chamber is ~15 m. A narrow gallery of 150 m long is connected to the main chamber. A parallel chamber, from the central part of the cave, of 50 m wide and 10 m deep runs for a distance of 75 m. It is observed that this chamber is connected to a stream at the deeper levels. The Borra Cave opens at an elevation of 705 m amsl in the form of a 100-m wide window. The interior of the cave recorded 92% humidity and air temperature of 21±2˚C. The interior of the cave distinctly exhibits a variety of impressive speleothems of various sizes and irregularly shaped stalactites and stalagmites. The stalactites range in length from ~0.1 to 3.5 m. The stalagmites are around 1.2 m long with columns of 6 m long and 0.75 m wide (Narayana *et al.,* 2014). Stalagmite sample BRA-3B was collected during December 2015 from the deep interior narrow gallery of the cave located ~300m south from the entrance of the cave with a small passage to reach a small terrace located 20 m above the ground surface of the cave. The total longitudinal length of the sample BRA-3B was measured as ~47 cm with an average diameter of ~6 cm.

3.2.3 Sub-sample Preparation

The stalagmites were cut into two equal halves along its growth axis using an ultra-thin diamond cutting blade of a DRAMET-make cutting machine (Fig. 3.1) at the PRL, Ahmadabad, and polished. Micro-milling of the samples was done without gaps using a New Wave Research Micro-mill (Fig. 3.3 and 3.4) at PRL, Ahmadabad, and obtained 1198and 420 sub-samples at 400 µm and 200 µm spacing for KG-6 and BRA-3B respectively. A carborundum drill bit of ~100µm was used for micromilling.

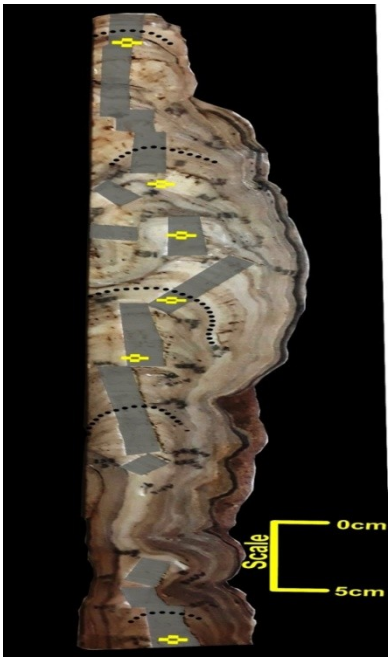

Fig. 3.5. **Stalagmite Slicing for sub-sampling**. Slice of BRA-3B stalagmite with showing sum-sampling along growth layers (grey). Yellow points are U-Th age points and black dotted lines are selected growth layers for Hendy's Test

The micromill system functions with automated milling coupled with visual and microscopic view and motorized sample stage. Stalagmite KG-6 (Fig. 3.2) shows very fine, straight, and clear laminations from the top down to 310 mm. At the bottom, it has a thick lamina with a few 'dirty' patches as shown in figure. 2.4a. Thirty two, eleven, and six distinct layers (Fig. 3.2) were identified and drilled for mineralogy, U-Th ages, and Hendy's test, respectively. Similarly, BRA-3B sample shows changes in its growth layers' (Fig. 3.5) direction such that the actual growth length of the sample was relatively smaller than the longitudinal length of the stalagmite. The sample was observed to be translucent and clear with few dark patches in growth layers. Eleven, six, and five distinct layers (Fig.3.5) were identified and drilled for mineralogy, U-Th ages, and Hendy's test.

3.3. Mineralogy of Stalagmites

It is important to determine the mineral composition of stalagmites as it involves in the estimation of initial concentration in its U-Th geochronology. Also, the compositions of stalagmite are very well utilized to deduce the dry and wet phases as per its aragonite or calcite mineralogy respectively. Furthermore, under controlled laboratory conditions of precipitation, isotopically rich oxygen in aragonite when compared to calcite by 0.6‰ at 25˚C (Tarutani *et al.,* 1969) is observed. Similarly, the carbon isotopes are enriched by 1.8‰ at 25˚C (Rubinson and Clayton, 1969). Therefore, it is inferred that more intake of oxygen and carbon isotope are natural in aragonite when compared to calcite, Hence, the mineralogy is very important for isotopic estimations in terms of inferring the monsoon intensity. The mineral compositions of the two stalagmite samples KG-6 and BRA-3B were determined using classical method of chemical etching and also using X-Ray Diffractometer as described below.

3.3.1. Chemical Etching Method

To obtain the mineralogy of the stalagmites KG-6 and BRA-3B sample, thin profile slices of the stalagmite were cut and immersed into Fiegl's solution for ten minutes (Kato *et al.,* 2003). This chemical etching method is useful in differentiating the aragonite and calcite layers in which the aragonite layers become black/dark and no change is observed in calcite/dolomite layers. This method is useful in targeting the actual aragonite layers for XRD analyses. To prepare Feigl's solution, 1 gram of Ag_2SO_4 was added to a mixture of 11.8 gram of $MnSO_4.7H_2O$ and 100cc of distilled water. The whole mixture was boiled, cooled and filtered. Subsequently, 1mL of

NaOH was added to the solution and kept it to get settled for three hours. The settled sample was filtered again and kept in a dark colored bottle to avoid exposure to the light to check for the mineralogy of the carbonate. The etching method showed calcite composition of the samples of KG-6 and BRA-3. However, few gray layers were also observed which appeared to be of different composition. Hence, XRD mineralogy was done for those layers.

3.3.2. X-Ray diffraction

A typical X-Ray powder diffraction pattern consists of diffraction peaks as a function of diffraction angle 2Θ.The diffraction occurs when an object scatters waves which ultimately produce constructive and destructive interference patterns with each other. The X-ray diffraction of the powdered sample follows Bragg's Law:

$$\lambda = 2d_{hkl} \sin\Theta$$

Where,

λ = Wavelength

d = distance between imaginary plane which form parallel intersecting repeated unit cells filled with atom as per miller indices

hkl = Miller indices

Θ = one half of the diffraction angle

The intensity of each diffraction peak is a pattern governed by the structure of the crystal and the physical configuration of the diffractometer.

Distinct gray growth layers in KG-6 (32) and BRA-3B (11) were observed in chemical etching method. Therefore, XRD was done to determine the mineralogy of

distinctly identified gray growth layers by Philips X-Ray Diffractometer using Nickel filtered copper (Cu) Kα radiation at the University of Hyderabad.

3.4. Geochronology

Radiocarbon ages of foraminifera separated from the marine core SK 170/2 were analysed to estimate the geochronology at different depths of the core. U-Th ages were estimated for the stalagmite samples KG-6 and BRA-3B. Details of applied methods are discussed below:

3.4.1. Radiocarbon dating of Foraminifera

The natural production of ^{14}C is a secondary effect of cosmic-ray bombardment in the upper atmosphere. After production, it gets oxidized to form $^{14}CO_2$. In this form, ^{14}C is distributed throughout the earth's surface. Metabolic processes maintain the ^{14}C content of the living organisms in equilibrium with atmospheric ^{14}C. Once metabolic processes stop, as at the death of an animal or plant, the amount of ^{14}C begins to decrease by decay at a rate measured by the ^{14}C half-life. The radiocarbon age of the given sample is based on measurement of residual ^{14}C content in it.

For a radiocarbon (^{14}C) age to be equivalent to its actual or calendar age, several assumptions are taken into account. These assumptions are: (i) The concentration of ^{14}C in each carbon reservoir has remained essentially the same over the ^{14}C time scale; (ii) There has been complete and quick mixing of ^{14}C throughout the carbon reservoirs world- wide: (iii) Carbon- isotope ratios in samples have not been affected except by ^{14}C decay since these sample materials ceased to be an active

part of one of the carbon reservoirs (as at the death of the organisms); (iv) The half-life of ^{14}C is accurately known as 5730 years ago, and (v) Natural levels of ^{14}C can be measured to appropriate levels of accuracy and precision.

As we assume that ^{14}C has remained constant in the biosphere during the past 50,000 years or so is not precisely true. Fortunately, numerous experiments have demonstrated that the mixing rate of ^{14}C in the atmosphere is rapid (of the order of two years even between hemispheres) so that we can consider the atmosphere as a whole. It is not possible to obtain a precise assessment of the constancy of the cosmic ray intensity since we are looking for comparatively small variations in ^{14}C content. Studies of the decay series of nuclides in meteorites indicate that there have been no major changes in cosmic ray intensity during the past 300,000 years.

Hence, the ages of carbonate material like foraminifera can be estimated using ^{14}C. However, a pretreatment of the material is essential before using the sample for age estimation as the impurities present can lead to addition of errors in age estimation. Hence, carbonate samples are pretreated with 100% H_3PO_4 to remove 50 to 85% of the carbonate which is further dried and hydrolyzed with H_3PO_4. From the pretreated carbonate sample, CO_2 is produced from which graphite powder is produced. The graphite powder is pressed into a target holder of Arizona design. The pressed graphite is then used for ^{14}C measurements following the procedures and calculations of Donahue et al., 1990, using 3-MV AMS system (Fig. 3.6) at University of Arizona.

Eight samples of mixed planktonic foraminifera (250-350μm) were handpicked under stereo zoom microscope and analyzed by AMS radiocarbon dating

method at NSF-Arizona AMS laboratory, University of Arizona, USA in the year 2006. Calibration to calendar year ages was performed using marine09 Radiocarbon calibration program (Stuvier and Riemer, 2009). Errors (1σ) in the age estimates range between ±37 and ±780years. A reservoir age correction of 400 years was applied for all the radiocarbon ages (Stuvier and Riemer, 1993; Dutta *et al,* 2001).The ^{14}C ages of marine fossils are considered on average to be 400 years older than contemporary terrestrial wood because the foraminifers derive their carbon from ocean water or the reservoir have lower $^{14}C/^{12}C$ ratios with respect to the atmosphere as they mix with deeper ^{14}C depleted water (Dutta et al., 2001).This happens because the ^{14}C ages of marine calcareous shells are observed to have considerable variance spatially due to variations in the regional ocean circulation patterns. This change, ΔR(s), is calculated for a given region (s) at any given time (t) as the difference between the regional marine ^{14}C age Rs(t) and the global model marine ^{14}C age Rg(t) (Stuiver and Braziunas 1993).

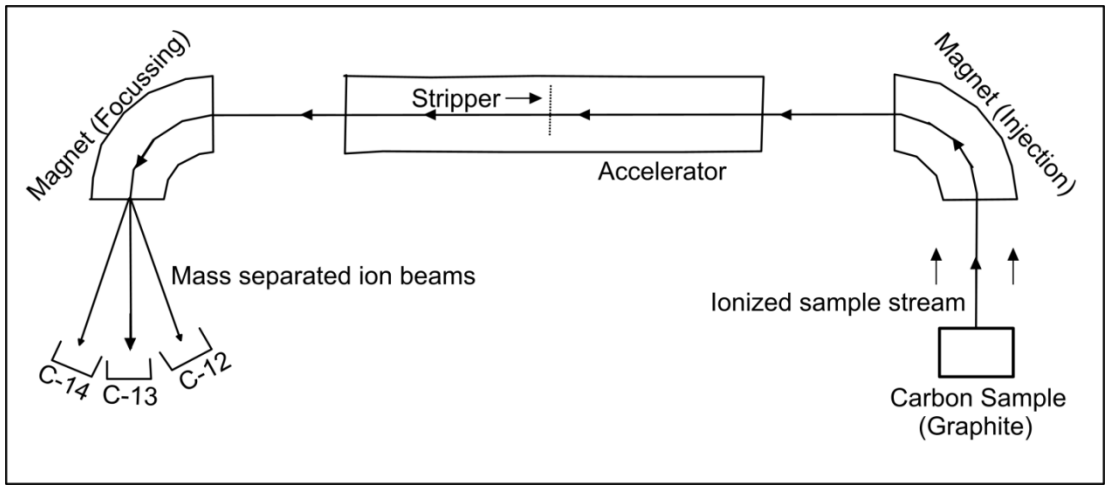

Fig.3.6.AMS Geometry. Geometrical layout of Anisotropic Mass Spectrometer (AMS) used for Radiocarbon age estimation

3.4.2. Marine Isotope Stages (MIS)

As mentioned in section 3.3.1, the bottom two ages were beyond the radiocarbon age calibration limit, the downcore ages were linearly extrapolated comparing with MIS 3.0 to 3.3 (24 ka BP to 53 ka BP) ages following Imbrie et al. (1984). Marine isotope stages (MIS) are also called as marine oxygen-isotope stages, or oxygen isotope stages (OIS). MIS are the stages of alternate stadial or cold and interstadial or warm climate stages of Earth's climate which have been deduced from oxygen isotope variability records from deep sea sediments using proxies like marine sediments, foraminifera, sapropels, etc. The stadial and interstadial are identified by characteristic oxygen isotope $\delta^{18}O$ enrichment and depletion respectively such that the odd MIS stages are identified as interstadial and odd stages as stadial. Following the oxygen isotope work of Urey in 1947, Emiliani (1955) developed MIS time scale for the Quaternary period and further extended for the early Earth Climate. During six million years of span, 100 stages have been identified among which few stages have sub-classifications as shown in figure 3.7. MIS chronostratigraphy also matches well with Milankovitch cycles of orbital forcing in terms of Earth's various movements knowns as orbital theory. Furthermore, MIS stages are also supported by dendrochronology, ice cores. It was further compensated by SPECMAP project in which marine sediments ages older than 50 ka was carried out based on stable oxygen curves which acted as a powerful stratigraphic tool to compare the deep-sea climatic records within a common time frame along with precision required for to Earth orbital cyclic modulation due to solar forcing.

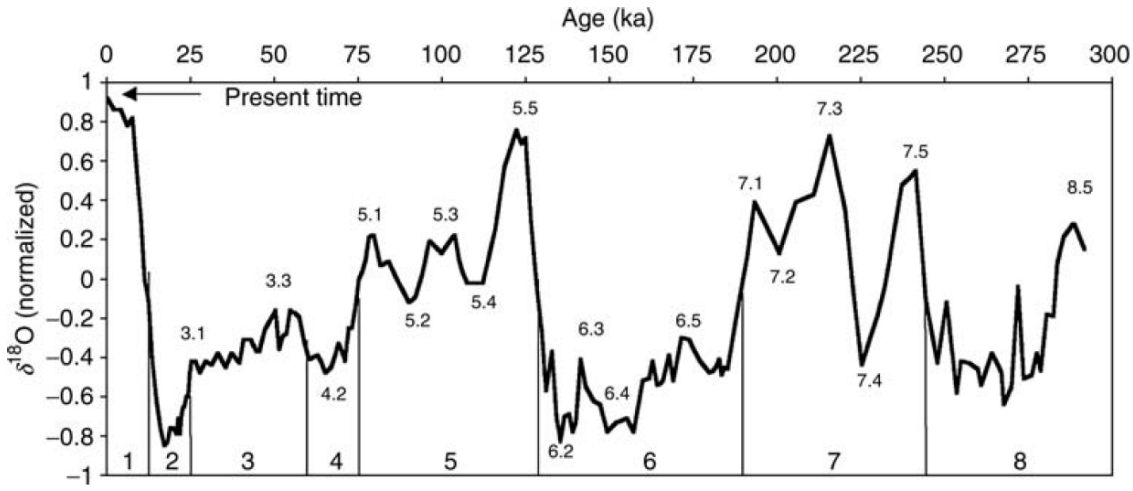

Fig. 3.7. SPECMAP isotopic stages are shown on the bottom of the 0-300 ka time scale (Martinson *et al.,* 1987 and Pisias *et al.,* 1984). Major isotopic events are shown along the isotopic curve, following definition by Pisias *et al.* (1984)

3.4.3. Age-Depth Model of Foraminifera

Based on the radiocarbon and compared MIS 3.0-3.3 ages, a linearly interpolated Age-Depth model was prepared to assign ages for each sub-sampled foraminifera. Using Age-Depth model, sedimentation rates were also calculated.

3.4.4. U-Th Ages of Stalagmites

U-Th geochronology of stalagmites is considered as one of the most accurate and a precise method as the decay rate of natural uranium (U) into a series of daughter isotope is known. There exist three U-series decay chains starting with naturally occurring radioactive isotopes: ^{238}U, ^{235}U, and ^{232}Th and ending with stable isotopes of ^{206}Pb, ^{207}Pb, and ^{208}Pb, respectively with more than a dozen of intermediate isotopes in which ^{234}U and ^{230}Th are mostly used for stalagmite geochronology. The half-lives of ^{238}U and ^{235}U are 4.47Ga and 0.7Ga, respectively

whereas their immediate daughter isotopes have half-life of very short term period that is 245ka for ^{234}U, 76 ka for ^{230}Th, and 33ka for ^{231}Pa. While the parent isotope's activity i.e. no. of decays per unit time, during Quaternary remains negligible, the activity of daughter isotope keeps on changing until it attains a secular equilibrium with parent isotope. However, for geochronological purpose an initial disequilibrium is necessary. Stalagmites can be dated accurately and precisely with the help of U-Th ages because their growth is based on the precipitation from natural water where the solubility of U is higher, whereas Th solubility is quite low. Hence, stalagmites are known to have significant U concentration and nearly negligible Th content giving rise to high U/Th ratio which is the prerequisite for U-Th geochronology.

U-Th ages also referred to as ^{230}Th or ^{238}U–^{234}U–^{230}Th ages, was used to determine ages of stalagmite. Eleven U-Th dates were obtained for KG-6 from a Thermo Fisher NEPTUNE multi-collector inductively coupled plasma mass spectrometer (MC-ICP-MS; Fig. 3.8) at High-Precision Mass Spectrometry and Environment Change Laboratory (HISPEC), National Taiwan University, Taiwan (Shen *et al.,* 2003, 2012). Details of the chemical procedures followed are described in Shen *et al.* (2003). Instrumental methods and off-line data reduction are described in Shen *et al.* (2002; 2012). Estimated ^{230}Th dates (relative to 1950 AD) with a 2σ error from ±44 to ±98 years are in correct stratigraphic order for KG-6 sample. Similarly, six U-Th dates were obtained for BRA-3B sample using MC-ICP-MS at Institute of Global Environmental Change, Xi'an Jiaotong University, Xi'an 710049, China. Estimated ^{230}Th dates (relative to 1950 AD) with a 2σ error from ±36 to ±271 years are in correct stratigraphic order for BRA-3B sample.

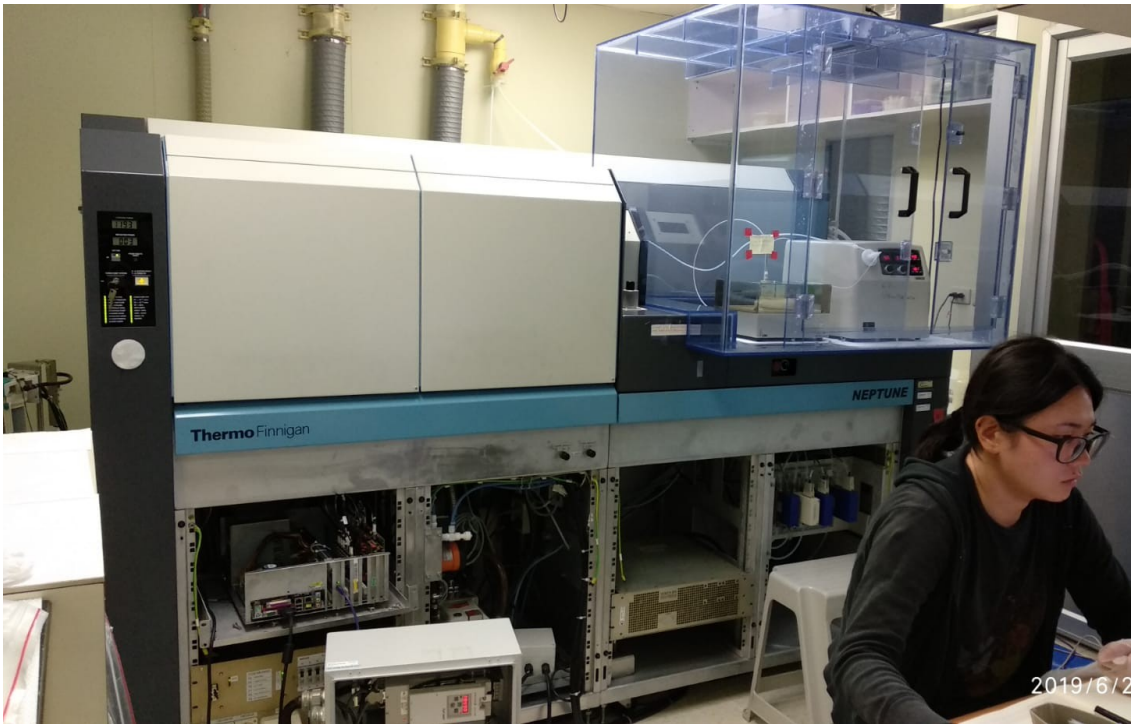

Fig. 3.8. MC-ICP-MS Lab at HISPEC, National University of Taiwan, where U-Th age estimation of stalagmites was carried out.

3.4.5. Age-Depth Model of Stalagmites

COPRA age-depth Model. At present, speleologists use various age models like StalAge, COPRA, OXCAL, Bacon to name a few (Scholz *et al.,* 2012). Each model comes with its own advantages and drawbacks. **Co**nstruction of **P**roxy **R**ecord for **A**ge models (COPRA) 1.0 Age model was run for the stalagmite sample KG-6 for establishing a normal stratigraphic order of crystallization in the given temporal span. COPRA 1.0 is interactive software that runs on the MATLAB interface (Breitenbach *et al.,* 2012). Prerequisites to using this model is monotonocity i.e. the older deposition is at the bottom and younger at the top. Based on the ages and errors associated with them, a normal distribution is built around the age and proxy data points. The software uses 2000 Monte-Carlo simulations (Fig. 3.9) to interpolate

between two data points. Age reversals and outliers can be identified and removed from the data set. The model also incorporates and interpolates ages between the hiatuses. The median of the distribution and the 95% confidence limits represent the final age model. The work flow of the model is shown in figure 3.10.

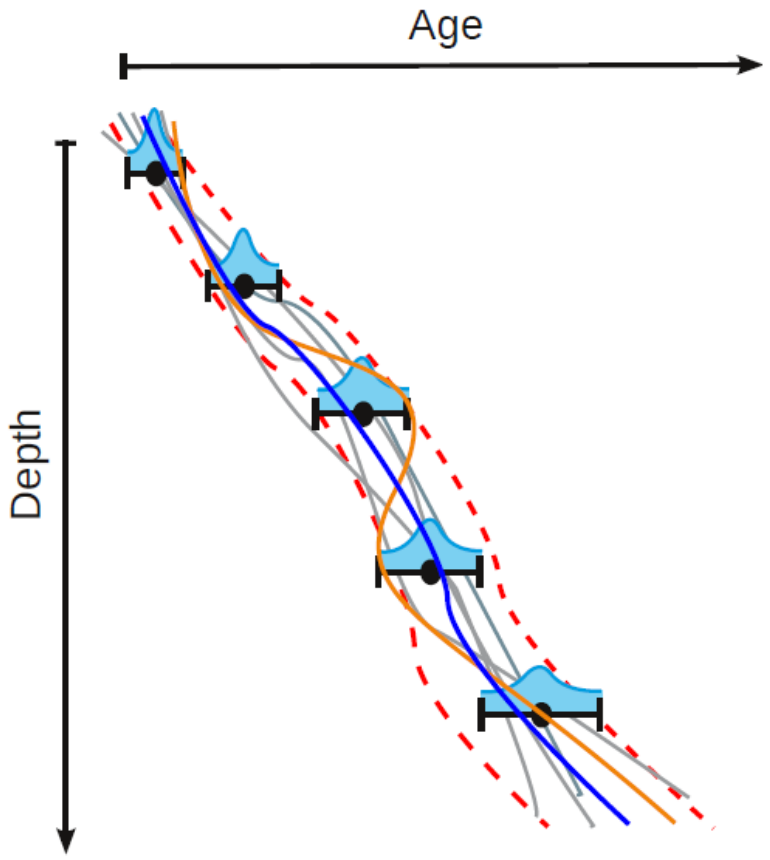

Fig. 3.9. COPRA age-depth model. Monte Carlo simulation of the age points and their interpolations.

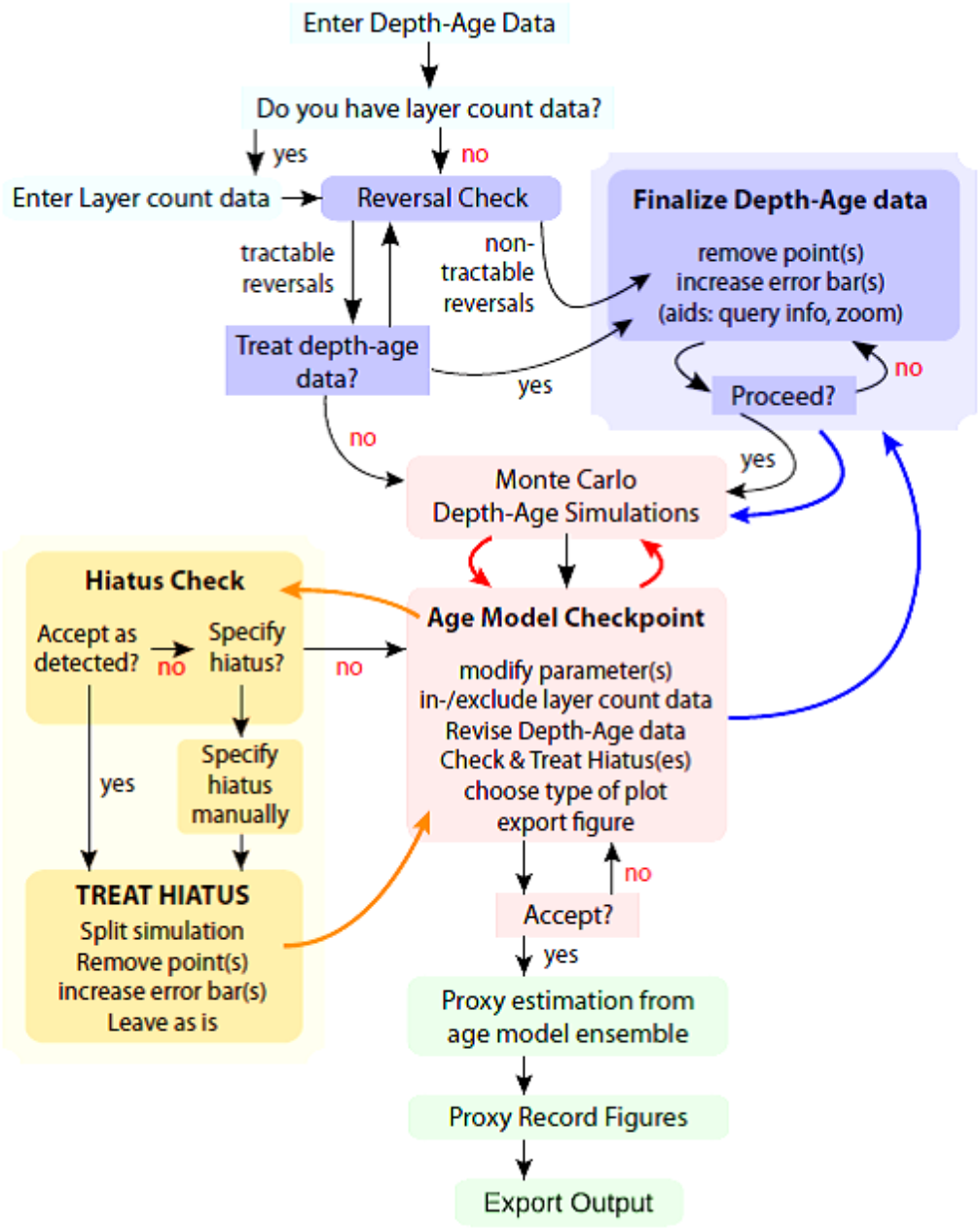

Fig. 3.10. COPRA Workflow. The COPRA work flow is divided into five broad sections which are color-coded as explained in the figure.

StalAge Age-Depth Model. The StalAge 1.0 age-depth model is able to detect and account for outliers and age inversions, includes stratigraphic information

in addition to monotonocity constraints, and provides 95% confidence limits for the uncertainty of the age model. The code is written for the use with the open source statistical software R. StalAge is applicable to problematic datasets that include outliers, age inversions, hiatuses and large changes in growth rate. The development of StalAge numerical model (Fig.3.11) involves simulation of speleothem growth, incorporation and temporal evolution of U-series isotopes and mass spectrometer analyses. The model is enriched with two major advantages: first, simulated age model is known and can be compared to the age model calculated by the algorithm. Second, outlier, age inversion, etc. can be simulated and the performances and robustness can also be tested.

Major outliers, if any, from the age data is screened that is all those ages which are not in stratigraphic order and delete or their error bars are enlarged to fit into stratigraphic order as per the convenience. Following major outlier screening, minor outliers and age inversion screening is performed by fitting error weighted straight lines through subsets consisting of three adjacent points. Further, monte carlo simulation is performed for every successive subset consisting of more than two data points to fit an error weighted straight line within the associated error bars. The simulated straight lines are extrapolated by half of the distance to previous/subsequent data point which allows a variation of one by sixth distance in simulation.

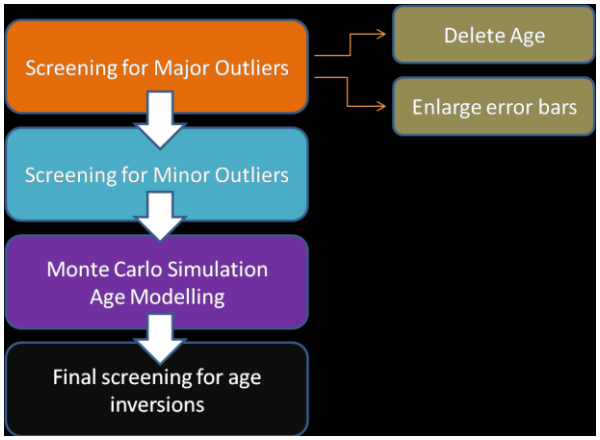

Fig. 3.11. StalAge age-depth model workflow. Flowchart of StalAge model summarizes the steps the model executes while interpolating the age model based on MonteCarlo simulations.

3.5. Stable Isotope Analyses

The oxygen and carbon stable isotopes of foraminifera and stalagmites have been analyzed using Gas bench IRMS at PRL, Ahmedabad.

3.5.1. Isotope Ratio Mass Spectrometer (IRMS)

IRMS works on the principle of mass spectrometer (Fig. 3.12) where ions are differentiated, based on the ratio of their mass, to ionic charge. A mass spectrometer is mainly composed of three components: (i) Ion Source- Where samples are ionized; (ii) Analyzer-which separates the different isotopologues using strong applied magnetic field; and (iii) Detector- where the isotopologues are collected and measured.

Ion source. A Thorium (Th) coated tungsten filament is used to produce electrons by passing ~3.5 A current which is accelerated upto ~70eV. These electrons after entering into source ionize CO_2 gas with an efficiency of 0.1%. To increase the ionization efficiency, a low magnetic field is applied due to which electrons starts

moving in spiral motion along the magnetic field. Collimating plates are used to focus the ion beams. The ionized gas molecules are accelerated towards analyzer using a high voltage of ~2.5kV which produces a kinetic energy to the charged molecules. It can empirically be expressed as:

$$qV = \frac{1}{2} mv^2 \quad [1]$$

Where,q = Charged molecule; V = Accelerating voltage; M = mass, and V = velocity

Analyzer. Having gained the kinetic energy, charged molecules enters into magnetic chamber of the analyzer and get separated based on their mass to charge ratio. In case of CO_2, three dominant beams with masses 44, 45, and 46 amu corresponding to $^{12}C^{16}O_2$, $^{13}C^{16}O_2$, and $^{12}C^{16}O^{18}O$ are produced. A directed curvilinear path, owing to Lorentz force, is followed by the beams. The force is balanced by the centripetal force on the beams which enters perpendicular to the direction of the magnetic field. It is empirically expressed as:

$$q(VxB) = mv^2/r \quad [2]$$

Where, q = ionic charge; V = Potential; and B = Magnetic Field.

Therefore, using equation [1] and [2],

$$r = \sqrt{[(2Vm)/(B^2q)]} \quad [3]$$

Where, r= Radius of curvature of singly charged ion.

Since, V, B, and q are kept constant; r of the singly charged ion is directly proportional to the square root of its mass (m). Hence, the ions with heavier mass i.e. 46 ($^{12}C^{16}O^{18}O$) are detected at the path of larger radius of curvature whereas the lighter mass at smaller radius of curvature.

Detector. The detectors are basically made up of faraday cups connected to very high resistors (~$10^9\Omega$) which measures the three ion beams. Faraday cups are metal cups where ions collide and get neutralized by losing their kinetic energy and charge which ultimately produces current. The produced current is further passed through external high resistors which is measured in IRMS as voltage across the resistance produced by ion and measured as proportional to the number of ions entering into faraday cups per unit time.

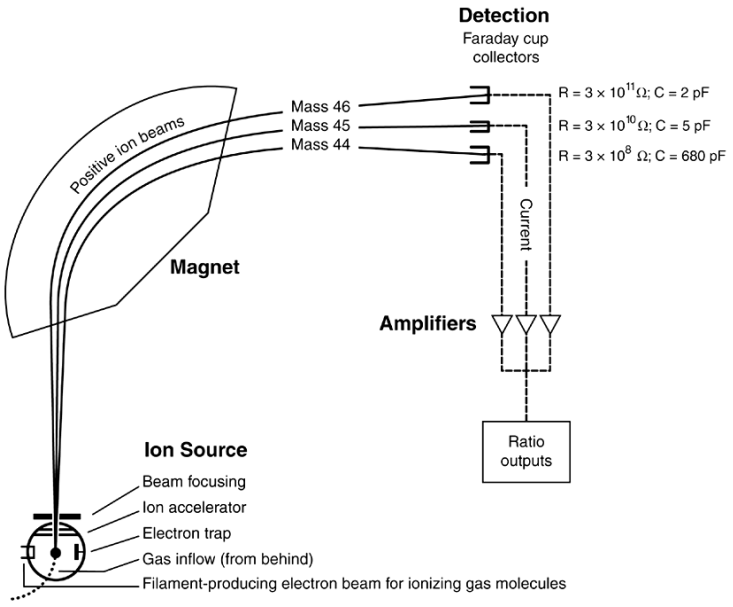

Fig. 3.12. IRMS. Schematic diagram of an isotope ratio mass spectrometer (Clark and Fritz, 2013)

Fig. 3.13. IRMS. Gas Bench Delta V-Plus IRMS lab at PRL, Ahmedabad

3.5.2. External Peripherals of IRMS

External peripherals are attached with IRMS system for automated sample preparation and injection of CO_2 and measurements of stable isotopes of carbon and oxygen. Following two peripherals are attached with Gas bench IRMS for isotopic analyses:

Sample Tray. Sample tray (Fig. 3.13) is the first peripheral component used for the introduction of sample to IRMS for isotopic measurements. Sample tray is basically an automated container having capacity of 88 samples to be mounted in one single batch of measurement. The temperature of the sample is regulated based on the type of sample to be measured. Tray temperature is fixed at 72±0.5˚C for carbonate samples.

Gas Bench or GC Column. The equilibrated gas for the sample is transferred to GC column or gas bench (Fig. 3.13). The water vapour produced along with equilibrated gas removed by hygroscopic gastight Nafion® tubing. Therefore, dry

gases are directed towards Valco loop and then transferred to GC column. GC column separates different gas compound released from the sample loop viz. CO2, H2, N2, etc. These compounds are further directed through Nafion® guard trap via open slit into IRMS.

3.5.3. $\delta^{18}O$ and$\delta^{13}C$ Isotope Measurements

For the measurements of oxygen and carbon stable isotopes in Delta v-plus, powdered carbonate samples were taken in 12 ml quartz vials and tightly capped. These tightly capped quartz vials were then put in the automated sample tray along with internal standard MMB (99.99% $CaCO_3$) vials, at an interval of every 10 samples, flushing with Helium (He) gas injection for 10 minutes. Once all the vials of the tray were flushed, ~0.1 ml of 100% orthophosphoric acid (H_3PO_4) was added in all the vials and kept for one hour at 72±0.5˚C temperature for complete dissolution and CO_2 production. The produced CO_2 was then injected into Delta V-plus IRMS through Gas bench. External precision (1σ) was better than ±0.08‰ and ±0.03‰ for $\delta^{18}O$ and $\delta^{13}C$, respectively.

3.5.4. $\delta^{18}O$ and $\delta^{13}C$ Isotope calculations for carbonates

The estimated raw data from IRMS provide results as per MMB laboratory standards. Hence, conversion of the raw results to international standards is essential. There are several standards (Table 3.1) available from IAEA for such conversions (Table 3.2 and 3.3). VPDB is widely used for carbonate samples. Therefore,

following Clark and Fritz (2013), conversion of local standard MMB to VPDB is done as stated below.

$$\delta^{18}O_{Sample\text{-}VPDB} = \delta^{18}O_{MMB\text{-}VPDB} + \delta^{18}O_{Sample\text{-}MMB} + [\delta^{18}O_{MMB\text{-}VPDB} \times \delta^{18}O_{Sample\text{-}MMB} \times 10^{-3}]$$

Similarly,

$$\delta^{13}C_{Sample\text{-}VPDB} = \delta^{13}C_{MMB\text{-}VPDB} + \delta^{13}C_{Sample\text{-}MMB} + [\delta^{13}C_{MMB\text{-}VPDB} \times \delta^{13}C_{Sample\text{-}MMB} \times 10^{-3}]$$

Given that MMB calibration to VPDB as:

$$\delta^{18}O_{MMB\text{-}VPDB} = -10.7‰; \delta^{13}C_{MMB\text{-}VDB} = 3.9‰$$

While equating results for laboratory standard to international standard, few corrections are essential for the isobaric contributions from several other isotopologues which have contributions to the masses detected at faraday cups. This correction is also called as Craig correction.

Craig correction. Removal of effects of $^{13}C^{16}O^{17}O$ from $^{12}C^{16}O^{18}O$ during the conversion of molecular ratios into atomic ratio for the estimation of $\delta^{18}O$ and $\delta^{13}C$ is called as Criag correction (Criag, 1957).

$$\delta^{18}O = 1.0010\ \delta_{46} - 0.0021\ \delta_{45}$$

$$\delta^{13}C = 1.0676\ \delta_{45} - 0.0338\ \delta_{46}$$

Where,

$$\delta_{45} = [(I_{45}/I_{44})\text{-}1] \times 10^3$$

$$\delta_{46} = [(I_{46}/I_{44})\text{-}1] \times 10^3$$

Here, I_{44}, I_{45}, and I_{46} are currents at faraday cups.

Table3.1. IAEA standards used for water and carbonate isotopic measurements				
Name	**δ‰**		**Nature of the sample**	**Reference Standard**
VSMOW	0	$^{18}O/^{16}O$	Water (Tropical)	VSMOW
SLAP	-55.50‰	$^{18}O/^{16}O$	Water (High latitude)	VSMOW
NBS-19	1.95‰	$^{13}C/^{12}C$	Calcite	VPDB
	-2.20‰	$^{18}O/^{16}O$		VPDB
Table3.2. Materials for inter-comparison				
GISP	-24.784±0.075	$^{18}O/^{16}O$	Water (high latitude)	VSMOW
NBS-18	-5.029±0.049	^{13}C	Calcite	VPDB
	-23.035±0.172	^{18}O		
IAEA-CO-1	2.48±0.025	^{13}C	Calcite	VPDB
	-2.437±0.073	^{18}O		

Table 3.3. Comparison between reported and measured IAEA standard values.				
Standard	**$\delta^{13}C$ Reported**	**$\delta^{13}C$ Measured**	**$\delta^{18}O$ Reported**	**$\delta^{18}O$ Measured**
NBS-19	1.95	2.1±0.07	-2.20	-2.22±0.08
IAEA-CO-1	2.48	2.42±0.072	-2.44	-2.49±0.03

3.6. Statistical Analyses

3.6.1. Z-Score

Z-score or standard score is a statistical estimation of numbers of standard deviations of a variable is away from the mean value of its population. This

estimation helps in comparison and correlation of the variables from different sets of data in terms of zero, positive or negative Z-scores. It is calculated as the ratio of the difference between variable and mean to the standard deviation.

$$\text{Z-Score} = [\ (x-\mu) / \sigma\ ]$$

Where,

x = variable

μ = mean of the population

σ = Standard deviation, $\sigma = \sqrt{\{(x-\mu)^2/n\}}$

n = population

Standard deviation (σ) shows the amount of variability within a given data set by calculating the difference between each data point and the mean. The calculated differences are then squared, summed and averaged to produce the variance. The squared root of the variance is termed as standard deviation which shows the original unit of estimation. Z-Score is considered a better tool than standard deviation because standard deviation (σ) shows the amount of variability within a given population by calculating the difference between each variable and the mean whereas Z-Sore is the number of standard deviations a given variable lies from the mean. The calculated Z-Score zero indicates the score to be identical to the mean or it represents the average value of the variable. Positive Z-Scores indicate the location of the variable form the mean on the upper side of the distribution curve whereas negative Z-Scores indicate the position in the lower side of the distribution curve. In a normal scenario, variables are observed to have a Z-Score between -3 and 3, meaning they lie within three standard deviations above and below the mean value of the population.

3.6.2. REDFIT Spectral Analyses

Spectral analysis is helps to understand the climate change processes and the variability recorded in a time series. Paleoclimate time series spectrum often shows a continuous decrease in the amplitude with increasing frequency which is called as red-noise. A first-order autoregressive (AR1) process can explain the climatic red-noise signature (Hasselmann, 1976) where AR1 model is often used as null hypothesis to assess whether or not the variability recorded in a time series is consistent with a stochastic origin of this type (Gilman *et al.,* 1963). Such a test involves estimation of an AR1 parameter from the time series under consideration. While, this process is straightforward for evenly sampled time series (Percival and Walden, 1993), it is quite complex for unevenly spaced paleoclimate data. Hence, Schulz and Mudelsee (2002) introduced a computer programme REDFIT which estimates the AR1 parameter directly from unevenly spaced time series. The programme is based on Lomb-Scargle Fourier transform (Lomb, 1976; Scargle, 1982, 1989) where the estimated AR1 model is transformed from the time to frequency domain. Comparison of the spectrum of the time series with that of the AR1 model allows testing the hypothesis that the time series originates from an AR1 process.

3.6.3 Wavelet Analyses

Wavelet analysis is now recognized as one of the important method to analyze time series with many different timescales or changes in variance (Torrence and Compo, 2001). It converts the time series into time-frequency domain which helps us in determining the periodicities along with its temporal control. The wavelet analyses involve a multi-step transformation such that it finds the Fourier transform of the time

series and then selects a wavelet function and a set of scales for analyses. Then, it constructs the normalized wavelet function for every selected scale and finds out the wavelet transform. It also determines the cone of influence and the Fourier wavelength at that scale. Assuming a background Fourier power spectrum (e.g., white or red noise) at each scale, it uses the chi-squared distribution to find the 95% confidence or 5% significant contour. Numerous climatic studies have used wavelet transforms (e.g. Tropical convection, Weng and Lau 1994; El Niño–Southern Oscillation, Wang and Wang 1996; atmospheric cold fronts, Gamage and Blumen 1993, etc.) The wavelet transform has also been used widely in paleomonsoon studies (e.g. Yadava and Ramesh, 2005; Lone *et al.,* 2014; Gautam *et al.,* 2019) to deduce the periodicities.

To determine the periodicities in the unevenly spaced $\delta^{18}O$ measurements, we performed wavelet analyses in the PAST platform (Hammer *et al.,* 2001) using the codes of Torrence and Compo (1998).Wavelet analysis is considered as a robust approach for analyzing localized variations in power in the time-frequency domain. Morlet function at 6 dB was used to perform the wavelet analyses which suits best in delineating the latent periodicities. Finite length of time series signals cause uncertainties to occur at the beginning and end of the power spectrum. The cone of influence in the wavelet plot limits these uncertainties to interpret the power spectrum. In the wavelet plot, Y-axis corresponds to a log scale with base 2 and X-axis corresponds to the modelled age.

3.7. Ocean Climate Data and Analyses

Sea surface height anomaly record for the year 1992-2013 using altimeter data which is a combination of TOPEX Poseidon, ERS, and Jason1 satellite altimeter were obtained from AVISO having a resolution of $1/3^{rd}$ of a degree for oceanographic studies for western BoB.

The primary objective of the TOPEX/POSEIDON project is to make precise and accurate global observations of the sea level for several years, substantially increasing understanding of global ocean general circulation and heat transport. Like TOPEX/POSEIDON satellite, the primary instruments in ERS and Jason1 is a radar altimeter which is similar to aircraft radar having a satellite altitude with comparatively very high height precision. These altimeters calculate the time of the radar signal pulses off the sea surface and their return to the satellite. A microwave radiometer based corrections for any errors in the time delay that is caused by water vapor in the path through the atmosphere is done.

3.8. GNIP Data and Analyses

The Global Network of Isotopes in Precipitation was initiated in 1958 by IAEA and WMO, and became operational in 1961. The objective was a systematic collection of basic spatial data on the isotope content of precipitation across global scales to determine temporal and spatial variations of both environmental stable isotopes and tritium in precipitation. While the initial driver, was to monitor atmospheric thermonuclear test fallout through the determination of the radioactive

hydrogen isotope Tritium, since the 1970s the focus changed to a become observation network of stable hydrogen and oxygen isotope data for hydrologic studies. For over 50 years, GNIP has provided global isotope data for the use in hydrological investigations water resources investigation, planning, conservation and development. The IAEA's Water Resources Programme and the World Meteorological Organization (WMO) have established a global network for surveying the stable $\delta^{18}O$ and δD and tritium concentrations in the worldwide precipitation since 1961. The data is archived at www.iaea.org/water/. In the present study, $\delta\ ^{18}O$ and the corresponding rainfall amount over the globe (Fig. 3.14) and India (Fig. 3.15) are comparatively used from the GNIP data.

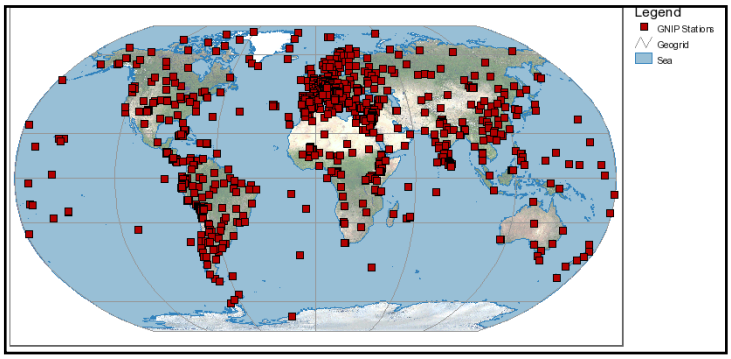

Fig. 3.14 GNIP Stations. Worldwide location of GNIP stations. (Source: IAEA)

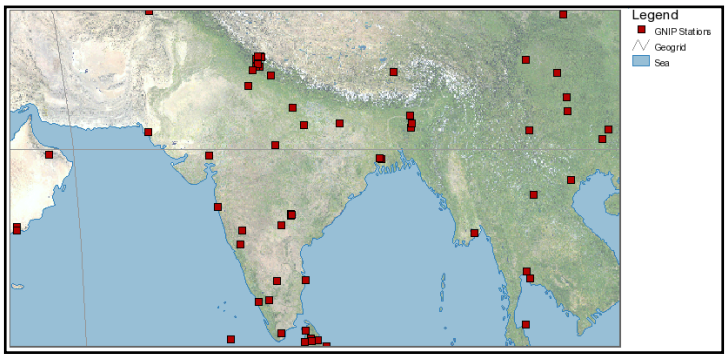

Fig. 3.15 GNIP Stations. Locations of GNIP stations in India. (Source: IAEA)

Chapter 4

Isotopic Variability: Inferences from Global Network of Isotopes in Precipitation Records

Chapter 4

Isotopic Variability: Inferences from Global Network of Isotopes in Precipitation Records

4.1 Introduction:

Urey (1947), on theoretical grounds, showed the isotope fractionations and suggested to utilize the isotopic fractionations as a tool for geological information. Subsequently, many researchers brought wide applications of isotopic fractionation in terms of geological investigation, environment, climate, etc. Isotope fractionation is the processes which affects the relative abundance of stable isotopes or the isotopic composition of a given sample irrespective of their phase.

Climatic parameters such as temperature, humidity, atmospheric circulation, etc., affects or change the ratio of heavier to lighter isotope of oxygen atom of the rain water. During the phase transition, δ is changed significantly (Fig. 4.1) due to evaporation of liquid water and condensation of vapour mass. It is important to understand the variation in isotopic composition of rainfall to utilize it in understanding the climate change. The International Atomic Energy Association (IAEA) and World Meteoric Organization (WMO) have operated the Global Network of Isotopes in Precipitation (GNIP) since 1961. This programme maintains a database of monthly precipitation isotope values at selected sites worldwide. This chapter deals with the latitudinal variation of isotopes in rain water based on the GNIP data from

3772 stations all over the world. The chapter discusses about fractionation and various isotopic effects in global precipitation.

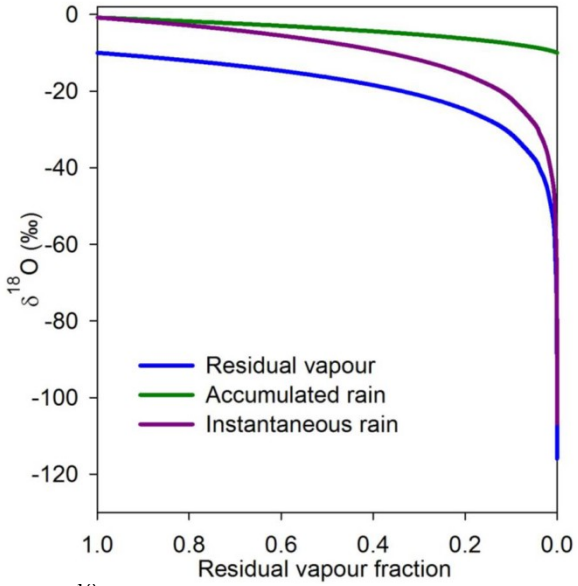

Fig. 4.1. Figure displays $\delta^{18}O$ change of the water vapor during the instantaneous rain and the accumulated rain formed from the water vapor when compared with the vapour fraction retained in the system. (Source: Lekshmy, 2015).

4.2. Equilibrium Fractionation

Physical condition, when δ values for reactant and products are unique and equilibrium is maintained between the two, is known as equilibrium fractionation. This occurs when the reactant and the products remain in contact for a sufficiently long time to achieve chemical equilibrium. During equilibrium fractionation, the total energy of the system is minimized such that the heavier isotope preferably goes into the compound having strong binding. For example, during the condensation of vapour mass, equilibrium fractionation of vapour formation and condensation takes place after attaining a thermodynamic equilibrium condition. This occurs only when the process is extremely slow and the system is a closed system (Dansgaard, 1964).

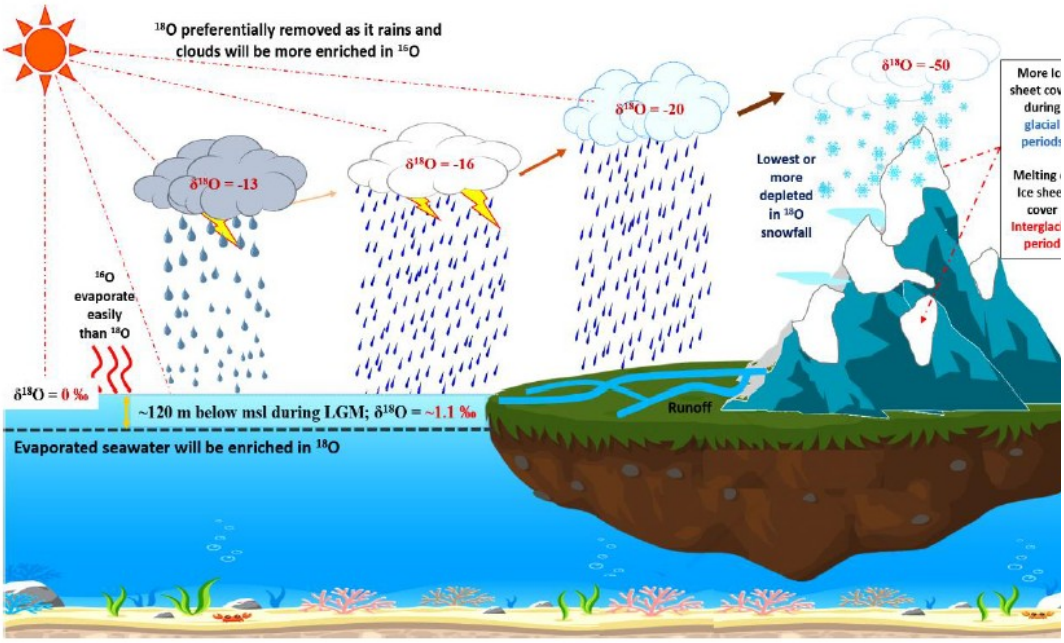

Fig. 4.2. Figure explains fractionation by Rayleigh distillation model where the primary evaporation takes place from the ocean. The direct precipitation, and runoff from land to sea refer are the local effects. Isotopic depletion is observed. Source: Clark and Fritz (2013).

4.3. Kinetic fractionation

Kinetic fractionation refers to the fractionation which occurs during the unidirectional reaction process such that no equilibrium is maintained between reactant and product. For example, kinetic fractionation takes place during the evaporation from ocean surface. During evaporation, diffusion rates of H_2O isotopologues are observed to be different (Craig and Gordon, 1965).

4.4. Rayleigh's Fractionation

Rayleigh's fraction describes about the system of multiple phase from which one phase is continuously extracted by fractional distillation (Rayleigh, 1896).

Rayleigh's equation describes about the fractionation of the system as described below:

$$R = N^{*} / N$$

Where, N* = Number of heavier isotopes;

N = Number of lighter isotopes

In a system where one phase is being extracted,

$$R/R_o = (X/X_o)^{\alpha-1}$$

Where,

R = Ratio of isotopes (e.g. $^{18}O/^{16}O$) in the system (vapour mass) from which rain is

extracted by condensation

R_o= Ratio of isotopes at initial conditions

X = Amount of relatively more abundant (lighter) isotope

X_o= Initial concentration of relatively more abundant (lighter) isotope

α = Fractionation factor

$$\text{Given, } X/X_o = f,$$

$$\text{Hence, } R = R_o f^{\alpha-1}$$

This is further transformed into δ notation as:

$$\delta = \delta_o + (\alpha-1)10^3 \ln f$$

The Rayleigh's equation and fractionation model holds good when following assumptions are considered: (a) Phase is continuously extracted from the multiphase system, (b) the abundance of higher isotope is much less than the lighter isotope, (c) System must be homogeneous, and (c) the process is isothermal

4.5. Water Isotopologues

Water (H_2O) is composed of combinations of isotopes of Hydrogen (H) and Oxygen (O). Hydrogen has three naturally occurring isotopes in which two isotopes that is ^{1}H or Protium (99.98%) and ^{2}H or Deuterium (0.02%) are stable. ^{3}H or Tritium is radioactive with a half life of 12.32 years. Isotopes of Hydrogen are strongly influenced by kinetic processes which causes significant fractionation relative to oxygen isotopes during precipitation and evaporation. Their fractionation mostly depends on the relative humidity of the ambient environment (Craig 1961; Craig and Gordon 1965; Merlivat and Jouzel 1979; Gat and Gonfiantini 1981; Clark and Fritz 2013). The oxygen isotopes have been discussed in section 1.2. of Chapter 1 while explaining about CO_2 isotopologues.

4.6. Isotopic effects in Global Precipitation

Ocean, covering ~70% of the earth, is the ultimate reservoir of water in the hydrological system. It is the main source of water in vapour, liquid, and solid forms in land and atmosphere. Well-Mixed ocean water has $\delta^{2}H$ and $\delta^{18}O$ close to 0‰ which is nothing but the absolute abundance for Vienna Standard Mean Oceanic Water (VSMOW). The $^{2}H/^{1}H$ ratio is measured to be 0.00015576 (Hagemann *et al.,* 1970) whereas it is 0.0020052 for $^{18}O/^{16}O$ (Baertschi, 1976). The isotopic composition of ocean water and related products change significantly due to

continuous evaporation, precipitation and other water mixing processes which cause inhomogeneous mixing and kinetic fractionation processes (Gat and Gonfiantini 1981; Rozanski *et al.,* 1993). Hence, H_2O isotopologues of rainwater, atmospheric moisture and seawater can be used to characterize sources of moisture and understand hydrological cycle of the modern climate (Dansgaard 1964; Rozanski and Sonntag 1982; Rozanski *et al.,* 1992, 1993; Gat 1996; Clark and Fritz 2013; Yang *et al.,* 2016). The H_2O isotopologues are observed to have various isotopic effects during the process of precipitation. These isotopic effects are briefed below.

4.6.1. Temperature effect

The mean annual surface air temperature shows a linear relation (Fig. 4.3) with mean annual $\delta^{18}O$ as shown by the GNIP records (Dansgaard 1964; Rozanski et al. 1993). The temperature effect is prominent in high latitudes when compared to tropics where it is almost negligible.

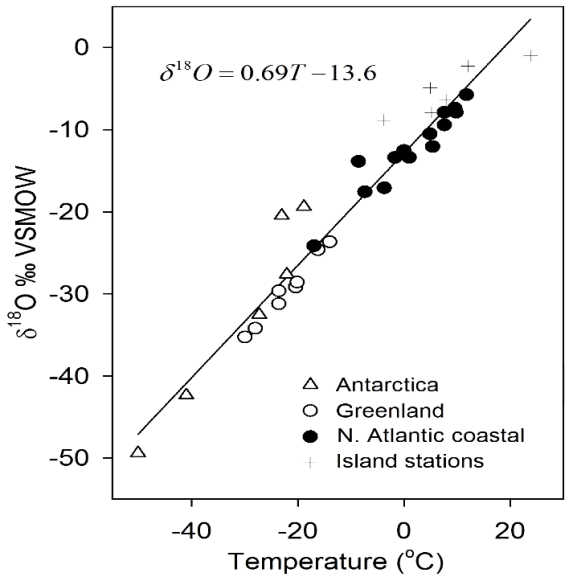

Fig. 4.3. Linear relation is observed between mean annual surface air temperature and $\delta^{18}O$ of GNIP record where $\delta^{18}O$ = 0.69T-13.6 (Dansgaard 1964; Rozanski et al. 1993).

From the temperature effect, vapour masses that evolve through rain out under cold condition will experience an enhanced depletion in ^{18}O and ^{2}H compared to warmer condition. These results from increased Rayleigh distillation of vapour mass and increased isotope fractionation at colder temperature. There exists a good positive correlation (R^2=0.60; Fig. 4.4) between mean air temperature and latitude. The correlation shows a parabolic best fit having an empirical equation of Mean Air Temp = -0.0068*(latitude)^2 + 0.0099*(latitude) + 24.477.

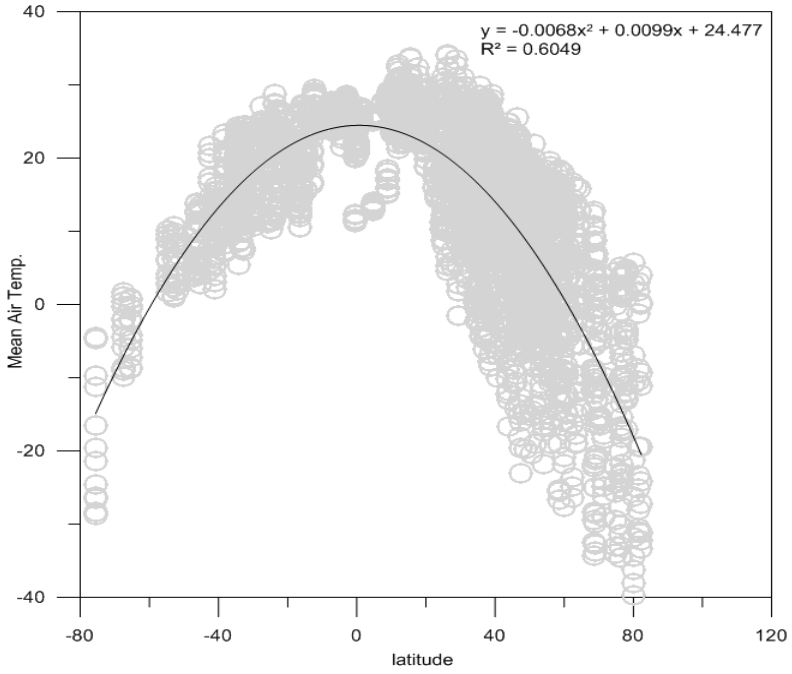

Fig. 4.4. Temperature effect as shown by mean air temperature and latitude. (Data source: GNIP).

4.6.2. Amount effect

Amount effect is observed as negative correlation between precipitation isotopic ratio and rainfall (Fig. 4.5). Amount effect deals with the basic principle of

Rayleigh's isotopic fractionation in which the newly formed condensate is enriched in ^{18}O and re-evaporation of isotopically lighter rain happens at the base of the cloud due to lower humidity. This is prominent is tropical latitudes where the isotopic composition of precipitation is controlled by the amount of rainfall (Dansgaard, 1964). Lekshmy (2015) have shown a negative relation between precipitation isotopic ratio and rainfall in the tropical rainfall from around the globe (Fig. 4.5). This is interpreted as depletion of $\delta^{18}O$ with more rainfall. Dansgaard (1964) has also shown a 1.5‰ change with per 100 mm monthly rain on 14 islands distributed at tropical latitudes.

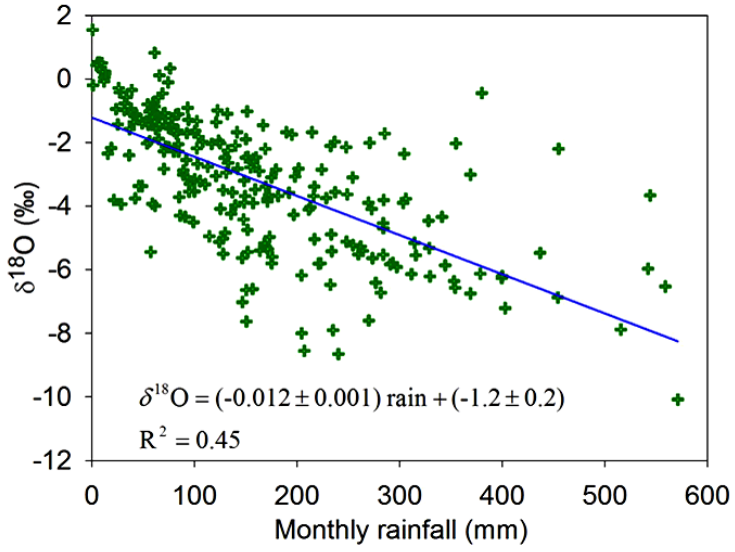

Fig. 4.5. Amount effect shown by $\delta^{18}O$ of tropical rainfall (Ref: Lekshmy, 2015)

4.6.3. Altitude Effect

Altitude effect causes depletion in $\delta^{18}O$ in the rainfall with increase in the latitude. As shown by the GNIP data (Fig. 4.6). This effect has also been reported by Clark and Fritz (2013). Decrease in the temperature favors the conversion increased vapor mass fraction into the precipitation. This can be understood from figure 4.7

given by Yonge *et al* (1989) that depletion is more towards mountain side whereas it is observed to be enriched when moved towards coast.

4.6.4. Continental effect

As the vapor (moist air) move away from the source region (ocean) across a continent, its isotopic composition changes more rapidly due to rainout influenced by topography variations and the extreme temperature characterizing the continental climate. The continental temperatures are associated with strong seasonal variation (Clark and Fritz 2013).

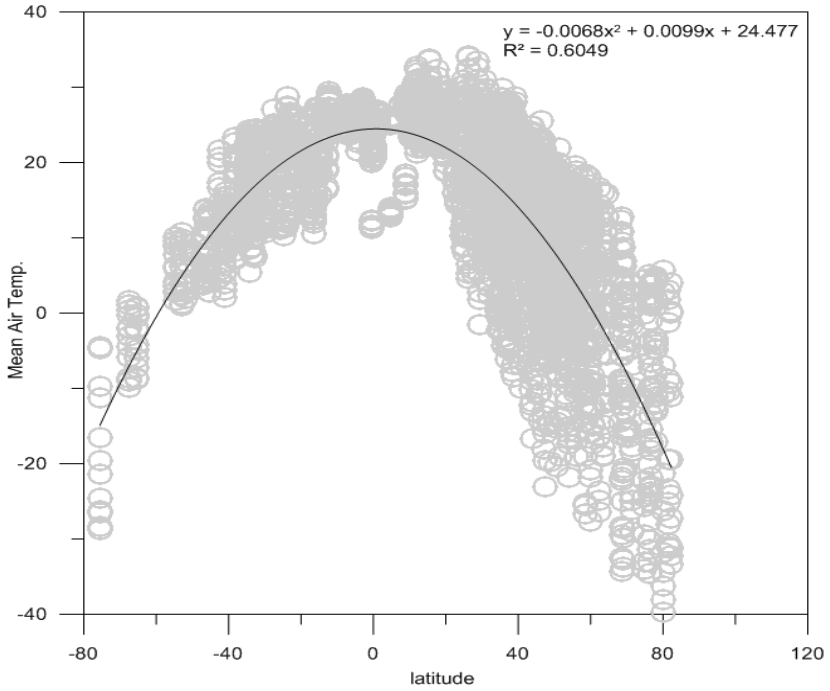

Fig. 4.6. Altitude effect as shown by GNIP data.

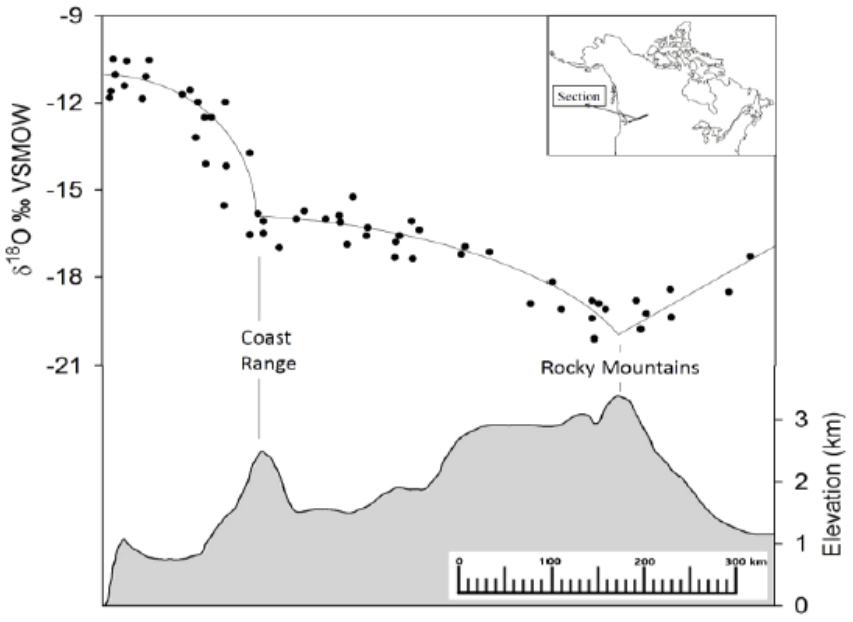

Fig. 4.7. Altitude effect observed in $\delta^{18}O$ in the rainfall (Ref. Yonge *et al*., 1989)

Coastal precipitation is associated with enriched rainfall than the central regions, which are associated with depleted rainfall with strong seasonal differences (Rozanski et al. 1993). While moving coast to inland, the rain has successively depleted 'δ' values. It is called the continental effect.

4.7. Latitudinal variation in rainfall isotopic properties

Dansgaard (1954) investigated the variation of heavy isotopes with latitude and altitude and stated that the fractionation ratio in freshwater decreases with increasing latitude and altitude. A parabolic curve can best describe the latitudinal variation of fractionation ratios $\delta^{2}H$ and $\delta^{2}O$. Rain fall enriched in $\delta^{18}O$ and $\delta^{2}H$ occurs during the winter spring dry season, associated with weather patterns of trade wind orographic showers and frontal systems. These results agree quite well with the global pattern shown by Feng et.al. (2009). As the season changes, the isotopic

composition of rain at any site will reflect two basic changes in the rain pattern. The first is the change of the source characteristic over the ocean due to the seasonal change in ocean temperature and air sea interaction condition affecting the δ-value, primarily. Furthermore, different seasons have different degrees of rain out as dictated by the temperature along the air mass trajectory (which fixes the position along the Rayleigh line).

Enriched concentration of δ^2H and $\delta^{18}O$ were observed during months with less rainfall and depleted concentration of δ^2H and $\delta^{18}O$ correlated with higher precipitation amount. This was called as amount effect by Dansgaard (1964). Rainfall enriched in $\delta^{18}O$ and δ^2H occurs during the winter/spring dry season associated with weather patterns of trade wind orographic showers and frontal system. The isotopic composition of rain is controlled by the temperature of condensation, the isotopic composition of the source vapour, and the length of time the raining air mass spends over the study area, as well as rain drops coalescing and equilibrating isotopically with surrounding vapour during the process of circulation within the cloud and transport to the land surface (Lee & Feng 2008; Rozanski et. al. 1993). Condensation of precipitation at lower temperature (higher in atmosphere) accelerates the removal of the heavier isotopologues from the vapour, with the end result that precipitation of $\delta^{18}O$ and δ^2H values from low temperature condensation are more depleted.

4.7.1. Latitudinal variation of $\delta^{18}O$

A parabolic curve (Fig. 4.8) fits best for the mean $\delta^{18}O$ versus latitude where enriched $\delta^{18}O$ concentration is observed in southern hemisphere when compared to the northern hemisphere. Furthermore, the variability range also is observed higher

towards high latitudes while moving from equator to the higher latitude. Bivariate polynomial correlation between latitude and $\delta^{18}O$ is:

$$\delta^{18}O = -0.0029*(\text{latitude})^{2} - 0.0122*(\text{latitude}) - 2.3077;\ R^2 = 0.55$$

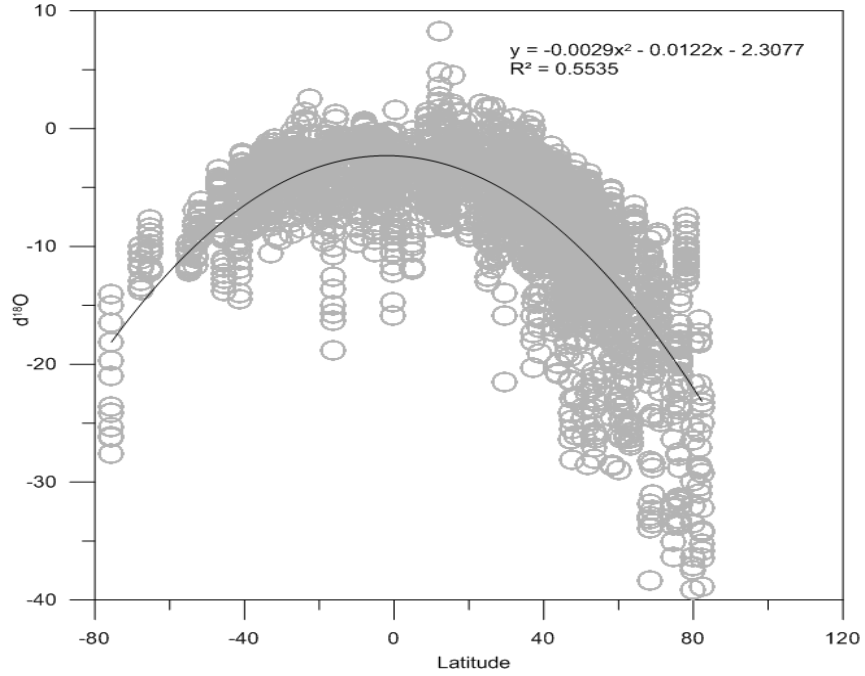

Fig. 4.8. Latitudinal variation of $\delta^{18}O$ in GNIP data.

The enrichment of $\delta^{18}O$ concentration towards southern hemisphere supports the continental effect as northern hemisphere has more land whereas southern hemisphere has more sea. To understand it further, $\delta^{18}O$ concentrations were classified into northern (Fig. 4.9) and southern hemisphere (Fig. 4.10). Latitudinal variation of $\delta^{18}O$ in northern hemisphere shows a R^2 of 0.54 whereas in southern hemisphere, latitudinal variation of $\delta^{18}O$ shows R^2 of 0.47. Continuous depletion in $\delta^{18}O$ concentration from tropics towards pole also supports the amount effect.

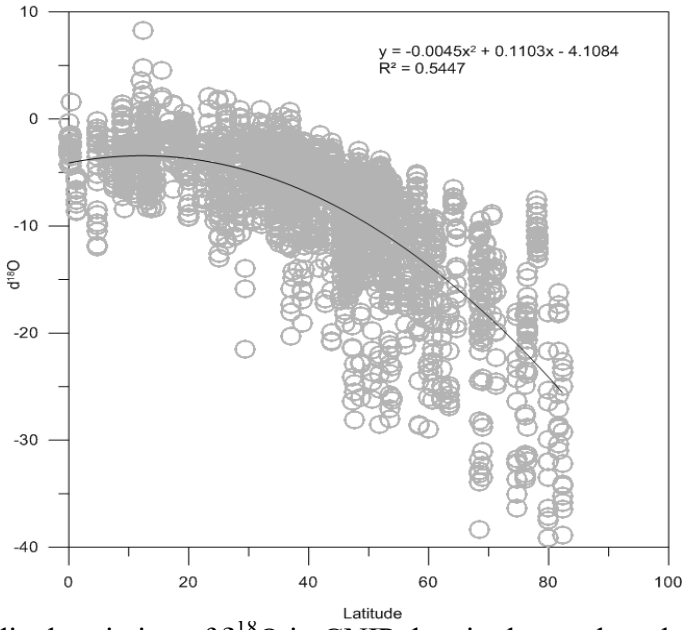

Fig. 4.9. Latitudinal variation of $\delta^{18}O$ in GNIP data in the northern hemisphere

Seasonal $\delta^{18}O$ variability during summer in the southern hemisphere (Fig. 4.11) and northern hemisphere (Fig. 4.12) was also studied to understand the changes in isotopic effects pertaining to $\delta^{18}O$ concentrations. Similarly, it was also studied for winter season in southern (Fig. 4.13) and northern hemisphere (Fig. 4.14). During summer season, better correlation (R^2=0.57) was observed in northern hemisphere when compared to southern hemisphere (R^2=0.35).

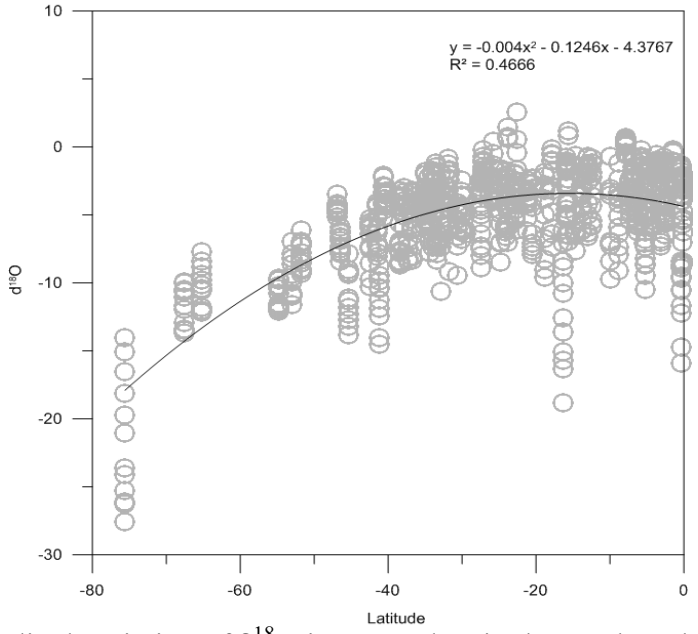

Fig. 4.10. Latitudinal variation of $\delta^{18}O$ in GNIP data in the southern hemisphere

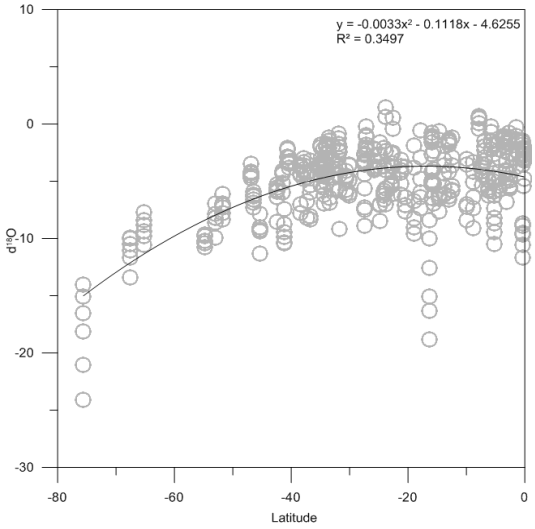

Fig. 4.11. Latitudinal variation of $\delta^{18}O$ in GNIP data in the southern hemisphere during summer

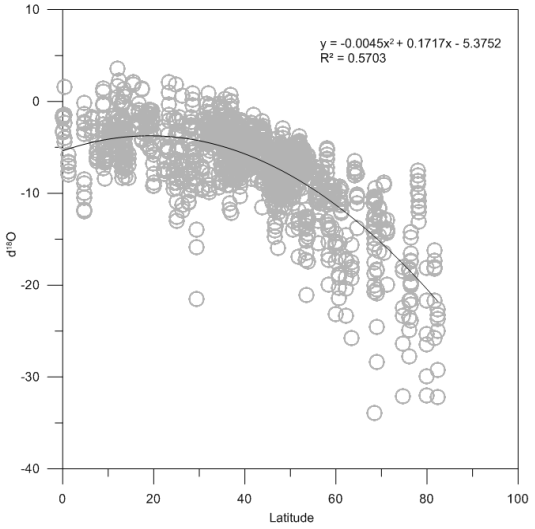

Fig. 4.12. Latitudinal variation of $\delta^{18}O$ in GNIP data in the northern hemisphere during summer

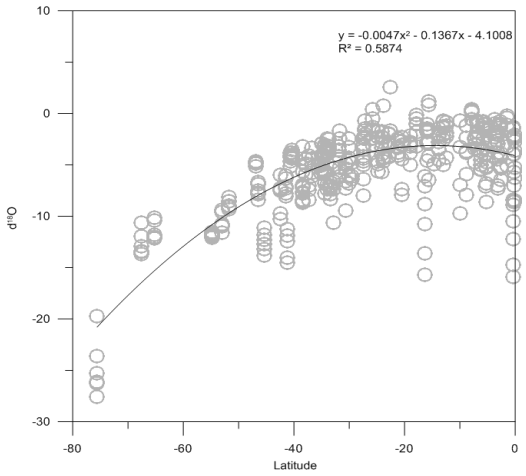

Fig. 4.13. Latitudinal variation of $\delta^{18}O$ in GNIP data in the southern hemisphere during winter.

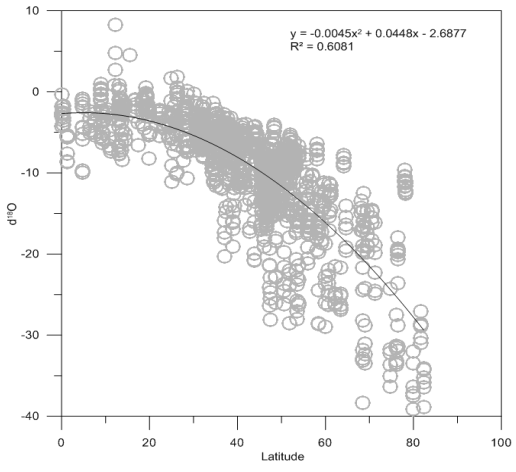

Fig. 4.14. Latitudinal variation of $\delta^{18}O$ in GNIP data in the northern hemisphere during winter.

This provides an understanding that isotopic variability is comparatively less in northern hemisphere than southern hemisphere during summer season. Similar isotopic properties are observed during winter season but with increased correlation such that latitudinal variation in both the hemisphere shows good positive correlation. However, northern hemisphere still hold slightly better correlation (R^2=0.61) than southern hemisphere (R^2=0.59). In other way it can be interpreted that latitudinal $\delta^{18}O$ variability is more consistent during winter season in both the hemispheres. As the frequency and intensity of rainfall during summer is higher, the fractionation and isotopic effects are also higher when compared to winter season giving rise to higher $\delta^{18}O$ variability. Thus, in order to cross validate, $\delta^{18}O$ variability during rainy season was also studied for southern (Fig. 4.15) and northern (Fig. 4.16) hemispheres. The latitudinal variations in the northern hemisphere show very good positive correlation (R^2=0.78) whereas northern hemisphere shows a poor positive correlation (R^2=0.25). This clearly indicate that canonical changes in isotopes due to amount effect,

elevation effect, altitude effects, continental effects, etc., play major role in isotopic variability in northern hemisphere.

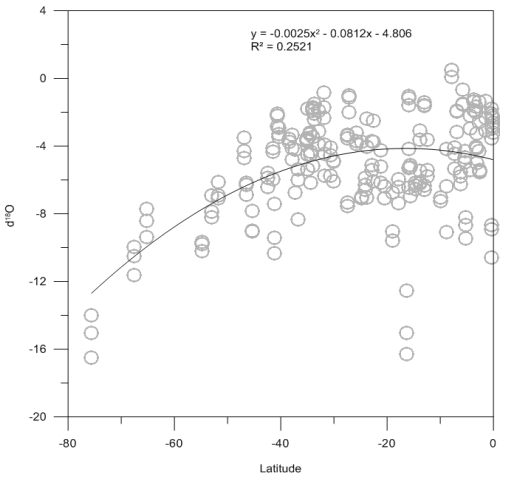

Fig. 4.15. Latitudinal variation of $\delta^{18}O$ in GNIP data in the southern hemisphere during rainy season.

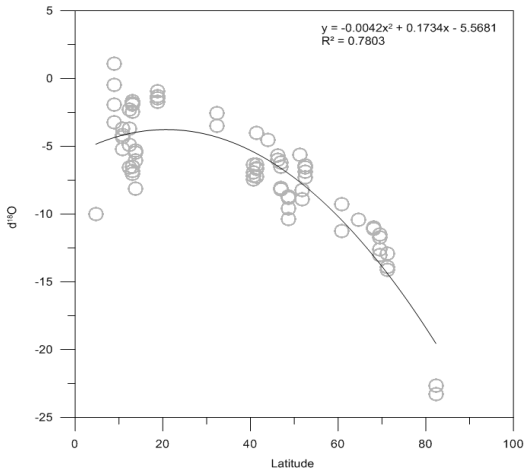

Fig. 4.16. Latitudinal variation of $\delta^{18}O$ in GNIP data in the northern hemisphere during rainy season.

4.7.2. Latitudinal variation of ^{2}H

The mean $\delta^{2}H$ value also varies in similar fashion with latitude like $\delta^{18}O$. A parabolic curve fits best for the mean $\delta^{2}H$ versus latitude having relatively enriched values in southern hemisphere when compared to the northern hemisphere when moving towards poles from tropics. The R^2 value for the curve is 0.55. This plot gives a polynomial equation as:

$$\delta^{2}H = -0.0243*(latitude)^{2} - 0.0874*(latitude) - 8.0553$$

Similar variability of $\delta^{2}H$ as in $\delta^{18}O$ variability was observed in southern (Fig. 4.17) and northern (Fig. 4.18) hemispheres. Almost similar correlation of ^{2}H is observed in both the hemisphere with latitude having R^2 of 0.52 and 0.56 for southern and northern hemispheres, respectively.

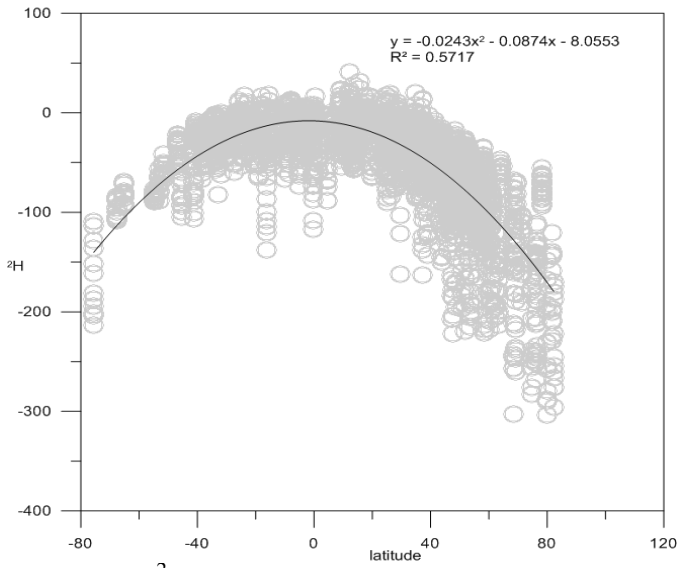

Fig. 4.17. Latitudinal variation of δ^2H in GNIP data.

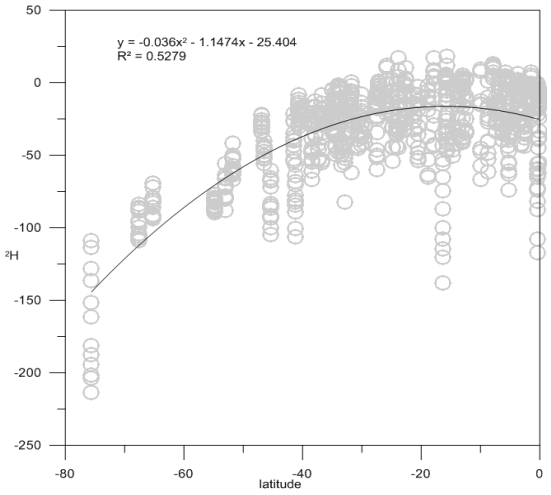

Fig. 4.18. Latitudinal variation of δ^2H in GNIP data of southern hemisphere

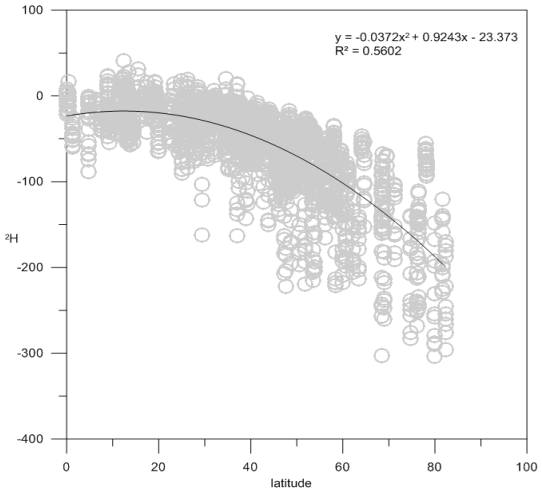

Fig. 4.19. Latitudinal variation of δ^2H in GNIP data of northern hemisphere

During summer season, the correlation between latitude and δ^2H in GNIP data of northern hemisphere (Fig. 4.19) holds better (R^2=0.59) than in the southern hemisphere (Fig. 4.20, R^2=0.43).

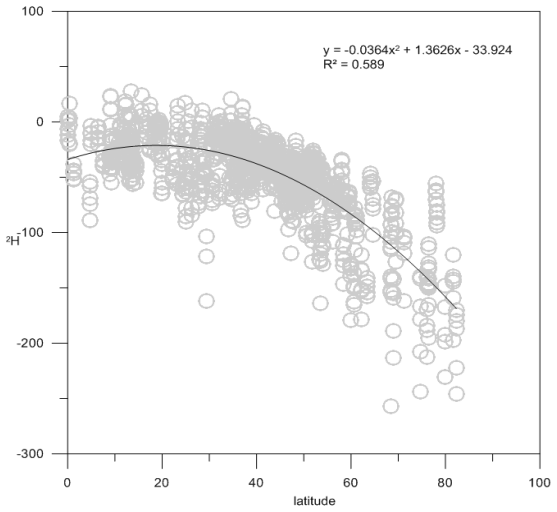

Fig. 4.20. Latitudinal variation of δ^2H in GNIP data of northern hemisphere during summer season.

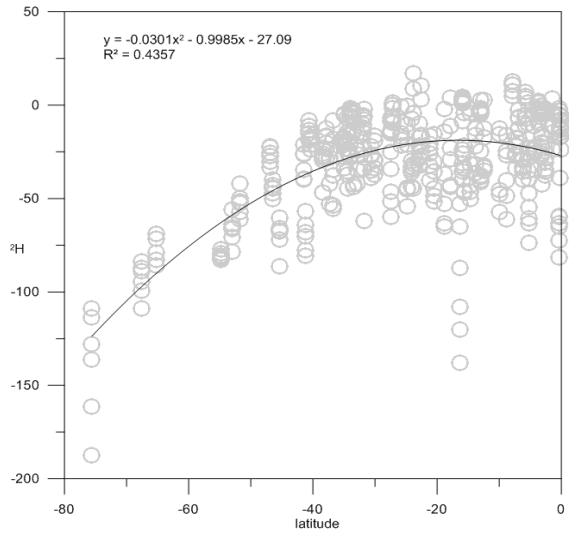

Fig.4.21. Latitudinal variation of δ^2H in GNIP data of northern hemisphere during summer season.

During winter season, the correlation between latitude and δ^2H in GNIP data of northern hemisphere (Fig. 4.21) holds better (R^2=0.61) than in the southern hemisphere (Fig. 4.22, R^2=0.62). δ^2H shows similar nature of variability as of $\delta^{18}O$ during winter.

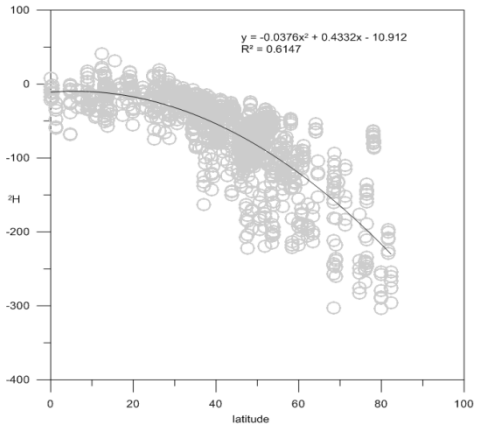

Fig. 4.22. Latitudinal variation of δ^2H in GNIP data of northern hemisphere during winter season.

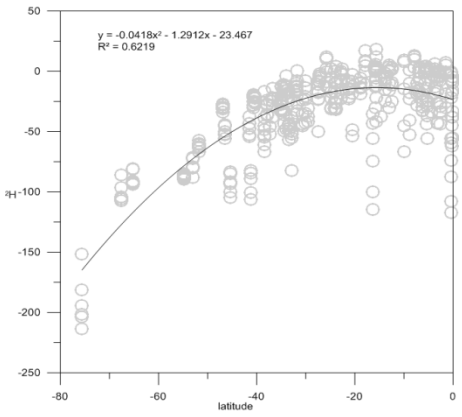

Fig. 4.23. Latitudinal variation of δ^2H in GNIP data of northern hemisphere during winter season.

4.8. Global Meteoric Water Line

Global Meteoric Water Line (GMWL) is defined as the average relation between $\delta^{18}O$ and $\delta^{2}H$ of natural water of land with no excessive evaporation (Craig 1961). The $\delta^{18}O$-$\delta^{2}H$ relation of global precipitation is associated with a slope of 8 which is matches with the ratio of the equilibrium fractionations (at 25°C, Clark and Fritz 2013). Craig (1961) has reported a global precipitation equation as $\delta^{2}H = 8.17 (\pm 0.17) \times \delta^{18}O + 11.27 (\pm 0.5)$. However, water which has evaporated or has mixed with the locally evaporated water, the slope of their $\delta^{18}O$-$\delta^{2}H$ plot shifts off to the meteoric water line, and intersects the GMWL at the point corresponding to the original un-evaporated composition of the water (Merlivat 1978; Gat and Gonfiantini 1981; Rozanski et al. 1993; Clark and Fritz 2013). Records of GNIP data from 3772 GNIP stations provide a GMWL equation as: $\delta^{2}H = 7.9769^{*} \delta^{18}O+9.126$ with a correlation coefficient R^2 of 0.99 (Fig. 4.23). This result is very precise to global meteoric lines obtained by Craig *et al.* (1956) and Rozanski *et al.* (1993).

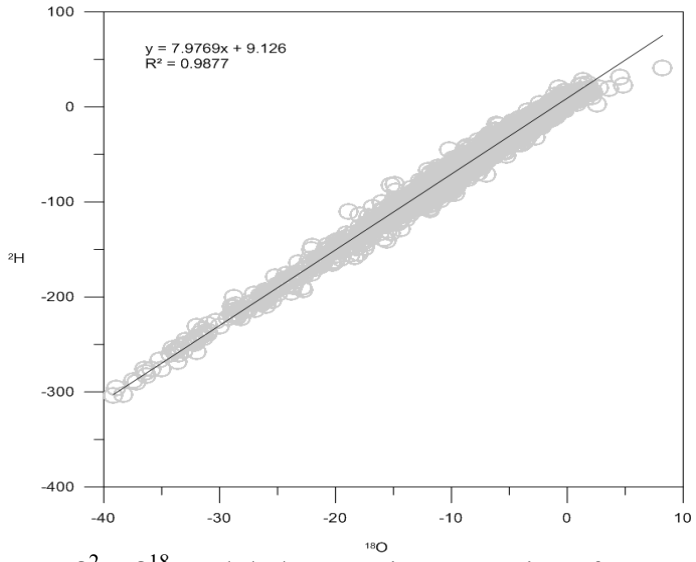

Fig. 4.23. $\delta^{2}H$-$\delta^{18}O$ Global Meteoric Water Line of GNIP data

4.9. Summary

Understanding the controlling factors of the variability of oxygen isotopic ratios ($\delta^{18}O$) of rainfall is of vital importance to interpret of $\delta^{18}O$ derived from climate proxies such as speleothem and foraminifera, etc. This chapter has explained various isotopic effects and fractionations which occur during rainfall using GNIP records from 3772 stations globally. Climatic parameters such as temperature, humidity, atmospheric circulation, etc., affects or change the ratio of heavier to lighter isotope of oxygen atom of the rain water. Chapter provides a clear idea about the interpretation of $\delta^{18}O$ concentration in terms of rainfall. It has also provided a clear picture of latitudinal variation of water isotopologues in northern and southern hemispheres during summer and winter and also during rainy seasons. Parabolic curves fit best for the isotope concentrations with latitude where enriched concentrations are observed in southern hemisphere when compared to the northern hemisphere. The latitudinal variations of isotopologues during the rainy season show very good positive correlations in the northern hemisphere whereas they show poor positive correlation in the southern hemisphere. This indicate that canonical changes in isotopes due to amount effect, elevation effect, altitude effects, continental effects, etc., play major role in isotopic variability in northern hemisphere during rainy season. $\delta^{18}O$ and $\delta^{2}H$ Bivariate plot shows an empirical equation very close to GMWL.

Chapter 5

Indian Monsoon Record from Bay of Bengal during last 46 ka

Chapter 5

Indian Monsoon Record from Bay of Bengal during last 46 ka

5.1. Introduction

The Indian monsoon is the main source for the freshwater of the major river systems in India and neighboring countries which ultimately debouch into the northern Indian Ocean causing seasonal changes in the waters of Upper Ocean. Northern Indian Ocean comprises water masses of Arabian Sea (AS) in the west and Bay of Bengal (BoB) and Andaman Sea (AnS) in the east coasts of the India. Except a few (Indus, Narmada, Tapti, etc. into Arabian Sea), major rivers (viz. Ganga, Brahmaputra, Mahanadi, Godavari, Krishna, Cauvery, etc.) of India, and (Irrawaddy, Salween, Meghna, etc.) of adjacent countries debouch into Bay of Bengal (BoB) with a total water flux of 2.95×10^{12} m^3/year (Sijinkumar *et al.,* 2016; Silva *et al.,* 2017). Annual rainfall over BoB varies between ~1m off the east coast of India to about 3m over the Andaman Islands (reference). The seasonal hydrographic changes are well recorded in the oceanic biota (e.g. planktic foraminifera), which is considered as one of the best proxy to understand the variability of monsoon in the past as they capture the seasonal oceanic changes in the shells during their growth.

Several workers have used planktic foraminifera from Arabian Sea (AS)and reconstructed the Indian paleomonsoon(For ex.,Sirocko *et al.,* 1993;Overpeck *et al.,* 1996; Naidu and Malmgren, 1996; Sarkar *et al.,* 2000; Gupta *et al.,* 2003; Anand *et al.,* 2008; Ramesh *et al.,* 2010; Singh *et al.,* 2010; Tiwari *et al.,* 2005, 2010; Govil

and Naidu., 2010; Naidu *et al.,* 1999, 2011; Saraswat *et al.,* 2013; Partin *et al.,* 2015; Singh *et al.,* 2016). Similarly, a few studies on foraminiferal species from BoB and AnS have also been carried out to reconstruct the monsoon system (Cullen *et al.,* 1981; Naidu *et al.,* 1999; Kudrass *et al.,* 2001; Rashid *et al.,* 2007, 2011; Govil and Naidu, 2011; Ahmad *et al.,* 2012; Raza *et al.,* 2014; Sijinkumar *et al.,* 2016; Gebregiorgis *et al.,* 2016; Silva *et al.,* 2017; Kumar *et al.,* 2018). However, the studies from BoB are scanty as compared to AS and the available literature warrants more attention and further studies as BoB witnesses the extreme hydrographic changes throughout the year because of large amount of freshwater influx and stratification. Although there are a few studies on the reconstruction of paleomonsoon employing $\delta^{18}O$ records of foraminifera species from BoB, but the relative differences of isotopic signatures from the near-surface dwelling and mixed layer depth (MLD) dwelling planktic foraminifera have not been studied for paleoceanographic implications. The study on relative differences of the isotopic signatures from different habitats within upper ocean water provides clues to the past changes in its stratification (e.g., Singh *et al.,* 2016; Kumar *et al.,* 2018).

While the surface water of BoB is known for fresh water induced changes, MLD is characterized by nearly homogenous nature resulting from intense mixing in the upper ocean by heat, momentum and freshwater flux (Narvekar and Prasanna Kumar, 2014). This mixed layer regulates the air-sea exchange process by mass and energy transfer in association with convection and cyclone genesis. The physical and chemical changes occurring in the mixed layer also modulates the oceanic productivity. In tropical Ocean, the structure and variability of mixed layer largely

depends on the regional oceanographic characteristics and atmospheric forcing (Narvekar and Prasanna Kumar, 2014).

The mixed layer during southwest monsoon (SWM, June-August) is observed as the deepest, and with the progress of SWM from June to August the mixed layer becomes deeper in most parts of the Bay of Bengal. However, along the western boundary and in the northern and eastern parts of the BoB the MLD remains shallow. During the northeast monsoon (NEM), deep MLD (30–40 m) is observed all over the Bay of Bengal except in the northern and eastern parts (Narvekar and Prasanna Kumar, 2014). Since, the hydrographic variability in the upper ocean is observed to be large when compared to the deeper portion in space and time, and, therefore, BoB is considered as an important region for climatic studies (Narvekar and Prasanna Kumar, 2014).

5.2. Foraminiferal Species

Two distinct planktic foraminiferal species – *Globigerina bulloides* and *Orbulina universa* – dwelling in surface and mixed layer water depths, have been studied. The two species exhibit distinct morphological characteristics and isotopic concentrations. Add some more information on these two species

This chapter discusses how these two species and their isotopic compositions can be used as paleoclimate proxies, and particularly to infer Indian monsoon, in the southwestern Bay of Bengal region. The main approach of this chapter was to test the sensitivity of monsoon induced near-surface and mixed layer depth hydrographic variability and to infer the causative processes responsible for the changes occurred in the upper ocean stratification, using $\delta^{18}O$ and $\delta^{13}C$ records of *Globigerina bulloides*

(near-surface dwelling) and *Orbulina universa,* (MLD dwelling), spanning for the last 46 ka BP. Further, correlation of $\delta^{18}O$ and $\delta^{13}C$ time series with the solar insolation and north Atlantic climatic changes have been done along with coupled regional ocean-atmospheric forcing, which have an integrated control over the Indian monsoon system.

5.3. AMS Radiocarbon chronology and sedimentation rates

Radiocarbon ages and an interpolated age model developed using six AMS radiocarbon ages are shown in Table 5.1 and Figure 5.1. Sedimentation rates, based on the age-depth model (Fig. 5.1), at the core location reveal that the top 6 cm (~1.1- ~5.1 ka BP) of the core was deposited at a rate of ~6.5 cm/kyr, whereas from 6 – 20cmdepth (i.e., ~5.1- ~10.7 ka BP) the sedimentation rate is recorded as ~5.8 cm/kyr. The sedimentation rate from 20 to 58 cm (i.e., between ~10.7- ~11.7 ka BP) of the core is ~12.3 cm/kyr. Further, the sedimentation rate of ~6.9 cm/kyr was estimated for the core from 58 to 104 cm length (i.e., during ~11.7- ~34.5 ka BP). Sedimentation rate of ~7.4 cm/kyr was estimated for the core between 104cm to 340 cm (~34.5-~46 ka BP). The results reveal that the sediment accumulation rate was higher during the early Holocene.

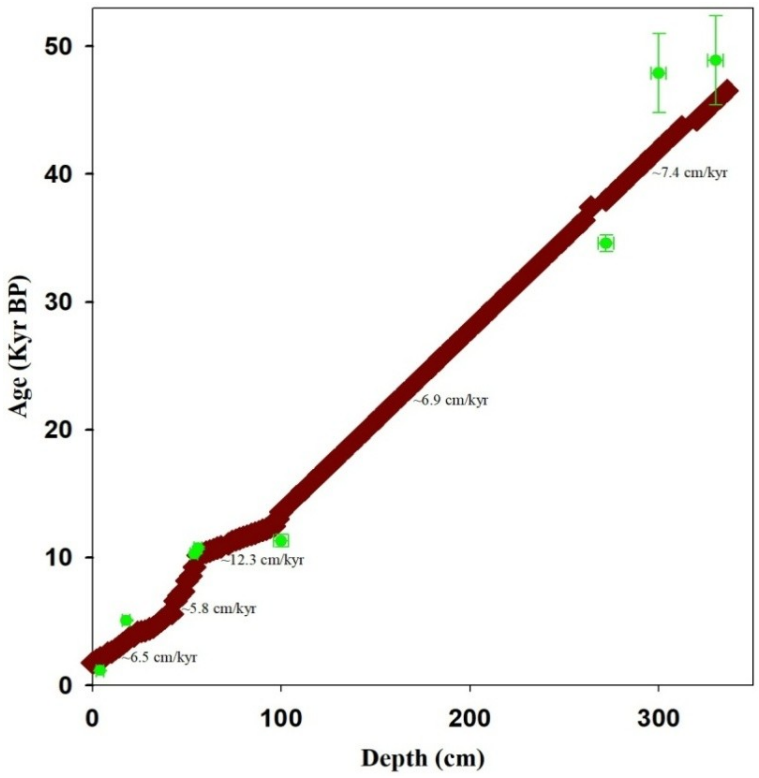

Fig. 5.1. Age-Depth Model. An interpolated age-depth model (maroon array/line) was prepared for 340 cm long SK-170/2 marine core recovered from Bay of Bengal using six calibrated AMS ages using marine09 Radiocarbon calibration program (Stuvier and Riemer, 2009) out of eight (green points with their errors) AMS radiocarbon ages.

Table 5.1. Radiocarbon and calibrated ages of eight samples of mixed planktic foraminifera for core SK-170/2 collected from southwestern BoB. Conversion to calendar years ages was performed using marine09 (Stuvier and Riemer, 2009).

Depth (cm)	Lab Code (AA#)	^{14}C age (yrs)	1σ Error (yrs)	Calibrated ^{14}C age (yrs)
4-6	AA92478	1132	±37	1,237-1,299
18-20	AA92479	5059	±44	3,509-3,380
54-56	AA92480	10269	±46	9,330-9,244
56-58	AA92494	10728	±99	10,370-10,002
100-104	AA92495	11698	±48	11,296-11,183
272-276	AA92481	34590	±650	38,288-36,543
300-304	AA92483	47900*	±3100	--
330-334	AA92485	48900*	±3500	--

*Ages could not be calibrated due to Radiocarbon age limits.

5.4. Isotopic variability

$\delta^{18}O$ variability

The $\delta^{18}O$ values in *Globigerina bulloides* vary between -2.86‰ and -0.52‰, with respect to VPDB, with an average of -1.89‰ (n=107; Fig.5.2). Similarly, $\delta^{18}O$ variability in *Orbulina universa* ranges from-3.60‰ to -0.37‰ with an average of -1.70‰ (n=106). Further, the $\delta^{18}O$ variability during MIS-1, MIS-2, and MIS-3 has been observed separately. The measured minimum, maximum and average values of $\delta^{18}O$ in *Globigerina bulloides* during MIS-1(n=42) are recorded as -2.38‰, -0.52‰, and -1.69‰, and in *Orbulina universa* the minimum, maximum and average values recorded are -3.60‰, -0.37‰, and -1.70‰, respectively. During MIS-2 a minimum, maximum and average $\delta^{18}O$ values recorded in *Globigerina bulloides* (n=38) are-2.86‰, -0.92‰, and -1.96‰, respectively. Similarly, $\delta^{18}O$ records of *Orbulina universa* show minimum, maximum and average values of 2.27‰, -0.37‰, and -0.98‰ respectively. *Globigerina bulloides* in bottom portion of the core with a radiocarbon age of ~46ka which forms a part of MIS-3, records $\delta^{18}O$ values (n=27) of -2.81‰, -1.25‰, and -2.08‰, in *Globigerina bulloides* as minimum, maximum and average concentrations, respectively. Similarly, *Orbulina universa* (n=26) exhibit the minimum, maximum and average $\delta^{18}O$ values as -2.79‰, -0.86‰, and -1.81‰, respectively.

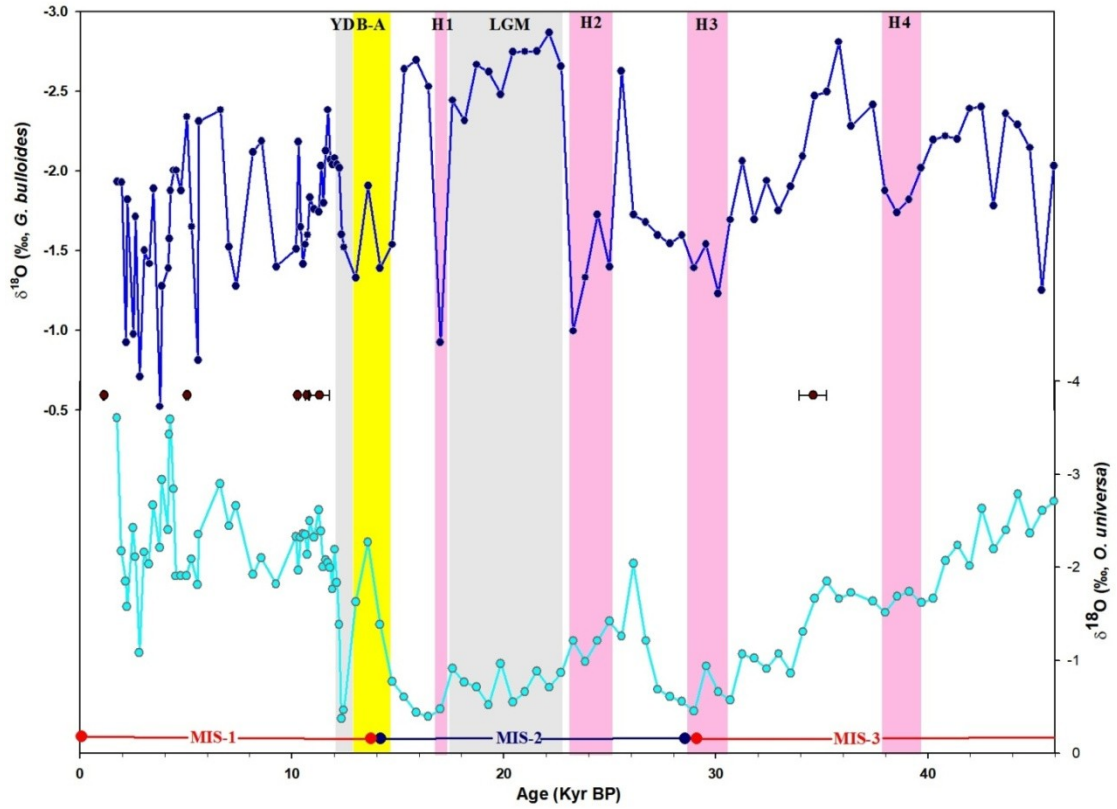

Fig. 5.2. $\delta^{18}O$ variability record. $\delta^{18}O$ variability record of planktic foraminifera *Globigerina bulloides* (blue) and *Orbulina universa* (cyan)obtained from core SK-170/2 recovered from southwestern Bay of Bengal.

$\delta^{13}C$ variability

$\delta^{13}C$ values, with respect to VPDB, in *Globigerina bulloides* vary between -4.55‰ and -3.97‰ with an average of -0.41‰ (n=107, Fig.5.3). Similarly, $\delta^{13}C$ variability in *Orbulina universa* ranges from -1.85‰ to 3.14‰ with an average value of 2.04‰ (n=106). The minimum, maximum, and average $\delta^{13}C$ values in *Globigerina bulloides* during MIS-1 (n=42) are recorded to be -0.11‰, 2.12‰ and 1.08‰, respectively. In the case of *Orbulina universa*, the minimum, maximum, and average $\delta^{13}C$ values were recorded as -1.54‰, 2.81‰, and 1.79‰, respectively. During MIS-2, *Globigerina bulloides* (n=38) recorded the minimum, maximum, and average $\delta^{13}C$ values as -4.55‰, 2.15‰, and -1.48‰ while *Orbulina universa* recorded as 1.00‰,

3.14‰, 2.44‰, respectively. The minimum, maximum and mean $\delta^{13}C$ values recorded in *Globigerina bulloides (n=27)* at the bottom part of the core (^{14}C age 46ka; MIS-3), are -1.65‰, 3.97‰, and -1.21‰, respectively; whereas in *Orbulina universa* $\delta^{13}C$ values (n=26) are -1.85‰, 3.06‰ and 1.85‰, respectively.

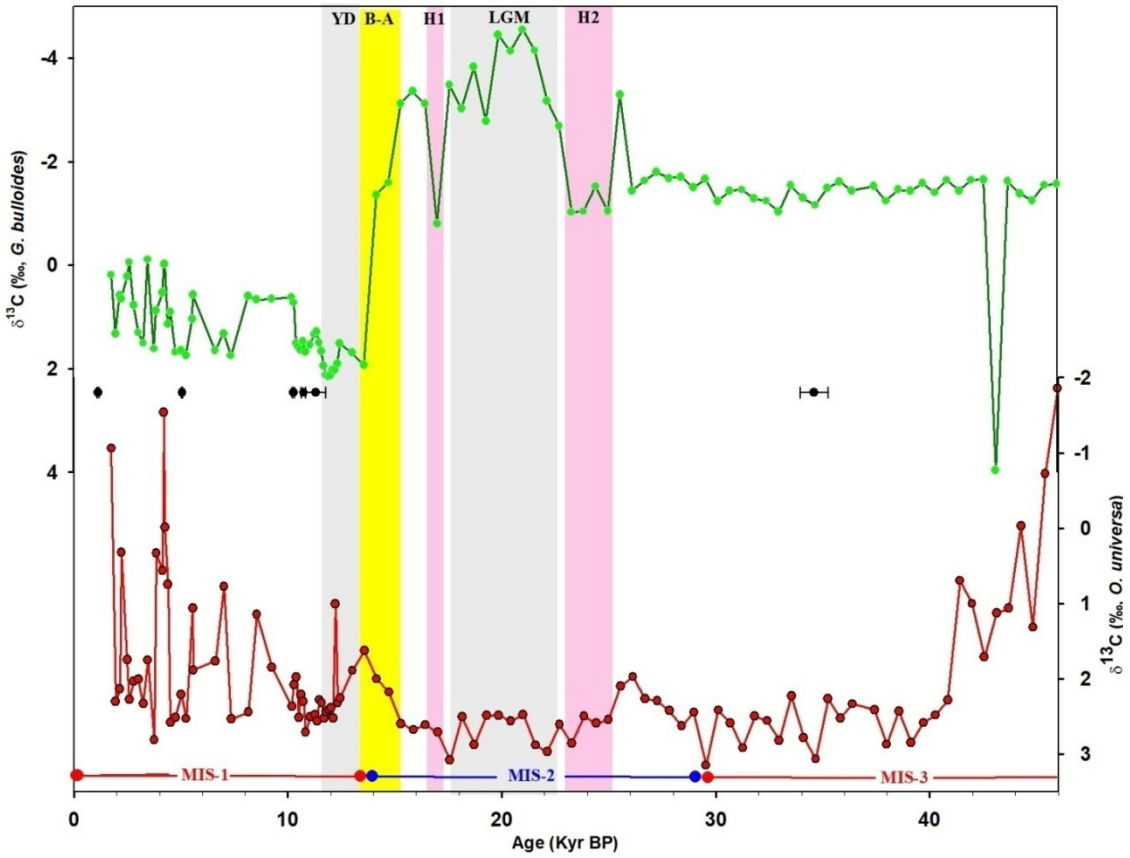

Fig. 5.3. $\delta^{13}C$ variability record. $\delta^{13}C$ variability record of planktic foraminifera *Globigerina bulloides*(Green) and *Orbulina universa* (red)obtained from core SK-170/2 recovered from southwestern Bay of Bengal.

5.5. Inferences from $\delta^{18}O$ and $\delta^{13}C$ variability

$\delta^{18}O$ and $\delta^{13}C$ variability in planktic foraminifera is not strictly governed by any thumb rule and, therefore, it can be inferred in many ways. Further, $\delta^{18}O$ of foraminiferal shell is interpreted as a function of the isotopic composition of the

ambient sea water besides its water temperature at which the calcification of the species takes place (Tiwari *et al.,* 2015). Hence, the isotopic composition of the shells can be used in reconstructing sea water temperature, if the shells have not undergone post depositional alteration (Niebler *et al.,* 1999; Birch *et al.,* 2013). Thus, $\delta^{18}O$ and $\delta^{13}C$ variability from species of different depth habitats can help in reconstructing the past oceanic thermal stratification (Birch *et al.,* 2013). Planktic foraminifera *Globigerina bulloides* dwells 0-50 m depth habitat and exhibits isotopic imprints of changes in near-surface water of the core location (Fairbanks et al., 1982). Therefore, it is interpreted that the downcore $\delta^{18}O$ variability in *Globigerina bulloides* as reflection of changes happening at the locale occurring mainly due to the NEM as the southwestern BoB receives most of the rainfall during NEM season. Based on $\delta^{18}O$-D studies of ocean surface waters over 10˚ N - 10˚ S latitudes of BOB, Achyutan *et al.* (2013) suggest that there was no direct rainfall or river influx in the vicinity of the core location during SWM. Similarly, a strong correlation between $\delta^{18}O$ and salinity (S), particularly during the winter, in surface waters of the BoB was observed (Kumar *et al.,* 2018). Mixed layer (50-200 m) dwelling planktic foraminifer *Orbulina universa* indicates rather more complex process as it experiences the consequent changes produced due to disturbances from coastally trapped and remotely forced currents (Narvekar and Prasanna Kumar, 2014). The $\delta^{18}O$ record of *Orbulina universa* indicates the reflection of changes occurring due to remotely forced currents and hence reflecting the regional aspects. Changes in the SWM (dominant Indian monsoon component) are directly linked to the changes occurred at regional scale, therefore, it is correlated with $\delta^{18}O$ variability of *Orbulina universa* as the reflection of changes in the SWM intensity. Therefore, the downcore variability of $\delta^{18}O$ records

of the two species can help us in understanding the temporal changes with respect to fresh water induced stratification in the southwestern BoB. Surface waters are generally observed to be enriched in ^{13}C when compared to the deeper subsurface water due to photosynthesis processes where ^{12}C is preferentially utilized in the formation of organic matter (Broecker and Peng, 1982). During upwelling, the stratification of the water column is disturbed and surface water receives cold and nutrient rich waters. Upwelling indicator *Globigerina bulloides*, calcified in upwelling waters, will have lower $\delta^{13}C$ because upwelling brings nutrient-rich and depleted $\delta^{13}C$ waters to the surface (Curry *et al.,* 1992; Naidu and Niitsuma, 2004). Naidu and Niitsuma (2004) have also suggested that a combination of higher calcification of *Globigerina bulloides* in the nutrient-rich waters and respired CO_2 would lead to the more negative $\delta^{13}C$. Hence, it is inferred that a depleted $\delta^{13}C$ value due to the consequence of disturbed stratification and enhanced upwelling along with respired CO_2, whereas enriched $\delta^{13}C$ corresponds to increased photosynthetic process when the ^{12}C brought by upwelling was too low for the fixation of ^{12}C by photosynthesis causing increased productivity. The high productivity in southwestern BoB is also correlated to cyclonic eddies as no evidence of upwelling was observed from the records during MIS- 2 and MIS-3, respectively. Hence, eddy pumping can be the potential mechanism for vertical transfer of nutrients (Prasanna Kumar *et. al.,* 2004) during MIS-1 and MIS-3 as the stratification was observed to be highest.

5.6. Upper ocean water hydrographic changes

The difference in $\delta^{18}O$ ($\Delta\delta^{18}O$*bulloides-universa*) and $\delta^{13}C$ concentrations of two planktic foraminifera *Globigerina bulloides* and *Orbulina universa* show large

isotopic differences between the water columns from surface to the mixed layer depth, respectively for the last 46 ka (Fig. 5.2 and 5.3). The variable records of $\delta^{18}O$ clearly reflect the convergence of water masses during MIS-1 ($\Delta\delta^{18}O$*bulloides-universa*= 0.1‰) and divergence ($\Delta\delta^{18}O$*bulloides-universa* = 2.94‰) during MIS-2. This $\delta^{18}O$ convergence-divergence suggests that the intensity of Indian monsoon in southwestern BoB was significantly different during MIS-1 and MIS-2, and is observed to be strongest during MIS-1 and weakest during MIS-2. Isotopic records further show that the Indian monsoon during MIS-3 ($\Delta\delta^{18}O$*bulloides-universa* = 0.27‰) was stronger than during MIS-2 but weaker than MIS-1. Therefore, the degree of divergence indicates relatively shallow and deep MLD during MIS-1 and MIS-2 respectively. Similarly, the MLD during MIS-3 was shallower than during the MIS-2 but deeper than MIS-1. This trend of stratification is also supported by the significant changes in $\delta^{13}C$ record with a sharp enrichment of ~2‰ at the onset of MIS-1 and depletion of ~1.2‰ at the onset of the last glacial maximum (LGM). Most enriched $\delta^{13}C$ concentrations of *Globigerina bulloides* during MIS-1 clearly indicate intense stratification such that upwelling was least as it received maximum solar energy resulting in enhanced productivity. On the contrary, MIS-2 indicates weakest stratification and nutrient rich cold water with depleted $\delta^{13}C$ supply was more to the surface water with the involvement of respired CO_2. Govil and Naidu (2010) also have shown that the productivity in the AS and BoB was higher during the interglacial than in glacial periods. Similarly, a moderate $\delta^{13}C$value during MIS-3 also supports the fact that MIS-3 was associated with higher productivity than MIS-2 but lower than MIS-1. Although optimum shell size range were selected where the disequilibrium reaches minima, the $\delta^{13}C$ record of *Orbulina universa* may still have

some effects of disequilibrium. Hence, *Orbulina universa* $\delta^{13}C$ may be imprecise to infer productivity in the mixed layer depth. Apart from photosynthesis and upwelling, other oceanic processes like cyclonic eddies may also have been responsible for surficial nutrient supply to the surface waters of BoB. Prasanna Kumar *et al*. (2004) identified cold-core eddies in the BoB and proposed eddy-pumping as a possible mechanism of vertical transfer of nutrients across the halocline to the oligotrophic euphotic zone during summer monsoon, when the upper ocean is highly stratified. This cold-core eddy was found to enhance the biological productivity by more than double. It is evident that cyclonic eddies exist and enhance biological productivity of the Bay of Bengal, not only in summer monsoon (Prasanna Kumar et al., 2004) but also in fall and spring inter-monsoons (Prasanna Kumar *et al.,* 2007). Though the surface chlorophyll concentrations as retrieved by satellite remote sensing may be perennially low, these cyclonic eddies, which appear to be ubiquitous in the Bay of Bengal, enhance biological productivity by 1.5 to 2 times its ambient value through eddy-pumping of nutrients. This has an overall implication for the basin-wide new production and export flux (Prasanna Kumar *et al.,* 2007). Therefore, it is attempted to correlate the cyclonic eddies as one of the main agents of the upper ocean changes in southwestern BoB during MIS-1 and MIS-3 when there was no upwelling as inferred from the records. In this regard, monthly means of sea surface height anomaly record for the year 1992-2013 using altimeter data (which is a combination of TOPEX Poseidon, ERS, and Jason1 satellite altimeter obtained from AVISO having a resolution of 1/3rd of degree) was analysed. The monthly means of sea surface height anomaly for the months of November (Fig. 5.4A), December (Fig. 5.4B), January (Fig. 5.4C), and composites of the months November, December,

January, and February (Fig. 5.4D) reveal that the core location lies in the region of cyclonic circulation pointing the persistence of cyclonic eddies. Cyclonic eddies have been observed to be potential mechanism of vertical transportation of nutrients. Hence, it is inferred that the nutrient supply in the southwestern BoB may be associated with cyclonic eddies too especially during the MIS-1 and MIS-3 when there was no or poor upwelling. The monthly mean composites (Fig. 6D) also suggest that the southward movement of East India Coastal Currents (EICC) aided with local alongshore winds create a window of cold and nutrient rich water upwelling by removing the blanket of surficial water. In this context, Keerthi *et al.*, (2012) also have linked interannual variability of the mixed layer tropical Indian Ocean to eddy and in situ hydrographic conditions. Further, Sree Lekha *et al.,* (2018) have suggested that the meso-scale eddies and Ekman transport likely plays a role in the export of freshwater from the coastal margins into the interior basin.

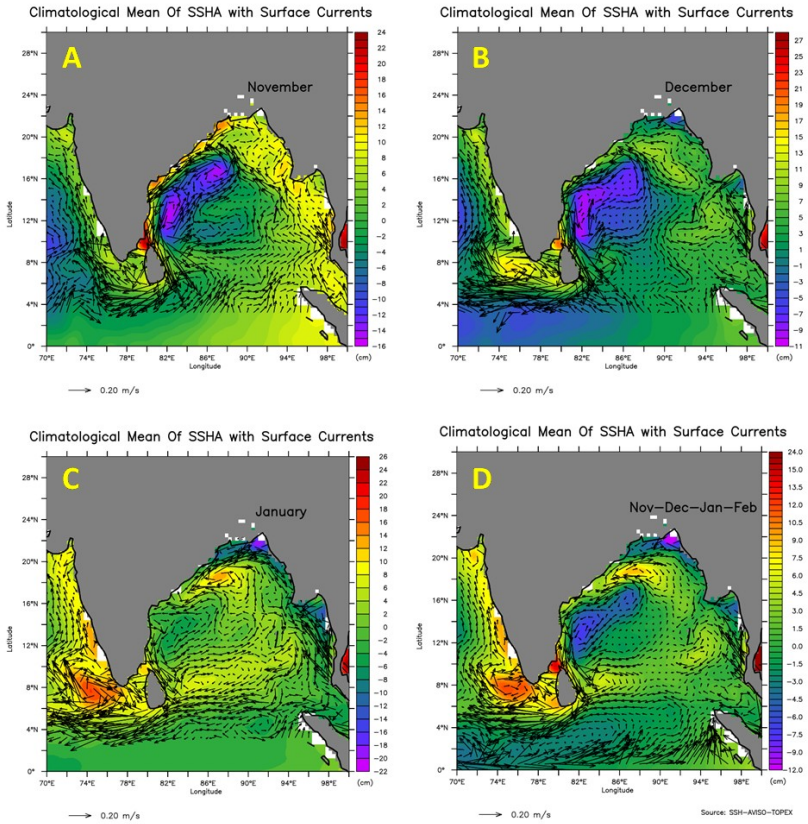

Fig. 5.4.Climatological Mean of sea surface height anomaly (SSHA) with surface currents. The monthly mean during November (A), December (B), January (C), and monthly mean composite of the months November, December, January, and February (D) of sea surface height anomaly record for the year 1992-2013 using altimeter data (which is a combination of TOPEX Poseidon, ERS, and Jason1 satellite altimeter) obtained from AVISO having a resolution of 1/3rd of a degree. (Source of data: Prasanna Kumar, NIO).

5.7. Indian Monsoon variability during MIS-1

The $\delta^{18}O$ record of *Globigerina bulloides* and *Orbulina universa* show a significant variability (Fig. Fig.5.2) with a major shift of 1.7‰ from LGM to the onset of MIS-1 or Holocene in *Orbulina universa* is clearly observed. Similar $\delta^{18}O$ amplitude shifts have also been reported from the BoB and AnS (Duplessey, 1982; Ahmad *et al.,* 2008; Raza *et al.,* 2014., Kumar *et al.,* 2018). Schrag *et al.* (1996) have substantiated ~1‰ of this shift due to ice-volume effect during Glacial to Holocene transition. Hence, subtracting 1‰ (from 1.7‰ of change in shift from LGM to

Holocene), the remaining 0.7‰ represents salinity function of local changes, where the local changes are the ratio of difference of evaporation (E) and precipitation (P) to surface runoff induced salinity at the core location (Kumar *et al.,* 2018). However, Cullen (1981) has demonstrated that sea surface salinity in the southern BoB during LGM may have been similar or slightly higher to modern salinity. Hence, it is considered that the 0.7 ‰ change, mainly due to E-P factor, makes surface water cooler by ~3˚C. Most depleted $\delta^{18}O$ during MIS-1 as recorded in *Orbulina universa* suggests intense SWM and a very wet period. However, an opposite trend with large shifts in $\delta^{18}O$ records of *Globigerina bulloides* is observed (Fig.5.2). It is understood that during onset of the Holocene the SWM strengthened and NEM was subdued. The $\delta^{18}O$ records of *Orbulina universa* and *Globigerina bulloides* show supportive evidences for SWM and NEM variability, respectively. The $\delta^{18}O$ records are observed to be similar in variability with other previously reported records from the BoB and AnS (Kudrass *et al.,* 2001; Rashid *et al.,* 2011; Raza *et al.,* 2014; Sijinkumar *et al.,* 2016; Silva *et al.,* 2017; Grebgroiges *et al.,* 2016; Kumar *et al.,*2018) and Arabian Sea (Naidu *et al.,*1996; Fleitmann *et al.,* 2003; Gupta *et al.,* 2003; Tiwari *et al.,* 2005; Anand *et al.,*2008; Kumar and Ramesh, 2015).

Further, $\delta^{18}O$ enrichment in *Orbulina universa* during ~9.2-8.1 cal kyr BP, ~5.5-4.5 cal kyr BP, and ~2.8 cal kyr BP and corresponding depletion in $\delta^{18}O$ records of *Globigerina bulloides* during ~8.5-8.1 cal kyr BP and ~5.0-4.2 cal kyr BP are clearly observed (Fig.5.2). The $\delta^{18}O$ record of *Orbulina universa* clearly exhibits comparatively higher depletion corresponding to strengthened SWM in early Holocene than during the late Holocene. The $\delta^{18}O$ values of *Globigerina bulloides* also compliment the *Orbulina universa* $\delta^{18}O$ variability record in which enriched

$\delta^{18}O$ during the early Holocene (weak NEM) and depleted $\delta^{18}O$ values (enhanced NEM) during the late Holocene are noted. The $\delta^{18}O$ enrichment during ~9.2-8.1 kyr in the study may be correlated with the ~8.2 kyr event reported from GISP2 ice core $\delta^{18}O$ record with significant temperature anomaly (Alley and Agustsdottir, 2005). During ~8.2 kyr event, cooling of approximately 6˚C in the Northern Hemisphere region has been estimated which may be similar to 5˚C cooling during the Heinrich events (Bard et al., 2000) and slightly smaller than the YD event of ~8˚C cooling (Dansgaard *et al.,* 1989). These cooling events are often related to melt water outflows into the North Atlantic Ocean and slowdowns of the Atlantic meridional oceanic circulation (AMOC; Alley and Agustsdottir, 2005). Similarly, ~5.5-4.5 cal kyr BP is correlated with $\delta^{18}O$ enrichment to ~4.2 kyr cooling event (Weiss *et al.,* 1993; Staubwasser *et al.,* 2003; Booth *et al.,* 2005) which is considered as the episode of weak monsoon (Kathayat *et al.,* 2016). The severe drought caused by this extreme climate event covered widespread areas from East Africa through the subcontinent of India and the Tibetan Plateau (Berkelhammer *et al.,* 2012) and eastward i.e., towards southeastern China (Wu and Liu, 2004). At approximately the same time, many civilizations (for ex., Harappan, Mesopotamian, etc.) around the globe witnessed their decline (Weiss *et al.,* 1993; Staubwasser *et al.,* 2003; Rashid *et al.,* 2011;Berkelhammer *et al.,* 2012).

The 4.2 ka event has also been discussed by various researchers through their high resolution stalagmite records (Yadava and Ramesh, 2005; Kathayat *et al.,* 2016; Band *et al.,* 2018; Dutt *et al.,* 2018), and several potential factors pointing to this event have been advocated employing relevant time series data such as reduced solar activity (Bond *et al.,* 2001; Müller *et al.,* 2006), changes in the thermohaline

circulation (Bianchi and McCave, 1999; Hong *et al.,* 2003), neo-glacial glacier advances (Wanner *et al.,* 2011), El Niño activity (Moy *et al.,* 2002). It is inferred that the rapid changes during MIS-1 may be the result of convergent factors of North Atlantic climate changes along with coupled ocean-atmospheric processes, which caused the abrupt climate shift towards an interglacial phase. These inferences are also supported by enriched $\delta^{13}C$ records of *Globigerina bulloides* during MIS-1 (Fig.5.3), and abrupt and persistent enrichment up to ~2.3‰ after Bølling-Allerød (B-A) event. This remarkable enrichment of $\delta^{13}C$ during MIS-1 may be the result of enhanced photosynthesis in the upper photic zone due to increased solar energy during the Holocene. The interpretation of the carbon isotopic composition proved to be more complicated than $\delta^{18}O$. Due to the preferential fixation of $^{12}CO_2$, by primary producers and subsequent transport and decomposition of organic matter below the euphotic zone, surface waters of the ocean are depleted in ^{12}C whereas the deeper ocean is ^{12}C-enriched. Thus, as a consequence of community production and respiration, $\delta^{13}C$ depth profiles are related to the oxygen concentration and inversely correlated with the nutrient concentration (Broecker and Peng 1982). Hence the $\delta^{13}C$ of surface dwelling foraminifers is used as a surface water fertility proxy (Bijma et al., 1999). The enrichment of $\delta^{13}C$ in both the studied species (*bulloides and universa*) during the early Holocene, whereas slightly depleted $\delta^{13}C$ during mid- and late- Holocene also suggest that the high productivity during the early Holocene was due to the onset of interglacial stage with enhanced photosynthesis and productivity. However, the modulations in SWM intensity have affected the productivity as observed minor shifts during the middle, and late Holocene.

5.8. Indian Monsoon variability during MIS-2

Indian monsoon record shows abrupt shifts during MIS-2 including the LGM, Heinrich event 1 (H1), Heinrich event 2 (H2), Bølling-Allerød (B-A) and Younger Dryas (YD). This is clearly observed in *Orbulina universa* $\delta^{18}O$ record (Fig. 5.2), which shows a cyclic pattern with sudden enrichment during ~28 to ~26 cal kyr BP and then a gradual depletion from ~26 to ~22 cal kyr BP. The high depletion in $\delta^{18}O$ during ~26 kyr is correlated with Dansgaard-Oeschger (D-O) events of the North Atlantic (Bond *et al.,* 1993). The $\delta^{18}O$ variability record of *Globigerina bulloides* also shows maximum depletion and enrichment during LGM and H1 respectively (Fig.5.2). Maximum depletion of $\delta^{18}O$ during LGM and its enrichment during HI indicate relatively strong monsoonal precipitation in LGM than in Heinrich Events, which are much colder within MIS-2 and MIS-3. Similar depletion and enrichment are observed in *Globigerina bulloides* $\delta^{18}O$ records during B-A and YD events, respectively. Depleted $\delta^{18}O$ in near-surface dwelling *Globigerina bulloides* suggests NEM dominance during the LGM at the core location as the area receives rainfall mainly due to the effect of the NEM. Enriched $\delta^{18}O$ in *Orbulina universa* (Fig. 5.2) also suggest a poor SWM during LGM and H1 event, and the intensified NEM may be responsible for the depletion of $\delta^{18}O$ values in *Globigerina bulloides* during the LGM. Similarly, $\delta^{13}C$ variability in *Globigerina bulloides* record (Fig.5.3) shows maximum depletion during the LGM indicating weak stratification, which in turn causing the supply of nutrient rich cold water with depleted $\delta^{13}C$ to the ocean surface. Based on this observation, it is stated that the NEM was dominant during the LGM when compared to MIS-1 (Holocene). Sijinkumar *et al*. (2016) also have reported weakened summer monsoon during the LGM, reduced ocean stratification by low

influx of freshwater and strengthened winter monsoon which resulted in intense vertical mixing. Furthermore, Rashid *et al.* (2011) have also shown a progressive enrichment of seawater $\delta^{18}O$ values between 30 kyr and 15.8 kyr BP, but the trend has truncated between 22.3 and 18.2 cal kyr BP owing to depletion of $\delta^{18}O$.

5.9. Indian Monsoon variability during MIS-3

The $\delta^{18}O$ variability observed during part of the MIS-3 is identified by H3 and H4 events as exhibited in $\delta^{18}O$ enrichment of *Globigerina bulloides* (Fig.5.2). However, similar variability is not depicted in $\delta^{18}O$ records of *Orbulina universa*. Heinrich events led to cooling in the northern Indian Ocean and reduced the convective precipitation, and as a result, isotopically enriched moisture was carried across India and over China from northern Indian Ocean (Pausata *et. al.,* 2011). Hence, the northern Indian Ocean acts as a source of moisture to the BoB. Further, as glaciers started melting during interglacial periods, the ocean became depleted in ^{18}O, which is recorded in marine microfossils. Gradual depletion of $\delta^{18}O$ is also observed from ~36 to ~29 cal kyr BP (Fig. 5.2), and a stable plateau like $\delta^{18}O$ variability is persisted between ~40 and ~36 kyr BP. A similar rhythmic $\delta^{18}O$ depletion trend is observed again up to ~45 cal kyr BP in *Orbulina universa* records (Fig.5.2). Since the data covers only the later part of MIS-3, it shows overall $\delta^{18}O$ enrichment indicating gradual weakening of the SWM in the late MIS-3. $\delta^{13}C$ variability of *Globigerina bulloides* shows (Fig.5.3) a consistent trend, except at ~43.1 cal kyr BP where it abruptly reaches to an enriched value of 3.97‰. Further, *Orbulina universa* $\delta^{13}C$ variability (Fig. 5.3) also shows enrichment between ~ 40 and ~29 cal kyr BP.

Enriched $\delta^{13}C$ is inferred to increase photosynthetic processes during MIS-2, when compared to MIS-1 which exhibits much lesser.

5.10. Time Series Analysis of Isotopes and Inferences

Inferences from Z-Score analysis

Z-score statistical analyses of the $\delta^{18}O$ (Fig. 5.5) and $\delta^{13}C$ (Fig. 5.6) time series of *Globigerina bulloides* and *Orbulina universa* clearly differentiates the southwest and northeast monsoon variability during the last 46 ka BP. The dominant phases of southwest and northeast monsoon are shown by cyan and red bars, respectively. The Holocene phase is clearly demarcated by the $\delta^{18}O$ of *Globigerina bulloides (Fig. 5.5)* and $\delta^{13}C$ of *Orbulina universa (Fig. 5.6)*.

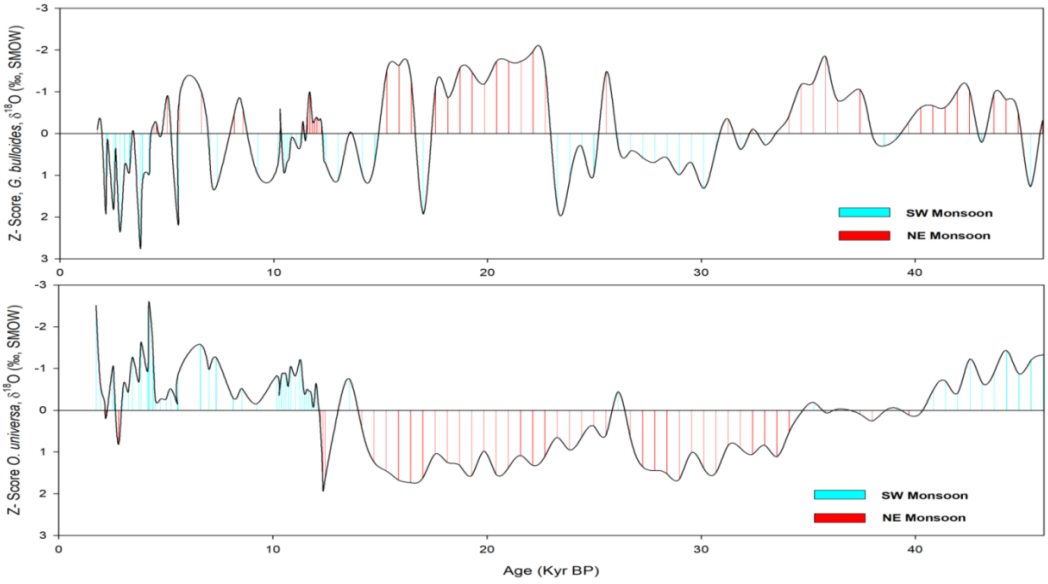

Fig. 5.5. Z-Score of $\delta^{18}O$ time series of *Globigerina bulloides* and *Orbulina universa*.

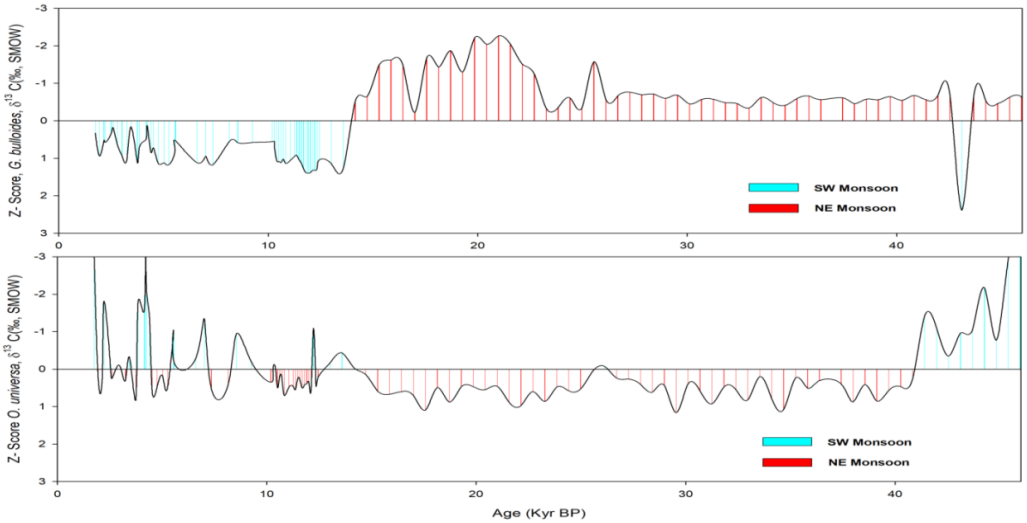

Fig. 5.6. Z-Score of $\delta^{13}C$ time series of *Globigerina bulloides* and *Orbulina universa*.

Inferences from REDFIT spectral analysis

REDFIT spectral analyses of the $\delta^{18}O$ and $\delta^{13}C$ time series of *Globigerina bulloides* and *Orbulina universa* has provided distinct periodicities. $\delta^{18}O$ Spectrum (Fig. 5.7) of *Globigerina bulloides* show periodicities of ~34kyrs, ~23kyrs, ~3.5kyrs, and a periodic range of ~1.3 to ~1.2 kyrs. Further, the $\delta^{18}O$spectrum of *Orbulina universa* (Fig. 5.8) also shows periodicities of ~125 kyr and ~80 kyr. The REDFIT analyses of $\delta^{18}O$ time series indicate that the periodicities follow the Milankovitch cycles and its associated cycles.

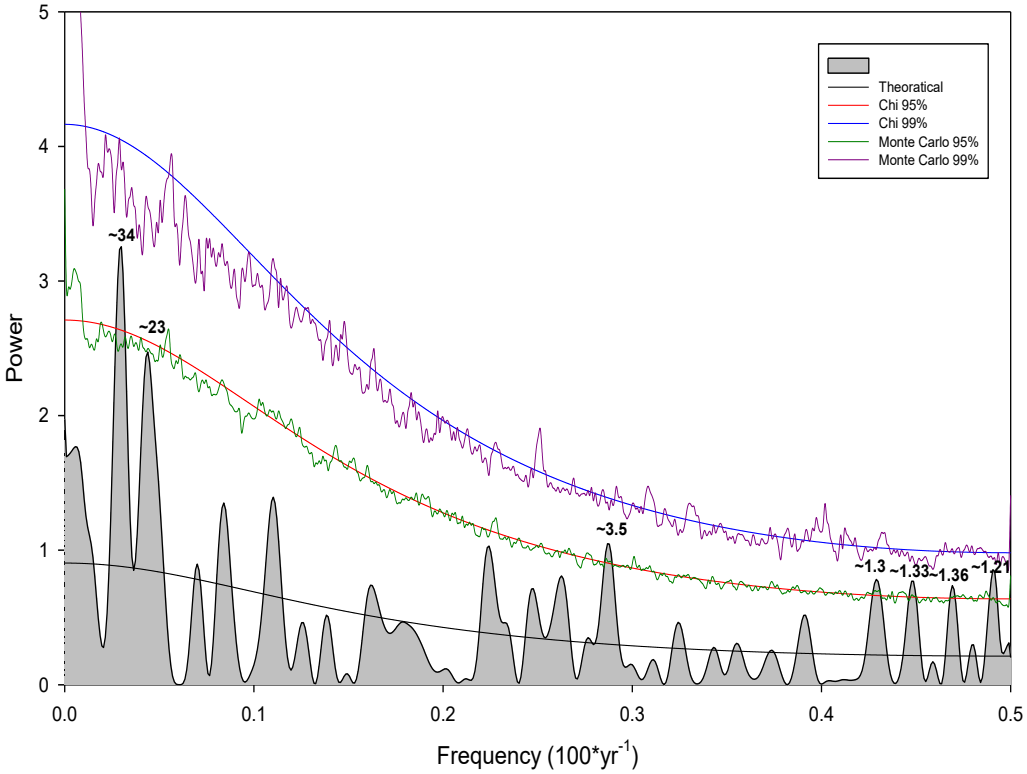

Fig. 5.7. REDFIT spectral analysis of *Globigerina bulloides* $\delta^{18}O$. Analyses show millennial scale periodicities indicating links to Sub-Milankovitch cycles.

The $\delta^{13}C$ REDFIT spectrum of *Globigerina bulloides* (Fig. 5.9) show a periodicity of ~65 kyr whereas $\delta^{13}C$ spectrum of *Orbulina universa* (Fig. 5.10) show periodicities of ~225 kyrs, ~3.25 kyrs, and ~2.5 kyrs. Hence, the $\delta^{13}C$ spectrums of the two species also suggest periodicities associated to Milankovitch cycle.

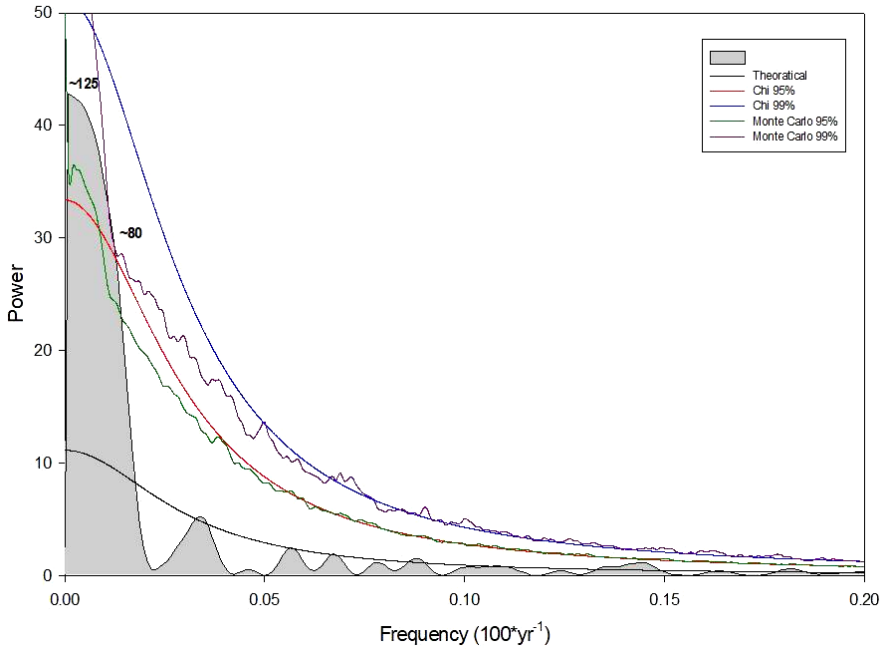

Fig. 5.8. REDFIT spectral analysis of *Orbulina universa* $\delta^{18}O$. Analyses show millennial scale periodicities indicating links to Sub-Milankovitch cycles.

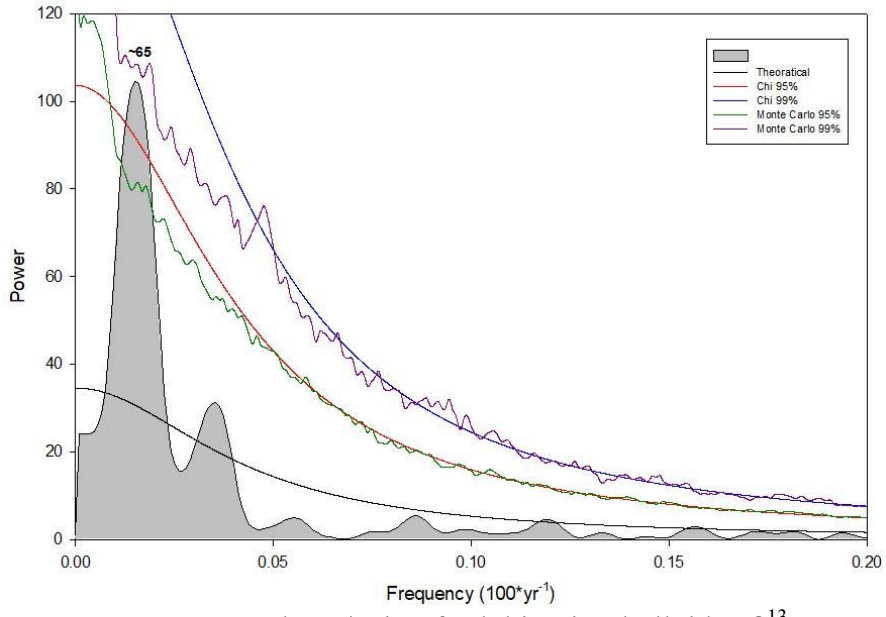

Fig. 5.9. REDFIT spectral analysis of Globigerina bulloides $\delta^{13}C$. Analyses show millennial scale periodicities indicating links to Sub-Milankovitch cycles.

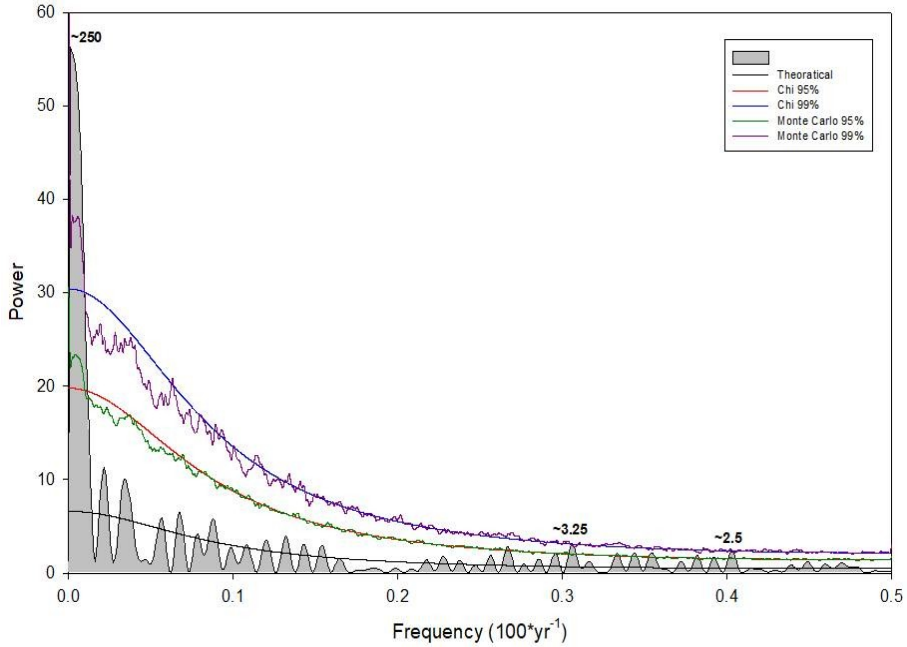

Fig. 5.10. REDFIT spectral analysis of Orbulina universa $\delta^{13}C$. Analyses show millennial scale periodicities indicating links to Sub-Milankovitch cycles.

Inferences from Wavelet analysis

The wavelet analyses of $\delta^{18}O$ and $\delta^{13}C$ time series of the two species reveal wide range of significant millennial scale periodicities (Fig.5.11). *Globigerina bulloides* $\delta^{18}O$ time series indicate periodicities of ~18.55kyr, ~13.12 kyr, ~9.3 kyr, ~6.56 kyr; whereas *Orbulina universa* $\delta^{18}O$ time series show periodicities of ~13.12 kyr, 9.3 kyr, 5.52 kyr, and ~3.9 kyr. Similarly, total $\delta^{13}C$ time series of *Globigerina bulloides* show periodicities at ~17.32 kyr, ~7.8 kyr, and ~1.38 kyr; whereas *Orbulina universa* $\delta^{13}C$ time series represent periodicities at ~11 kyr, ~9.3 kyr, ~6.56 kyr, and ~2.32 kyr. An attempt was made to understand the periodicities within MIS-1 (Fig.5.12) and to correlate the cyclic changes with boundary conditions. *Globigerina bulloides*$\delta^{18}O$ time series during MIS-1 indicate periodicities of ~4.2

kyr, ~1.2kyr, and 0.8 kyr, but $\delta^{13}C$ time series doesn't show any significant periodicity. *Orbulina universa* $\delta^{18}O$ time series show periodicities of ~3.6 kyr and ~2.4 kyr, whereas $\delta^{13}C$ time series indicate periodicities of ~4.2 kyr and ~1.6 kyr.

Millennial scale periodicities are inferred to be associated with orbital scale variability representing 23 kyr precession cycle and changes in global ice volume. In this context, millennial scale variability is often related to Dansgaard-Oeschger (D-O) variability of ~1.47 kyr (Grootes and Stuvier, 1997), first observed in Greenland ice core records (Dansgaard *et al.,* 1993; Johnson *et al,* 1992). Now D-O variability has been reported globally (Voelker, 2002; Schulz, 2002), which is further manifested by harmonics of ~3 ka and ~4.5 ka (Alley *et al.,* 2001). Hence, the periodicities of ~4.2 and ~3.9 kyrs are correlated to the Heinrich events of North Atlantic climate change and the periodicity of ~2.32 can be linked to the changes in Indian monsoon system as suggested by Naidu and Malmgren (1995) and Ahmad *et al.* (2012). A 4.4 kyr cycle has been reported by Rao and Tiwari (2009) and Ahmad *et al.* (2012). Further, the oceanic circulation changes, at sub-Milankovitch cycle, may also have influenced the Asian monsoon and atmospheric CO_2 at 2.2 kyr cycle (Naidu and Malmgren, 1995). Similarly, Magny (1993) also have shown a 2.3 kyr cycle of atmospheric ^{14}C. Denton and Karlen (1973) have suggested that glacier expansion and contraction is linked to the higher and lower atmospheric ^{14}C respectively. Also, the changes in ^{14}C have been inferred due to modulating cosmic flux and climate induced oceanic changes (Stuvier and Braziunas, 1989). Periodicities of ~7.8, ~6.56, and ~5.52 kyrs can be inferred as associated to ocean convective processes coupled with ocean-atmospheric interactions. The periodicities of ~18.55, ~17.32, ~13.12, ~11, and ~9.3

kyrs are further attributed to harmonics of 23 kyr insolation equinoxes associated with some lead/lags.

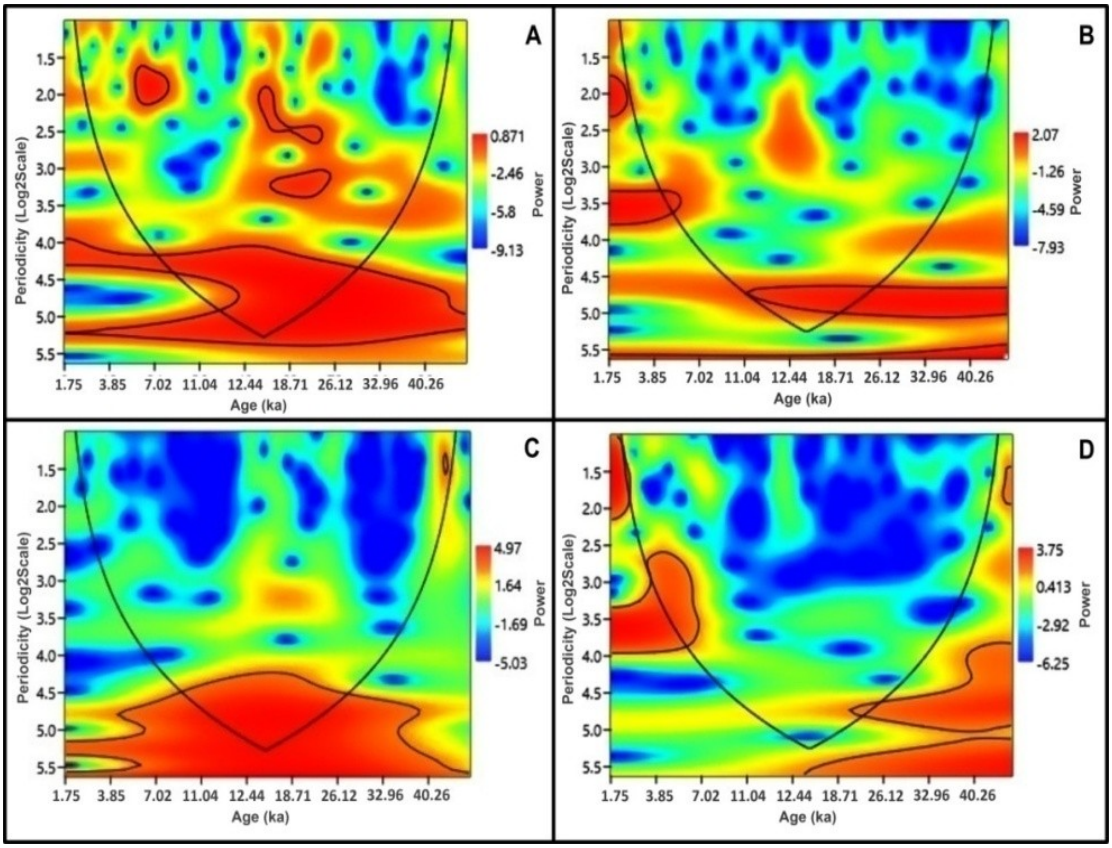

Fig. 5.11. Wavelet plots of total $\delta^{18}O$ and $\delta^{13}C$ time series. Spectral power (variance,‰^{2}) is shown by columns ranging from weak (deep blue) and strong (deep red) color bands. Black cone demarcates the upper boundary in which identified frequencies can be interpreted for periodicities. Irregular black curves delineate 95% confidence limit of time-frequency region. Fig. 5.11A and 5.11B shows the wavelets of total $\delta^{18}O$ time series of *Globigerina bulloides* and *Orbulina universa*, respectively, whereas Fig. 5.11C and 5.11D shows total $\delta^{13}C$time series of *Globigerina bulloides* and *Orbulina universa*, respectively

5.11. Regional Coherence

The *Orbulina universa* $\delta^{18}O$ record (Fig.5.13K) have been compared with other $\delta^{18}O$ records of different planktic foraminifera species from BoB (Fig. 5.13C, Rashid

et. al., 2011; Fig. 5.13I, Kudrass *et. al.,* 2001; Fig. 5.13J, Govil and Naidu, 2017), AnS (Fig. 5.13B, Grebgroiges *et. al.,* 2016; Fig. 5.13D, Kumar *et. al.,* 2018; Fig. 5.13E,Sijinkumar *et al.,* 2011; Fig. 5.13F,Silva *et al.,* 2017; Figs. 5.13G and 5.13H, Raza *et al.,* 2014) and with polar ice core records (Fig. 5.13A, GISP record) to understand their regional and inter-hemispheric links. *Orbulina universa* $\delta^{18}O$ variability records of this study can be compared with GISP2 $\delta^{18}O$records and also with $\delta^{18}O$ variability records observed during MIS-1, MIS-2, and MIS-3 from BoB and AnS. This indicates

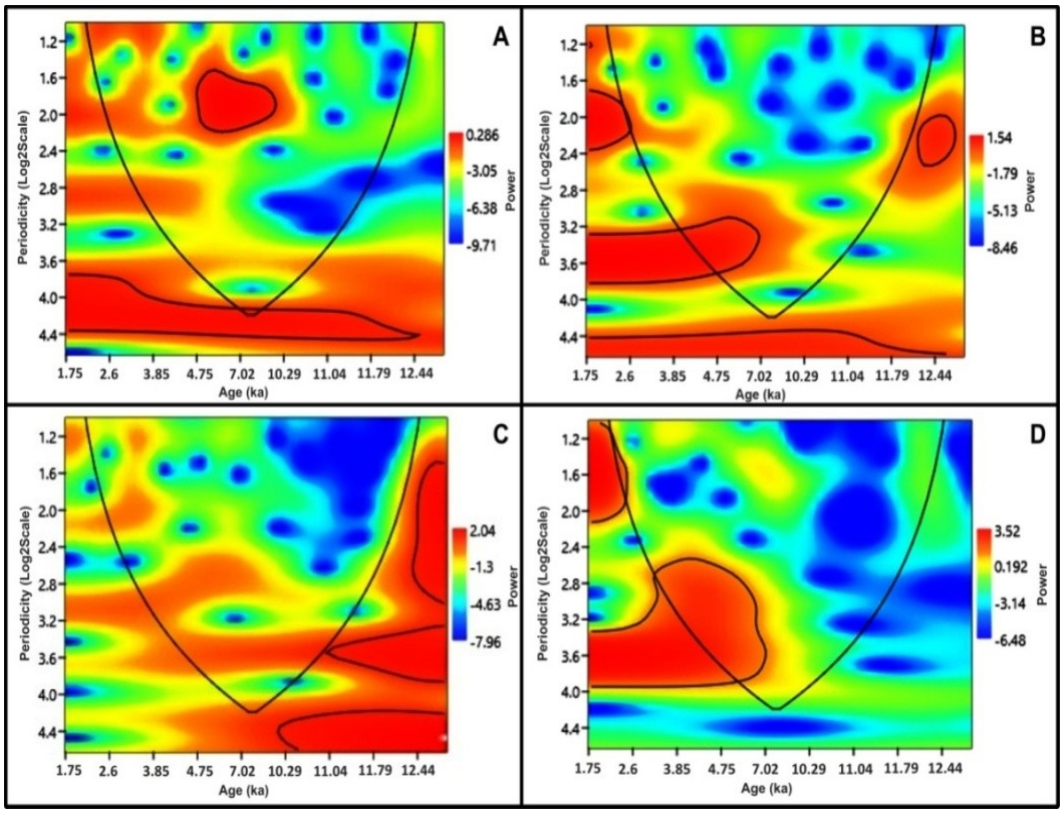

Fig. 5.12. Wavelet plots of $\delta^{18}O$ and $\delta^{13}C$ time series during MIS-1. Spectral power (variance,‰^{2}) is shown by columns ranging from weak (deep blue) and strong (deep red) color bands. Black cone demarcates the upper boundary in which identified frequencies can be interpreted for periodicities. Irregular black curves delineate 95% confidence limit of time-frequency region. Fig. 5.12A and 5.12B shows the wavelets of MIS-1$\delta^{18}O$ time series of *Globigerina bulloides* and *Orbulina universa* respectively, whereas Fig. 5.12C and 5.12D shows MIS-1$\delta^{13}C$time series of *Globigerina bulloides* and *Orbulina universa*, respectively.

that the processes, which have controlled the hydroclimate in southwestern BoB, happen to be similar to the climate changes that occurred in other parts of BoB and AnS. The concordance of *Orbulina universa* $\delta^{18}O$ variability with polar records suggest that the climatic changes occurring in North Atlantic and at high latitudes have direct control over tropical climatic system causing the variability in secular equilibrium in space and time (Overpeck and Webb, 2000; Gupta *et al.,* 2003; Fleitmann *et al.,* 2003; Hong *et al.,* 2003; Wanner *et al.,* 2011; Kathayat *et al.,* 2016; Gautam *et al.,* 2019).

This link has been elucidated by Atlantic meridional overturning circulation (AMOC) when much fresh melt water enters the North Atlantic Ocean. Due to the fresh water intake, the seawater at high latitudes is freshened abruptly, and the AMOC slows down or even stops which results in large decrease in northward heat transfer and the precipitous cooling of the North Atlantic region (Broecker, 1997; Knutti et al., 2004; EPICA Community Members, 2006; Barker *et al.,* 2009; Cheng *et al.,* 2012; Chiang and Friedman, 2012). This concordance has also been linked to the south(north) shifts of the mean latitude position of the Inter Tropical Convergence Zone (ITCZ) and to the weakening (strengthening) of the monsoonal intensity by many workers (Broccoli *et al.,* 2006; Clement and Peterson, 2008; Chiang and Friedman, 2012).

5.12. Summary

The $\delta^{18}O$ and $\delta^{13}C$ record of *Globigerina bulloides* and *Orbulina universa* from Bay of Bengal strongly indicate Northeast Monsoon (NEM) and Southwest

Monsoon (SWM) variability, respectively. The $\delta^{13}C$ record of upwelling species *Globigerina bulloides* has shown a remarkable variability during the last 46 ka with global climatic shifts. The $\Delta\delta^{18}O$*bulloides-universa* indicates that the intensity of Indian monsoon in the southwestern Bay of Bengal (BoB) was significantly different during MIS-1, MIS-2, and MIS-3 where monsoon was strongest during MIS-1 followed by MIS-3, whereas it was weaker during MIS-2. This is reflected by the shallow and deep Mixed Layer Depth (MLD) during MIS-1 and MIS-2, respectively. The MLD during MIS-3 was shallower than the MIS-2 but deeper than MIS-1. Most enriched $\delta^{13}C$ concentrations of *Globigerina bulloides* during MIS-1 also indicate intense stratification and weak upwelling. On the contrary, MIS-2 indicates weakest stratification due to the supply of nutrient rich cold water along with depleted $\delta^{13}C$ to the ocean surface. Similarly, a moderate $\delta^{13}C$ value during MIS-3 supports the fact that MIS-3 was associated with higher productivity than MIS-2 but lower than MIS-1. Sea surface height anomaly data suggest that the core location lies in the region of persistent cyclonic eddies as the southwestern BoB experiences more cyclonic events. Hence, it is advocated that the nutrient supply in the southwestern BoB may be associated with cyclonic eddies, particularly during the MIS-I. Millennial periodicities of $\delta^{18}O$ and $\delta^{13}C$ records clearly exhibit interhemispheric links and the rapid changes are due to convergent factors of north Atlantic climate changes and coupled ocean-atmospheric processes. It is inferred that downwind transport of atmospheric signal from the North Atlantic drives the changes in the Indian monsoon. The study further reveals that high productivity during early Holocene, i.e. onset of active interglacial stage, was due to enhanced photosynthesis (productivity). The modulations in SWM intensity affected the productivity because of minor shifts

during the mid- and late- Holocene. The $\delta^{18}O$ and $\delta^{13}C$ records from MIS-2 indicate strong NEM and weak SWM during the LGM. Regional correlation of the $\delta^{18}O$ records suggest that the processes which have controlled the hydroclimate in southwestern BoB were similar to those occurred in other parts of BoB and AnS. The variability of monsoon over last 40 kyr BP reconstructed in this study by using isotopic ratios of selected planktic foraminifera species are in broad agreement with other monsoon reconstructions based on $\delta^{18}O$ from BoB, which suggests that the forcing mechanisms of monsoon appears to be similar in the entire north Indian Ocean.

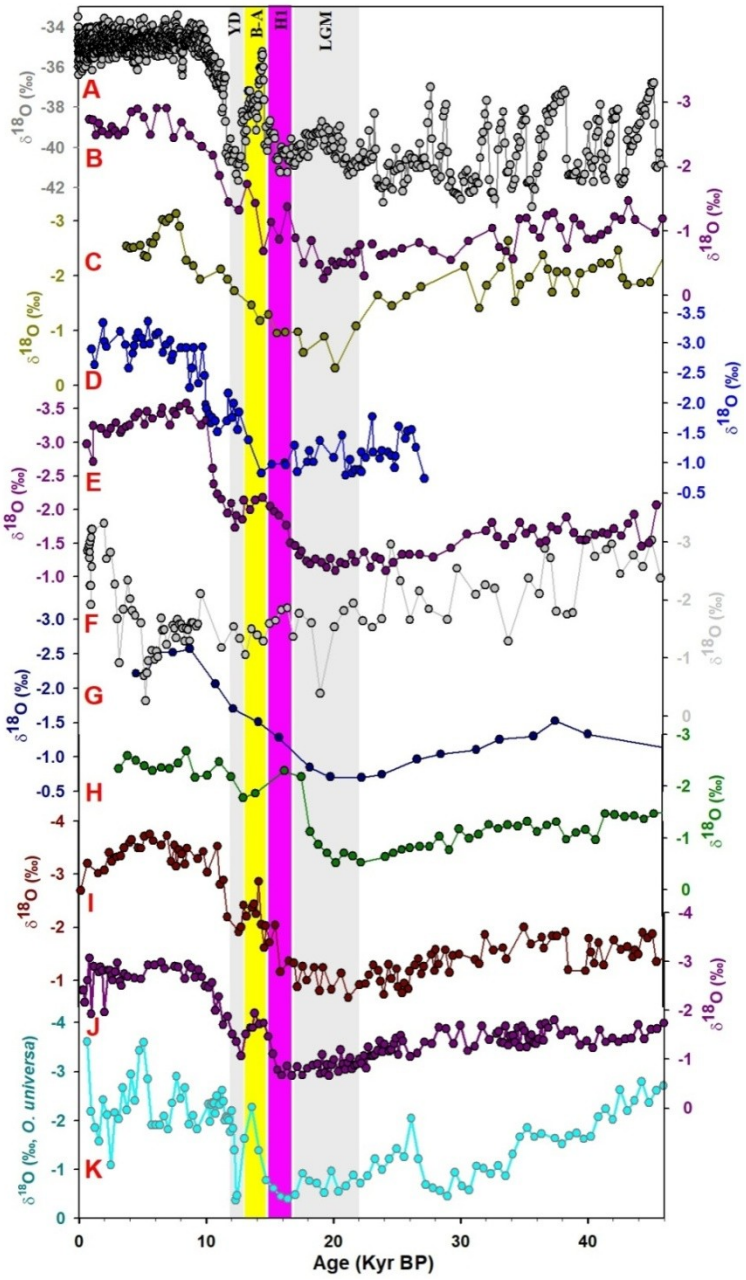

Fig. 5.13. Regional Coherence. $\delta^{18}O$ variability record of planktic foraminifera *Orbulina universa* obtained from core SK-170/2 (present study; K) is compared with GISP record (A: Dansgaard et al., 1993), Andaman Sea (B: Grebgroiges et al., 2016; C: Kumar et al., 2018; E: Sijinkumar et al., 2011; F: Silva et al., 2017; G and H: Raza et al., 2014), and Bay of Bengal record (D: Rashid et al., 2011; I: Kudrass et al., 2001; J: Govil and Naidu, 2017).

Table 5.2. Statistics of $\delta^{18}O$ and $\delta^{13}C$ variability in core SK-170/2 collected from southwestern BoB

	Globigerina bulloides		*Orbulina universa*	
	$\delta^{18}O$	$\delta^{13}C$	$\delta^{18}O$	$\delta^{13}C$
Total time series				
Minimum	-2.86 ‰	-4.55 ‰	-3.60 ‰	-1.85 ‰
Maximum	0.52 ‰	3.97 ‰	-0.37 ‰	3.14 ‰
Average	-1.89 ‰	-0.41 ‰	-1.70 ‰	2.04 ‰
MIS-1				
Minimum	-2.38 ‰	-0.11 ‰	-3.60 ‰	-1.54 ‰
Maximum	-0.52 ‰	2.12 ‰	-0.37 ‰	2.81 ‰
Average	-1.69 ‰	1.08 ‰	-1.70 ‰	1.79 ‰
MIS-2				
Minimum	-2.86 ‰	-4.55 ‰	-2.27 ‰	1.00 ‰
Maximum	-0.92 ‰	2.15 ‰	-0.37 ‰	3.14 ‰
Average	-1.96 ‰	-1.48 ‰	0.98 ‰	2.44 ‰
MIS-3				
Minimum	-2.81 ‰	-1.65 ‰	-2.79 ‰	-1.85 ‰
Maximum	-1.25 ‰	3.97 ‰	-0.86 ‰	3.06 ‰
Average	-2.08 ‰	-1.21 ‰	-1.81 ‰	1.85 ‰

Chapter 6

Indian Monsoon during Bølling-Allerød Period: Records from Stalagmite of Kailash Cave

Chapter 6

Indian Monsoon during Bølling-Allerød Period: Records from Stalagmite of Kailash Cave

6.1. Introduction

During the last deglacial period, every component of the Earth system experienced large scale changes as recorded in the northern hemispheric (NH) ice sheets: melting of ice, sea level rise (~120 m), and increase in the atmospheric CO_2 (~100 ppmv, Denton *et al.,* 2010; Clarke *et al.,* 2012). The plausible cause has been attributed to changes in insolation and consequent migration of Inter Tropical Convergence Zone (ITCZ; Clarke *et al.,* 2012). As the Indian Summer Monsoon (ISM), an integral component of the Earth's tropical climate dynamics, affects the socio-economic conditions of the Indian subcontinent (Lone *et al.,* 2014; Kathayat *et al.,* 2016; Huguet *et al.,* 2018; Band *et al.,* 2018), and as recurrence of abrupt climate change might be a possible scenario in conjunction with anthropogenic climate influence (Partin *et al.,* 2015). Hence, understanding the response of ISM to abrupt climate change is of fervent interest. It has been reported that the tropical regions can warm polar areas through atmospheric teleconnection (Ding *et al.,* 2011) as the sea-ice extent in the poles are perturbed by the tropics and *vice versa* (Yuan and Martinson, 2011). Recent studies link ISM variability with dry (wet) ISM phase to cold (warm) climate events in North Atlantic (Gupta *et al.,* 2013; Mohtadi *et al.,* 2014; Band *et al.,* 2018). Also, recent coupled general circulation model (CGCM) simulations have suggested that change in the North Atlantic, especially the Arctic melt water discharge can also affect the warming process of the NH (Chiang and Friedman, 2012) and can be linked to changes in the East Asian Monsoon. However, the link of ISM variability to changes in Southern Hemisphere (SH) remains elusive (Clemens *et al.,* 1991; Kathayat *et al.,* 2016). Here, we present a new

centennially resolved 2200 years record of ISM variability during 14.8 to 12.6 ka from Kailash cave, eastern India, located in the core ISM area. This age range offers the signatures of the two major climatic events i.e. the Bølling-Allerød (B-A) and the onset of the Younger Dryas (YD) corresponding to abrupt warming and cooling events, respectively, that occurred during the last deglaciation. The onset of B-A (~14.7 ka) was associated with an abrupt heat migration from SH to NH resulting in rapid increase of temperature in a very short duration of 1-3 years in the moisture source region of Greenland (Steffenson *et al.,* 2008). It has been suggested that during the B-A transition, a reorganization of the prevailing atmospheric circulation enhanced a northward advection of moisture and heat, which resulted in increasing the Greenland temperature, causing cooling of the SH by the northward migration of southern westerlies (Anderson *et al.,* 2009). This phenomenon has been explained conventionally by the bipolar see-saw mechanism, which is closely linked to the Atlantic meridional overturning circulation (AMOC) and associated atmospheric teleconnections which modulate the thermodynamic exchange between the south and north Atlantic (Pedro *et al.,* 2015; Stocker and Johnsen, 2003). Similarly, the sudden influx of freshwater into the AMOC triggered the YD event at ~12.8 ka. The warm and cold events at higher northern latitudes are associated with wet and dry events of ISM respectively, in the tropics (Gupta *et al.,* 2013; Mohtadi *et al.,* 2014; Band *et al.,* 2018). Hence, suitable inter-hemispheric mechanism that could link ISM variability is an important research theme which demands attention.

The main aim of this chapter was to generate a high resolution $\delta^{18}O$ record to identify and understand the controlling factors and possible inter-hemispheric linkages that modulated the Indian Summer Monsoon (ISM) during the last deglacial. The results were also compared with published Ice Rafted Debris (IRD) flux (Weber *et al.,* 2014) along with other proxies.

6.2. Mineralogy and Isotopic Equilibrium Growth

The mineralogy of the stalagmite is an important criterion to estimate the initial value for ^{230}Th dating methods. The chemical staining resulted in no dark/black layers which confirmed the mineral composition of the sample KG-6 to be calcite. Furthermore, thirty-two distinct layers selected for XRD analyses (Fig. 6.1) also confirm the mineralogy of KG-6 stalagmite to be calcite. Results of Hendy's test (Fig. 6.2) show that there is no significant variation except at the flanks of the growth layers, as the growth layers converge at the flanks. Insignificant correlation between $\delta^{18}O$ and $\delta^{13}C$ indicate that the deposition was likely under isotopic equilibrium.

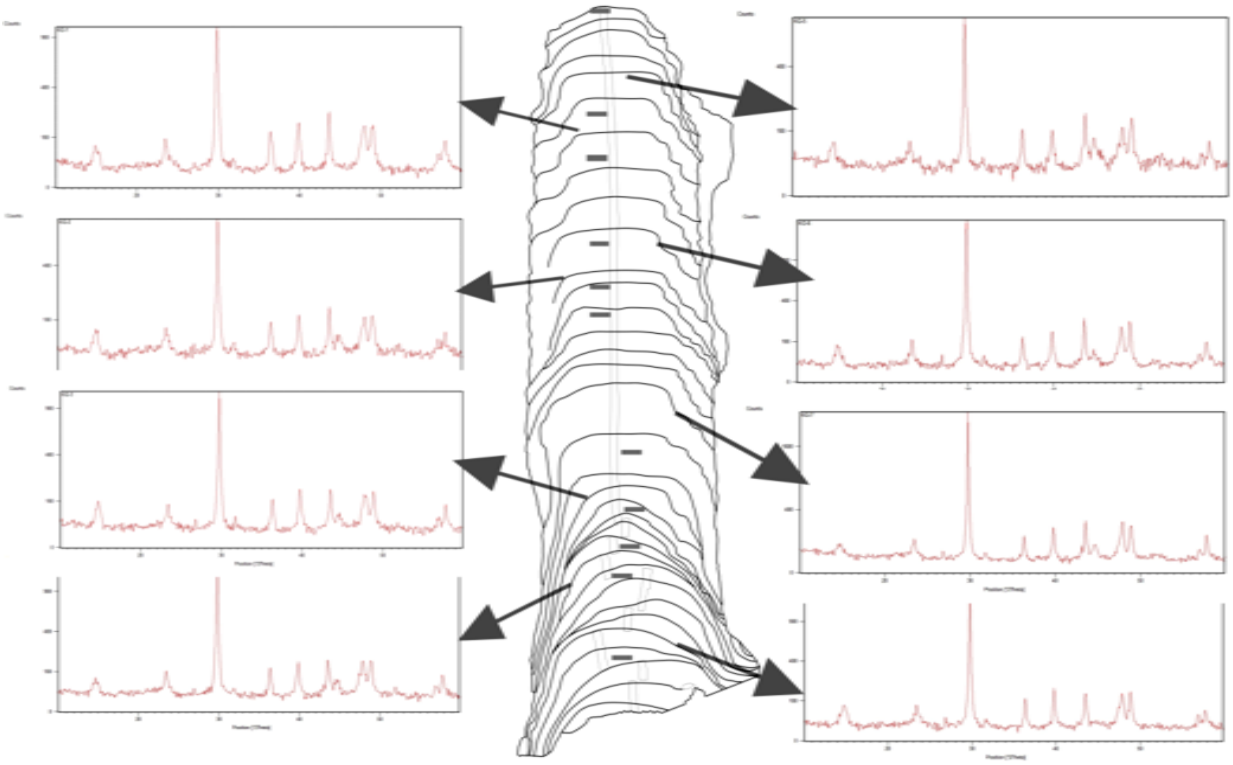

Fig. 6.1. XRD mineralogy of Stalagmite KG-6, Kailash Cave, Chhattisgarh, India. Results show the composition of the stalagmite is calcite throughout the sample.

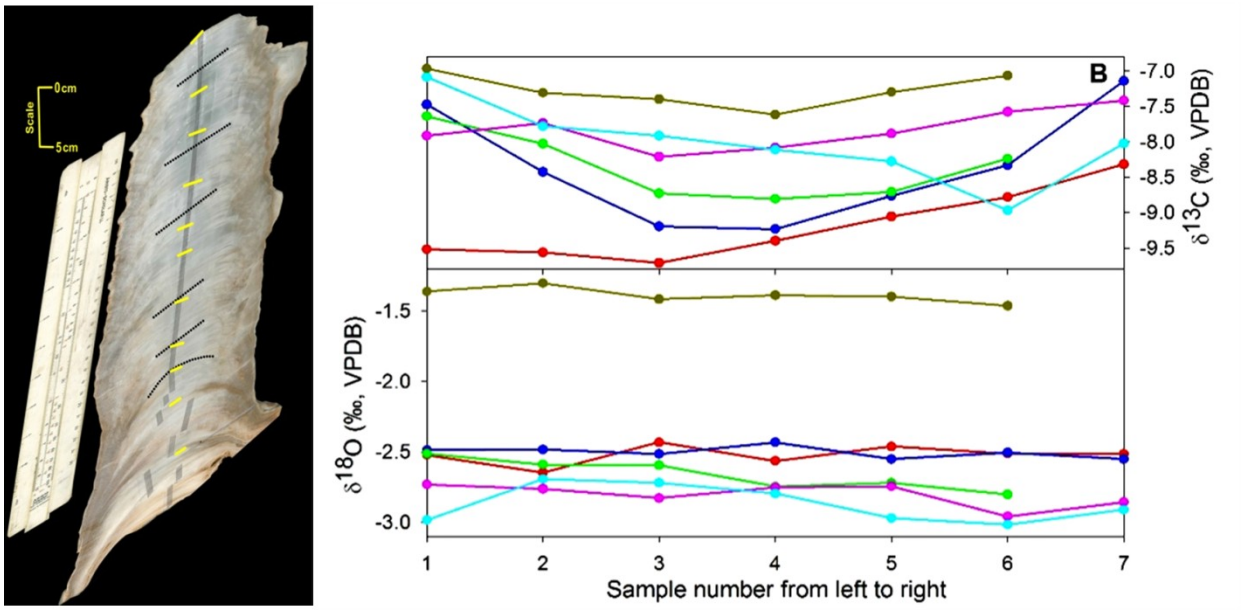

Fig. 6.2. Hendy's Test of Stalagmite sample KG-6. Horizontal black lines on the sample slice show the selected layers for Hendy's Test. Right panels show the $\delta^{18}O$ and delta $\delta^{13}C$ of the samples selected for Hendy's test.

6.3. U-Th Chronology of Stalagmite

Eleven U-Th dates were obtained (Table 6.1) from a Thermo Fisher NEPTUNE multi-collector inductively coupled plasma mass spectrometer (MC-ICP-MS) at High-Precision Mass Spectrometry and Environment Change Laboratory (HISPEC), National Taiwan University, Taiwan (Shen *et al.,* 2003, 2012). Constructing Proxy Records from Age Model (COPRA; Breitenbach *et al.,* 2012) for the stalagmite sample was run with the given geochronological data for an age model (Fig. 6.3) in order to establish a normal stratigraphic order of crystallization in the given temporal span.

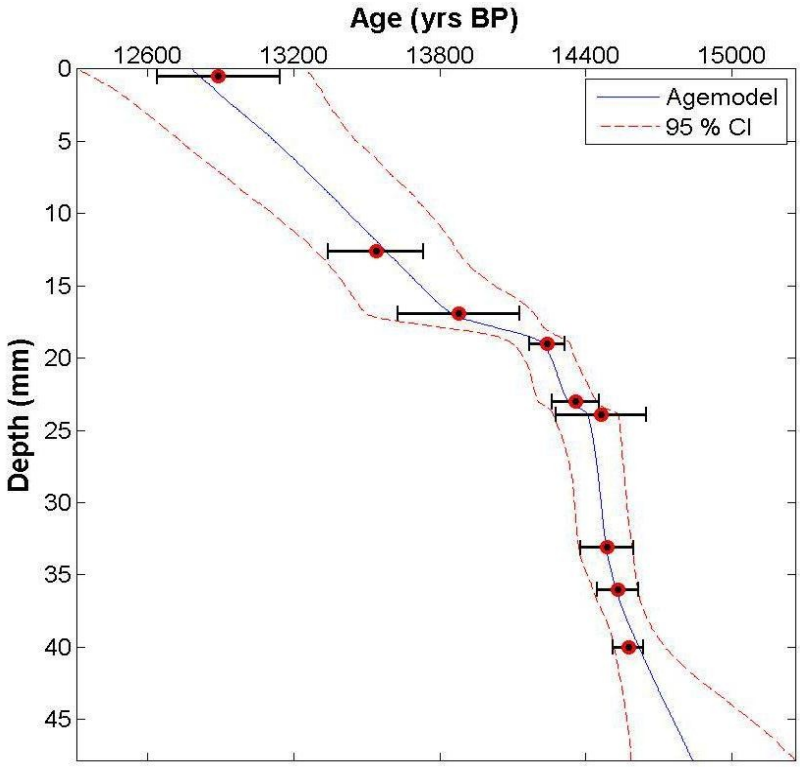

Fig. 6.3. COPRA age-depth model. COPRA selected ten ages out of eleven collected from different depths of 43 cm long stalagmite of Kailash Cave, Chhattisgarh, India, to model the age in correct age progression.

6.4. Isotopic variability during Bølling-Allerød

$\delta^{18}O$ Variability

The stalagmite (KG-6) $\delta^{18}O$ record (Fig. 6.4) consists of 1186 measurements with temporal resolution varying from a minimum of ~2 months to ~10 years during ~14.8-12.6 ka with $\delta^{18}O$ values varying from -6.1‰ to 0.37‰ with an average of -2.55‰ and appear to be cyclic in nature associated with several episodes of dry (^{18}O enriched) and wet (^{18}O depleted) events relative to the long term average. The $\delta^{18}O$ time series shows nine (Fig.6.4) centennial scale oscillations varying in their amplitudes and temporal spans, identified with three persistent and distinct stages in each cycle as: first abrupt onset, second transient stable, and third relatively longer and gradual termination stages. The onsets of ISM intensification are identified by the

Table 6.1: Uranium and Thorium isotopic compositions and ^{230}Th ages for KG-6 stalagmite.

Depth	Weight	^{238}U		^{232}Th		□^{234}U		[^{230}Th/^{238}U]		^{230}Th/^{232}Th		Age (yr ago)		Age (yr ago)		Age (yr BP)		□$^{234}U_{initial}$	
cm	g	ppb[a]		ppt		measured[a]		activity[c]		atomic (x 10^{-6})		uncorrected		corrected [c,d]		relative to 1950 AD		corrected[b]	
0.5	0.05084	97.97	± 0.20	2263	± 12	512.3	± 3.7	0.1746	± 0.0018	124.6	± 1.5	13,292	± 152	12,892	± 251	12,826	± 251	531.2	± 3.9
6.7	0.06255	89.87	± 0.16	199.4	± 7.4	504.7	± 3.1	0.18247	± 0.00079	1356	± 51	13,998	± 71	13,960	± 73	13,894	± 73	525.0	± 3.2
8.1	0.05046	97.44	± 0.13	355.2	± 9.2	511.8	± 2.3	0.18398	± 0.00089	832	± 22	14,045	± 77	13,982	± 83	13,916	± 83	532.4	± 2.4
19	0.06262	159.98	± 0.34	238.3	± 7.4	515.8	± 4.1	0.18715	± 0.00070	2071	± 65	14,266	± 70	14,241	± 71	14,175	± 71	537.0	± 4.2
23	0.07537	160.56	± 0.33	996.7	± 6.7	530.1	± 3.6	0.19141	± 0.00090	508.4	± 4.0	14,465	± 81	14,359	± 96	14,293	± 96	552.0	± 3.7
23.9	0.02688	47.675	± 0.053	463	± 17	520.1	± 2.3	0.1905	± 0.0023	324	± 13	14,634	± 164	14,463	± 185	14,397	± 185	541.8	± 2.4
33.1	0.05873	271.03	± 0.32	1246.5	± 8.5	544.4	± 1.8	0.1946	± 0.0013	697.5	± 6.5	14,565	± 102	14,487	± 109	14,421	± 109	567.1	± 1.9
35.3	0.05041	275.07	± 0.35	496.6	± 9.4	558.6	± 2.6	0.1987	± 0.0013	1815	± 36	14,763	± 105	14,733	± 106	14,667	± 106	582.3	± 2.7
36	0.05245	279.29	± 0.46	1643	± 10	556.3	± 3.0	0.19682	± 0.00077	551.8	± 4.0	14,630	± 68	14,531	± 84	14,465	± 84	579.5	± 3.1
37.3	0.05899	246.95	± 0.25	1533.9	± 9.0	556.9	± 1.8	0.1955	± 0.0015	518.9	± 4.9	14,534	± 117	14,429	± 128	14,363	± 128	580.0	± 1.9
40	0.05629	387.33	± 0.74	679.0	± 8.4	568.3	± 3.4	0.19802	± 0.00066	1862	± 24	14,603	± 61	14,574	± 63	14,508	± 63	592.1	± 3.5

Analytical errors are 2σ of the mean.

[a] $[^{238}U] = [^{235}U] \times 137.818$ (±0.65‰) (Hiess et al., 2012); □$^{234}U = ([^{234}U/^{238}U]_{activity} - 1) \times 1000$.

[b] □$^{234}U_{initial}$ corrected was calculated based on ^{230}Th age (T), i.e., □$^{234}U_{initial} =$ □$^{234}U_{measured} X e^{□^{234}*T}$, and T is corrected age.

[c] $[^{230}Th/^{238}U]_{activity} = 1 - e^{-□^{230}T} + (□^{234}U_{measured}/1000)[□_{230}/(□_{230} - □_{234})](1 - e^{-(□^{230}-□^{234})T})$, where T is the age.

Decay constants are 9.1705 x 10^{-6} yr^{-1} for ^{230}Th, 2.8221 x 10^{-6} yr^{-1} for ^{234}U (Cheng et al., 2013), and 1.55125 x 10^{-10} yr^{-1} for ^{238}U (Jaffey *et al.,* 1971).

[d] Age corrections were calculated using an estimated atomic $^{230}Th/^{232}Th$ ratio of 4 (± 2) x 10^{-6}.

Those are the values for a material at secular equilibrium, with the crustal $^{232}Th/^{238}U$ value of 3.8. The errors are arbitrarily assumed to be 50%.

most ^{18}O depleted values, while the terminations are marked by the maximum enrichment in^{18}O. Extreme five wet and six dry events (Fig. 6.4) are identified in the $\delta^{18}O$ time series of the stalagmite sample. It is also observed that the ISM attained stability at ~13.8 ka, prior to which an abrupt climate change (B-A) persisted, which is well recorded in the growth rate of the sample, which also has been visually interpreted from the growth layers where The stable phase of ISM shows clean translucent color and the opaque layers exhibit dirty patches from B-A event.

Although $\delta^{18}O$ variations in paleoclimatic proxies are often interpreted in terms of local climatic variations such as temperature, amount of precipitation, the $\delta^{18}O$ values of tropical rain are not correlated with the mean annual surface air temperature. Model based simulations show that $\delta^{18}O$ in precipitation is influenced by strong moisture transport by ISM winds and upstream rainfall with a significant negative $\delta^{18}O$ correlation (Midhun and Ramesh, 2015). This negative correlation of $\delta^{18}O$ with the amount of ISM precipitation is also known as the amount effect (Wang *et al.,* 2001; Yuan *et al.*, 2004; Yadava and Ramesh, 2007; Lone *et al.,* 2014; Allu *et al.,* 2014; Sinha *et al.,* 2015), which is applied to most of the Indian and the entire Indian monsoon domain. It is manifested as ^{18}O depletion during the intense monsoon (wet) and ^{18}O enrichment during weaker monsoon (dry). We, therefore, interpret the stalagmite $\delta^{18}O$ record in terms of past changes in the ISM rainfall. Few recently published stalagmite $\delta^{18}O$ records from Asia (Breitenbach *et al.,* 2010; Dayem *et al.,* 2010; Pausata *et al.,* 2011; Berkelhammer *et al.,* 2012; Dutt *et al.,* 2015), however, reflect $\delta^{18}O$ variability to past changes in moisture source, changes in isotopic fractionation at the source, and changes in transport pathways as well as the $\delta^{18}O$ of Bay of Bengal (BoB) surface water. It has also been widely reported that the ISM circulation and associated moisture penetrate northeastward, deep into East Asia resulting in a significant concept that the component of east Asia summer monsoon (EASM) precipitation is derived essentially from the ISM domain (Ding 2004; Clemens *et al.,* 2010; Pausata *et al.,* 2011).

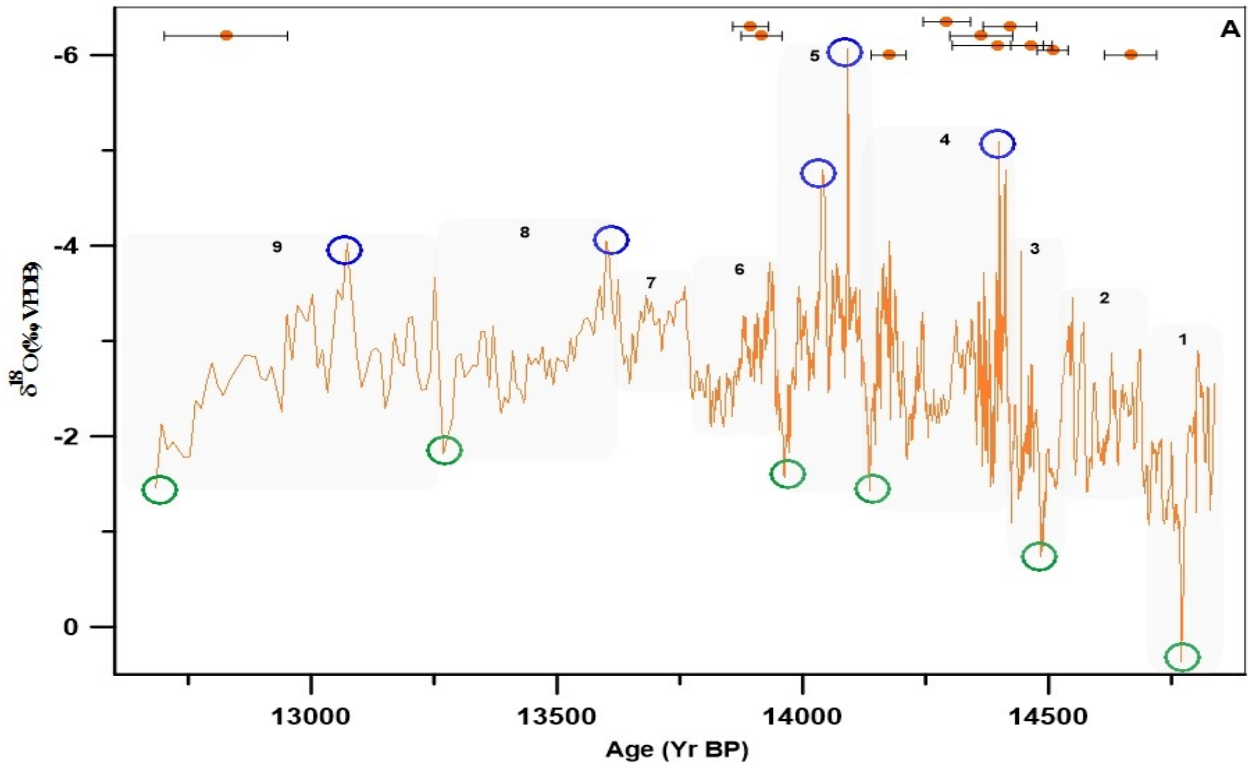

Fig. 6.4. $\delta^{18}O$ variability. $\delta^{18}O$ record for ~2.1 kyr from ~14.9 ka to ~12.7 ka obtained from stalagmite KG-6. $\delta^{18}O$ values vary from 0.37 ‰ to -6.07‰ with an average of -2.55 ‰. The major oscillations range between -2 to -4 ‰.The $\delta^{18}O$ values appear to be cyclic in nature with nine major cycles as shown in grey boxes 1 to 9. Horizontal error bars indicate the age control. Blue and green circles represent extreme wet and dry events, respectively.

$\delta^{13}C$ Variability

The carbon in stalagmite is mainly derived from soil CO_2 having $\delta^{13}C$ of 0.9‰ and bedrock having $\delta^{13}C$ of +1‰. Carbon isotope evolution is a complex process where photosynthesis, biological activities play important role. C-3 plants produce biogenic carbon with $\delta^{13}C$ -36‰ to -22‰ with respect to VPDB in humid and tropical region wheras C-4 plants produce $\delta^{13}C$ of -12‰ with respect to in semi arid region. Hence, $\delta^{13}C$ of cave deposits such depends upon relative concentration from these two types of vegetation along with soil and bedrock. It is important to note that the change in vegetation is a cycle of centennial scale.

$\delta^{13}C$ record of the stalagmite KG-6 (Fig. 6.5) shows variability from -2‰ to -11‰ with respect to VPDB during the B-A period. However, an average variability range between -6‰ to -10‰. Isotopic concentrations above and below the average range indicate anomalous nature of climatic variability. The $\delta^{13}C$ variability record shows similar variability with $\delta^{18}O$ variability record where an increasing trend of depletion was observed during 14.9 to 14 ka BP. Unlike $\delta^{18}O$ records, an abrupt enrichment (average $\delta^{13}C$ of -2.5‰) in $\delta^{13}C$ record was observed soon after 14 ka BP which persisted for about a century after which the depletion was abruptly regained in the $\delta^{13}C$ record with an average $\delta^{13}C$ value of -10‰. The sudden enrichment after 14 ka is inferred to the reduction in the rainfall which caused enrichment of $\delta^{13}C$ in the stalagmite.

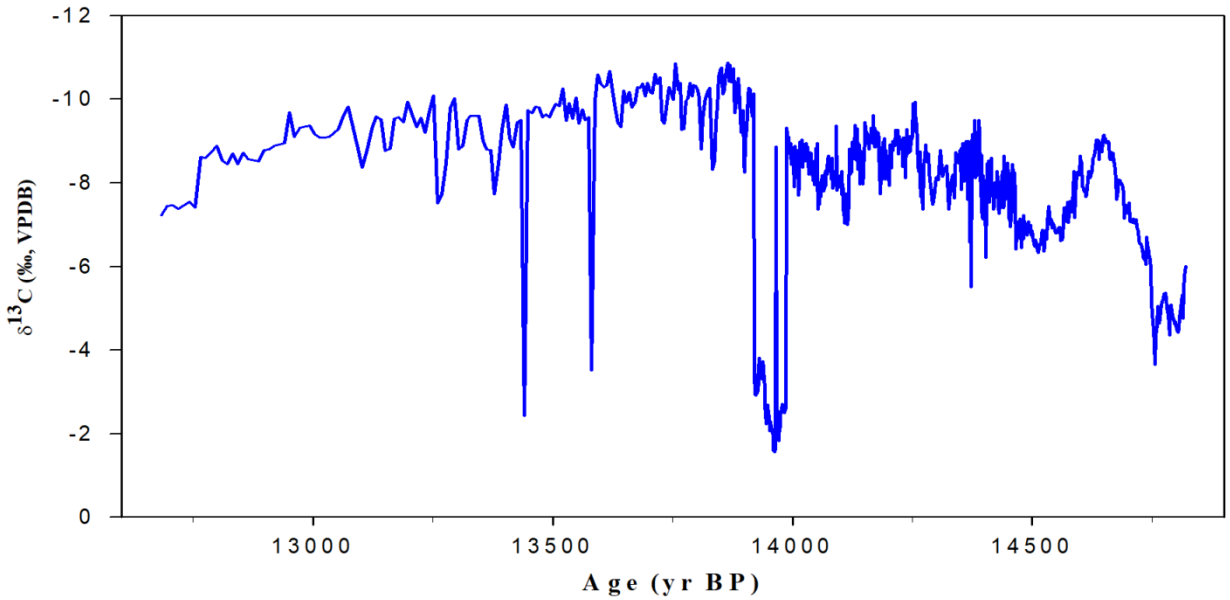

Fig. 6.5. $\delta^{13}C$ Variability. $\delta^{13}C$ record for ~2.1 kyr from ~14.9 ka to ~12.7 ka obtained from stalagmite KG-6. $\delta^{13}C$ values vary from 0.37 ‰ to -6.07‰ with an average of -2.55 ‰. The major oscillations range between -1.5 to -11 ‰.The $\delta^{13}C$ values show abrupt enrichment for about a century after 14 ka BP.

Further, shallow enrichment trend in $\delta^{13}C$ variability was observed with intermittent abrupt enrichment, however for periods, in the variability record during 13.6 and 13.4 ka BP.

These abrupt enrichment in the $\delta^{13}C$ records primarily indicate the onset on cyclic monsoon cycles as indicated in $\delta^{18}O$ variability records. $\delta^{13}C$ record show a similar nature of variability as shown by $\delta^{18}O$ records between 13.8 ka BP to 12.7 ka BP. Gradual enrichment during YD is also indicated by $\delta^{13}C$ record.

6.5. Time Series Analyses of Isotopes and Inferences

Inferences from Z –Score analyses

Z-scores of $\delta^{18}O$ and $\delta^{13}C$ time series indicate similar wet (cyan in Fig. 6.6) and dry (red in Fig. 6.6) phases of Indian monsoon system. The $\delta^{18}O$ time series indicate that there existed dominant dry phase during 14.9 to 14.4 ka BP which was terminated by the onset of intense rainfall for about a century around 14.4 ka BP. Although the intensity of wet phases were observed to have increased but dry phases were also persisting. Hence, it can be inferred that increase in the intensity of rainfall created a transition phase where dominant dry phases where gradually changing towards wet phases. The cyclonic episodes are also indicated around 14.1 ka BP. Further, cyclic nature of monsoon system is depicted during 14 ka to 12.7 ka BP in the $\delta^{18}O$ record with dominant wet phase. The wet was gradually terminated at the onset of YD. The dry phase of YD onset is also depicted in the $\delta^{18}O$ record. A dry phase around 14 ka BP is shown by the z-score of $\delta^{18}O$ record.

A similar variability of $\delta^{13}C$ z-score (Fig. 6.6) is observed which indicate dry phase of the monsoon system during 14.9 ka BP to 14.5 ka BP. Unlike $\delta^{18}O$ record, the $\delta^{13}C$ z-score show early beginning of wet phase from 14.5 ka BP till 14 ka BP. An abrupt dry phase after ~14 ka BP is observed in the $\delta^{13}C$ z-score for about a century after which the wet phase was regained with similar intensity till the beginning of YD during 12.8 ka BP.

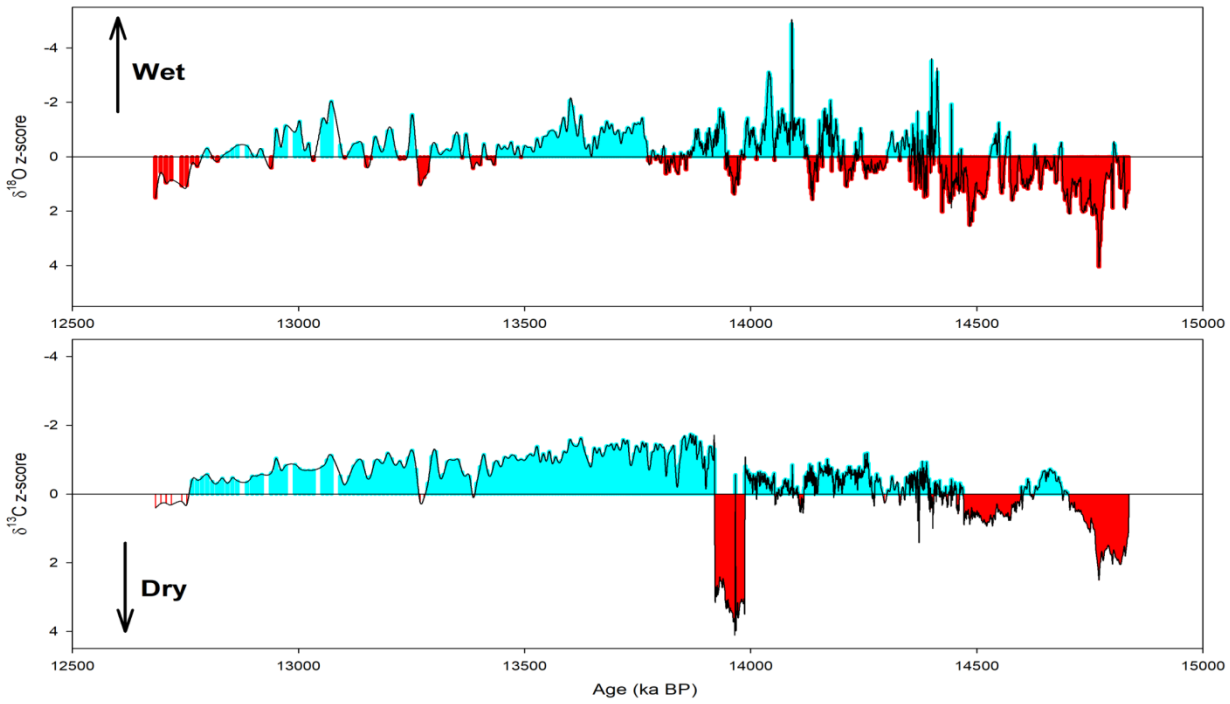

Fig.6.6. Z-Score of $\delta^{18}O$ and $\delta^{13}C$ time series of KG-6 stalagmite, Kailash Cave, Chhattisgarh. Negative (Cyan) and positive (red) z-scores indicate wet and dry phases, respectively.

Inferences from REDFIT Spectral analyses

To estimate the periodicities in the unevenly spaced spectrum of $\delta^{18}O$ measurements, time-series analyses using REDFIT (Schulz &Mudelsee, 2002) was performed to delineate the influence of both solar and non-solar frequencies during the recent deglacial period in PAST programme. The analyses for the time series were performed to identify the periodic components. 99% and 95% confidence levels along with their Monte Carlo counterparts were marked to identify the periodic components in the spectrum.

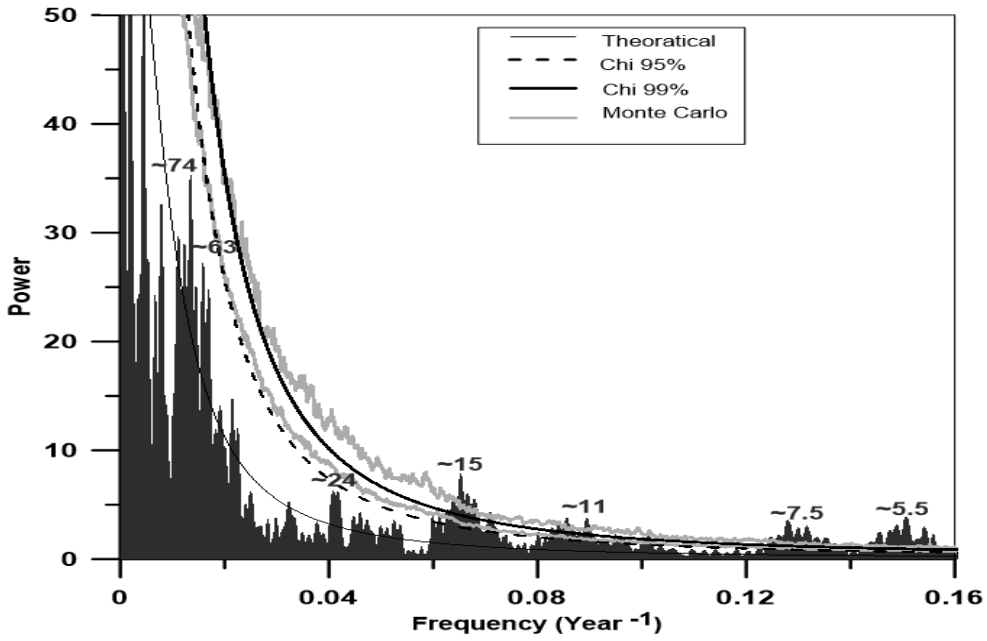

Fig. 6.7. REDFIT Spectral analysis of $\delta^{18}O$ time series. The graph shows frequency-power spectrum having theoretical, Chi 95% and chi 99% along with their monte carlo simulations.

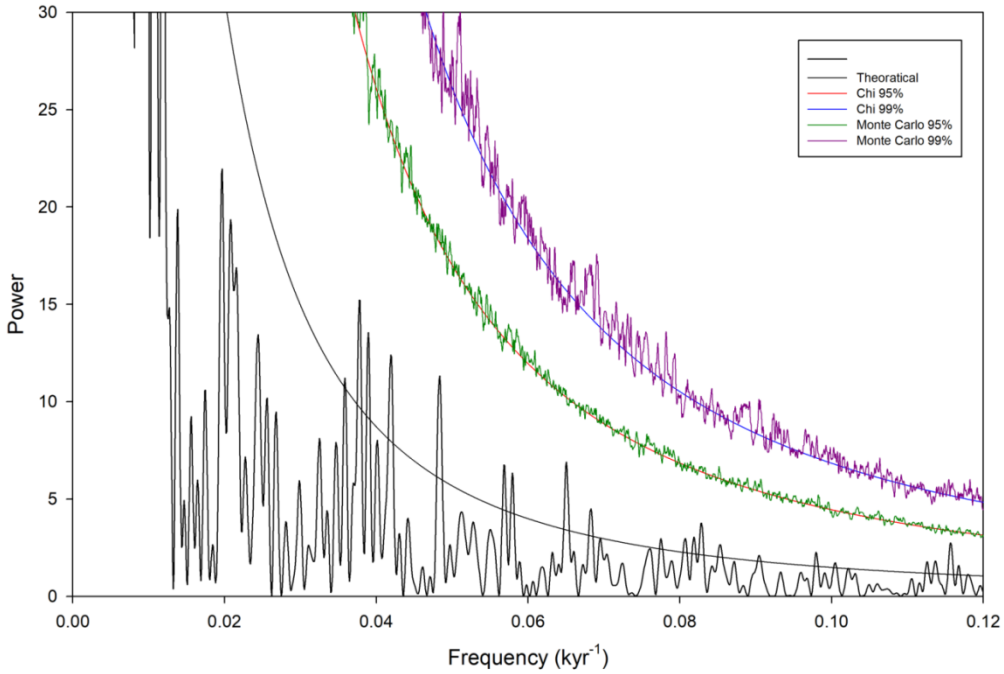

Fig. 6.8. REDFIT Spectral analysis of $\delta^{13}C$ time series. The graph shows frequency-power spectrum having theoretical, Chi 95% and chi 99% along with their monte carlo simulations.

Spectral analyses of the time series from ~14.8 ka to ~ 12.7 ka revealed periodicities of ~ ~74, ~63, ~24, ~15, ~11, ~7.5, and ~5.5 years. The observed cycles indicated a strong link of ISM intensities to solar activities and regional ocean-atmosphere coupling processes responsible. The periodicity of ~24 years is correlated with the magnetic reversals of Sun's magnetic field, known as Hale cycle. Likewise, cycles of ~15, and ~11 years are related to the 11 year Schwabe sunspot cycle. Also, periodicities of ~7.5 and ~5.5 years represent the multiple of Hale and Schawbe cycle. The currently accepted sunspot cycle varies between 9 to 13 years of periodicity (Olvera, 2005; Yadava and Ramesh, 2007). Moore *et al.,* (2006) have also reported that the causative processes for 11 years cycles are most likely due to climate system and unlikely due to sunspot cycles. Similarly, satellite based solar observation since 1978 (Wilson, 1957) have shown that solar magnetic activity modulates the energy received at the top of the atmosphere that may be origin of the cycle in the weather and climate of the earth. The 11 years variations in the sun were also observed in several features such as faculae, flares, radiobursts, etc. (Yadava and Ramesh, 2007). Thus, it is clearly understood that ISM intensities were directly controlled by solar activities during last deglacial. Furthermore, Ruzmalkin (1999) has also suggested that ~11 years solar cycle activity forcing of climate could be through stochastic resonance with El Nino Southern Oscillations (ENSO). Hence, it was inferred from the spectra that solar activities were among the main processes involved in last glacial termination resulting in intense ISM during the recent last deglacial. Agnihotri *et al.,* 2002 has observed periodicities of ~77 and ~113 years in TSI which could be correlated to the periodicities of ~74 years of KG-6 spectra. The centennial periodicity can also be correlated to the long term persistence of ISM intensity in the late phase when ISM attained stable phase i.e., after Bølling-Allerød and before younger drayas (YD). Many earlier workers (Cohmap, 1988; Clemens *et al.,* 1991; Anderson and Prell, 1993) have also reported that the ISM strengthening during the last deglaciation was the consequence of

increasing Northern Hemisphere insolation and changing glacial boundary conditions which created relatively greater heating of the Asian landmass. Dykoski *et al.,* (2005) has related the changes in atmospheric $\Delta^{14}C$ to solar activities because solar wind intensity is reduced during periods of lowered sunspot activity, which increases the influx of galactic cosmic rays, and in turn increases the production of ^{14}C in the atmosphere and vice versa.. Further, Bond *et al.,* (2001) suggest that the ^{14}C record and the millennial events seen in North Atlantic sediment cores are related. They correlated the core record with the $\Delta^{14}C$ record and explained in large part by a solar forcing mechanism. Thus, the periodicities observed in stalagmite KG-6 can also be related to periodicities observed in $\Delta^{14}C$ spectra. The periodicities of ~76.1 years in $\Delta^{14}C$ can be related to cycles of ~74 years respectively indicating a strong solar influence on ISM intensities on decadal to centennial scale.

Since, the variability of $\delta^{13}C$ time series has shown a complex process of deposition, no significant periodicity (Fig.6.8) was deduced from REDFIT analyses of the time series data.

Inferences from Wavelet analysis

The wavelet analyses of KG-6 $\delta^{18}O$ time series (Fig. 6.9) having a resolution of 1.82 years reveal wide range of significant periodicities. Periodicities of ~500 to 460, ~330, ~287, ~143, ~116.5, ~60, ~29, and a poor periodicity of ~7.3 years were observed in the KG-6 $\delta^{18}O$ time series. Further, the wavelet analysis for 14 to 12.6 ka (average resolution: 4.93 years) showed periodicities of ~284, ~147, ~66, and ~25 years. Similarly, periodicities of ~142, ~115, ~81, ~58, ~29, ~14, and ~3.6 years were revealed from the wavelet analyses of the $\delta^{18}O$ time series from 14.8 to 14 ka which has an average resolution of 0.90 years. It is suggested that the 500 to ~460 year cycle in KG-6 $\delta^{18}O$ record depicts the centennial scale variability in coupled ocean-atmospheric processes. A ~512 year cycle in $\Delta^{14}C$ (Stuvier *et al*, 1993) has been suggested to be due to variations in ocean circulation specifically, by changes in North Atlantic Deep Water

(NADW) formation that control incorporation of ^{14}C into the ocean. Similarly, ~356 year cycle in $\Delta^{14}C$ may correspond to the ~330 year cycle in KG-6 $\delta^{18}O$. Furthermore, it is also suggested that the periodicities of ~284 and ~287 years may be the harmonic multiple of ~500 to ~460 years periodicities. Similarly, periodicities of ~142 to ~147 years may also correspond to harmonic multiples of the coupled ocean-atmospheric cycles. In this regard, it is worth to note ~148 year cycle in $\Delta^{14}C$ which support the association of the cycles with ocean variability. Periodicity of ~81 year in KG-6 $\delta^{18}O$ record may correspond to Gleissberg solar insolation cycle. Similarly, the periodicities of ~116.5 and ~115 year may also be associated with solar insolation. Cycles of ~117 year and ~81.6 year have been noted in the sunspot cycles. The periodicities of ~58, ~60, and ~66 years can be related to oceanic processes involved in controlling the ISM intensity changes.

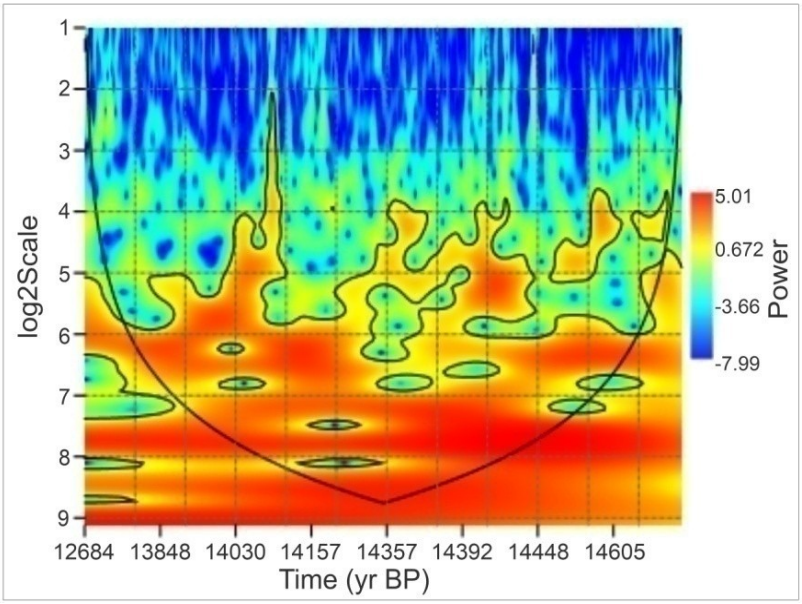

Fig. 6.9: Wavelet analyses of KG-6 stalagmite $\delta^{18}O$ record. Spectral power (variance, $‰^2$) is shown by columns ranging from weak (deep blue) and strong (deep red) color bands. Black cone demarcates the upper boundary in which identified frequencies can be interpreted for periodicities. Irregular black curves delineate 95% confidence limit of time-frequency region.

The wavelet analysis of KG-6 $\delta^{13}C$ time series (Fig. 6.10) revealed periodicities of ~499 years, ~329 years, ~143 years, ~58 years, and ~9.5 years. The centennial scale periodicities are observed to be dominant in the $\delta^{13}C$ time series which may indicate the change in the centennial scale vegetation patterns associated with the monsoonal changes in the region. The centennial scale periodicities of ~499 years can be correlated with the ~512 year cycle in $\Delta^{14}C$ (Stuvier *et al.,* 1993) due to the changes in North Atlantic Deep Water (NADW) formation that control incorporation of ^{14}C into the ocean. Similarly, ~356 year cycle in $\Delta^{14}C$ may correspond to the ~329 year cycle in KG-6 $\delta^{13}C$. The ~143 cycle may again correspond to as harmonic multiples of the coupled ocean-atmospheric cycles. Further, the periodicity of ~9.5 years is linked to year Schwabe sunspot cycle.

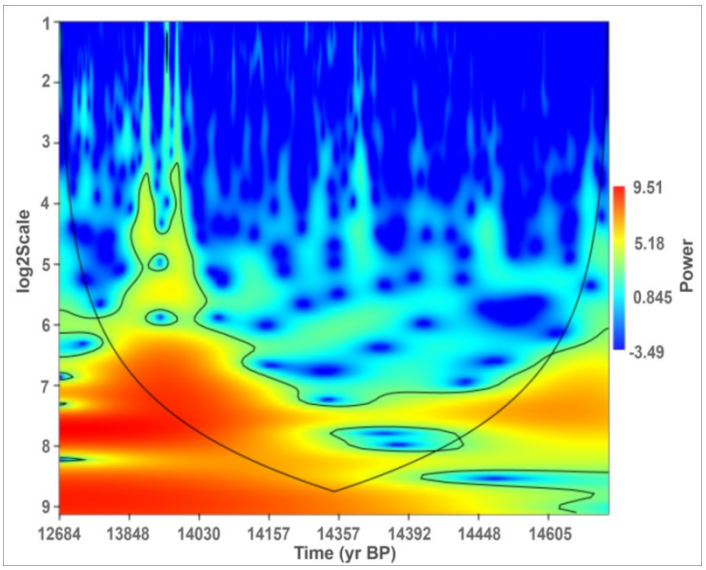

Fig. 6.10: Wavelet analyses of KG-6 stalagmite $\delta^{18}O$ record. Spectral power (variance, $‰^2$) is shown by columns ranging from weak (deep blue) and strong (deep red) color bands. Black cone demarcates the upper boundary in which identified frequencies can be interpreted for periodicities. Irregular black curves delineate 95% confidence limit of time-frequency region.

Kerr (2000) recognized a 65-80 year cycle in Atlantic SST, corresponding to Atlantic multidecadal oscillation. Similarly, Delworth and Mann (2000) found an approximate variability of ~70 years in a 330 year proxy based reconstruction of SST and also in instrumental records. The spatial pattern of this variability has been regarded to be of hemispheric or even global scale. Agnihotri *et al.,* (2002) also found an approximate ~60 year periodicity in multi proxy results of surface productivity from Arabian Sea which in turn reflect ISM wind intensity. It is also noteworthy from the recent data (1871-1900) analyses (Goswami, 2006; Krishnamurthy and Shukla, 2001) that there exist no trend or climate change signal in ISM data but contain coherent multidecadal variability with an approximate periodicity of 55-60 years. Joseph (1976) also showed a ~60 year interdecadal changes in monsoon rainfall associated with interdecadal changes in the trace of storms and cyclones in the Bay of Bengal. We infer these decadal periodicities to be extremely important periodic changes in ISM intensities due to the coupled ocean-atmospheric processes. Period of ~ 29 year may be related to 33-38 year cycle reported by Stocker (1994) which has been attributed to fluctuations in thermohaline circulation in the North Atlantic. Lone *et al.,* (2014) have related ~33 year cycle to solar and/or ocean-atmospheric circulation changes. Furthermore, Tiwari *et al.,* (2012) have reported a ~32 year solar cycle from tree ring record of western Himalaya. Also, ~33 year cycle from various stalagmite records from China has also been reported (Ku and Li., 1998; Paulsen *et al.,* 2003; Zhang *et al.,* 2013). We assume that the periodicity of ~29 years may be the consequence of integrated solar and oceanic circulation processes. Inferred poor periodicities of ~14 and ~7.3 years can also be linked to oceanic processes as it has been inferred from North Atlantic Oscillation and of SST of the tropical, northern, and southern Atlantic respectively (Melice and Servain, 2002; Domminget and Latif, 2000).A 14 year cycle was also detected in the Peru (Quelcaya) ice records (Melice and Roucou, 1998). Thus, it is interesting to note from the periodicities of KG-6 $\delta^{18}O$ record that ISM

shifts are essentially associated with the integrated changes in solar and coupled ocean-atmospheric processes.

6.6. Regional Coherence

The stalagmite KG-6 $\delta^{18}O$ record (Fig. 6.11) is compared with speleothem data from the Maboroshi cave, Japan; Hulu and Dongge caves, China; Timta cave, Himachal Pradesh, India; Valmiki Cave, Andhra Pradesh, India; Moomi cave, Yemen; and the Gunung Buda cave, Borneo; to understand the intensity and extent of coherence to spatially demarcate the boundary of ISM forcing factors. The onset of B-A is well marked in all the caves as shown in figure 6.11, indicating a good agreement between the records. Coherence with other caves provides an evidence of the growth of the stalagmite in secular isotopic equilibrium eliminating all chances of kinetic fractionation. These similar patterns of $\delta^{18}O$ shifts also indicate that the hydroclimate at all these sites was governed more or less from vapor masses responding to a similar forcing mechanism (post glacial warming, as indicated by GISP record, Fig. 6.11A). As the timing of stabilization of the monsoon, it is noteworthy that the $\delta^{18}O$ records of the Maboroshi cave (Fig. 6.11B), Hulu (Fig. 6.11C) and Dongge caves (Fig. 6.11D) stabilize much later than those from the Timta (Fig. 6.11E), Kailash (Fig. 6.11F), and Valmiki cave (Fig. 6.11G) records of India. This may be due to the fact that ISM sub-domain receives moisture dominantly from the Indian Ocean, whereas the East Asian sub-domain gets moisture mainly from the Pacific (Clarke *et al.,* 2012). Similarly, the enrichment in ^{18}O towards YD (~12.8 ka) is observed in all the cave records. Hence, it can be inferred that while these caves recorded similarly to post glacial warming, they differed during the stable phases of the monsoon because during ISM, asymmetric pressure patterns across the Equator leads to cross equatorial flow connecting the Mascarene High in the Southern Hemisphere and the Monsoon Trough over India. This transports moisture

from the southern Indian Ocean to south Asia (Wang, 2006). Hence, it is likely that the trigger for large scale convection, originated from the southern hemisphere, modulating the monsoon strength over the Indian subcontinent must have controlled the monsoonal variability at all the cave sites coupled with local climatic attributes. Also it has been well reported that the ISM circulation and associated moisture penetrate northeastward, deep into East Asia resulting a significant concept that the component of east Asia summer monsoon (EASM) precipitation is derived essentially from the ISM domain (Ding 2004; Clemens *et al.* 2010; *Pausata et al.,* 2011) as perceived from the coherent $\delta^{18}O$ records. A prominent dry phase (Older Dryas?) around 13.7-13.8 ka (Fig. 6.11) in the $\delta^{18}O$ records of all the caves appear to have some leads and lags, because of differences in the age models and the associated age uncertainties. We suspect that the dry phase around 13.7-13.8 ka may have consequently locked B-A period causing ISM to attain a stable phase henceforth.

6.7. Interhemispheric Links - Teleconnection

The KG-6 $\delta^{18}O$ record is compared with polar records to identify possible inter-hemispheric links modulating the ISM. Variations in $\Delta^{14}C$ (a surrogate for cosmic ray flux modulated by solar activity) compares well with changes in the ISM in early part of the record (Fig.6.12A). Similarly, the synchronous variability of GISP $\delta^{18}O$ record (Fig. 6.12B) with KG-6 record during the same interval clearly indicates a direct linkage with ISM variability with clear cut signatures of the B-A event; likewise, the YD event in both the isotopic records provide evidence of climatic interaction between the poles and the tropics, linked to the contemporaneous ITCZ migration towards further north and advection of moisture resulting in the intensification of the ISM and ^{18}O enrichment in Greenland ice (Steffenson *et al.,* 2008, Fig.6.12). The B-A and YD events have been more or less in antiphase relation in both the hemispheres (Pedro *et al.,*

2015) and are explained using the bipolar seesaw mechanism pertaining to the cross equatorial flow (Shen *et al.,* 2010). The stalagmite $\delta^{18}O$ record compares well with the Arabian Sea monsoon run-off record (Saraswat *et al.,* 2013; Fig.6.12D). It has been shown that the atmospheric CH_4 record is important as it varies in phase with Greenland and Antarctic climate change during the deglaciation (Marcott *et al.,* 2014). This offers a means of synchronization of tropical proxy records with polar records. Atmospheric CH_4 is primarily produced by land-based sources, such as tropical and boreal wetlands, where methane emissions are driven by changes in temperature and hydrology. Methane, therefore, serves as an indicator of terrestrial biosphere. Here, the rapid rise and fall of methane during B-A and YD events, respectively, and a plateau like record of CH_4 (Fig.6.12E and F) during the stable phase of ISM (as observed in stalagmite KG-6 of this study) are quite alike. Similarly, CO_2 records too, compared with the KG-6 $\delta^{18}O$ record (Fig. 6.12G), suggests interhemispheric teleconnection, reinforced by rising atmospheric CO_2 which allowed the Earth to emerge from the last ice age (Denton *et al.,* 2010).

Higher atmospheric CO_2, driven by the reorganization of ocean and atmospheric circulation that accompanied northern stadials, is a key factor to complete the deglaciation. Specifically, it was the long duration of stadial conditions made possible by large and unstable ice sheets that extracted enough CO_2 from the deep ocean to warm the Earth; and sustained the melting of NH ice sheets for several thousand years after NH summer insolation started to decline. Comparison of proxy records across latitudes clearly shows a controlling pathway of ISM pertaining to the changes occurring in the polar climatic patterns. We also compare high resolution KG-6 $\delta^{18}O$ record with the EPICA Dronning Maud Land (EDML) and TALOS $\delta^{18}O$ records (Fig. 6.12H) and also with the new high resolution ice rafted debris (IRD) record (Fig. 6.12I).

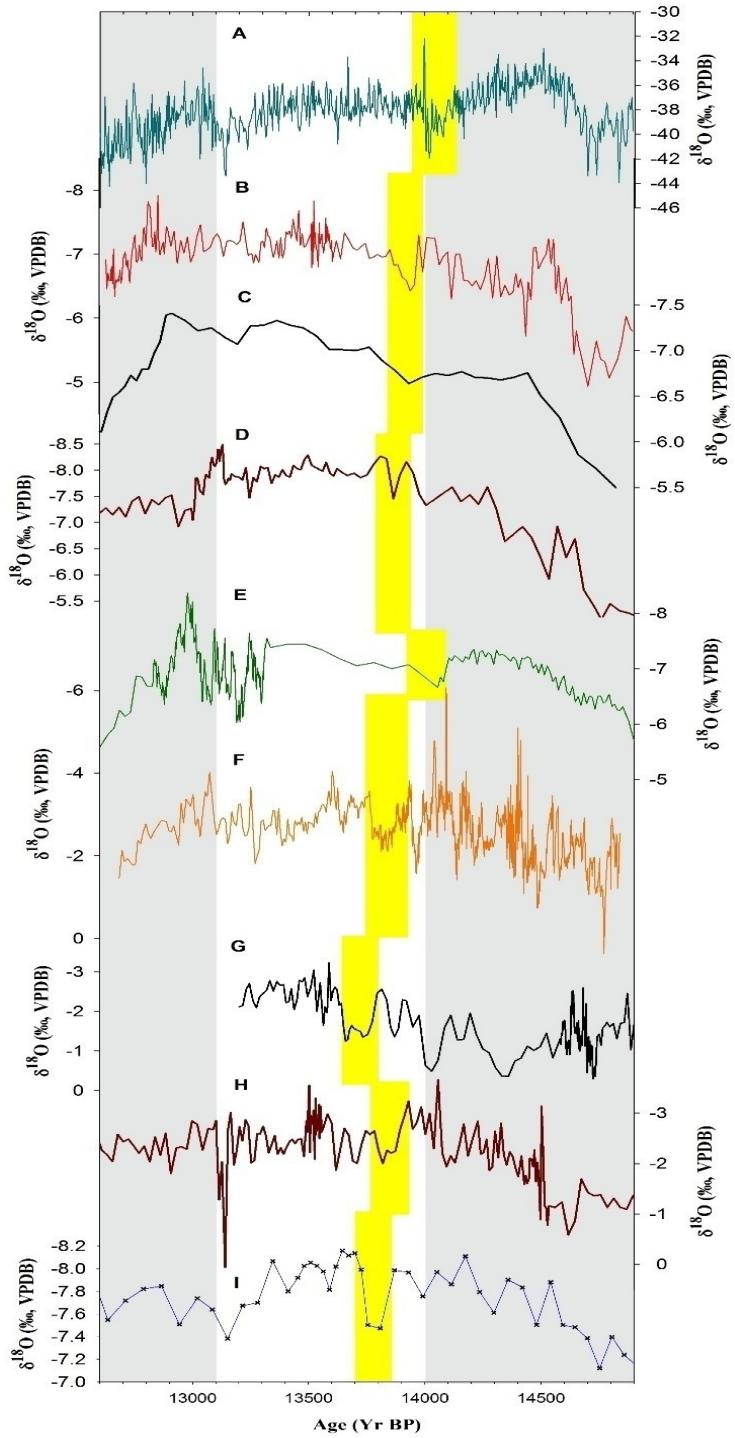

Fig.6.11: Coherence of stalagmite $\delta^{18}O$ with other proxy records. Records for the period 14.8 ka to 12.6 ka from **A**. GISP2 core, Greenland (Stuvier and Grootes, 2009). **B**. Maboroshi cave, Japan (Shen *et al.,* 2010) **C.** Hulu cave, China (Wang *et al.,* 2001)**D.** Dongge cave, China (Dykoski *et al.,* 2005) **E.** Timta cave, India (Sinha *et al.,* 2005)**F.** Kailash cave, eastern India (this study) **G.** Moomi cave, Socotra Island, Yemen (Shakun *et al.,* 2007)and **H.** Gunung Buda Cave, Borneo (Partin *et al.,* 2015) have been compared. Shaded grey band represents the onset of B-A event in all the proxies and yellow bands indicate a dry event (Older Drayas?) after B-A which may have reorganized the ocean-atmospheric processes modulating the hydroclimate and stable ISM.

The latter corresponds to elevated temperature shifts in the Southern Ocean documented as abrupt shifts in the Antarctic climate and associated ice sheet dynamics (Weber et al., 2014). The KG-6 $\delta^{18}O$ record and those of EDML and TALOS show a remarkably synchronous variability, indicating a significant influence on ISM of SH during the last deglaciation.

Similarly, the increased rate of depletion of ^{18}O from -5.09‰ to 0.36‰ with the increase in IRD flux during ~14.7-14 ka is well marked as the onset of B-A. It is interesting to note that the higher IRD flux reflect more depletion of ^{18}O as in the case of stalagmite KG-6. Further, relatively lower IRD flux during YD is also coherent with the enrichment in ^{18}O trend in KG-6. Also, the temporal shifts in IRD flux are coherent with significant variable temporal lags in KG-6 $\delta^{18}O$ record. These periodic changes in IRD flux with KG-6 $\delta^{18}O$ gives the hint of probable link between the two, such that changes in SH also have control on ISM indicating higher the IRD flux, more intense the monsoon. The AID6 (~14.7 ka) peak in the IRD record co-occurs with MWP-1A (Weber et al., 2014) which provides direct evidence for inter-hemispheric climatic link. It is also noteworthy that following AID7 event (~16 ka), Antarctic bottom water formation was reduced and subsurface water surrounding Antarctica, the Circumpolar Deep Water (CDW) began to warm and migrate further southward (Weber et al., 2014; Zhang et al., 2016). This poleward migration of CDW helped to accelerate the thinning of ice shelves by basal melting, inducing Southern Ocean upwelling and Antarctic Cold Reversal (ACR), which ultimately shifted ITCZ northward resulting in the intensification of ISM. While comparing our records with SH-IRD flux, it was noted that the intensification of ISM during the onset of B-A was probably modulated by the ocean thermal forcing from the transport of warm CDW to the base of the ice shelves, which resulted higher freshwater input in the Southern Ocean and ultimately in the rise of sea level.

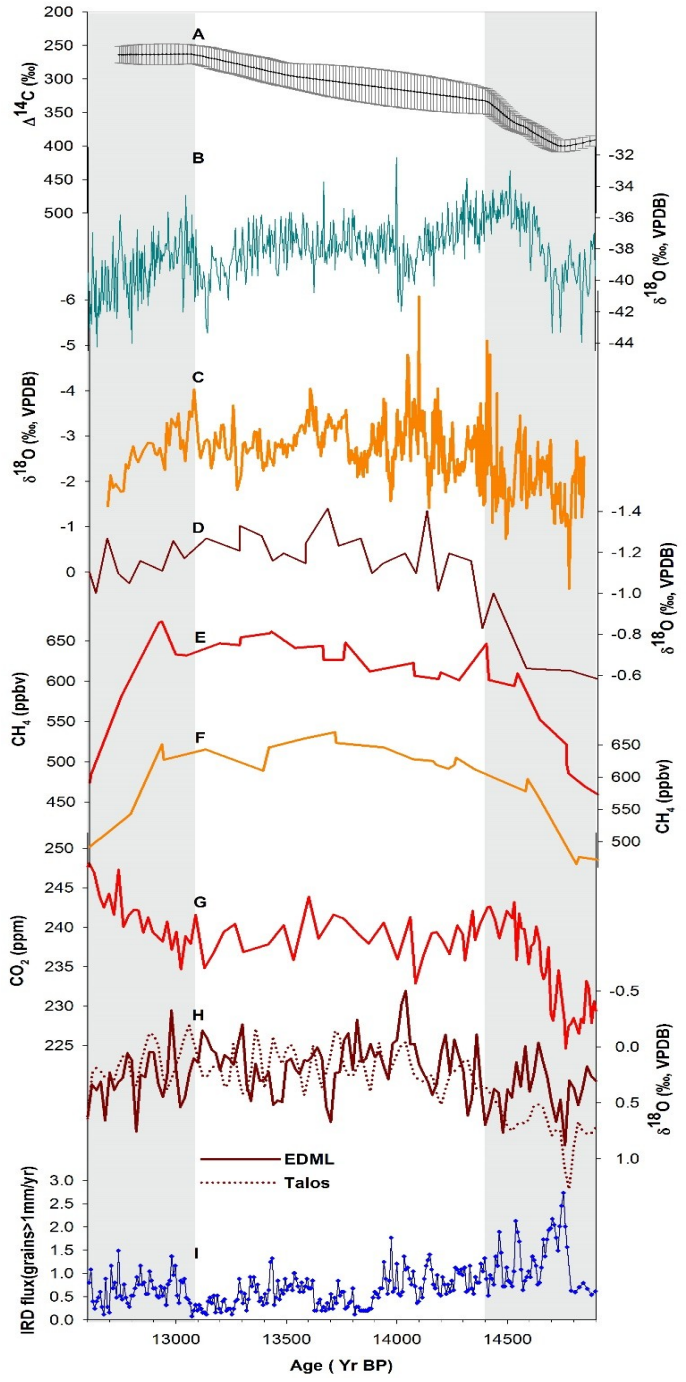

Fig. 6.12: Interhemispheric comparison of KG-6 $\delta^{18}O$ record. A. $\Delta^{14}C$ (Riemer *et al.,* 2009) **B.** GISP2 ice core $\delta^{18}O$ record (Stuvier and Grootes, 2009; data retrieved from NOAA, USA) **C.** Kailash cave, KG-6 $\delta^{18}O$ record (This study) **D.** Indian Ocean $\delta^{18}O$ record (Saraswat *et al.,* 2013) **E**. EDML CH_4 (data retrieved from NOAA, USA) **F.** EDC CH_4 (data retrieved from NOAA, USA) **G** AICC CO_2 (data retrieved from NOAA, USA) **H.** EDML and TALOS $\delta^{18}O$ records (data retrieved from NOAA, USA) **I.** IRD Flux rate (Weber et al., 2014) provides inter-hemispheric relations and teleconnections. Two gray shaded portions indicate B-A and YD events from right to left, respectively.

This freshwater input must have caused widespread surface cooling in SH and increase in the Southern Ocean sea ice cover. Consequently, it established ACR and the bipolar seesaw.

Furthermore, last deglaciation induced a reorganization of global atmospheric circulation patterns characterized by a southward shift in the SH westerlies, increased upwelling in the Southern Ocean, rising atmospheric CO_2 and global temperature (Anderson *et al.,* 2009). This reorganization may plausibly be the result of the dry period (~ 13.7-13.8 ka) which occurred after B-A event. Atlantic Meridional Oceanic Circulation had a critical role in the glacial–interglacial rise of atmospheric CO_2 and may have acted as a modulator of both the timing and the magnitude of CO_2 and CH_4 changes during the last glacial termination, either directly, through changes in ocean circulation, or indirectly, through the redistribution of heat and the associated climate response. ACR, as seen in the proxies, is ultimately a response to the strengthening of the AMOC. Hence, to summarize, although there is no denying the fact that NH has direct impact on ISM, we observe that there exists a probable causal link of ISM with SH too at the onset of B-A event and thereafter. Zhang *et al.,* (2016) have also reported a similar signature from their stalagmite $\delta^{18}O$ records from Haozhu cave, central China. Also, this has been suggested from the records of Hequing Basin, Southern China (An *et al.,* 2011) that SH latitudinal cooling produces stronger ISM by enhancing cross-equatorial atmospheric pressure gradient. Clemens (1991) also has documented the consistence of modern annual and inter-annual coupling between stronger monsoons and increased ocean-atmosphere latent heat flux from the southern subtropical Indian Ocean. He also speculated from the zero-phase relationship that SST estimated from higher southern latitudes, under great influence of obliquity forcing, may show significantly greater coherence with the monsoon. However, Kathayat *et al.,* (2016) contradicts this link and suggest that tropical-subtropical monsoonal regions may themselves be a part of bipolar see-saw mechanism rather than being influenced by SH variations. They also add that SH temperature

changes are too small and gradual to affect ISM. Hence, links of SH with ISM variability requires more attention, further investigations and discussions to understand the actual interhemispheric forcing and controlling mechanisms.

6.8. Summary

In this chapter, $\delta^{18}O$ and $\delta^{13}C$ records of stalagmite KG-6 from Kailash cave have been discussed. The isotopic records represent significant high resolution southwest monsoon variability reconstruction during ~14.7–12.6 ka, which covers Bolling-Allerod (B-A) and Younger Dryas Events. The variability of isotopic records is inferred as the consequence of the changes that occurred in the coupled ocean-atmospheric system, in addition to solar forcing. The results indicate that there could be a significant SH contribution in modulating the climate pattern of ISM. However, it still remains a destitute inference and demands more attention to understand the forcing and controlling mechanisms.

Chapter 7

Indian Summer Monsoon during Mid-Holocene

Chapter 7

Indian Summer Monsoon during Mid-Holocene

7.1.Introduction

Mid- Holocene climate has been considered as one of the most complex processes which resulted in abrupt climate changes throughout the world as it represents a major transition in global climate. Mid-Holocene is believed to have observed a significant social and cultural transformation in many parts of the world. This climate transition has been appreciated as the analogy of the ongoing and forthcoming global climate change (Budyko *et al.,* 1978; Kellogg, Kutzbach and Guetter, 1986; Mitchell, 1990). However, it is a matter of long debate and adequate research to prove this. Mid-Holocene thus, offers a good example of the nature and magnitude of changes in climate and biota that could occur over the long term in specific regions, and, based on what happened in the past, their possible impact on human societies. A number of records spanning across the Mediterranean, Middle East, North Africa, North America, India, and China suggest that there was a significant large-scale climate shift at approximately 4 ka B.P. which caused extinction of major civilizations like Indus valley, Yangtze valley, Greece, Egypt, etc (Weiss and Bradley, 2001; Thompson *et al.,* 2002; Booth *et al.,* 2005; Rashid *et al.,* 2011; Berkelhammer *et al.,* 2012; Weiss, 2012; Ruan *et al.,* 2016; Railsback *et al.,* 2018; Kathayat *et al.,* 2018; Band *et al.,* 2018). It has been reported as dominant arid phase due to weakened Indian Summer Monsoon (ISM) in Indian subcontinent (Rashid *et al.,* 2011; Giosan

et al., 2012; Berkelhammer *et al.,* 2012; Dixit *et al.,* 2014, 2018; Kathayat *et al.,* 2017, 2018; Dixit *et al.,* 2018; Band *et al.,* 2018; Walker et al., 2019). Mid-Holocene climate transition correlates very well with other northern low-latitude records resulting directly from the orbitally induced lowering of summer insolation affecting ITCZ position and low-latitude precipitation patterns along with solar forcing (Wang *et al.,* 2005). However, a few results have also shown flood events during this time interval (Huang et al., 2010, 2011; Wu *et al.,* 2017). Hence, a clear understanding of the abrupt climate change during mid-to late Holocene from high resolution proxy data is very important for both climatic and archaeological perspectives.

A high resolution $\delta^{18}O$ and $\delta^{13}C$ variability record of stalagmite from Borra Cave, Araku Valley, India is presented in this chapter for mid Holocene age covering a temporal span of ~925 years from ~4.79 ka BP to ~3.87 ka BP at an average resolution of ~2.2 years. The main focus of the chapter is listed below:

- To identify and understand the feedback mechanism that influenced ISM during the mid- Holocene from the high resolution $\delta^{18}O$ and $\delta^{13}C$ variability record.
- To identify/understand whether dry period around 4.2 ka BP was a continuous and/or are there any intermittent wet periods, if so how long.
- The work also aims to observe the potential tie ups between the abrupt climate changes with the history of civilizations.

The details of sample collection and sub-sampling for geochronology and isotopic analyses for paleoclimatic inferences are discussed in Chapter 3. The stalagmite BRA-3B was cleaned with jet water for physical examination of any major or minor

physical change along the growth lines. The mineralogy of BRA-3B growth layers are discussed below.

7.2.Mineralogy and Isotopic Equilibrium Growth

Mineralogy of the stalagmite growth layers is essential to estimate the initial value for ^{230}Th geochronological method and also for the oxygen and carbon stable isotopic analyses. In this regard, classical staining and modern XRD methods, as discussed in Chapter 3, both were used. Fiegl's solution chemical staining method showed no dark or black layers which confirmed the mineral composition of the stalagmite BRA-3B to be calcite. However, some feeble spot of patchy darkness were observed at few places on the sample slice along the growth layers. Hence, eleven such layers from the dark patchy area were selected for XRD analyses (Fig.7.1) which also confirmed their composition to be of calcite. Hence, it was finally understood that the composition of stalagmite BRA-3B is calcite throughout.

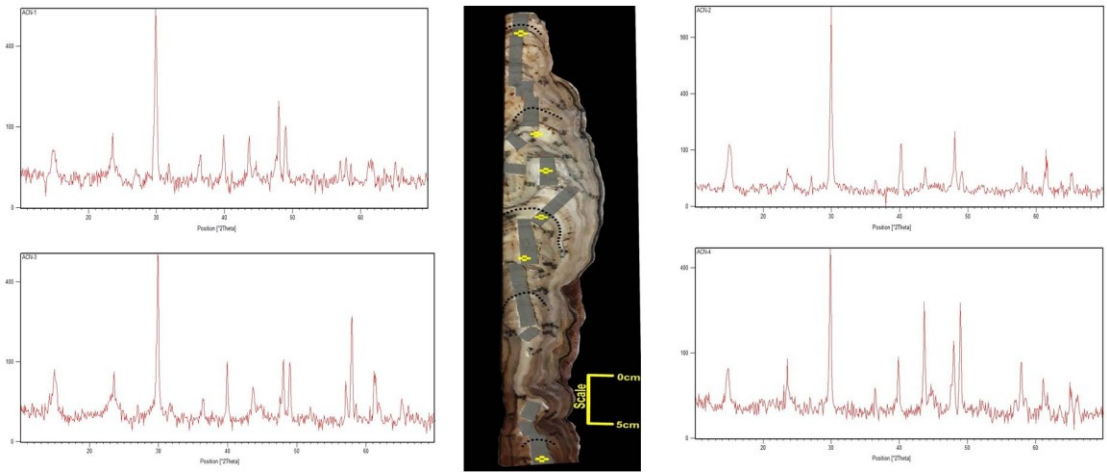

Fig. 7.1. XRD mineralogy of stalagmite BRA-3B. The XRD mineral composition of the stalagmite BRA-3B revealed as of calcite throughout.

Hendy's test (1971) for isotopic equilibrium growth of the stalagmite sample BRA-3B shows (Fig.7.2) that there is no significant latitudinal variation in the concentrations of $\delta^{18}O$ and $\delta^{13}C$ in individual growth layers. No significant correlation is also observed between $\delta^{18}O$ and $\delta^{13}C$ which indicate that the stalagmite was deposited under isotopic equilibrium.

7.3.U-Th Chronology of Stalagmite

Six ^{230}Th ages (Table 7.1) of the sample were obtained, using the facility at Xi'an Jiaotong University, China, employing Thermo-Finnigan Neptune-*plus* multi-collector inductively coupled plasma mass spectrometer (MC-ICP-MS) following the methods described in Cheng *et al*. (2000, 2013). Standard chemical procedure (Edwards et al., 1987) was used to separate uranium and thorium. A triple-spike (^{229}Th-^{233}U-^{236}U) isotope dilution method was used to correct instrumental fractionation and to determine U/Th isotopic ratios and concentration (Cheng *et al.,*

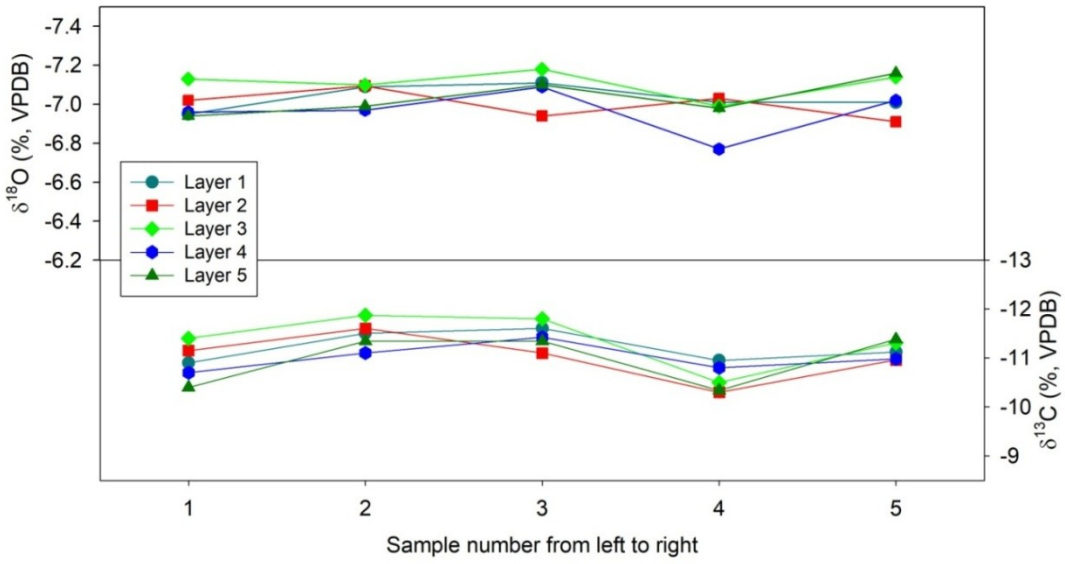

Fig.7.2. Hendy's Test. Five distinct growth layers were drilled along latitudes for Hendy's test of stalagmite BRA-3B. The isotopic composition is observed to be in same range within the growth layer.

2013). U-Th isotopes were measured on a MasCom multiplier behind the retarding potential quadrapole in the peak jumping mode using the standard procedure (Cheng *et al.,* 2000). Uncertainties in U/Th isotope measurement were calculated at 2σ level. StalAge 1.0 age-depth model (Fig. 7.3) was run for BRA-3B stalagmite using six ^{230}Th ages to establish a normal stratigraphic order of crystallization in the given temporal span of ~4.79 ka BP to ~3.87 ka BP.

7.4. Isotopic variability during the Mid-Holocene

The $\delta^{18}O$ and $\delta^{13}C$ measurements (Fig. 7.4) make a time series of 420 data points of BRA-3B with an average temporal resolution of 2.21 years for a period from ~4.79 ka to ~3.87 ka. The $\delta^{18}O$ and $\delta^{13}C$ time series show cyclic variabilities where onsets of ISM are identified as abrupt depletion in $\delta^{18}O$ and $\delta^{13}C$ values and the terminations are marked by the gradual enrichment.

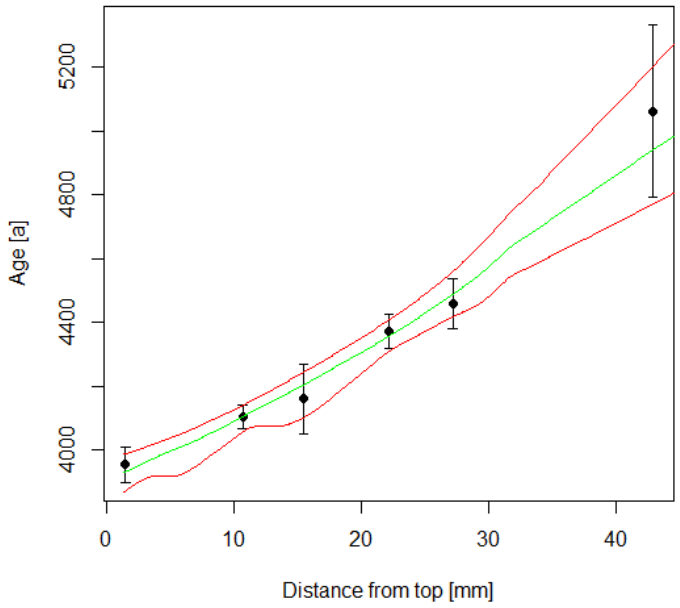

Fig. 7.3. StalAge 1.0 Age-Depth model. Black dots with error bars indicate the measued U-Th ages with their errors. Green line shows the interpolated age with buffer red lines.

.Table. 7.1. U-Th ages of Stalagmite BRA-3B		
Depth (mm)	**Age**	**Error**
85	3954	55
122	4104	36
165	4160	111
211	4372	53
257	4458	78
480	5062	271

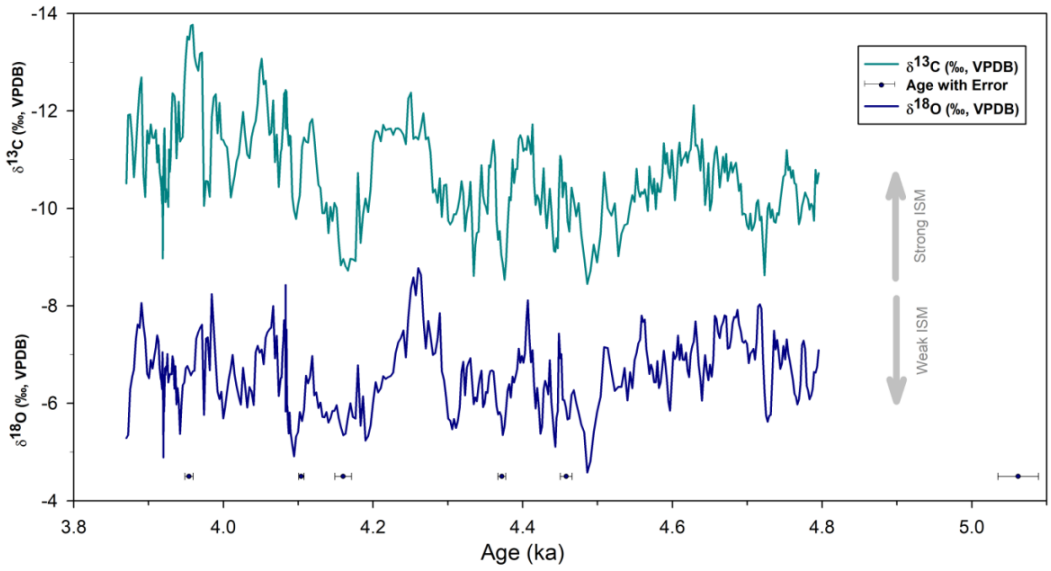

Fig. 7.4. $\delta^{18}O$ and $\delta^{13}C$ time series of BRA-3B stalagmite from Borra Cave, Andhra Pradesh. Dark cyan and blue curves indicate $\delta^{13}C$ and $\delta^{18}O$ time series, respectively. black points with error bars indicate the measure U-Th ages of the stalagmite.

Desphande et al. (2012) have reported present day $\delta^{18}O$ ranging from -8‰ to -6‰ at the cave location. Hence, employing this range to be normal variability in the study area, the additional depleted and enriched values may indicate wet and dry events

respectively. Therefore, six distinct wet phases are identified as depleted concentrations in the $\delta^{18}O$ time series of BRA-3B stalagmite during the periods of 4.5-4.47 ka BP, 4.44-4.41 ka BP, 4.38-4.29 ka BP, 4.23-4.08 ka BP, and 4.04-3.99 ka BP The isotopic values of this study demarcate three major dry periods on centennial scale including the global 4.2 ka event exhibiting enriched $\delta^{18}O$ values for ~150 years duration from 4.23 ka BP to 4.08 ka BP.

7.5. Time Series Analyses of Isotopes and Inferences

Inferences from Z-Score analysis

The z-score plots of $\delta^{18}O$ and $\delta^{13}C$ records clearly show the major wet (cyan, Fig. 7.5) and dry (red, Fig. 7.5) phases. The z-score of $\delta^{18}O$ shows six distinct wet phases and five distinct dry phases whereas the z-score of $\delta^{13}C$ record shows four distinct wet and dry climate phases. The dry and wet phases show a cyclic nature. Long term dry event is inferred beginning at 4.2 ka BP from the z-score time series analysis of the two isotopic records.

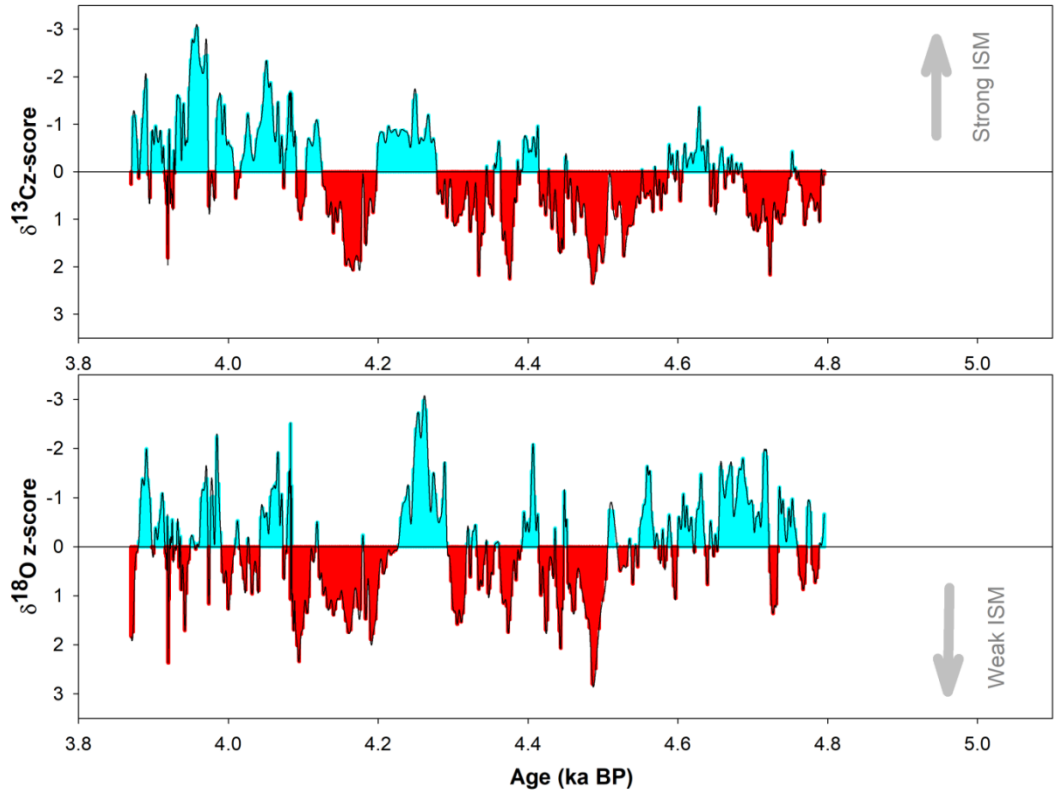

Fig. 7.5. Z-Score of $\delta^{18}O$ and $\delta^{13}C$ time series. Negative Z-score (cyan) indicate wet phases whereas positive z- score (red) indicate dry phases of Indian summer monsoon.

Inferences from REDFIT analysis

The REDFIT analysis of $\delta^{18}O$time series (Fig. 7.6) of stalagmite BRA-3B revealed periodicities of ~11.5 years, ~9.8 years, ~9.0 years, ~8.1 years, ~7.7 years, ~6.25 years, and ~5.5 years. Similarly, $\delta^{13}C$ time series (Fig. 7.7) of BRA-3B also showed ~12.5 years, ~7.5 years, ~6.5 years, and ~5.5 years. The periodicities from the two time series directly show their link to solar insolation periodicities. The inferred cycles are directly linked to ~ 11 year Schwabe cycle and its arithmetic multiples.

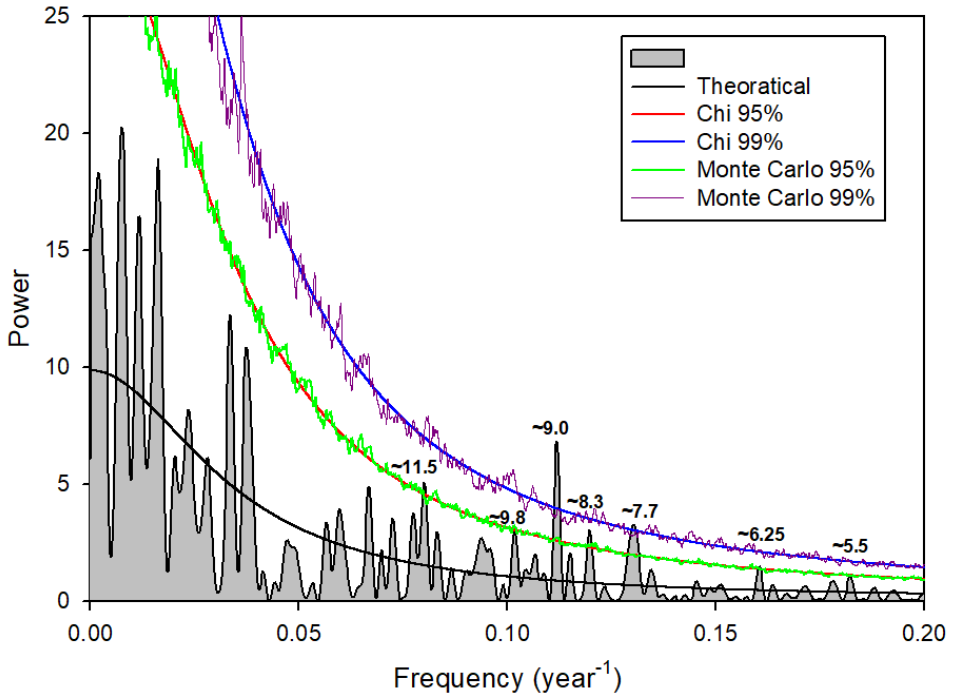

Fig. 7.6. REDFIT Spectral analysis of $\delta^{18}O$ records. Graphs shows power-frequency plot with 95% and 99% chi square along with monte carlo simulations.

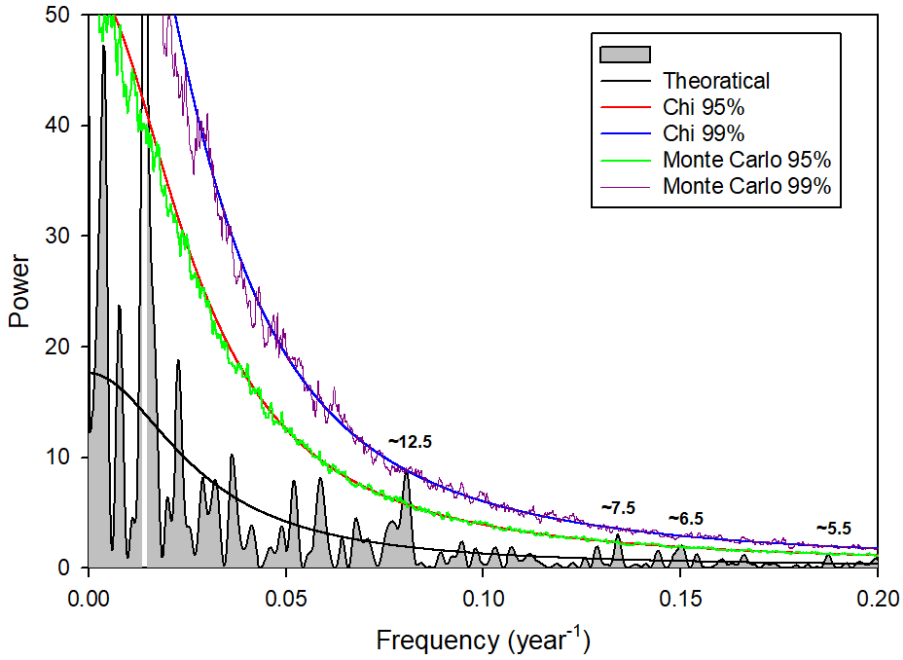

Fig. 7.7. REDFIT Spectral analysis of$\delta^{13}C$ records. Graphs shows power-frequency plot with 95% and 99% chi square along with monte carlo simulations.

Inferences from Wavelet analysis

The wavelet analysis was carried out for the $\delta^{18}O$ (Fig.7.8) and $\delta^{13}C$ (Fig. 7.9) time series having average temporal resolution of~2.21 years. Periodicities of ~283, ~162, ~93, ~70, ~47, ~37, ~25, and ~16 years were observed in the $\delta^{18}O$ time series. Similarly, periodicities of ~239, ~152, ~119, ~107, ~71, ~54, and ~28 years were revealed from the wavelet analyses of the $\delta^{13}C$ time series.

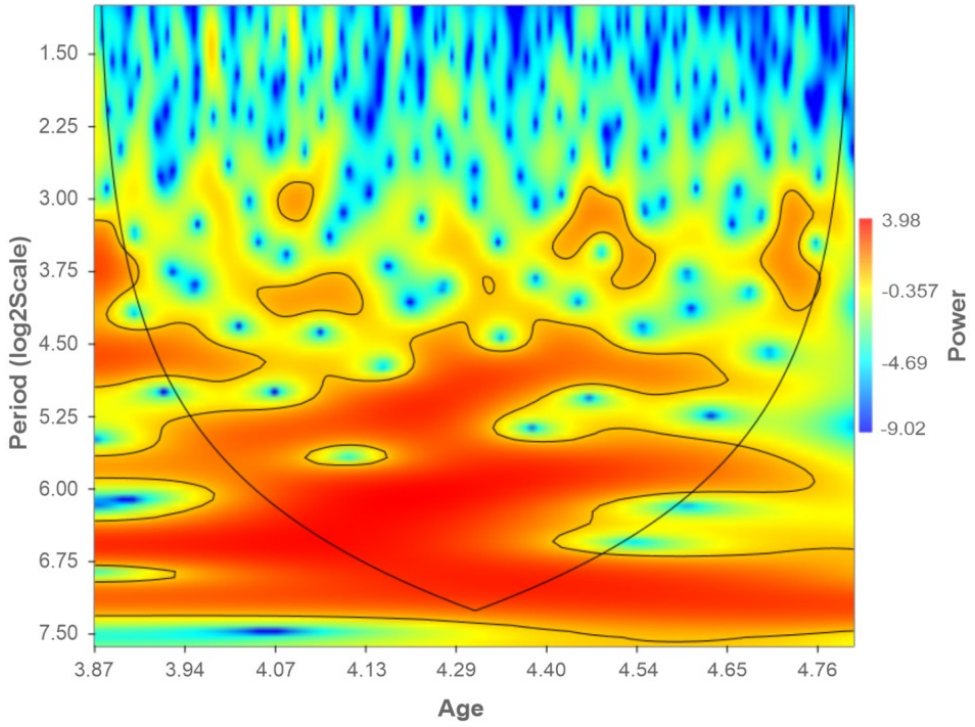

Fig 7.8. Wavelet plot of $\delta^{18}O$ time series. The wavelet analysis was carried out for the $\delta^{18}O$time series having average temporal resolution of~2.21 years. Periodicities of ~283, ~162, ~93, ~70, ~47, ~37, ~25, and ~16 years were observed in the $\delta^{18}O$ time series.

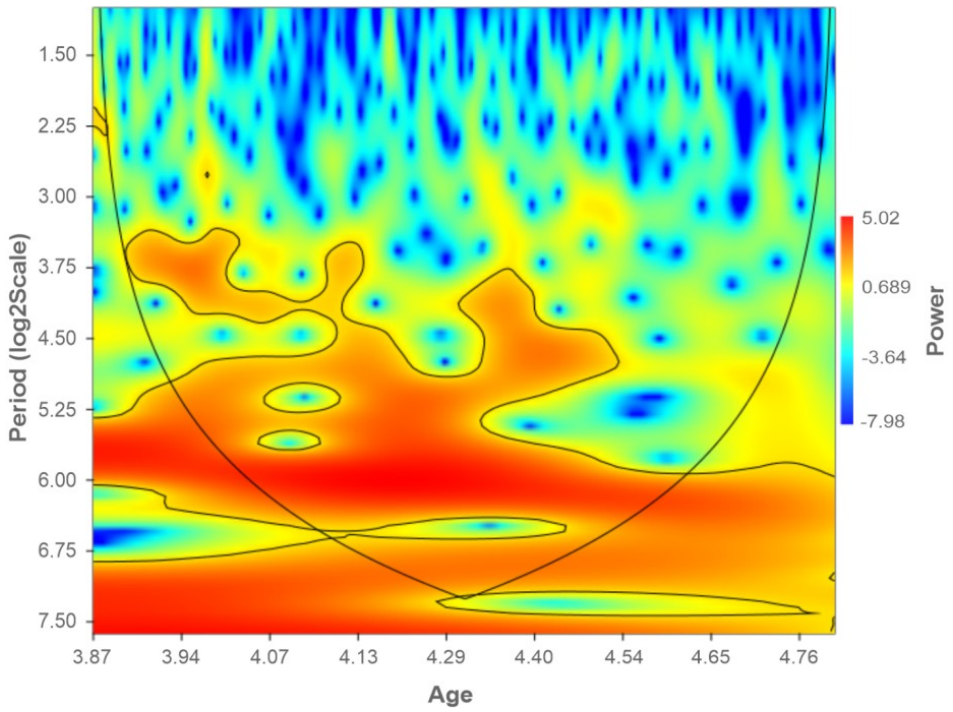

Fig. 7.9. Wavelet plot of $\delta^{13}C$ time series. The wavelet analysis was carried out for the$\delta^{13}C$time series having average temporal resolution of ~2.21 years. Periodicities of ~239, ~152, ~119, ~107, ~71, ~54, and ~28 years were revealed from the wavelet analyses of the $\delta^{13}C$ time series.

7.6. Inferences from $\delta^{18}O$ and $\delta^{13}C$ Records

The $\delta^{18}O$ variations in paleoclimate proxies are usually interpreted in terms of local climatic changes such as temperature and amount of precipitation. However, $\delta^{18}O$ values in tropical rain are not correlated with the mean annual surface air temperatures. The temporal $\delta^{18}O$ variations in monsoonal rainfall and consequently in speleothems from tropical country like India have been interpreted dominantly to reflect upstream changes in the ISM strength (Sinha et al., 2011; Berkelhammer et al., 2012). Model based simulations also show that $\delta^{18}O$ in precipitation is influenced by strong moisture transport by ISM winds and upstream rainfall with a significant negative $\delta^{18}O$ correlation (Midhun and Ramesh, 2015). Additionally, a local effect may also be contributing; it is a negative correlation of $\delta^{18}O$ with the local amount of

ISM precipitation, known as amount effect (Wang et al., 2001; Yuan et al., 2004; Yadava and Ramesh, 2007; Lone et al., 2014; Allu et al., 2014; Sinha et al., 2015) which is applied to most of the Indian monsoon domain. $\delta^{18}O$ depletion and enrichment is manifested during the intense (wet) and weak monsoon (dry) respectively (e.g., Berkelhammer et al., 2012; Cheng et al., 2012; Breitenbach et al., 2015; Dutt et al., 2015; Kathayat et al., 2016, 2017; Gautam et al., 2019). However, since the cave has wide open entrance kinetic fractionation may also be operative in parallel. Nonetheless, during wet season when major growth of the speloethem occurs and humidity is high the kinetic fractionation effect may have been negligible. We therefore interpret the stalagmite $\delta^{18}O$ record in terms of past changes in the intensity of ISM.

The carbon in stalagmite is mainly derived from soil CO_2 ($\delta^{13}C$= -9‰; Craig and Keeling, 1963) and bedrock ($\delta^{13}C$= +1‰). However, the carbon isotope evolution is a complex process; the photosynthetic pathways, closed/open type dissolution and biological activities play a major role (Band and Yadava, 2020). Moreover, a cave system with wide opening is prone to kinetic isotope fractionation as well. C3 type plants produce biogenic carbon with $\delta^{13}C$ ranging from -36‰ to -22‰ with respect to VPDB in humid and tropical region (Badeck et. al., 2005), whereas C4 type plants in semi-arid regions produce $\delta^{13}C$ value of -12‰ with respect to VPDB (Bender, 1968). In summary, $\delta^{13}C$ of cave deposits (stalagmites) depends on relative concentration of these two types of vegetation. Hence, climatically controlled vegetation change may modulate the $\delta^{13}C$ of cave deposits. Therefore, enrichment and depletion of$\delta^{13}C$ can be inferred in terms of humid-moist and arid climate respectively. This directly

reflects the wet and dry ISM as shown by depleted and enriched $\delta^{18}O$ respectively in the stalagmites.

7.7.ISM variability during Mid-Holocene

The $\delta^{18}O$ variability (Fig. 7.4) shows that the ISM variability before ~4.2 ka event was of ~25 years cycle, of gradual decline during ~4.8 to ~4.5 ka BP and gradual incline during ~4.5 to ~4.3 ka BP. This periodicity was absent during prolonged weakening of ISM for ~130 years over ~4.2 to 4.1ka BP. ISM regained its strength, however, at reduced periodicity of ~10 years corresponding to higher frequency of ISM having similar intensity after ~4.1ka BP. Similar change is reflected in $\delta^{13}C$ variability record (Fig. 7.4) with prolific isotopic depletion(~2.6‰)and attainment of ~10 year periodicity after ~4.1 ka BP by ISM. The coherence between $\delta^{18}O$ and $\delta^{13}C$ variability record (Fig. 7.4) suggest the direct response of ISM on the vegetation pattern in the region. It is also interesting to observe from the z-scores of the variability records (Fig. 7.5) that there have been alternate wet and dry ISM phases for the entire time series where dry phases were dominant during ~4.5 to ~4.1 ka BP (Fig. 7.5) with intermittent impoverished wet phase for a small time period.We have observed higher amplitudes of the intermittent wet phase with $\delta^{18}O$ depletion of -1.8 ‰ during ~ 4.3 ka BP to ~ 4.2 ka BP (Fig. 7.4 and 7.5). Band (2016) observed a maximum $\delta^{18}O$ depletion of ~1‰ and attributed it to intensified local moisture that resulted because of moisture change from Arabian Sea to Bay of Bengal. The additional depletion of ~ -0.8 ‰ in $\delta^{18}O$ that we have observed may be the result of local moisture changes, and this additional enforcement of moisture could be attributed to the frequent cyclones that occur in Bay of Bengal. The sensitivity of

tropical cyclones intensification and wind shear on inner core moisture transport has also been suggested by Emanuel and Zhang (2017). Further, additional enforcement of moisture from atmospheric rivers traversing from north pacific towards Asia (Skinner *et al.,* 2020) may have caused more depletion.Also, Chen *et al.* (2008) have reported contrasting intense moisture in arid central Asia (ACA)and correlated it to persistently high SST in the North Atlantic Ocean, high air temperatures in mid-latitudes and still high summer insolation during the mid-Holocene; this caused a peak in effective moisture in ACA, through enhanced moisture transport from the North Atlantic and increased cyclonic activities. Therefore, the ISM variability linked to North Atlantic may also be a potential cause for the intermittent climatic change during the prolonged dry/arid phase. We attribute these changes to the flood events as reported from China (Huang *et al.,* 2010, 2011; Wu *et al.,* 2017; Tan *et al.,* 2018). However, this needs more research for better understanding of the intermittent wet events during mid-Holocene.

Coherent periodicities inferred from the $\delta^{18}O$ and $\delta^{13}C$ wavelet analyses (Fig. 7.8 and 7.9) reflect a strong link between ISM variability and solar cycles.Centennial periodicities of ~239, ~152, ~119, and ~107 years can be related to the centennial scale solar cycles of ~245, ~155, ~120, and ~110 years of periodicities as reported by Hong *et al.,* (2003). Centennial periodicities of ~150-152 and ~117-114 years have been reported by Warrier *et al.,* (2017) and Gupta *et al.,* (2003). Decadal periodicities of ~93, ~71-70, ~54, ~47, ~28, ~25, and ~16 years can also be linked to solar periodicities. Periodicity of ~93 years can be related to Gleissberg cycle, and periodicities of ~71-70 years can be linked to solar sunspot and Gleissberg cycles (Hong *et al.,* 2003).Decadal periodicity of ~54 years may be related to ~60 year of

Suess cycle. Periodicity of ~28-25 years is related to Hale cycle. Similarly, the ~16 year cycles may be related to sunspot cycles. Therefore, the time series spectrums of $\delta^{18}O$ and $\delta^{13}C$ records strongly suggest that the ISM variability has been directly modulated by solar cycles.

7.8.The 4.2 ka event

The 4.2 ka event, defined as the beginning of the Meghalayan stage by the International Commission on Quaternary Stratigraphy, has been reported as two century long global climate aridity (e.g. Cullen *et al.,* 2000; Staubwasser *et al.,* 2003; Berkelhammer *et al.,* 2012; Dixit *et al.,* 2014; Cheng *et al.,* 2015; Kathayat *et al.,* 2018) associated major impact on several civilizations around the globe (e.g., Weiss *et al.,* 1993; Enzel *et al.,* 1999; Stanley *et al.,* 2003; Staubwasser *et al.,* 2003; Marshall *et. al.,* 2011; Liu and Feng, 2012; Dixit *et al.,* 2014; Weiss, 2016; Railsback *et al.,* 2018; Kathayat *et al.,* 2018). This event has been linked to a weakening of the Indian summer monsoon (ISM) which deurbanized of the Indus Valley Civilization (Staubwasser *et al.,* 2003; Madella and Fuller, 2006; Dixit *et al.,* 2014; Giosan *et al.,* 2012; Berkelhammer *et al.,* 2012; Hong *et al.,* 2014; Hong *et al.,* 2016; Kathayat *et al.,* 2017; Dixit *et al.,* 2018). However, the timing, structure and magnitude of the 4.2 ka event have been debatable topic. Primary records (Berkelhammer *et al.,* 2012) from northeastern India have shown an abrupt onset of the event at ~4.1 ka BP. Many other results from other parts of the Asia also have reported similar records, however, the time and the structure varies. Kathayat *et al.,* (2018) have reported 4.2 ka events as three-phase structure: dry-wet-dry rhythmic phases of ISM. The record also supports the rhythmic wet-dry-wet state of the 4.2 ka event; however, the intensity of

the phases varies along with their time frame such that the arid phase of ~130 years continuity was undulated by intermittent small wet events at ~4.18 ka and ~4.11 ka BP (Fig. 7.10). Having compared the isotopic records from Indian sector, four major distinct dry phases as enriched $\delta^{18}O$ values (Fig.7.10) were identified where the temporal length and the intensity of the phases vary widely. This may be due to leads and lags of the age-depth modelling approaches. It is interesting to note that the monsoon cyclic process has remained conducive but their strength diminished impetuously. Although ~4.2 ka event is observed to be the major arid phase due to locked ISM, it is of the opinion that the dry phase I and II (Fig. 7.10) during the ~25 years inclining cycle of ISM must have played a crucial precursor for the Dry phase III or ~4.2 ka event to occur. Hence, it may be inferred that climate induced deurbanization of Bronze aged mature Harappan civilization and changes in their lifestyle must have started from the Dry Phase I and II ultimately witnessing extinction during Dry Phase III. Subsequently, it is interesting to observe prolific depletion in $\delta^{13}C$ at around 4.07 ka BP which caused mixed-farming economy using cattle traction for ploughing permanent fields with changed and intensified agrarian system towards the beginning of nordic bronze age (Tegtmeier, 1993 and Fries, 1995, Fokken, 2009) in civilizations of other parts of the world.

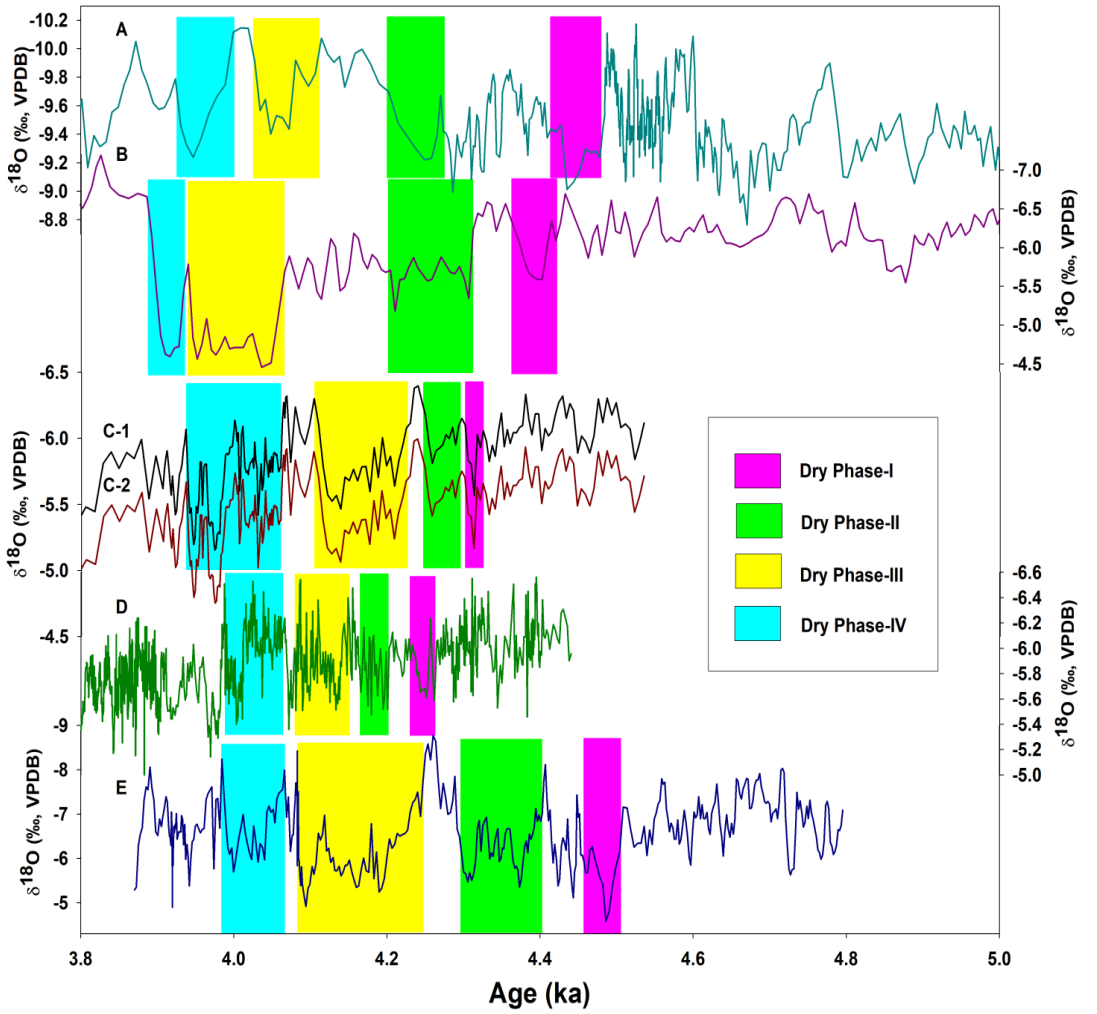

Fig. 7.10.Comparison of 4.2 ka event from Indian cave records. Isotopic record was compared with the published data of cave isotopic records from Indian sector (7A, Bittoo Cave, Kathayat et al., 2016; B, Mawmluh Cave, Berkelhammer et al., 2012; C-1 and C-2, Mawmluh Cave, Kathayat et al., 2018; D; Sahiya Cave, Kathayat et al., 2018) with our records, and it was found that four major distinct dry phases as enrichment in $\delta^{18}O$ values where the temporal length and the intensity of the phases vary widely. This may be due to leads and lags of the age-depth modelling approaches

7.9.Regional Coherence

During mid-Holocene, the decline in terrestrial air temperature was observed in the higher latitudes (Steig *et al.,* 1998) and aridity in the low latitudes (Dykoski *et al.,* 2005; Wang *et al.,* 2005), which have also been referred as "*cool poles, dry tropics*" (Mayewski *et al.,* 2004). The aridity in the low latitudes has been a debatable topic in

terms of gradual (Wang *et al.,* 2005; Fleitman *et al.,* 2007) and abrupt climate change(Berkelhammer 2012; Sarkar *et al.,* 2015; Kathayat *et al.,* 2018). While open system like lacustrine environment, where lake level changes are directly proportional to the difference between precipitation and evaporation, reflects the gradual nonlinear response of ISM (Fleitman *et al.,* 2007), whereas closed system proxy such as stalagmite would be free from this gradual nonlinear phenomenon as it grows due to continuous dripping of seepage water. Hence, any abrupt change in the stalagmite signals would reflect the abrupt climate change. The abrupt changes have also been linked to thermohaline circulation (Turney *et al.,* 2005) and solar insolations (Morill *et al.,* 2003; Wang *et al.,* 2005). Also, the winter cooling and concomitant increase in the Eurasian snow cover has been reported, which is often referred to as snow cover monsoon linkages (Ye and Bao, 2001). Hence, we have attempted to see whether our results exhibit any regional coherence with other observations in the region.

Our $\delta^{18}O$ time series shows a clear coherence with other records (Fig.7.11). The coherence of four dry phases was clearly identified from all the $\delta^{18}O$ records (Fig.7.11) but they vary in their temporal ranges. Based on an observationally derived relationship between total solar irradiance and the open solar magnetic field, Steinhilber *et al.,* (2009) reported that the open solar magnetic field can be obtained from the cosmogenic radionuclide ^{10}Be measured in ice cores. Thus, ^{10}Be allows reconstructing total solar irradiance much further back than the existing record of the sunspot number which is usually used to reconstruct total solar irradiance. We correlated our results with the derived total change in the solar irradiance (Fig.7.11A) which suggests a significant coherence, however, with a little lead in ΔTSI. This lead

is observed to be within the limit of errors in age estimation of the stalagmite BRA-3B. Hence, it is very clear from the spectrum that solar insolation has directly controlled the ISM variability during mid-Holocene. Moreover, it can be observed from the coherence of our δ^{18}Orecords with polar GISP2 (Fig. 7.11B, Grootes *et al.,* 1997) record and other records from China (Fig. 7.11C, Hong *et al.,* 2003; Fig. 7.11D, Dykoski *et al.,* 2005;Fig. 7.11E, Dong *et al.,* 2010), and Oman (Fig.7.11G, Fleitmann *et al.,* 2007;Fig. 7.11H, Arz *et al.,* 2006) that the similar feedback mechanism played a role in modulating the ISM spatially and temporally. Hence, it can be inferred from the regional coherence that the main feedback mechanism for the ISM variability is due to change in the solar insolation and the associated periodicities.

7.10. Summary

Results have emphasized on the clear temporal demarcations of wet and dry phases during mid Holocene. The results suggest a ~25 years and ~10 years cycles before and after 4.2 ka event. Results indicate dry phases dominant during ~4.5 ka to ~4.1 ka with small but intense intermittent wet phase caused due to intensified local moisture. Centennial periodicities inferred from δ^{18}O and δ^{13}C time series strongly suggest that the ISM variability has been directly modulated by solar cycles. The records show rhythmic wet-dry-wet state of the 4.2 ka event; however, the intensity of the phases varies along with their time frame such that the arid phase of ~130 years continuity was undulated by intermittent small wet events at ~4.18 ka and ~4.11 ka BP. Four dry phases have been identified during ~4.79 ka BP to ~3.87 ka BP in which dry phase I and II during the ~25 years inclining cycle of ISM must have played a crucial

precursor for the Dry phase III or ~4.2 ka event to occur. Hence, it may be inferred that climate induced deurbanization of Bronze aged mature Harappan civilization and changes in their lifestyle must have started from the Dry Phase I and II ultimately witnessing extinction during Dry Phase III. Subsequently, it is interesting to observe prolific depletion in $\delta^{13}C$ at around 4.07 ka BP which caused mixed-farming economy using cattle traction for ploughing permanent fields with changed and intensified agrarian system towards the beginning of nordic bronze age in civilizations of other parts of the world.The$\delta^{18}O$ time series shows a clear coherence change in solar insolation which suggest that the solar insolation has directly controlled the ISM variability during mid-Holocene. Similar coherence with records from China and Oman indicate that the similar feedback mechanism played in modulating the ISM spatially and temporally.

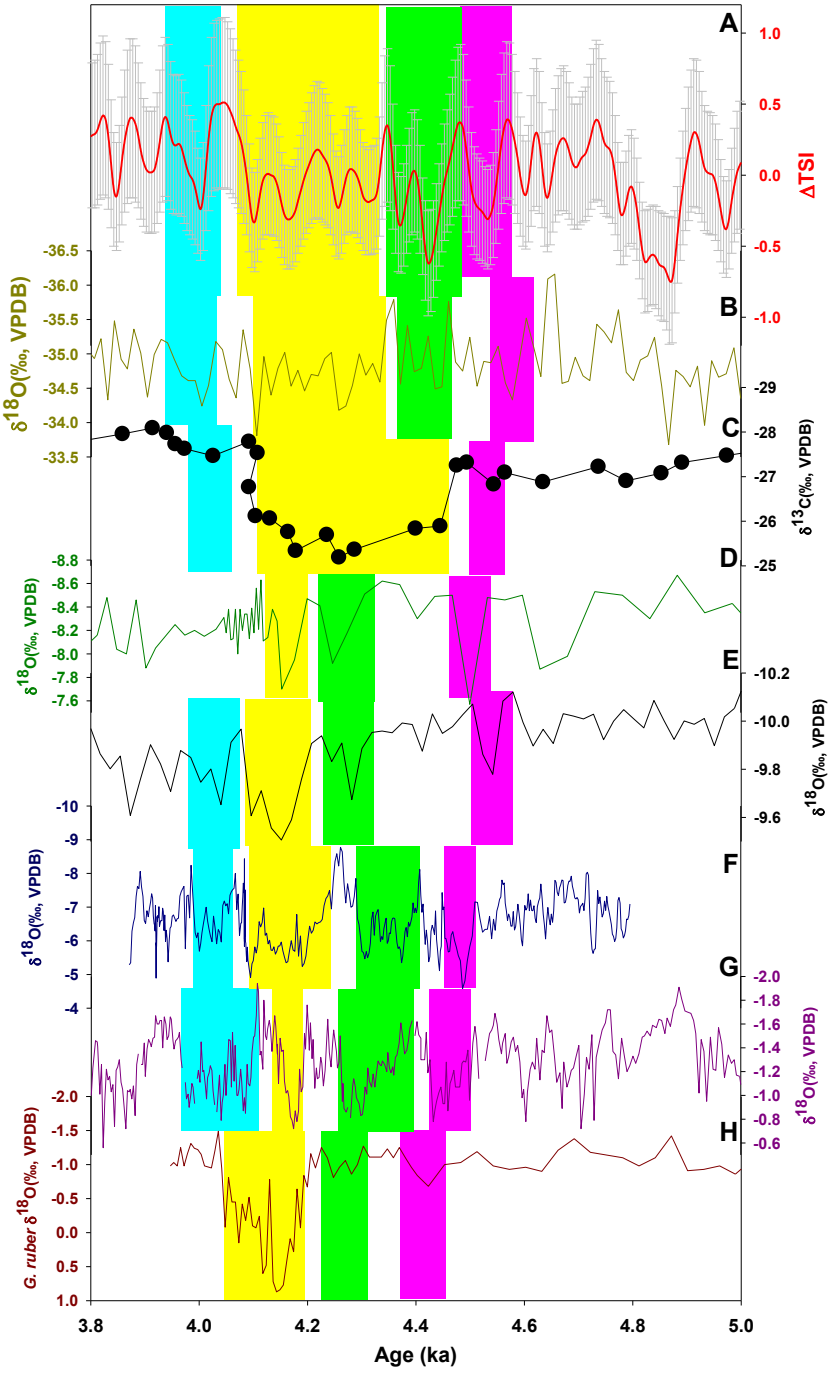

Fig. 7.11. Regional coherence. The stalagmite BRA-3B $\delta^{18}O$ time series (F) shows a clear coherence with total solar irradiance and the open solar magnetic field (A, Steinhilber et al., 2009), polar GISP2 (B, Grootes et al., 1997) record and other records from China (C, Hong et al., 2003; D, Dykoski et al., 2005; E, Dong et al., 2010), and Oman (G, Fleitmann et al., 2007, and H, Arz et al., 2006) so that the similar feedback mechanism played in modulating the ISM spatially and temporally.

Chapter 8

Summary and Future Research Scope

Chapter 8

Summary and Future Research Scope

8.1. Summary

The present research work emphasizes the mechanism and variability of monsoon system during the late Quaternary employing the marine and continental records. The results of the study help in understanding local, regional coherences, and tele-connections of the monsoon system. Main component of the thesis comprises records from both marine and continental archives i.e, foraminifera of sediment core and stalagmites from the caves of eastern India. $\delta^{18}O$ and $\delta^{13}C$ isotopic analysis of two planktic foraminifera viz., *Globigerina bulloides* and *Orbulina universa* recovered from a marine sediment core in southwestern Bay of Bengal as marine proxy records, and stalagmite samples from Kailash Cave and Borra Cave, respectively, as continental record to understand the Indian monsoon system. The temporal range for the marine record accounts for the last 46 ka BP, whereas stalagmites provide ages of Bølling-Allerød to Younger Dryas (YD) and Mid-Holocene. The findingsfrom the marine and continental records are summarized below.

8.1.1. Indian monsoon inferred from southwestern Bay of Bengal records

The $\delta^{18}O$ and $\delta^{13}C$ isotopic records of *Globigerina bulloides* and *Orbulina universa* from Bay of Bengal unravel the Indian monsoon variability during the last 46 ka BP. The isotopic variability records of *Globigerina bulloides* and *Orbulina*

universa are inferred to reflect Northeast Monsoon (NEM) and Southwest Monsoon (SWM) variability, respectively. The $\Delta\delta^{18}O$*bulloides-universa* indicates that the intensity of Indian monsoon in the southwestern Bay of Bengal (BoB) was significantly different during MIS-1, MIS-2, and MIS-3 where monsoon was strongest during MIS-1 followed by MIS-3, but was weaker during MIS-2. This is reflected in the isotopic records which indicate shallow and deep Mixed Layer Depth (MLD) during MIS-1 and MIS-2, respectively. The MLD during MIS-3 was shallower than the MIS-2 but deeper than MIS-1. The $\delta^{13}C$ record of upwelling species *Globigerina bulloides* has shown a remarkable variability during the last 46 ka with global climatic shifts. Most enriched $\delta^{13}C$ concentrations of *Globigerina bulloides* during MIS-1 also indicate intense stratification and weak upwelling. On the contrary, MIS-2 indicates weakest stratification due to the supply of nutrient rich cold water along with depleted $\delta^{13}C$ to the ocean surface. Similarly, a moderate $\delta^{13}C$ value during MIS-3 supports the fact that MIS-3 was associated with higher productivity than MIS-2 but lower than MIS-1. Sea surface height anomaly data suggest that the core location lies in the region of persistent cyclonic eddies as the southwestern BoB experiences more cyclonic events. Hence, it is advocated that the nutrient supply in the southwestern BoB may be associated with cyclonic eddies, particularly during the MIS-I. Millennial periodicities of $\delta^{18}O$ and $\delta^{13}C$ records clearly exhibit interhemispheric links and the rapid changes are due to convergent factors of north Atlantic climate changes and coupled ocean-atmospheric processes. It is inferred that downwind transport of atmospheric signal from the North Atlantic drives the changes in the Indian monsoon. The study further reveals that high productivity during early Holocene, i.e. onset of active interglacial stage, was due to

enhanced photosynthesis (productivity). The modulations in SWM intensity affected the productivity because of minor shifts during the mid- and late- Holocene. The $\delta^{18}O$ and $\delta^{13}C$ records from MIS-2 indicate strong NEM and weak SWM during the LGM. Regional correlation of the $\delta^{18}O$ records suggest that the processes which have controlled the hydroclimate in southwestern BoB were similar to those occurred in other parts of BoB and AnS. The variability of monsoon over last 40 kyr BP reconstructed in this study by using isotopic ratios of selected planktic foraminifera species are in broad agreement with other monsoon reconstructions based on $\delta^{18}O$ from BoB, which suggests that the forcing mechanisms of monsoon appears to be similar in the entire north Indian Ocean. The results are listed below.

- *G. bulloides* and *O. universa* $\delta^{18}O$ and $\delta^{13}C$ can be reliable proxy for Indian monsoon reconstruction.
- The $\Delta\delta^{18}O_{bulloides\text{-}universa}$ indicates that intensity of Indian monsoon was stronger during MIS-1 followed by MIS-3, whereas it was weaker during MIS-2.
- Shallow and deep MLD were persistent during MIS-1 and MIS-2.
- MLD during MIS-3 was shallower than the MIS-2 but deeper than MIS-1.
- Most enriched $\delta^{13}C$ concentrations of *G. bulloides* during MIS-1 indicate intense stratification and poor upwelling.
- MIS-2 indicates weakest stratification due to the supply of nutrient rich cold water with depleted $\delta^{13}C$ to the ocean surface.
- Moderate $\delta^{13}C$ value during MIS-3 supports the fact that MIS-3 was associated with higher productivity than MIS-2 but lower than MIS-1.

- Millennial periodicities of $\delta^{18}O$ and $\delta^{13}C$ records exhibit interhemispheric coupled ocean-atmospheric and planetary cycle linkages.
- High productivity during early Holocene was due to enhanced photosynthesis.
- $\delta^{18}O$ and $\delta^{13}C$ records from MIS-2 indicate strong NEM and weak SWM during LGM.
- Regional correlation of $\delta^{18}O$ records suggest that hydroclimate in southwestern BoB were similar to the other parts of BoB and Andaman Sea.

8.1.2. Indian monsoon during B-A and YD as inferred from Kailash Cave stalagmite

The stalagmite (KG-6) $\delta^{18}O$ and $\delta^{13}C$ records represent significant high resolution Southwest monsoon variability reconstruction during ~14.9–12.7 ka which covers Bølling-Allerød (B-A) and Younger Dryas Events. The variability of the records is inferred as the consequence of the changes that occurred in the coupled ocean-atmospheric system, in addition to solar forcing. It is also inferred from the time series analyses that the coupled ocean-atmospheric system was dominant during stadial or glacial phase which gave rise to its termination during B-A event. The results indicate that there could be a significant SH contribution in modulating the climate pattern of ISM. However, it still remains a destitute inference and demands more attention to understand the forcing and controlling mechanisms. The main inferences from the isotopic analyses of KG-6 stalagmite are listed below.

- Significant high resolution southwest monsoon variability reconstruction during ~14.7–12.6 ka which covers Bolling-Allerod (B-A) and Younger Dryas Events.

- Monsoonal variability and their periodicities were the consequence of the changes that occurred in dominant coupled ocean-atmospheric system.
- Results indicate significant Southern Hemisphere contribution in modulating the climate pattern of southwest monsoon.

8.1.3. Indian monsoon inferred from Borra Cave, Andhra Pradesh during the Mid-Holocene

The stalagmite (BRA-3B) $\delta^{18}O$ and $\delta^{13}C$ records from Borra cave have helped in clearly demarcating wet and dry phases during mid-Holocene. The isotopic variability records suggest a ~25 years and ~10 years cycles before and after 4.2 ka event. Records also show that dry phases were dominant during ~4.5 ka to ~4.1 ka with small but intense intermittent wet phase caused due to intensified local moisture. Centennial periodicities inferred from $\delta^{18}O$ and $\delta^{13}C$ time series strongly suggest that the ISM variability has been directly modulated by solar cycles. The isotopic variability records suggest a rhythmic dry-wet state of the 4.2 ka event with an arid phase of ~130 years. This aridity was undulated by intermittent small wet events at ~4.18 ka and ~4.11 ka BP. The $\delta^{18}O$ and $\delta^{13}C$ time series shows a clear coherence change in solar insolation which suggest that the solar insolation has directly controlled the ISM variability during mid-Holocene. This coherence suggests that the similar feedback mechanism played in modulating the ISM spatially and temporally. The major outcomes of the chapter are listed below.

- Significant high resolution southwest monsoon variability has been reconstructed during Mid-Holocene.
- Six wet and four dry phases are identified during ~4.8- ~3.8 ka BP.

- Major dry period existed in three phases with intermittent short wet phases during 4.2 ka. Intermittent wet periods may be associated with flood events.
- The isotopic variability records suggest a ~25 years and ~10 years cycles before and after 4.2 ka event, respectively.
- The dry phase caused change in the vegetation patterns.
- Major dry phase caused global extinction and/or migration of civilizations Centennial periodicities inferred from $\delta^{18}O$ and $\delta^{13}C$ time series strongly suggest that the ISM variability has been directly modulated by solar cycles.

8.2. Future Research Scope

- High resolution generation of the isotopic data is needed for the entire Late Quaternary period for better understanding of the feedback mechanism of the Indian monsoon
- Multiproxy records for the stalagmites is needed for the cross validation of the inferences made. In this regards trace element analyses and fluid inclusion studies of the stalagmites are essential.
- The future research may focus on the correlation of proxy records with physical processes such as ENSO, etc.
- More isotopic studies on Globigerina bulloides and Orbulina universa should be done to validate their reliability as proxy for Indian monsoon variability from the geological past.
- High resolution U-Th geochronologies for the stalagmites are needed. Since, no facility for U-Th in India is available so far, it is very important to establish the U-Th geochronological facility in India.

References

Adyalkar, P., G. 1977. Hydrogeology of karstic terrains (limestone areas). In: Exploration techniques for groundwater. COSTED, Chennai, India, pp 128–142.

Agnihotri, R., Dutta, K., Bhushan, R., Saumyajulu, B. L. K. 2002. Evidence for solar forcing on Indian monsoon during the last millennium. Earth. Planet. Sci. Lettr. V. 198. pp. 521-527.

Allu, N. C., Tiwari, M., Yadava, M. G., Dung, N. C., Shen C., Belagaonkar, S. P., Ramesh R., Laskar, A. H. 2014. Stalagmite $\delta^{18}O$ variations in southern India reveal divergent trends of Indian Summer Monsoon and East Asian Summer Monsoon during the last interglacial. Quaternary International. http://dx.doi.org/10.1016/j.quaint.2014.12.014.

An, Z., Clemens, S. C., Shen, J., Qiang, X., Jin, Z., Sun, Y., Prell, W. L., Luo, J., Wang, S., Xu, H., Cai, Y., Zhou, W., Liu, X., Liu, W., Shi, Z., Yan, L., Xiao, X., Chang, H., Wu, F., Ai, L., Lu, F. 2011. Glacial-Interglacial Indian Summer Monsoon dynamics. Science. V. 333. pp. 719-723.

Anderson, et al. 2009. Wind driven upwelling in the Southern Ocean and the deglacial rise in the atmospheric CO_2.Science. V.323. pp. 1443-1448.

Arz, H.W., F. Lamy, and J. Pätzold. 2006. A pronounced dry event recorded around 4.2 ka in brine sediments from the northern Red Sea. Quaternary Research, Vol. 66, Issue 3, pp. 432-441, doi:10.1016/j.yqres.2006.05.006

Badeck, F.W., G. Tcherkez, S. Nogues, C. Piel, Ghashghaie, J., 2005. Post photosynthetic fractionation of stable carbon isotopes between plant organs: a widespread phenomenon. Rapid communications in mass spectrometry, 19 (11), 1381-1391.

Baertschi, P. 1976. Absolute ^{18}O content of standard mean ocean water. Earth and Planetary Science Letters V. *31*(3), pp. 341–344.

Band, S., Yadava, M.G., Lone, M.A., Shen, C., Sree, K., Ramesh, R., 2018. High-resolution mid-Holocene Indian Summer Monsoon recorded in a stalagmite from the Kotumsar cave, Central India. Quat. Int. https://doi.org/10.1016/j.quaint.2018.01.026

Baskar, S., R. Baskar, Natuschka Lee; A. Kaushik; P. K. Theophilus. 2007. Precipitation of iron in microbial mats of the spring waters of Borra Caves, Vishakapatnam, India: some geomicrobiological aspects. Environmental Geology. v. 56(2). DOI: 10.1007/s00254-007-1159-y.

Bender, M. M.,1968. Mass spectrometric studies of carbon 13 variations in corn and other grasses. Radiocarbon, 10 (2), 468-472

Berkelhammer, M., Sinha, A., Stott, L., Cheng, H., Pausata, F., Yoshimura, K., 2012. An abrupt shift in the Indian monsoon 4000 years ago, Climates, land- scapes, and civilizations, pp. 75-88.

Booth, R. K., Jackson, S. T., Forman, S. L., Kutzbach, J. E., Bettis Iii, E., Kreigs, J., and Wright, D. K., 2005. A severe centennial-scale drought in midcontinental North America 4200 years ago and apparent global linkages. Holocene, 15, 321–328.

Breitenbach, et al. 2010. Strong influence of water vapor source dynamics on stable isotopes in precipitation observed in Southern Meghalaya, NE India, Earth Planet. Sci. Lett., 292, 212–220, doi:10.1016/j.epsl.2010.01.038.

Breitenbach, et al. 2012. Constructing Proxy Records from Age models (COPRA). Clim. Past. V.

8. pp. 1765–1779.
Breitenbach, S.F.M., Lechleitner, F.A., Meyer, H., Diengdoh, G., Mattey, D., Marwan, N., 2015. Cave ventilation and rainfall signals in dripwater in a monsoonal setting – a monitoring study from NE India. Chemical Geology, 402, 111–124.
Bradley, R.S. 2014. Paleoclimatology: Reconstructing Climates of the Quaternary (3rd edition). *Elsevier/Academic Press, San Diego*. ISBN: 9780123869135.
Bradley, R.S., Eddy, J.A. 1991. Records of past global changes. In, Global changes of the Past (Ed. r.s. Bradley) University corporation for Atmospheric research, Boulder, pp. 5-9.
Bryson, R.A. and Swain,A.M. 1981. Holocene variations of monsoon rainfall in Rajasthan, Quat. Res., V.16, pp.135-145.
Budyko, M. I., K. Vinnikov, O. A. Drozdov and H. A. Efimova, 1978: Forthcoming climatic changes. Izv, Akad. Nauk. USSR Ser. Geogr. V. 6,pp. 5.
Cai, Y., Zhang, H., Cheng, H., An, Z., Edwards, R.L.,Wang, X., Tan, L., Liang, F., Wang, J., Kelly, M. 2012. The Holocene Indianmonsoon variability over the southern Tibetan Plateau and its teleconnections. Earth Planet. Sci. Lett. 335–336, 135–144.
Canavan R.W., Slomp C.P., Van Cappellen P., van den Berg G. A. and Zwolsman J. J. G.; Trace metal geochemistry in a fresh water lake sediment; Geophysical Research Abstracts, Vol. 8, 05727, 2006.
Chen, F. et al., 2008. Holocene moisture evolution in arid central Asia and its out-of-phase relationship with Asian monsoon history. Quat. Sci. Rev., 27(3), 351–364, doi:10.1016/j.quascirev.2007.10.017.
Cheng, H., Sinha, A., Wang, X., Francisco W. C., Edwards, R. L. 2012. The Global Paleomonsoon as seen through speleothem records from Asia and the Americas. Clim Dyn. V.39. pp.1045–1062. DOI 10.1007/s00382-012-1363-7.
Chiang and Friedman. 2012. Extratropical cooling, interhemispheric thermal gradients, and tropical climate change.Ann. Rev.Earth Planet Sci. V.40. pp. 383.
Cheng, H., Edwards, R., Hoff, J., Gallup, C., Richards, D., Asmerom, Y., 2000. The half-lives of uranium-234 and thorium-230. Chemical Geology, 169, 17–33.
Cheng, H., Zhang, P., Spötl, C., Edwards, R., Cai, Y., Zhang, D., Sang, W., Tan, M., An, Z., 2012. The climatic cyclicity in semi arid- arid central Asia over the past 500,000 years. Geophysical Research Letters, 39.
Cheng, H., Edwards, R.L., Shen, C.-C., Polyak, V.J., Asmerom, Y., Woodhead, J., Hellstrom, J., Wang, Y., Kong, X., Spötl, C., 2013. Improvements in ^{230}Th dating, ^{230}Th and ^{234}U half-life values, and U–Th isotopic measurements by multi-collector inductively coupled plasma mass spectrometry. Earth and Planetary Science Letters 371, 82–91.
Cheng, H., Sinha, A., Verheyden, S., Nader, F.H., Li, X.L., Zhang, P.Z., Yin, J.J., Yi, L., Peng, Y.B., Rao, Z.G., Ning, Y.F., Edwards, R.L., 2015. The climate variability in northern Levant over the past 20,000 years. Geophysical Research Letters, 42, 8641-8650.
Cullen, H., P. DeMenocal, S. Hemming, G. Hemming, F. Brown, T. Guilderson, and F. Sirocko, 2000. Climate change and the collapse of the Akkadian empire: Evidence from the deep sea. Geology, 28(4), 379-382.
Clarke, et al. 2012. Global climate evolution during the last deglaciation. PNAS. E1134–E1142. www.pnas.org/cgi/doi/10.1073/pnas.1116619109.
Clemens, S., Prell W., Murray, D., Shimmield, G., and Weedon, G. 1991. Forcing mechanisms of Indian ocean monsoon. Nature. Vol. 353. pp. 720-725.
Clemens, S. C., Prell, W. L. & Sun, Y. 2010. Orbital-scale timing and mechanisms driving Late

Pleistocene Indo-Asian summer monsoons: Reinterpreting cave speleothem δ 18O. Paleoceanography. V.25**,** PA4207.
Clark, I. D., Fritz, P.2013. Environmental isotopes in hydrogeology. CRC press.
CLIMAP Project Members. 1976. The surface of the ice-age Earth,Science, V. 191, pp.1131-1137.
COHMAP Members 1988 . Climatic changes of the last 18, 000 years: observations and model simulations, Science, 241,1043-1052
Craig, H.1961. Isotopic variations in meteoric waters. Science.
Craig, H. 1957. Isotopic standards for carbon and oxygen and correction factors for mass-spectrometric analysis of carbon dioxide, Geochimica et cosmochimica acta. v.12 (1), pp.133-149.
Craig, H., & Gordon, L. I. 1965. Deuterium and oxygen 18 variations in the ocean and the marine atmosphere.
Croll, J. 1867. On the eccentricity of the Earth's orbit, and its physical relations to the glacial epoch. *Philosophical Magazine,* 33, 426-445.
Cullen, H., P. DeMenocal, S. Hemming, G. Hemming, F. Brown, T.Guilderson, and F. Sirocko, 2000. Climate change and thecollapse of the Akkadian empire: Evidence from the deep sea. Geology, 28(4), 379-382.
Dansgaard, W., Stable isotopes in precipitation. Tellus, 1964, 16, 436–468.
Dar et al. 2014. Review: Carbonate aquifers and future perspectives of karst hydrogeology in India. Hydrogeology Journal. DOI 10.1007/s10040-014-1151-z
Das Brijraj K., Haake Birgit-Gaye; Geochemistry of Rewalsar Lake sediment, Lesser Himalaya, India: implications for source-area weathering, provenance and tectonic setting; Geosciences Journal Vol. 7, No. 4, p. 299 − 312, December 2003.
Dayem, et al. 2010. Lessons learned from oxygen isotopes in modern precipitation applied to interpretation of speleothem records of paleoclimate from eastern Asia. Earth Plante, Sci. Lett. V.295 (1). Pp. 219-230.
Edwards, R. L., J. Chen, and G. Wasserburg 1987. ^{238}U- ^{234}U- ^{230Th}- ^{232}Th systematics and the precise measurement of time over the past 500,000 years. Earth and Planetary Science Letters, 81 (2), 175-192.
Emrich, K., et al. 1970. Carbon isotope fractionation during precipitation of calcium cabronate. Earth. Planet. Sci. Lett. V. 11 (8),363-371
Enzel, Y., L. Ely, S. Mishra, R. Ramesh, R. Amit, B. Lazar, S. Rajaguru, V. Baker, and A. Sandler, 1999. High-resolution holocene environmental changes in the thar desert, northwestern india. Science, 284 (5411), 125-128.
Enfield, D. B., Mestas-Nunes, A.M. 1999. Multiscale varibailites in global sea surface temperature and their relationship with toposheric climatic patterns. Journal of Climate. V.9. pp.2719-2733.
EPICA Community Members. 2006. One-to-one coupling of glacial climate variability in Greenland and Antarctica. Nature. V. 444**.** pp. 195–198.
Edwards, R. L., J. Chen, and G. Wasserburg 1987. ^{238}U- ^{234}U- ^{230Th}- ^{232}Th systematics and the precise measurement of time over the past 500,000 years. Earth and Planetary Science Letters, 81 (2), 175-192.
Emiliani, C., 1955. Pleistocene temperatures. Journal of Geology 63, 538-578.
Enzel, Y., L. Ely, S. Mishra, R. Ramesh, R. Amit, B. Lazar, S. Rajaguru, V. Baker, and A.

Sandler, 1999. High-resolution Holocene environmentalchanges in the Thar desert, northwestern India. Science, 284 (5411), 125-128.

Fairchild, I. J., Frisia, S., Borsato, A., & Tooth, A. F. 2006. Speleothems.

Feng, X., Faiia, A. M., and Posmentier, E. S. 2009. Seasonality of isotopes in precipitation: A global perspective, J. Geophys. Res.- Atmos. V. 114, D08116, https://doi.org/10.1029/2008JD011279.

Fleitmann, D., S. J. Burns, A. Mangini, M. Mudelsee, J. Kramers, I. Villa, U. Ne, A. A. Al-Subbary, A. Buettner, D. Hippler, 2007. Holoceneitcz and indian monsoon dynamics recorded in stalagmites from Oman and Yemen (socotra). Quaternary Science Reviews, 26 (1), 170-188.

Fleitmann, D., S. J. Burns, A. Mangini, M. Mudelsee, J. Kramers, I. Villa, U. Ne, A. A. Al-Subbary, A. Buettner, D. Hippler, 2007. Holocene itcz and indian monsoon dynamics recorded in stalagmites from oman and yemen (socotra). Quaternary Science Reviews, 26 (1), 170-188.

Fokkens, H., 2009. 'Die Wirtschaft der Nordischen Bronzezeit: mehr als Getreide saen und Vieh zuchten', in M. Bartelheim and H. Stauble (eds.), *Die wirtschaft lichen Grundlagen derBronzezeit Europas* [*The Economic Foundations of the European Bronze Age*], Forschungen zur Archaometrie und Altertumswissenschaft , 4. Rahden: Verlag Marie Leidorf, 85–104

Fries, J. C., 1995. *Vor- und frühgeschichtliche Agrartechnik auf den Britischen Inseln und dem Kontinent. Eine vergleichende Studie* , Internationale Archaologie. Espelkamp: Verlag Marie Leidorf

Gat, J. R., Gonfiantini, R.1981. Stable isotope hydrology. Deuterium and oxygen-18 in the water cycle.

Gat, J. R., Oxygen and hydrogen isotope in hydrologic cycle. Annu. Rev. Earth Planet Sci., 1996, 24, 225–262.

Gat, J. R., In Stable Isotope Hydrology: Deuterium and Oxygen-18 in the Water Cycle. Technical Report Series No. 210 (eds Gat, J. R. and Gonfiantini, R.), IAEA, Vienna, 1981, pp. 21–33.

Gautam, P.K, A.C. Narayana, S.T. Band, M.G. Yadava, R. Ramesh, Chung-Che Wu,Chuan-Chou Shen. 2019. High-resolution reconstruction of Indian summer monsoon during theBolling-Allerod from a central Indian stalagmite.Palaeogeography, Palaeoclimatology, Palaeoecology 514, 567–576

Gamage, N., and W. Blumen. 1993: Comparative analysis of lowlevel cold fronts: Wavelet, Fourier, and empirical orthogonal function decompositions. Mon. Wea. Rev. V. 121, pp.2867–2878

Godfrey, J. S., & Mansbridge, J. V. 2000. Ekman transports, tidal mixing and the control of temperature structure in Australia's northwest waters. Journal of Geophysical Research. V.105, pp.24021–24044.

Gordon, A., L. 2005. Oceanography of the Indonesian Seas and their throughflow. Oceanography. v. 18, pp. 14–27. https://doi.org/10.5670/oceanog.2005.01.

Goswami, B. N. 2006 in Wang B.2006. The Asian Monsoon. pp. 295-302.

Gupta, et al. 2013. Solar forcing of the Indian summer monsoon variability during the Allerød period. 2013. Sci. Rep. 3, 2753; DOI:10.1038/srep02753.

Gupta A., K., Anderson, D., M., Overpeck, J.T. 2003. Abrupt changes in the Asian southwest

monsoon during the Holocene and their links to the North Atlantic Ocean. *Nature,* 421, 354-356.

Guptha, M., V., S., Naidu, P., D., Haake, B., G., Schiebel, R**.** 2005. Carbonate and Carbon fluctuations in the Eastern Arabian Sea over 140ka: Implications on productivity changes? *Deep-Sea Research II* 52, 1981-1993..

Giosan, L., P. D. Clift, M. G. Macklin, D. Q. Fuller, S. Constantinescu, J. A. Durcan, T. Stevens, G. A. Duller, A. R. Tabrez, K. Gangal, et al., 2012. Fluvial landscapes of the Harappan civilization, Proceedings of the NationalAcademy of Sciences, 109 (26), E1688-E1694.

Giosan, L., P. D. Clift, M. G. Macklin, D. Q. Fuller, S. Constantinescu, J. A. Durcan, T. Stevens, G. A. Duller, A. R. Tabrez, K. Gangal, et al., 2012. Fluvial landscapes of the harappan civilization, Proceedings of the National Academy of Sciences, 109 (26), E1688-E1694.

Gilman, D.L., Fuglister, F.J., Mitchel Jr., J.M. 1963. On the power spectrum of red noise. Journal of the Atmospheric Sciences, V. 20 (2), pp. 182–184.

Grootes, P.M., and M. Stuiver., 1997. Oxygen 18/16 variability in Greenland snow and ice with 10^3 to 10^5-year time resolution. Journal ofGeophysical Research, 102, 26455-26470.

Gupta, A. K., D. M. Anderson, and J. T. Overpeck, 2003. Abrupt changes inthe Asian southwest monsoon during the Holocene and their links to the north Atlantic Ocean. Nature, 421 (6921), 354-357.

Gonfiantini, R., The δ-notation and the mass-spectrometric measurement techniques. In Stable Isotope Hydrology: Deuterium and Oxygen-18 in the Water Cycle. Technical Report Series No. 210 (eds Gat, J. R. and Gonfiantini, R.), IAEA, Vienna, 1981, pp. 103

Gopalan,A. K. S., Gopalakrishna, V. V., Ali, M. M., Sharma, R. 2000. Detection of Bay of Bengal eddies from TOPEX and in situ observations Mar. Res. v.58,pp.721-734.

GSI. 1997. Geological map series of carbonate areas of India, Geological survey of India, Calcutta, India

Hammer, et al. 2001. PAST: Paleontological statistics software package for education and data analysis. Palaeontologia Electronica 4, 1–9.

Hagemann, R., Nief, G., Roth, E.1970. Absolute isotopic scale for deuterium analysis of natural waters. Absolute D/H ratio for SMOW 1. Tellus V. *22*(6), pp. 712–715.

Hasselmann,K. 1976. Stochastic climate models. Part I, theory. Tellus. V. 28. pp. 473-485.

Hendy, C.H., 1971. The isotopic geochemistry of speleothems-I. The calculation of the different modes of formation on the isotopic composition of speleothems and their applicability as paleoclimatic indicators. Geochim. Cosmochim. Acta. V.35. pp. 801–824.

Hendy, C., 1971. The isotopic geochemistry of speleothems. The calculation of the effects of different modes of formation on the isotopic composition of speleothems and their applicability as palaeoclimatic indicators. Geochim. Cosmochim. Acta, 35 (8), 801-824, doi:10.1016/0016-7037(71)90127-X.

Hong, Y.T. B. Hong, Q.H. Lin, Y.X. Zhu, Yasuyuki Shibata, Masashi Hirota, Masao Uchida, X.T. Leng, H.B. Jiang, H. Xua, H. Wang, L. Yi., 2003. Correlation between Indian Ocean summer monsoon and North Atlantic climate during the Holocene. Earth and Planetary Science Letters, 211, 371-380

Hong, B., Hong, Y., Uchida, M., Shibata, Y., Cai, C., Peng, H., Zhu, Y., Wang, Y., Yuan, L., 2014. Abrupt variations of Indian and East Asian summer monsoons during the last deglacial stadial and interstadial. Quaternary Science Reviews, 97, 58-70.

Huang, C. C., Pang, J., Zha, X., Zhou, Y., Su, H., and Li, Y., 2010. Extraordinary floods of

4100–4000 a BP recorded at the Late Neolithic ruins in the Jinghe River gorges, Middle Reach of the Yellow River, China, Palaeogeogr. Palaeocl., 289, 1-9.
Huang, C. C., Pang, J., Zha, X., Su, H., and Jia, Y., 2011. Extraordinary floods related to the climatic event at 4200 a BP on the Qishuihe River, middle reaches of the Yellow River, China, Quaternary Sci. Rev., 30, 460–468.
Huguet C., Routh, J., Fietz, S., Lone, M.A., Kalpana, M.S., Ghosh, P., Mangini, A., Kumar, V., Rangarajan, R. 2018. Temperature and monsoon tango in a Tropical stalagmite: Last Glacial-Interglacial Climate Dynamics. Nat. Sci.Rep. V.8.pp.5386. DOI:10.1038/s41598-018-23606-w.
IGBP PAGES/ World Data Center for Paleoclimatology. Data Contribution Series # 2006–118. NOAA/NCDC Paleoclimatology Program, Boulder, CO, USA.
Joseph. 1976. Climatic changes in monsoon and cyclones. Proc. Symp. Trop. Monsoon, IITM, Poona, India. pp. 378-387.
Kathayat, G., Cheng, H., Sinha, A., SpÖtl, C., Edward, R. L., Zhang, H., Li, X., Yi, L, Ning, Y., Cai, Y., Lui, W. L., Breitenbach, S. F. M. 2016. Indian monsoon variability on millennial-orbital timescales. Nat. Sci. Reports. V.6. pp.24374. doi: 10.1038/srep24374 (2016).
Kato, K.,Wada, H., Fujioka, K., 2003. The application of chemical staining to separate calcite and aragonite minerals for micro-scale isotopic analyses. Geochem. J. 37, 291–297.
Kathayat, G., Cheng, H., Sinha, A., Yi, L., Li, X., Zhang, H., Li, H., Ning, Y., Edwards, R.L. 2017. The Indian monsoon variability and civilization changes in the Indian subcontinent. Science advances, 3, 1701296.
Kellogg, W. W., and R. Schware. 1981. Climate change and Society. Consequences of Increasing Atmospheric Carbon Dioxide. Westview Press.
Kerr, R.A. 2000. A North Atlantic climate pacemaker for the centuries. Science. V. 288(5473). pp. 1984-1986.
Krishnamurthi, V. and Shukla, J. 2001.Observed and model simulated interannual variability of the Indian monsoon. Mausam. V.52. pp.133-150.
Komaya M., Kawashima M., Takamatsu T., Glasby G. P., Stoppers P.; Mineralogy and geochemistry of sediments from Lakes Taupo and Waikaremoana, New Zealand; New Zealand Journal of Marine and Freshwater Research, 1989, Vol. 23: 121-130.
Koretsky Carla M, Haas Johnson R, Miller Douglas and Ndenga Noah T; Seasonal variations in pore water and sediment geochemistry of littoral lake sediments (Asylum Lake, MI, USA); Geochemical Transactions 2006, 7:11 doi: 10.1186/1467-4866-7-11.
Ku, T.-L., Li,, H.-C. 1998. Speleothems as high-resolution paleoenvironment archives: records from northeastern China. Proceedings of the Indian Academy of Sciences. Earth and Planetary Sciences, 107, pp. 321–330.
Kumar, A.1985. Karst landform of Upper Kapili River, Assam. Facets of geomorphology. Thinker's Library, Anil Kumar, India, 212 pp..
Kutzbach, J. E., Guetter, P. J. 1986. The influence of changing orbital parameters and surface boundary conditions on climate simulations for the past 18 000 years. J. Atmos. Sci. V. 43, pp. 1726-1759.
Landsberg, H., 1966. Physical Climatology. DuBois, Pa.: Gray Co.
Lekshmy, P. R. 2015. Stable isotopic studies on monsoon vapour/clouds and precipitation over Kerala, PhD Thesis p. 133.
Levitus, S., R. Burgett, , Boyer, T. 1994. *World Ocean Atlas 1994, Salinity*. Vol. 3, NOAA

Atlas NESDIS. v. 3, pp. 99.
Lee, J. E., Fung, I. .2008. "Amount effect" of water isotopes and quantitative analysis of post-condensation processes. Hydrological Processes, 22(1), 1–8. https://doi.org/10.1002/hyp.6637
Liu, F., Feng, Z. 2012. A dramatic climatic transition at ~4000 cal. yr BP and its cultural responses in Chinesecultural domains. Holocene 22, 1181-1197, 2012.
Lomb, N.R. 1976. Least-squares frequency analysis of unequally spaced data. Astrophysics and Space Science. V. 39, pp.447–462.
Lone, M. A., S. M. Ahmad, N. C. Dung, C. C. Shen, W. Raza, and A. Kumar., 2014. Speleothem based 1000-year high resolution record of Indian monsoon variability during the last deglaciation. Palaeogeogr. Palaeoclimatol, Palaeoecol., V. 395, pp. 1-8, doi:10.1016/j.palaeo.2013.12.010.
Madella, M., Fuller, D.Q., 2006. Palaeoecology and the HarappanCivilisation of South Asia: a reconsideration. Quaternary Science Reviews 25, 1283–1301.
Marshall, M.H., Lamb, H.F., Huws, D., Davies, S.J., Bates, R., Bloemendal, J., Boyle, J., Leng, M.J., Umer, M., Bryant, C. 2011. Late Pleistocene and Holocene drought events at Lake Tana, the source ofthe Blue Nile. Global and Planetary Change, 78, 147–161.
Martinson, D.G., Pisias, N.G., Hays, J.D., Imbrie, J., Moore, T.C., and Shackleton, N.J., 1987. Age dating and the orbital theory of the ice ages: Development of a high-resolution 0 to 300,000 year chronostratigraphy. Quaternary Res. v. 27, pp. 1–29.
Marcott, S.A., Bauska, T.K., Buizert, C., Steig, E.J., Rosen, J.L., Cuffey, K.M., Fudge, T.J., Severinghaus, J.P., Ahn, J., Kalk, M.L., McConnell, J.R., Sowers, T., Taylor, K.C., White, J.W.C., Brook, E.J., 2014. Centennial-scale changes in the global carbon cycle during the last deglaciation. Nature V.514. pp. 616–619.
Marshall, M.H., Lamb, H.F., Huws, D., Davies, S.J., Bates, R., Bloemendal, J., Boyle, J., Leng, M.J., Umer, M., Bryant, C. 2011. Late Pleistocene and Holocene drought events at Lake Tana, the source of the Blue Nile. Global and Planetary Change, 78, 147–161.
Mayewski, P. A., E. E. Rohling, J. C. Stager, W. Karlen, K. A. Maasch, L. D.Meeker, E. A. Meyerson, F. Gasse, S. van Kreveld, K. Holmgren, et al., 2004. Holocene climate variability. Quaternary research, 62 (3), 243-255.
McCreary, J. P., Jr., P. K. Kundu, and R. L. Molinari. 1993. A numerical investigation of dynamics, thermodynamics and mixed layer processes in the Indian Ocean, Prog. Oceanogr., 31, 181 – 244, doi:10.1016/0079- 6611(93)90002-U.
Melice, J.L., Servain, J. 2002. The tropical Atlantic meridional SST gradient index and its relationship with the SOI, NAO, and southern ocean. Climate dynamics. V. 20. Pp.447-464.
Melice, J. L., Roucou, P. 1998. Decadal time scale variability recorded in the Quelcaya summit ice core $\delta^{18}O$ isotopic ratio series and its relation with the sea surface temperature. Climate Dynamics. V. 14. Pp. 117-132.
Midhun, M., and R. Ramesh, 2015. Validation of $\delta^{18}O$ as a proxy forpast monsoon rain by multi-GCM simulations, Clim. Dyn., doi:10.1007/s00382-015-2652-8.
Milankovitch, M., M. 1941. Canon of insolation and the ice-age problem. Beograd: Konglich Serbische Akademie. English translation by the Israel Program for Scientific Translations, Published for the US department of Commerce, and the National Science, Foundations, Washington, DC (1969).
Miyama, T., McCreary Jr, J. P., Jensen, T. G., Loschnigg, J., Godfrey, S. & Ishida, A. 2003

Structure and dynamics of the Indian Ocean cross-equatorial cell. Deep-Sea Res. II, V. 50, pp. 2023- 2047.

Mitchell, J. F. B., Ingram, W. B. 1990: On CO_2 and Climate: A diagnostic study of changes in cloud and precipitation. J. Climate.

Murty, K., S., 1988. Karst hydrogeology: India. In: Proc. 21st IAH Congress, Karst Hydrogeology and Karst Environment Protection, Guilin, China 10–15 October 1988, pp 446–450.

Narayana, A.C., Yadava, M.G., Dar, F.A., Ramesh, R., 2014. The spectacular Belum and Borra Caves of Eastern India. In: Kale, V.S. (Ed.), Landscapes and Landforms of India. 978-94-017-8029-2, pp. 189

Nair K.M., Padmalal D., Kumaran K.P.N., Sreeja R., Limaye Ruta B., Srinivas Reji; Late quaternary evolution of Ashtamudi–Sasthamkotta lake systems of Kerala, south west India; Journal of Asian Earth Sciences 37 (2010) 361–372.

Ng Sai L., King Roger H..2004. Geochemistry of Lake Sediments as a Record of Environmental Change in a High Arctic Watershed ; Chemie der Erde 64 (2004) 257–275. Research Department, The Egyptian Meteorological Authority, Egypt Egyptian Atomic Energy Authority, Nasr City, Egypt; Spatial and temporal variation of rainwater stable isotopes in Egypt and the east Mediterranean; A. M. El-Asrag1, S. A. Al-Gamal2, A.

Partin et al. 2007. Millenial-scale trends in west pacific warm pool hydrology since the last glacial maximum. Nature. V. 449. pp. 452-455.

Partin et al. 2015. Gradual onset and recovery of the Younger Dryas abrupt climate event in the tropics. Nat. Commun. 6:8061. doi: 10.1038/ncomms9061.

Paulsen, D.E., Li, H.-C., Ku, T.-L. 2003. Climate variability in central China over the last1270 years revealed by high-resolution stalagmite records. Quat. Sci. Rev. 22, 691–701.

Pausata et al. 2011. Chinese stalagmite delta O-18 controlled by changes in the Indian Monsoon during a simulated Heinrich event. Nat. Geosci. V.4 (7). Pp. 474-480.

Pedro et al. 2015. The spatial extent and dynamics of the Antarctic Cold Reversal. Nat. GeoSci. doi: 10.1038/NGEO2580.

Pisias, N.G., Martinson, D.G., Moore, T.C., Shackleton, N.J., Prell, W., Hays, J., and Boden, G., 1984. High resolution stratigraphic correlation of benthic oxygen isotopic records spanning the last 300,000 years. Mar. Geol.V. 56, pp. 119–136.

Potemra, J.T., Luther, M.E. O'Brien, J.J.. 1991. The seasonal circulation of the upper ocean in the Bay of Bengal, J. Geophys. Res. V. 96, V. 12, pp. 667

Prell, W.L., Hutson, W.H., Williams, D.F., Be, A.W.H., Geitzenauer, W. and Molfinos, B., 1980. Surface circulation of the Indian ocean during the last glacial maximum approximately 18 ,000 yrs. B . P . Quat. Res. V.14, pp.309-336

Raza, W., Ahmad, S. M., Lone, M. A., Shen, C., Sarma, D.S., Kumar, A. 2017. Indian summer monsoon variability in southern India during the last deglaciation: Evidence from a high resolution stalagmite $\delta^{18}O$ record. Plaeogeography, Paleoclimatology, Paleoecology. doi:10.1016/j.palaeo.2017.07.003.

Railsback, L.B., Liang, F., Brook, G., Voarintsoa, N.R.G., Sletten, H.R., Marais, E., Hardt, B., Cheng, H., Edwards, R.L., 2018. The timing, two-pulsed nature, and variable climatic expression of the 4.2 ka event: A review and new high-resolution stalagmite data from Namibia. Quaternary Science Reviews 186, 78–90, 2018.

Rashid, H., E. England, L. Thompson, and L. Polyak, 2011. Lateglacial to Holocene Indian

summer monsoon variability basedupon sediment, Terr. Atmos. Ocean. Sci., 22(2), 215–228

Rayleigh J. W. S. 1896. Theoretical considerations respecting the separation of gases by diffusion and similar processes. Philos. Mag. V. 42, pp. 493–593

Rashid, H., E. England, L. Thompson, and L. Polyak, 2011. Late glacial to Holocene Indian summer monsoon variability based upon sediment, Terr. Atmos. Ocean. Sci., 22(2), 215–228

Rozanski, Kazimierz, Araguás-Araguás, L., & Gonfiantini, R. 1993. Isotopic patterns in modern global precipitation. Climate Change in Continental Isotopic Records, pp. 1–36.

Reimer, P. J. et al. 2009. INTCAL09 and Marine 09 radiocarbon age calibration curves 0-50,000 years cal BP. Radiocarbon. V. 51, pp.1111–1150.

Reppin, J., F. A. et al., 1999: Equatorial currents and transports in the upper central Indian Ocean: Annul cycle and interannual variability, J. Geophys. Res., V104, pp. 15495–15514.

Ruan, J., Kherbouche, F., Genty, D., Blamart, D., Cheng, H., Dewilde, F., Hachi, S., Edwards, R. L., Régnier, E., and Michelot, J.-L., 2016. Evidence of a prolonged drought ca. 4200 yr BP correlated with prehistoric settlement abandonment from the Gueldaman GLD1 Cave, Northern Algeria, Clim. Past, 12, 1–14, https://doi.org/10.5194/cp-12-1-2016, 2016.

Ruzmaikin. 1999. Can El Nino amplify thesolar forcing of Climate? Geoph. Res. Lett. 26, 2255.

Sarkar, S., S. Prasad, H. Wilkes, N. Riedel, M. Stebich, N. Basavaiah, and D. Sachse, 2015. Monsoon source shifts during the drying Mid-Holocene:Biomarker isotope based evidence from the core `monsoon zone'(cmz) of India,Quaternary Science Reviews, 123, 144-157.

Saraswat et al. 2013. Deglaciation in the tropical Indian ocean driven by interplay between the regional monsoon and global teleconnection. Earth Planet. Sci. Lett. V. 375. pp.166-175.

Sarkar, S., S. Prasad, H. Wilkes, N. Riedel, M. Stebich, N. Basavaiah, and D. Sachse, 2015. Monsoon source shifts during the drying mid-holocene: Biomarker isotope based evidence from the core `monsoon zone'(cmz) of india, Quaternary Science Reviews, 123, 144-157.

Schulz and Mudelsee. 2002. REDFIT: estimating red-noise spectra directly from unevenly spaced paleoclimatic time series. Comput. Geosci. 28, 421–426.http://dx.doi.org/10.1016/S0098-3004(01)00044-9.

Shakun et al. 2007. A high resolution, absolute-dated deglacial speleothem record of Indian Ocean climate from Socotra Island. Earth Planet. Sci. Lett. 259, 442–456.http://dx.doi.org/10.1016/j.epsl.2007.05.004.

Shen, C.C., Cheng, H., Edwards, R.L., Moran, S.B., Edmonds, H.N., Hoff, J.A., Thomas, R.B., 2003. Measurement of at to gram quantities of 231 Pa in dissolved and particulate fractions of seawater by isotope dilution thermal ionization mass spectroscopy. Anal. Chem. V. 75. pp. 1075–1079. http://dx.doi.org/10.1021/ac026247r.

Shen, C.C., Wu, C.C., Cheng, H., Edwards, R.L., Hsieh, Y.T., Gallet, S., Chang, C.C., Li, T.Y., Lam, D.D., Kano, A., Hori, M., Spötl, C. 2012. High-precision and high-resolution carbonate 230Th dating by MC-ICP-MS with SEM protocols. Geochim. Cosmochim. Acta. V. 99 pp. 71–86. http://dx.doi.org/10.1016/j.gca.2012.09.018.

Shen et al. 2010. East Asian monsoon evolution and reconciliation of climate records from Japan ad Greenland during the last deglaciation. Quat. Sci. Rev. V. 29. pp. 3327-3335.

Sinha et al. 2015. Variability of Southwest Indian summer monsoon precipitation during the

Bølling-Ållerød. Geology 33, 813–816. http://dx.doi.org/10.1130/G21498.1.
Scargle, J.D. 1982. Studies in astronomical time series analysis. II. Statistical aspects of spectral analysis of unevenly spaced data. The Astrophysical Journal. V. 263 (2), V. 835–853.
Scargle, J.D. 1989. Studies in astronomical time series analysis. III. Fourier transforms, autocorrelation functions, and cross-correlation functions of unevenly spaced data. The Astrophysical Journal. V. 343 (2), pp. 874–887.
Scholz, D., and D. Hoffmann, 2011.StalAge-An algorithmdesigned for construction of speleothem age models, Quat. Geochronol.,6(3–4), 369–382.
Schotterer, U., Oldfield, F. and Frölich, K., Global Network for Isotopes in Precipitation, IAEA, Vienna, 1996, pp. 1–48
Sengupta, D., Ravichandran, M. 2001. Oscillations of Bay of Bengal sea surface temperature during the 1998 summer monsoon, Geophys. Res.Lett. V. 28, pp.2033 – 2036.
Singh J, et al. 2006. Tree-ring-based hydrological records for western Himalaya, India, since AD 1560. Clim Dyn. V. 26, pp.295-303.
Sinha, A., M. Berkelhammer, L. Stott, M. Mudelsee, H. Cheng, and J. Biswas, 2011. The leading mode of Indian summer monsoon precipitation variabilityduring the last millennium, Geophysical Research Letters, 38 (15).
Singhvi A.K., Kale V.S.; Paleoclimatic studies in India- Last ice age to the present; Published by Shri SK Sahani, Executive Secreatary on behalf of Indian National Science Academy, Bahadur Shah Zafar Marg, New Delhi-110002 and printed at Aakriti Graphics, New Delhi
Sinha, A., et al., 2015. Trends and oscillations in the Indian summer monsoon rainfallover the last two millennia. Nat. Commun. 6306–6309. https://doi.org/10.1038/ncomms7309.
Skinner, B.C., Lora, M.J., Payne, E.A., Poulsen, J.C., 2020. Atmospheric river changes shaped mid-latitude hydroclimate since the Mid-Holocene. Earth and Planetary Science Letters. v. 541. 116293.
Sobha.V, Abhilash P.R., Santhosh S., Hashim.K.A and Valsalakumar E.; Geochemistry of Different Aquatic Systems in Thiruvananthapuram, Southern Kerala; Proceedings of the World Congress on Engineering 2009 Vol I, WCE 2009, London, UK.
Soleimani B. Soleimani; Paleoclimate Reconstruction during Pabdeh, Gurpi, Kazhdumi and Gadvan Formations (Cretaceous-Tertiary) Based on Clay Mineral Distribution; International journal of civil and environmental engineering, 1:2, 2009.
Sonda F., Ledru M. P. and Delaun M.; Geochemical markers of palaeo-environments: relations between climatic changes, vegetation and geochemistry of lake sediments, southern Brazil; Applied Geochemistry, Suppl. Issue No. 2, pp. 165-170, 1993
Srivastava, R., Ramesh, R., Prakash, S., Anilkumar, N. and Sudhakar, M., Oxygen isotope and salinity variations in the Indian sector of the Southern Ocean. Geophys. Res. Lett., 2007, 34, L24603
Staubwasser, M., Sirocko, F., Grootes, P.M., andSegl, M., 2003, Climate change at the 4.2 ka BP termination of the Indus valley civilizationand Holocene south Asian monsoon variability:Geophysical Research Letters, v. 30,p. 1425–1425, doi:10.1029/2002GL016822
Steig, E. J., C. P. Hart, J. W. White, W. L. Cunningham, M. D. Davis, and E. S. Saltzman, 1998. Change in climate, ocean and ice-sheet conditions in the Ross Embayment, Antarctica at 6 ka, Ann. Glaciol., 27.
Steinhilber, F., Abreu, J.A., Beer, J., Brunner, I., Christl, M., Fischer, H., Heikkilä, U., Kubik,

P.W., Mann, M., McCracken, K.G., Miller, H., Miyahara, H., Oerter, H., Wilhelms, F., 2012. 9,400 years of cosmic radiation and solar activity from icecores and tree-rings. Proceedings of the National Academy of Sciences of theUnited States of America 109

Steffenson et al. 2008. High resolution Greenland ice core data show abrupt climate change happens in few years. Science. V. 321. Pp.680-684.

Stocker, T.F. 1994. The variable ocean. Nature 36, 221–222.

Stocker and Johnsen. 2003 A minimum thermodynamic model for the bipolar seesaw. Paleoceanography. doi: 10.1029/2003PA000920

Sreedhar Arun K., Balakrishnan S., Pappu Shanti and Kumar Akhilesh; Clay mineralogical studies of sediments and strontium isotope analyses on calcretes at the prehistoric site of Attirampakkam, Tamil Nadu; Current Science, Vol. 94, No. 6, 25 March 2008.

Sultan Khawar, Shazili Noor Azhar; Rare earth elements in tropical surface water, soil and sediments of the Terengganu River Basin, Malaysia; Journal of Rare Earths, Vol. 27, No. 6, Dec. 2009, p. 1072..

Stuiver and Grootes. 2000. GISP2 oxygen isotope ratios. Quat. Res., V. 53, pp. 277–284.

Tan, L., Cai, Y., Cheng, H., Edwards, L. R., Gao, Y., Xua, H., Zhang, H., An, Z., 2018. Centennial-to decadal-scale monsoon precipitation variations in the upper Hanjiang River region, China over the past 6650 years. Earth and Planetary Science Letters 482, 580-590

Tegtmeier, U., 1993.*Neolithische und bronzezeitlichePflugspuren in Norddeutschland und den Niederlanden*,ArchaologischeBerichte, 3. Bonn: Holos

Thamban, M., Purnachandra Rao, V., Schneider, R. R., & Grootes, P. M. 2001. Glacial to Holocene fluctuations in hydrography and productivity along the southwestern continental margin of India. *Palaeogeography, Palaeoclimatology, Palaeoecology*, V. *165*(1–2), 113–127.

Tiwari, R.K., Yadav, R.R., Kaladhar Rao, K.P.C**.** 2012. Empirical orthogonal function spectra of extreme temperature variability decoded from tree rings of the western Himalayas. In: Sharma, A.S., et al. (Eds.), Extreme Events and Natural Hazards: The Complexity Perspective. Geophys. Monogr. Ser., vol. 196. AGU, Washington, D. C., pp. 169–176. http://dx.doi.org/10.1029/2011GM001133.

Tegtmeier, U., 1993. *Neolithische und bronzezeitliche Pfl ugspuren in Norddeutschland und den Niederlanden* , Archaologische Berichte, 3. Bonn: Holos.

Thompson, L.G., Mosley-Thompson, E., Davis, M.E., Henderson, K.A., Brecher, H.H., Zagorodnov, V.S., Mashiotta, T.A., Lin, P.-N., Mikhalenko, V.N., Hardy, D.R., Beer, J., 2002. Ice core records: evidence of Holocene climate change in tropical Africa. Science, 298, 589-593.

Torrence, C., Compo, G.P., 1998. A practical guide to wavelet analysis. Bull. Am. Meteorol. Soc. 79 (1), 61–78.

Turney, C., M. Baillie, S. Clemens, D. Brown, J. Palmer, J. Pilcher, P. Reimer, and H. H. Leuschner, 2005. Testing solar forcing of pervasive holocene climate cycles, Journal of Quaternary Science, 20 (6), 511-518..

Urey, H. C. 1947. The thermodynamic properties of isotopic substances. J. Chem. Soc., pp. 562 581,

Wadia D.,N. 1939. Geology of India. Macmillan, London

Wang, B. 2006. The Asian Monsoon (Springer).

Wang et al. 2001. A high-resolution absolute-dated Pleistocene monsoon record from Hulu Cave, China, Science. V. 294, pp. 2345–2348, doi:10.1126/science.1064618.

Warrier, A. K., Sandeep, K., Shankar, R. 2017. Climatic periodicities recorded in lake sediment magnetic susceptibility data: Further evidence for solar forcing on Indian summer monsoon. Geoscience Frontiers 8, 1349-1355.

Wang, Y., H. Cheng, R. L. Edwards, Y. He, X. Kong, Z. An, J. Wu, M. J. Kelly, C. A. Dykoski, and X. Li (2005), The holocene asian monsoon: links to solar changes and north atlantic climate, Science, 308 (5723), 854-857.

Weiss, H., 2012, Quantifying collapse: The late third millennium Khabur Plains, *in* Weiss, H., ed., Seven generations since the fall of Akkad: Wiesbaden, Harrassowitz Verlag, p. 1–24.

Weiss, H., M. Courty, W. Wetterstrom, F. Guichard, L. Senior, R. Meadow, and A. Curnow, 1993. The genesis and collapse of third millennium north Mesopotamian civilization, Science, 261 (5124), 995–1004.

Wang and Y. Wang. 1996: Temporal structure of the Southern Oscillation as revealed by waveform and wavelet analysis. J. Climate. V. 9, pp. 1586–1598.

Weiss, H., and Bradley, R.S., 2001, What drives societal collapse?: Science, v. 291, p. 609–610, doi:10.1126/science.1058775.

Warrier, A. K., Sandeep, K., Shankar, R. 2017.Climatic periodicities recorded in lake sediment magnetic susceptibility data: Further evidence for solar forcing on Indiansummer monsoon. Geoscience Frontiers 8, 1349-1355.

Wang, Y., H. Cheng, R. L. Edwards, Y. He, X. Kong, Z. An, J. Wu, M. J. Kelly,C. A. Dykoski, and X. Li (2005), The Holocene Asian monsoon: links to solarchanges and north Atlantic climate, Science, 308 (5723), 854-857.

Weiss, H., 2012, Quantifying collapse: The late thirdmillennium Khabur Plains, *in* Weiss, H., ed.,Seven generations since the fall of Akkad: Wiesbaden,HarrassowitzVerlag, p. 1–24.

Weiss, H., M. Courty, W. Wetterstrom, F. Guichard, L. Senior, R. Meadow, and A. Curnow, 1993. The genesis and collapse ofthird millennium north Mesopotamian civilization, Science, 261(5124), 995–1004.

Weiss, H., and Bradley, R.S., 2001, What drives societal collapse?: Science, v. 291, p. 609–610, doi:10.1126/science.1058775.

Weng, H., and K.-M. Lau. 1994. Wavelets, period doubling, and time-frequency localization with application to organization of convection over the tropical western Pacific. J. Atmos. Sci. V. 51, pp. 2523–2541.

Wu, L., Zhu, C., Ma, C., Li, F., Meng, H., Liu, H., Li, L., Wang, X., Sun, W., and Song, Y. 2017. Mid-Holocene palaeoflood eventsrecorded at the Zhongqiao Neolithic cultural site in the JianghanPlain, middle Yangtze River Valley, China, Quaternary Sci. Rev., 173, 145–160.

Wu, L., Zhu, C., Ma, C., Li, F., Meng, H., Liu, H., Li, L., Wang, X., Sun, W., and Song, Y. 2017. Mid-Holocene palaeoflood events recorded at the Zhongqiao Neolithic cultural site in the Jianghan Plain, middle Yangtze River Valley, China, Quaternary Sci. Rev., 173, 145–160.

Wang, Y., Cheng, H., Edwards, R.L., He, Y., Kong, X., An, Z., Wu, J., Kelly, M.J., Dykoski, C.A., Li, X., 2005. The Holocene Asian monsoon: links to solar changes and north Atlantic climate. Science 308, 854-857.

Weber et al. 2014. Millennial scale variability in Antarctic ice-sheet discharge during the last deglaciation. doi:10.1038/nature13397.

Webb A. 2002. Statistical Pattern Recognition, 2nd (Eds.) Hoboken NJ, pp. 496, John Wiley.
Wyrtki, K .1973. Physical oceanography of the Indian Ocean. Vol. 3 of Ecological studies: analysis and synthesis. In B. Zeischel, & S. A. Gerlach (Eds.), Biology of the Indian Ocean (pp. 18-36). London: Chapman and Hall Ltd.
Yadava, M.G. and Ramesh, R. 2007. Significant longer-term periodicities in the proxy record of the Indian monsoon rainfall. New Astron. 12, 544–555. http://dx.doi.org/10.1016/j.newast.2007.04.001.
Yonge, C. J., Goldenberg, L., & Krouse, H. R. 1989. An isotope study of water bodies along a traverse of southwestern Canada. Journal of Hydrology V. 106(3-4), pp. 245–255.
Yuan and Martinson. 2000. Antarctic sea ice extent variability and its global connectivity. J. Clim. V.13. pp. 1697-1717.
Yuan et al. 2004. Timing, duration, and transitions of the last interglacial Asian monsoon, Science. V.304, pp.575–578, doi:10.1126/science.1091220.
Yuan D, Cheng H, Edwards RL, Dykoski CA, Kelly MJ, Zhang M, Qing J, Lin Y, Wang Y, Wu J, Dorale JA, An Z, Cai Y. 2004. Timing, duration, and transitions of the last interglacial Asian monsoon. Science 304: 575–578.
Yadava, M., and R. Ramesh, 2007. Significant longer-term periodicities in the proxy record of the Indian monsoon rainfall, New Astron., 12 (7), 544-555, doi:10.1016/j.newast.2007.04.001.
Yadava, M., & Ramesh, R. 1999. Speleothems—Useful proxies for past monsoon rainfall.
Yadava, M., R. Ramesh, Pant, G. 2004. Past monsoon rainfall variations in peninsular India recorded in a 331-year-old speleothem, The Holocene, V. 14 (4), 517-524, doi:10.1191/0959683604hl728rp.
Yadava, M., & Ramesh, R. 2005. Monsoon reconstruction from radiocarbon dated tropical Indian speleothems. The Holocene. V. *15*(1), pp. 48–59.
Yang, H., Johnson, K. R., Griffiths, M. L., & Yoshimura, K. 2016. Interannual controls on oxygen isotope variability in Asian monsoon precipitation and implications for paleoclimate reconstructions. *Journal of Geophysical Research: Atmospheres*, *121*(14), 8410–8428.
Yu, L., 'Brien, J. O, Yang, J. 191. On the remote forcing of the circulation in the Bay of Bengal, J. Geophys. Res. V. 96, pp. 449-454.
Yuan, D., Cheng, H., Edwards, R. L., Dykoski, C. A., Kelly, M. J., Zhang, M., Qing, J.,Lin, Y.,
Wang, Y., Wu, J., Dorale, J. A., An, Z., Cai, Y. 2004. Timing, duration, and transitions of the last interglacial Asian monsoon. Science 304:575–578.
Yadava, M., and R. Ramesh, 2007. Significant longer-term periodicities in theproxy record of the Indian monsoon rainfall, New Astron., 12 (7), 544-555,doi:10.1016/j.newast.2007.04.001
Zhang, H. et al. 2016. Antarctic link with East Asian summer monsoon variability during the Heinrich Stadial–Bølling interstadial transition. Earth. Planet. Sci. Lett. V 453, pp 243-251.
Zhang, H.-L., Yu, K.-F., Zhao, J.-X., Feng, Y.X., Lin, Y.-S., Zhou,W., Liu, G.-H. 2013. East Asian Summer Monsoon variations in the past 12.5 ka: high-resolution δ18O record from a precisely dated aragonite stalagmite in central China. J. Asian Earth Sci. 73, 162–175. http://dx.doi.org/10.1016/j.jseaes.2013.04.015.

List of Publications

Articles

Gautam, P. K., Narayana, A. C., Band, S. T., Yadava, M. G., Ramesh, R., Shen, C.C. 2019. High-resolution reconstruction of Indian summer monsoon during the Bølling-Allerød from a central Indian stalagmite. Paleogeo., paleoclim., Paleoeco. V. 514. P. 567-576.

Gautam, P. K., Narayana, A. C., Band, Kiran P. K., Bhavani, P.G., Yadava, M. G., Jull, A. J.T. 2020. Indian monsoon variability over the last 46 ka: Isotopic records of planktonic foraminifera from southwestern Bay of Bengal. Journal of Quaternary Science. DOI: 10.1002/jqs.3263. MSP No. 3263. pp. 1-14.

Narayana, A.C., **Gautam, P. K.,** Kumar, P., K., Yadava, M., G., Varaprasad, V., Kathayat, G., Cheng, H., Xiyu, D., Jani, R. A. 2020. Mid-Holocene Indian Summer Monsoon Variability: Insights from stalagmite $\delta^{18}O$ and $\delta^{13}C$ Isotope records. climate Dynamics. (under review).

Seminar/Symposia/Conference

Gautam, P. K., Narayana, A. C., Band, S. T., Yadava, M. G., Ramesh, R., Shen, C.C. 2016. High Resolution deglacial monsoon $\delta^{18}O$ record from a new stalagmite from the Kailash Cave, Central India. Geophysical Research Abstracts, European Geophysical Union, General Assembly, EGU2016-9006, Vol. 18.

Gautam, P. K., Narayana, A. C., Yadava, M. G., Ramesh, R., Wu, C.C., Shen, C.C. 2015. Multidecadal and Centennial Periodicities in Indian Monsoon inferred from high resolution stalagmite $\delta^{18}O$ record. National Climate Science Conference. Divecha Centre for Climate Change, Indian Institute of Science, Banglore.

Gautam, P. K., Narayana, A. C., Yadava, M. G., Ramesh, R., Wu, C.C., Shen, C.C. 2015. A New High Resolution Stalagmite $\delta^{18}O$ Record of Deglacial Monsoon Variations from Central India. Session 1.3 Centennial and millennial scale variability in intensity of the Asian monsoon in the late Quaternary and Holocene. AGU Chapman Conference, June, 2015.

Gautam, P. K., Narayana, A. C., Ramesh, R., Yadava, M. G., Panigrahi, C. P. 2014. Origin and Evolution of Limestone Caves of Chhattisgarh and Orissa, India: Role of Geomorphic, Tectonic and Hydrological Processes. American Geophysical Union Fall Meeting. 2014. EP21C-3552.

Palaeogeography, Palaeoclimatology, Palaeoecology 514 (2019) 567–576

Contents lists available at ScienceDirect

Palaeogeography, Palaeoclimatology, Palaeoecology

journal homepage: www.elsevier.com/locate/palaeo

High-resolution reconstruction of Indian summer monsoon during the Bølling-Allerød from a central Indian stalagmite

P.K. Gautam[a], A.C. Narayana[a,*], S.T. Band[b], M.G. Yadava[b], R. Ramesh[b], Chung-Che Wu[c], Chuan-Chou Shen[c]

[a] Centre for Earth, Ocean, and Atmospheric Sciences, University of Hyderabad, Gachibowli, Hyderabad 500 046, India
[b] Physical Research Laboratory, Navrangpura, Ahemadabad 380 009, India
[c] High-Precision Mass Spectrometry and Environmental Change Laboratory (HISPEC), Department of Geosciences, National Taiwan University, Taipei 10617, Taiwan, ROC

ARTICLE INFO

Keywords:
Paleoclimate
Inter-hemispheric links
Coupled ocean-atmosphere
Wavelet analysis
U-Th dates
Kailash cave of India

ABSTRACT

Although the Indian monsoon during the last deglaciation has been reconstructed from marine sediments from the Indian Ocean, a detailed high resolution (decadal or less) reconstruction from terrestrial records such as speleothems has been lacking from the core monsoon zone of India. Such reconstructions can help determine whether the monsoon is controlled by insolation alone or also other feedbacks within the Earth system. We present here a new data set of high resolution record based on 1186 measurements of $\delta^{18}O$ from a 43-cm long speleothem from the Kailash Cave, Central India that record Indian Summer Monsoon (ISM) rainfall changes encompassing the Bølling-Allerød interstadial (14.8 to 12.6 ka). The growth rates varied from 0.6 to 37.1 mm/year, with the monsoon strength. This is also confirmed by the $\delta^{18}O$ record, with a rapid increase in the rainfall during 14.8 to 14.5 ka, stabilizing subsequently, and exhibiting centennial and multi-decadal oscillations. Our results corroborate an earlier observation that although the boundary conditions during the last several millennia and the Bølling-Allerød were very different, multi-decadal and centennial climate dynamics may have been similar. In addition to solar insolation, our results show a relation of ISM shifts to coupled ocean-atmospheric processes. Strong link of Indian Summer Monsoon (ISM) variability to proxy records from the southern hemisphere is also noted in this work.

1. Introduction

During the last deglacial period, every component of the Earth system experienced large scale changes as recorded in the northern hemispheric (NH) ice sheets: melting of ice, sea level rise (~120 m), and increase in the atmospheric CO_2 (~100 ppmv, Denton et al., 2010; Clarke et al., 2012). The plausible cause has been attributed to changes in insolation and consequent migration of Inter Tropical Convergence Zone (ITCZ; Clarke et al., 2012). As the Indian Summer Monsoon (ISM), an integral component of the Earth's tropical climate dynamics, affects the socio-economic conditions of the Indian subcontinent (Lone et al., 2014; Kathayat et al., 2016; Huguet et al., 2018; Band et al., 2018), and as recurrence of abrupt climate change might be a possible scenario in the future under anthropogenic climate influence (Partin et al., 2015), understanding the response of ISM to abrupt climate change is of fervent interest. It has been reported that the tropical regions can warm polar areas through atmospheric teleconnections (Ding et al., 2011) as the sea-ice extent in the poles are perturbed by the tropics and vice versa (Yuan and Martinson, 2000). Recent studies link ISM variability with dry (wet) ISM phase to cold (warm) climate events in North Atlantic (Gupta et al., 2013; Mohtadi et al., 2014; Band et al., 2018). Also, recent coupled general circulation model (CGCM) simulations have suggested that change in the North Atlantic, especially the Arctic melt water discharge can also affect the warming process of the NH (Chiang and Friedman, 2012) and can be linked to changes in the East Asian Monsoon. However, the link of ISM variability to changes in Southern Hemisphere (SH) remains elusive (Clemens et al., 1991; Kathayat et al., 2016). Here, we present a new centennially resolved 2200 years record of ISM variability during 14.8 to 12.6 ka from Kailash cave, central India, located in the core ISM area. This age range offers the signatures of the two major climatic events i.e. the Bølling-Allerød (B-A) and the onset of the Younger Dryas (YD) corresponding to abrupt warming and cooling events, respectively, that occurred during the last deglaciation. The onset of B-A (~14.7 ka) was associated with an

* Corresponding author.
E-mail address: acnes@uohyd.ernet.in (A.C. Narayana).

https://doi.org/10.1016/j.palaeo.2018.11.006
Received 23 May 2018; Received in revised form 29 October 2018; Accepted 1 November 2018
Available online 08 November 2018
0031-0182/

JQS Journal of Quaternary Science QRA Quaternary Research Association

Indian monsoon variability during the last 46 kyr: isotopic records of planktic foraminifera from southwestern Bay of Bengal

P. K. GAUTAM,[1] A. C. NARAYANA,[1]* P. KIRAN KUMAR,[2] P. G. BHAVANI,[1] M. G. YADAVA[2] and A. J. T. JULL[3]
[1]Centre for Earth, Ocean, and Atmospheric Sciences, University of Hyderabad, Hyderabad, India
[2]Geosciences Division, Physical Research Laboratory, Ahmadabad, India
[3]NSF-Arizona AMS Facility, University of Arizona Tucson, Arizona, USA

Received 17 November 2019; Revised 13 November 2020; Accepted 17 November 2020

ABSTRACT: The Indian monsoon carries large amounts of freshwater to the northern Indian Ocean and modulates the upper ocean structure in terms of upwelling and productivity. Freshwater-induced stratification in the upper ocean of the Bay of Bengal is linked to the changes in the Indian monsoon. In this study, we test the usefulness of $\delta^{18}O$ and $\delta^{13}C$ variability records for *Globigerina bulloides* and *Orbulina universa* to infer Indian monsoon variability from a sediment core retrieved from the southwestern Bay of Bengal encompassing the last 46 kyr record. Results show that the northeast monsoon was dominant during the Last Glacial Maximum. Remarkable signatures are observed in the $\delta^{18}O$ and $\delta^{13}C$ records during the Marine Isotope Stage (MIS) 3 to MIS-1. Our study suggests that Indian monsoon variability is controlled by a complex of factors such as solar insolation, North Atlantic climatic shifts, and coupled ocean–atmospheric variability during the last 46 kyr. Copyright © 2020 John Wiley & Sons, Ltd.

KEYWORDS: Bay of Bengal; foraminifera; Indian Monsoon; Indian Ocean; Late Quaternary

Introduction

The Indian monsoon is regarded as one of the most dynamic and powerful circulation systems manifested by the seasonal wind reversal driven by the north–south movement of the Inter-Tropical Convergence Zone (ITCZ) across the equator, causing enormous change in the hydrological system (Wyrtki, 1971). The monsoon system directly and/or indirectly controls the hydrology, economy, culture, society, land use, vegetation, etc., across the Indian subcontinent. Earlier studies on palaeomonsoons indicate that several ancient civilisations suffered due to the adverse changes in the Indian monsoon causing severe drought and/or floods (Staubwasser *et al.*, 2003; Rashid *et al.*, 2011; Gupta *et al.*, 2013; Lone *et al.*, 2014; Partin *et al.*, 2015; Kathayat *et al.*, 2018; Band *et al.*, 2018; Gautam et al, 2019). Hence, a clear long-term understanding of Indian monsoon variability is of vital interest for a better understanding of ocean circulation and ocean–atmosphere interactions in the past and for better predictions of the monsoon. The Indian monsoon is the main source of freshwater for the major river systems in India and neighbouring countries which ultimately debouch into the northern Indian Ocean causing seasonal changes in the waters of the upper ocean. The northern Indian Ocean comprises water masses of the Arabian Sea (AS) in the west and the Bay of Bengal (BoB) and Andaman Sea (AnS) in the east. Except a few (the Indus, Narmada, Tapti, etc. which flow into the AS), major rivers *viz.* the Ganga, Brahmaputra, Mahanadi, Godavari, Krishna, Cauvery, etc. in India, and Irrawaddy, Salween, Meghna, etc. in adjacent countries debouch into the BoB with a total water discharge of 2.95×10^{12} m^3/year (Sijinkumar *et al.*, 2016; Da Silva *et al.*, 2017). Annual rainfall over the BoB varies between −1 m off the east coast of India to about 3 m over the Andaman Islands (Rajeevan *et al.*, 2012).

The seasonal hydrographic changes are well recorded in the oceanic biota (e.g. planktic foraminifera), which are considered to be one of the best proxies for understanding Indian monsoon variability in the past as they capture the seasonal oceanic changes in their shells during their growth. Several researchers have used planktic foraminifera from the AS and reconstructed the Indian palaeomonsoon (e.g. Sirocko *et al.*, 1993; Overpeck *et al.*, 1996; Naidu and Malmgren, 1996; Sarkar *et al.*, 2000; Gupta *et al.*, 2003; Anand *et al.*, 2008; Ramesh *et al.*, 2010; Singh *et al.*, 2010; Tiwari *et al.*,2005, 2010; Govil and Naidu, 2010; Naidu *et al.*,1999, 2011; Saraswat *et al.*, 2013; Partin *et al.*, 2015; Singh *et al.*, 2016). Similarly, a few studies on foraminiferal species from the BoB and AnS have also been carried out to reconstruct the monsoon system (Cullen, 1981; Naidu *et al.*, 1999; Kudrass *et al.*, 2001; Rashid *et al.*, 2007, 2011; Govil and Naidu, 2011; Ahmad *et al.*, 2012; Raza *et al.*, 2014; Sijinkumar *et al.*, 2016; Gebregiorgis *et al.*, 2016; Da Silva *et al.*, 2017; Kumar *et al.*, 2018). However, studies from the BoB are scanty as compared with those from the AS and the available literature warrants more attention and further studies as the BoB witnesses extreme hydrographic changes throughout the year because of the large freshwater influx and stratification. Although there are a few studies on the reconstruction of palaeomonsoons, employing $\delta^{18}O$ records of foraminiferal species from the BoB, the relative differences of isotopic signatures from the near-surface dwelling and mixed layer depth (MLD)-dwelling planktic foraminifera have not been studied for their palaeoceanographic implications. The study on relative differences in the isotopic signatures from different habitats within upper ocean water provides clues to the past changes in its stratification (e.g. Singh *et al.*, 2016; Kumar *et al.*, 2018).

While the surface water of the BoB is known for freshwater-induced changes, MLD is characterised by its nearly homogenous nature resulting from intense mixing in the upper ocean by heat, momentum and freshwater flux (Narvekar and Prasanna Kumar, 2014). This mixed layer regulates the air–sea exchange process by mass and energy transfer in association

*Correspondence: A. C. Narayana, as above.
E-mail: acnarayana@gmail.com
[1]Present address: Geological Survey of India, Northern Region, Lucknow, India
[2]Present address: Isotope Climatology and Environmental Research Centre, Institute for Nuclear Research, Debrecen, Hungary

Plagiarism Report

Late Quaternary Indian Monsoon Variability: Inferences from Marine and Continental Records

by Pawan Kumar Gautam

Submission date: 14-Dec-2020 10:15AM (UTC+0530)
Submission ID: 1474331284
File name: Thesis_PKGautam_12ESPE04.pdf (16.08M)
Word count: 29083
Character count: 151625

Late Quaternary Indian Monsoon Variability: Inferences from Marine and Continental Records

ORIGINALITY REPORT

24%	3%	24%	1%
SIMILARITY INDEX	INTERNET SOURCES	PUBLICATIONS	STUDENT PAPERS

PRIMARY SOURCES

1	P.K. Gautam, A.C. Narayana, S.T. Band, M.G. Yadava, R. Ramesh, Chung-Che Wu, Chuan-Chou Shen. "High-resolution reconstruction of Indian summer monsoon during the Bølling-Allerød from a central Indian stalagmite", Palaeogeography, Palaeoclimatology, Palaeoecology, 2019 Publication	19%
2	mines.gov.in Internet Source	<1%
3	E. K. RALPH. "PROBLEMS OF THE RADIOCARBON CALENDAR", Archaeometry, 6/1967 Publication	<1%
4	Yadava, M.G.. "Significant longer-term periodicities in the proxy record of the Indian monsoon rainfall", New Astronomy, 200710 Publication	<1%
5	Submitted to Pamukkale Üniversitesi Student Paper	

Student's publication